Nanobody derivatization for molecular study and perturbation of cancer cell invadopodia

Tim Hebbrecht

Promotor: Prof. Dr. Jan Gettemans

2019 - 2020

Thesis submitted to fulfil the requirements for the degree of
Doctor (PhD) of Biomedical Sciences

Department of Biomolecular Medicine
Faculty of Medicine and Health Sciences
Ghent University

Nanobody derivatization for molecular study and perturbation of cancer cell invadopodia

By Ir. Tim Hebbrecht

Department of Biomolecular Medicine, Faculty of Medicine and Health Sciences
Campus Rommelaere
Albert Baertsoenkaai 3
9000 Gent
Belgium

Cover illustration

Photographs were taken by Tim Hebbrecht at the Rommelaere complex. The picture in front is the AF488 signal detected inside the FastGene FAS-digi Geldoc device (NIPPON genetics, Dueren, Germany). The picture at the back is a view through a window showing the historical charms of the Rommelaere complex.

Promotor

Prof. Dr. Jan Gettemans
Nanobody lab
Department of Biomolecular Medicine
Faculty of Medicine and Health Sciences
Campus Rommelaere
Ghent University

Dean

Prof. dr. Piet Hoebeke

Rector

Prof. dr. ir. Rik Van de Walle

Tim Hebbrecht was supported by the Concerted Actions Program (GOA) of Ghent University and an Emmanuel van der Schueren grant of the Flemish cancer society (Kom op tegen kanker).

Advisory Committee

Prof. Dr. Marleen Van Troys
Department Biomolecular Medicine
Ghent University

Prof. Dr. Ir. An Hendrix
Department of Human Structure and Repair
Ghent University

Examination Committee:
Chairman

Prof. Dr. Bruno Verhasselt
Department of Diagnostic Sciences
Ghent University

Members

Dr. Cécile Vincke
Department of Bioengineering Sciences
VUB

Prof. Dr. Frank Peelman
Department of Biomolecular Medicine
Ghent University

Prof. Andre Skirtach
Department of Biotechnology
Ghent University

Dr. Stephan Stremersch
Department of Pharmaceutics
Ghent University

Prof. Dr. Nadine Van Roy
Department of Biomolecular Medicine
Ghent University

Table of Contents

List of Abbreviations

AahI'	*Androctonus australis* hector toxin
Ab	Antibody
ADAM	A disintegrin and metalloprotease
ADCC	Antibody-dependent cytotoxicity
ADCC	Antibody-dependent cellular cytotoxicity
ADF	Actin depolymerizing factor or cofilin
AdPROM	affinity-directed protein missile
AF488	Alexa Fluor 488
AF647	Alexa Fluor 647
AhA	Azidohomoalanine
AID	Auxin-inducible degron
Anap	3-(6-acetylnaphthalen-2-ylamino)-2-aminopropanoic acid
Arg	Abl-related gene
Arp2/3	Actin-related protein 2/3
ASC	Apoptosis-associated speck-like protein
ASO	Antisense oligonucleotide
ATP	Adenosine triphosphate
AuNP	Gold nanoparticles
AzK	N^{ε}-(2-azidoethoxy)carbonyl-L-lysine
BARAC	Biarylazacyclooctynone compound
BSBMB	Belgian Society of Biochemistry and Molecular Biology
BTTAA	2-[4-((bis[(1-tert-butyl-1H-1,2,3-triazol-4-yl)methyl]amino)methyl)-1H-1,2,3-triazol-1-yl]acetic acid
BTTES	2-[4-((bis[(1-tertbutyl-1H-1,2,3-triazol-4-yl)methyl]amino)-methyl)-1H-1,2,3-triazol-1-yl]ethyl hydrogen sulfate
CAS9	CRISPR-associated gene
CBD	Chitin binding domain
CD7	Cluster of Differentiation 7
Cdc42	Cell division cycle 42
CDR	Complementarity determining region
CEA	Carcinoembryonic antigen (or CD66e)
CH	Constant domain of heavy chain
CIP4	Cdc42-interacting protein 4
CouAA	(S)-1-carboxy-3-(7-hydroxy-2-oxo-2H-chromen-4-yl)propan-1-aminium

CRIB	Cdc42- and Rac-interactive binding region
CRIG	Cancer Research Institute Ghent
CRISPR	Clustered regularly interspaced short palindromic repeat DNA sequences
CRL	Cullin-RING E3 ubiquitin ligase
CSF-1	Colony-stimulating factor-1
c-Src	Cellular Src kinase
CuAAC	Cu(I)-catalyzed Azide-Alkyne Click Chemistry
Cy5	Cyanine 5
Cy7	Cyanine 7
dAb	Single domain antibody
Dansyl Ala	Dansylalanine
DBCO	Dibenzocyclooctyne-amine
DHFR	Dihydrofolate reductase
DIBO	Dibenzocyclooctynes
DIFO	Difluorocyclooctyne
DNA	Deoxyribonucleic acid
DNA-PAINT	DNA point accumulation for imaging in nanoscale topography
DNP	Dinitrophenyl
DOX	Doxicicilne
DRF	Diaphanous-related formin
DTT	Dithiothreitol
E. coli	*Escherichia coli*
ECM	Extracellular matrix
EGF	Epidermal growth factor
EGFP	Enhanced green fluorescent protein
EGFR	Epidermal growth factor receptor
ELISA	Enzyme-linked immuno sorbent assay
EMT	Epithelial–mesenchymal transition
Ena-VASP	Enabled vasodilator stimulated phospoprotein
EtcK	Nε-(3-ethynyltetrahydrofuran-2-carbonyl)-L-lysine
EVH1	Ena-VASP homology 1
Fab	Fragment antigen-binding
FACS	Fluorescence-activated cell sorter
FAK	Focal adhesion kinase
FGE	Formylglycine-generating enzyme
fGly	Formylglycine
FH1	Formin-homology 1
FH2	Formin-homology 2
FRI	Fluorescence reflectance imaging
FWR	Frame work region
GA	Glutaraldehyde
G-actin	Monomeric actin
GBD	GTPase binding domain
GEF	Guanine nucleotide exchange factor
GFP	Green fluorescent protein
GPCR	G protein-coupled receptor

GQD	Graphene quantum dots
GTP	Guanosine triphosphate
HA	Hemagglutinin
HCAb	Heavy chain antibody
HEK293T	Human embryonic kidney cells
HeLa	Henrietta Lacks cervix cell line
HEPES	4-(2-hydroxyethyl)-1-piperazineethanesulfonic acid
HER2	Human Epidermal growth factor Receptor 2
HGF	Hepatocyte growth factor
HIV	Human immunodeficiency viruses
HNSCC61	Head and neck squamous carcinoma cancer cells
Hpg	Homopropargylglycine
HRP	Horseradish peroxidase
HypE	Huntingtin-associated yeast-interacting protein E
IEDDA	Inverse electron-demand Diels–Alder cycloadditions
IFP	Interstitial fluid pressure
IgG	Immunoglobulin G
IgNAR	Immunoglobulin new antigen receptor
IMAC	Immobilized metal affinity chromatography
JMY	Junction-mediating and regulatory protein
IPL	Intein-mediated protein ligation
IR	Infrared
ITC	Isothermal titration calorimetry
LPETG	Sortag consisting of Leu – Pro – Glu – Thr – Gly
LplA	Lipoic acid ligase
Malf1	Malassezia furfur cell surface protein
MamC	Magnetosome protein MamC of Magnetococcus marinus strain MC-1
MDA-MB-231	Breast cancer cells
MESNA	2-Mercaptoethane sulfonate sodium
MET	Mesenchymal to epithelial transition
*Mj*TyrRS/*Mj*tRNA^{Tyr}	*Methanocaldococcus jannaschii* Tyr tRNA synthetase/tRNA^{Tyr}
MHC	Major histocompatibility complex
MMP	Matrix metalloproteinase
MOM	Mitochondrial outer membrane
MT1-MMP	Membrane type I matrix metalloproteinases
MWCO	Molecular weight cut off
NAD(P)H	Nicotinamide adenine dinucleotide phosphate
Nb	Nanobody
Nck1	Non-catalytic region of tyrosine kinase adaptor protein 1
NHE1	Sodium hydrogen exchanger
NHS	N-hydroxysuccinimide
NMR	Nuclear magnetic resonance
NPC	Nuclear pore complex
NPF	Nucleation promoting factors
NSF	Nanobody Service Facility
NTA	Amino-terminal acidic region

N-WASp	Neural Wiskott-Aldrich syndrome protein
o-AzbK	N^{ε}-(o-azidobenzyloxycarbonyl)-L-lysine
PAG	Propargylglycine
PAGE	Polyacrylamide gel electrophoresis
PALM	Photo-activated localization microscopy
pAzF	Para-azido phenylalanine
PBMC	Peripheral blood mononuclear cell
PC-3	Prostate cancer cells
PCR	Polymerase chain reaction
PDGF	Platelet derived growth factor
PE38	Pseudomonas Exotoxin A
PEG	Polyethyleenglycol
PET	Positron emission tomography
P-EtF	P-ethinylphenylalanine
PFA	Paraformaldehyde
PH	Pleckstrin homology
$PI(3,4)P_2$	Phosphatidylinositol-(3,4)-biphosphate
$PI(3,4,5)P_3$	Phosphoinositol-(3,4,5)-triphosphate
$PI(4,5)P_2$	Phosphatidylinositol-(4,5)-biphosphate
PI3K	Phosphoinositide 3-kinase
PrgF	P-propargyloxy-L-phenylalanine
Protein-i	Protein interference
Ptk2	*Potorous tridactylis* epithelial kidney cells
Rac1	Ras-related C3 botulinum toxin substrate 1
RFP	Red fluorescent protein
Rho	Ras homologous
RING	Really interesting new gene
RNA	Ribonucleic acid
RNAi	RNA interference
ROS	Reactive oxygen species
SCAR	Suppressor of cAR
scFv	Single-chain variable fragment
SDS	Sodium dodecyl sulfate
SEC	Size exclusion chromatography
SH3	SRC Homology 3 domain
SHP2	Src homology region 2-containing protein tyrosine phosphatase 2
shRNA	Short hairpin RNA
SIM	Structured illumination microscopy
siRNA	Small interfering RNA
smFRET	Single molecule fluorescence resonance energy transfer
SMLM	Single molecule localization microscopy
SPAAC	Strain-promoted alkyne-azide cycloaddition
SPECT	Single-photon emission computed tomography
SrtA	Sortase A
STED	Stimulated emission depletion microscopy

STORM	Stochastic optical reconstruction microscopy
SYNJ2	Synaptojanin2
T-ALL	T-cell acute lymphoblastic leukemia
TAM	Tumor associated macrophage
TAMRA	Tetramethylrhodamine
TBTA	Tris-(benzyltriazolylmethyl)amine
TCEP	Tris[2-carboxyethyl]phosphine
TGFβ	Transforming growth factor β
Tgase	Transglutaminase
THPTA	Tris-(3-hydroxypropyltriazolylmethyl)-amine
TIRF	Total internal reflection fluorescence
Tks5	Tyrosine kinase substrate with five SH3 domains
TMP	Trimethoprim
TOCA1	Transducer of Cdc42-dependent actin assembly protein 1
tRNA	Transfer RNA
TTL	Tubulin tyrosine ligase
Tub	Tubulin-derived recognition sequence
VCA	Verprolin-homology (V), cofilin-homology or central (C) and acidic (A) region
VEGF	Vascular endothelial growth factor
VH	Variable domain of the heavy chain of a conventional Ab
VHH	Variable domain of the heavy chain of a HCAb
VHL	von Hippel-Lindau
VL	Variable domain of the light chain of a conventional Ab
VNAR	Variable domain of immunoglobulin new antigen receptors
WAML	WASp and missing-in-metastasis like protein
WAS	Wiskott-Aldrich syndrome
WASH	WASp and SCAR homologue protein
WASp	Wiskott-Aldrich syndrome protein
WAVE	WASP family verprolin-homologous protein
WAWH	WASp without WH1 domain protein
WH1	WASp homology 1
WH2	WASp homology 2
WHAMM	WASp homologue associated with actin, membranes, and microtubules
WIP	WASp-interacting protein
XLT	X-linked thrombocytopenia
YFP	Yellow fluorescent protein

List of Tables

List of Videos

List of Figures

Summary

Metastasis is a known lethal factor for cancer patients which is still not evident to prevent. It is one of the hallmarks of cancer. Metastasis is the process in which cancer cells escape from the primary tumor to disseminate through the body and to create a secondary tumor. To succeed in the spreading, such cancer cells hijack the normal cellular functions to become motile and invasive. Those invasive properties are a result of the actin cytoskeleton changes. Invasive cancer cells use specialised actin based membrane structures, called invadopodia, to facilitate their escape from a primary tumor leading to the dissemination. To study these invadopodia, the nanobody technology is utilised. Nanobodies are the smallest antigen binding fragment derived from the variable part of *Camelidae* heavy chain antibodies. Because of the high specificity and selectivity of nanobodies, it is possible to target specific invadopodium proteins which aid the study of the structure and the regulation of invadopodia as well as the contribution to invasion in the metastatic pathway.

The aim of this study is to reveal the function of neural Wiskott-Aldrich syndrome protein, N-WASp, in the invadopodium pathway by using nanobodies. N-WASp is one of the key players in the metastatic pathway through invadopodia due to its role in the actin polymerisation. The second goal of the study is to create a tool that enables a more accurate imaging compared to the existing methods by using the nanobody technology.

In the first part, nanobodies were generated to target the C-terminal domain of N-WASp, the VCA domain. Through its VCA domain, N-WASp is able to bind directly to actin monomers and Arp2/3 (actin related protein 2/3). Together they form a complex which is the precursor for a fast actin polymerisation. This is required to start the formation of an invadopodium. Following immunisation, a series of possible nanobodies were generated and had to be characterised first. After the characterisation and the measurement of the binding capacities, the nanobodies were implemented to analyse the role of N-WASp in the invadopodium pathway. The VCA nanobodies were able to

create inhibiting effects by reducing the number of invadopodia. However, they exert only small influence on the extracellular matrix degradation. Those results lead to the hypothesis that N-WASp found its main purpose in the invadopodium formation. Due to less invadopodia, the ECM degradation is slightly decreased as well.

In the second part, the nanobody technology is expanded to create a better imaging tool. Since the nanobodies are smaller compared to conventional antibodies, they enable a reduction in distance between the target and a dye (also known as linkage error). This results in higher resolution properties compared to the existing methods (e.g. conventional immunostaining, fusion proteins …). In this part, two ways are presented to attach a dye to a recombinant nanobody: by using the sortase A enzyme or by incorporating para-azido phenylalanine, an unnatural amino acid. The inclusion of an alkyne or azido group, allowed performing Cu(I)-catalyzed Azide-Alkyne Click Chemistry (CuAAC) to attach a fluorophore on the nanobody. When such fluorescent nanobodies were obtained, they were used for immunocytochemistry to visualise their target. However, the nanobodies face the same obstacles as antibodies. Due to fixation, the immunoreactivity of proteins can be altered. Further, those fluorescent nanobodies need fixed cells since they are not able to breach through the membrane of living cells. However, photoporation enables the delivery of fluorescent nanobodies into living cells. The combination of fluorescent nanobodies with photoporation creates a new instrumental strategy which allows a new and more precise way of doing research. Besides, due to the smaller linkage error, the labelled nanobodies are an interesting tool for super resolution microscopy to image invadopodia and other small structures more precisely.

Altogether, this study used the nanobody technology to analyse the role of N-WASp in the invadopodium pathway and to create a tool that allows better imaging of certain cellular structures.

Samenvatting

Van metastase of uitzaaiing is het geweten dat het een lethale factor is voor vele kankerpatiënten en dat het nog steeds moeilijk is om dit te voorkomen. Het is dan ook één van de gevreesde kenmerken van kanker. Metastase is het proces waarbij kankercellen ontsnappen uit de primaire tumor om zich te verspreiden doorheen het lichaam en zo een secundaire tumor te vormen. Echter, om in deze uitzaaiing te slagen, misbruiken dergelijke kankercellen de normale functies van de cel om beweeglijk en invasief te worden. Die invasieve eigenschappen zijn o.a. een resultaat van veranderingen in het actine cytoskelet. De invasieve kankercellen gebruiken namelijk actine gebaseerde membraan structuren, ook wel invadopodia genoemd, om net hun vrijkomen van de primaire tumor en hun verspreiding mogelijk te maken. In deze studie wordt er gebruik gemaakt van nanobodies om deze invadopodia te bestuderen. Nanobodies zijn het kleinste antigen herkennende domein dat afkomstig is van het variabele domein van zware keten antilichamen, die terug gevonden worden in kameelachtigen. Door de hoge specificiteit en selectiviteit van nanobodies, is het mogelijk om specifieke invadopodium eiwitten te visualiseren en op die manier zowel de structuur als de regulatie van een invadopodium te gaan bestuderen, als ook de invloed van dergelijke eiwitten op metastasering.

Het doel van deze studie is om de functie van het neurale Wiskott-Aldrich syndroom eiwit (N-WASp) in de invadopodium pathway te achterhalen door gebruik te maken van nanobodies. N-WASp is één van de hoofdrolspelers tijdens de invadopodium gerelateerde metastase door zijn rol in de actine polymerisatie. In het tweede deel is het doel vooral het creëren van een tool die het mogelijk maakt om accuratere beeldvorming te verkrijgen in vergelijking met de reeds bestaande methoden. Hierbij ligt de nanobody technologie ook aan de basis.

In het eerste deel worden er nanobodies opgewekt tegen het C-terminale domein van N-WASp, het VCA domein. Via dit domein kan N-WASp een directe interactie aangaan met

actine monomeren en met Arp2/3 (een actine gerelateerd eiwit 2/3). Tezamen vormen ze een complex wat uiteindelijk de precursor voor een snelle actine polymerisatie wordt. Dit is een vereiste om de invadopodium vorming van start te laten gaan. Door de immunisatie, ontstaan er een groot aantal nanobodies die eerst gekarakteriseerd moeten worden. Na deze karakterisatie en na het bepalen van de bindingscapaciteiten, worden de nanobodies gebruikt om de rol van N-WASp te analyseren in de invadopodium pathway. De resultaten tonen aan dat de VCA nanobodies in staat zijn om het aantal invadopodia te verminderen en een kleine invloed uit te oefenen op de extracellulaire matrix degradatie. Deze resultaten leidden tot de hypothese dat de rol van N-WASp hoofdzakelijk terug te vinden is tijdens de vorming van een invadopodium. De kleine, niet significante verlaging van de degradatie wordt dan verklaard doordat er minder invadopodia zijn en dus ook minder ECM degradatie.

In het tweede deel wordt de nanobody technologie uitgebreid om een betere beeldvormingstool te verkrijgen. Doordat nanobodies kleiner zijn in vergelijking met conventionele antilichamen, bezitten ze het voordeel dat de afstand tussen het target eiwit en de fluorescente molecule kleiner is. Deze afstand wordt ook wel de 'linkage error' genoemd. Hierdoor kan er een hogere resolutie verkregen worden dan de reeds bestaande methoden (zoals een conventionele immunokleuring, fusie eiwitten …). In dit deel worden er twee methoden voorgesteld om een fluorescente molecule te koppelen aan een recombinant nanobody: enerzijds door gebruik te maken van het enzym sortase A en anderzijds door de inbouw van een para-azido phenylalanine, een onnatuurlijk aminozuur. Dit heeft als gevolg dat er een alkyne of azido groep aanwezig is die het toelaat om Cu(I)-gekatalyseerde Azide-Alkyne Click Chemie (CuAAC) uit te voeren en op die manier een fluorofoor op het nanobody te plaatsen. Eenmaal een dergelijk fluorescent nanobody verkregen is, kan dit gebruikt worden in immunocytochemie om de target te visualiseren. De nanobodies ondervinden echter dezelfde problemen als antilichamen. Door het fixeren is het mogelijk dat de immunoreactiviteit van eiwitten gewijzigd wordt. Aangezien (fluorescente) nanobodies niet doorheen het membraan van levende cellen geraken, is de fixatie nog steeds nodig. Alhoewel, fotoporatie maakt het mogelijk om fluorescente nanobodies binnen te brengen in levende cellen. Door de combinatie van fluorescente nanobodies met de fotoporatie techniek, wordt er dan ook een nieuwe strategie gecreëerd die het toelaat om onderzoek te doen op een nieuwe en preciezere manier in levende cellen. Daarnaast kunnen de fluorescent gemerkte nanobodies als een belangrijke tool gezien worden voor super resolutie microscopie net doordat ze een kleine 'linkage error' hebben. Hierdoor kunnen kleine structuren, zoals een invadopodium, met meer precisie in beeld gebracht worden.

Algemeen kan besloten worden dat de nanobody technologie in deze studie gebruikt is om enerzijds de rol van N-WASp in de invadopodium vorming te analyseren en anderzijds om een tool te creëren dat een betere beeldvorming van bepaalde cellulaire structuren toelaat.

Part I

General introduction

Chapter 1
A nanobody or VHH

1.1 The discovery of heavy chain antibodies

The human body makes antibodies to defend itself against infections and harmful diseases. These IgG antibodies are 150 kDa in size[1], 12-15 nm in dimensions and consist of two light and two heavy chains. The heavy chain is composed of three constant (CH1, CH2 and CH3) and one variable domain (VH), while the light chain only consists of one constant (CL) and one variable domain (VL). Due to the high specificity and affinity between an antibody and its target[2] and due to the enormous diversity of the antigen binding domains[2], scientists have been searching for (recombinant) antibody formats that are as small as possible and which have applications as therapeutics, research tools or diagnostics. Such formats can be seen as next-generation antibody fragments (Figure 1A)[3]. The first antibody fragment consisted of four immunoglobulin domains (CH1, VH, CL and VL) and is called a 'fragment antigen-binding' or Fab (55 kDa)[3, 4]. Some difficulties were found when a Fab fragment is expressed recombinantly. Because two different polypeptides are required to associate and have to be linked through a disulfide bond, the assembly and folding of Fab fragments became a challenge[5, 6]. Besides, the light chains are likely to form undesired homo-dimers, making the challenge even bigger[5, 6]. Once formed properly, Fabs possess high stability over time[5].

Due to these obstructions, the search was going on to find and to engineer antibody fragments which were able to be expressed as a single polypeptide[7]. A single-chain variable fragment (scFv) (25-28 kDa) consists only of the variable domains of an antibody (VH and VL) which are linked using a synthetic linker peptide ($(Gly)_n$ or $[(Gly)_n\text{-}Ser]_p$) (Figure 1A)[3, 4, 6-8]. Next to a linker peptide, a disulfide bond can be used as well[9]. This fragment yielded better expression levels in microorganisms[4, 10] and could be used for *in*

vivo experiments[7, 11]. However, the intracellular, cytoplasmic expression of scFvs remained challenging as scFvs are unstable over a period of time and some scFvs showed a reduced affinity compared to the Fab fragments[5, 6, 8]. This is because the orientation of the paratope is only mediated by hydrophobic interactions of the VH with VL, while Fab also has the stability of the disulfide bridge between CH1 and CL[6, 8]. Both Fab and scFv enhance pharmacokinetics for tissue penetration[4], but can often suffer from loss of antigen binding[12]. So, the urge to find better antibody fragments was still existing. In the late 1980s, a fragment existing of only a variable domain (VH or VL) was generated and called a single domain antibody (dAb) (Figure 1A)[13]. Such a single immunoglobulin domain has four framework regions (FWR) and three complementarity determining regions (CDRs) (Figure 1B). Because in conventional antibodies the antigen recognition site needs six CDRs (three CDRs from the VH and three CDRs from the VL), an dAb could be faced with a big 'recognition problem' due to the split of the original paratope into two[4, 14].

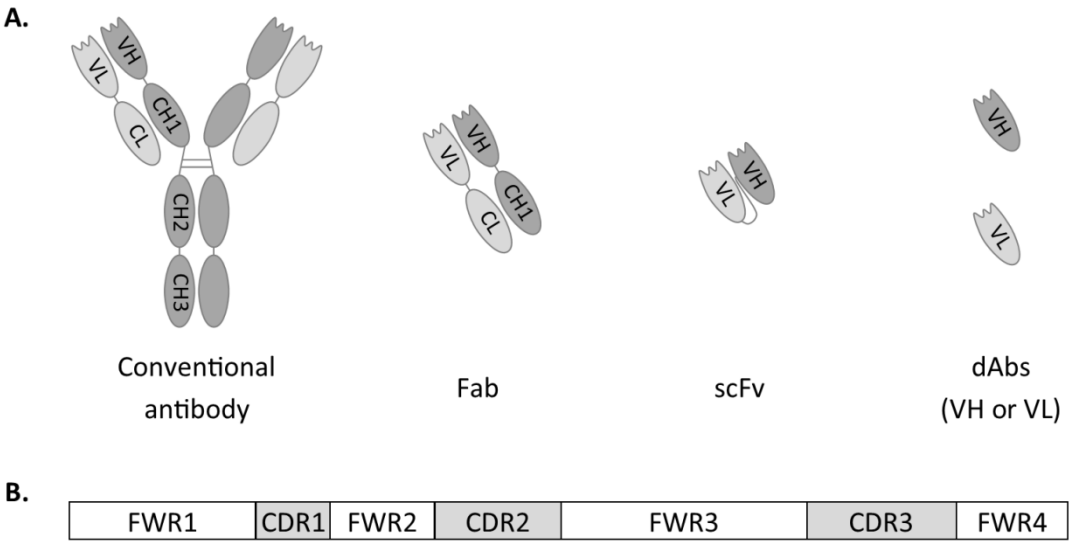

Figure 1: Antibody and antibody fragments. (**A**) Starting from the conventional antibody, different antibody fragments were made such as fragment antigen-binding (Fab), single-chain variable fragment (scFv) and the variable domain (VH or VL) or single domain antibodies (dAbs). (**B**) A dAb consists of four frame work regions (FWR) and three complementarity-determining regions (CDRs).

A breakthrough in the search is to be situated in the early 1990s. Hamers-Casterman and co-workers discovered a different kind of antibodies[15, 16]. Compared to conventional antibodies (150 kDa) (Figure 2A), this new type of antibody was only 90 kDa in size and was called heavy chain antibody (HCAb) (Figure 2B)[17]. HCAbs lack the light chains and are composed of a CH3, a CH2 and a variable domain (VHH)[17, 18]. Those HCAbs are found in animals from the *Camelidae* family such as dromedaries (*Camelus dromedaries*), camels (*Camelus bactrianus*), llamas (*Lama glama*) and alpacas (*Vicugna pacos*)[17, 19]. A few years later in 1995, another variant of the HCAbs was found in cartilaginous fishes (*Chondrichthyes*) such as nurse sharks (*Ginglymostoma cirratum*), wobbegong sharks

(*Orectolobus maculates*) and dogfish sharks (*Squalus acanthias* and *Mustelus canis*)[20, 21]. This variant is called immunoglobulin new antigen receptor or IgNAR and is composed of five constant domains and one variable domain (Figure 2D)[18, 21]. The fact that HCAbs are produced by the immune system, is due to a defective splicing site which causes the elimination of the CH1 region resulting in the lack of interaction site for the light chain[17, 22]. Based on similar interests, the HCAbs were used as a starting point to make antibody fragments leading to the VHH or nanobody (Figure 2C).

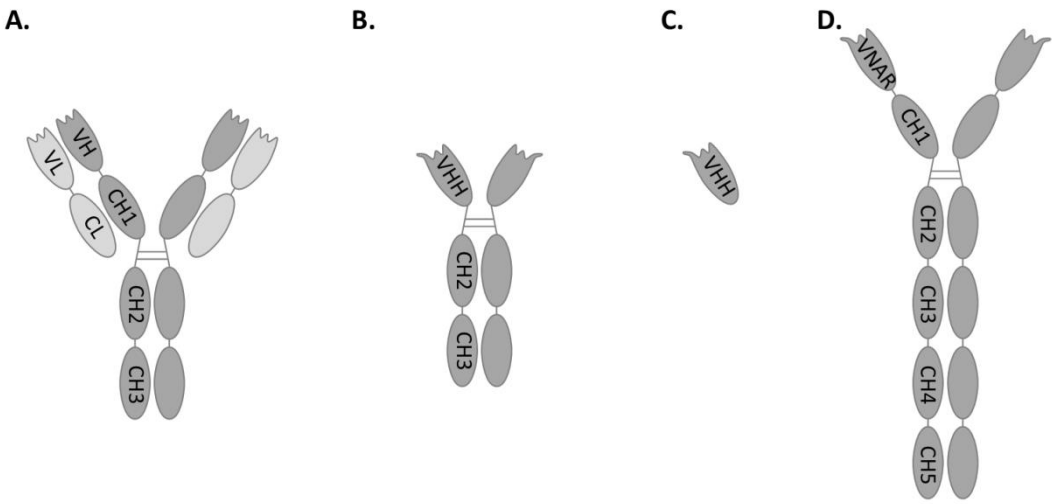

Figure 2: Heavy chain antibodies. Next to the conventional antibodies (**A**), *Camelidae* have a second pool of antibodies. Those are lacking the light chain and are called heavy chain antibodies (HCAbs) (**B**). This discovery resulted in the VHH or the nanobody (**C**), the counterpart of the VH. Next to *Camelidae*, a variant of the HCAbs is found in some shark species and those are called immunoglobulin new antigen receptor or IgNAR (**D**).

1.2 **Nanobodies**

1.2.1 VH versus VHH

Structurally, both VH (Figure 3A) and VHH (Figure 3B) are composed of nine β strands which are organised in a four-stranded and a five-stranded β sheet[17, 19]. A VH and a VHH are similar in size and both have four FWRs and three CDRs (Figure 1B). However, some important differences lead to the preference for VHHs for downstream applications. For a VH the distinction between a CDR and a FWR is obvious, but when looking at VHHs the difference is far less clear[22, 23]. It has been suggested that some amino acids in the FWR for many nanobodies take part in the binding and hence, co-determine the affinity for the antigen[22, 23]. Besides, there are two main differences between a VH and VHH of which the first is found in the frame work region 2 (FWR2). Highly conserved amino acids

in the VH are needed to interact with the VL to have a proper orientation of the paratope[8, 19]. Those amino acids are typically hydrophobic (Val42, Gly49, Leu50, Trp52) and they may cause undesired aggregation, accounting for their 'sticky' properties[17, 19, 24, 25]. In case of VHHs, those hydrophobic amino acids are replaced by more hydrophilic amino acids (mostly Phe42, Glu49, Arg50, Gly52), making the VHHs more soluble[6, 17-19, 25]. The second difference is found in the length of the CDR1 and CDR3, which is larger in case of VHH compared to VH[17, 19, 22]. The advantage of the extended loops gives a nanobody better antigen binding affinities then the VH or VL[17, 19, 22]. While the CDRs of the VH and VL contribute similarly to antibody specificity, the CDR3 in VHHs contributes for the most part of the antigen recognition (at least 60-80% of the antigen binding)[1, 8, 23]. This explains why the length of a CDR3 loop in VHHs varies broadly in length (3 – 28 amino acids) compared to a human VH (8 – 15 amino acids)[8, 26]. Notably, the CDR3 loop is on average shorter in llama than in dromedary[17, 27]. Furthermore, the extended CDR3 gives the advantage of binding cryptic epitopes and antigen cavities which are unreachable to conventional antibodies[15, 17-19, 22]. For nanobodies with a long CDR3, the CDR3 works as a finger-like structure that is able to reach cavities, such as active sites of enzymes[8, 18, 28]. For nanobodies with a less longer CDR3, the shape of the nanobody creates a convex paratope that is able to interact more into concave epitopes[15, 18, 22, 28]. In some cases the long CDR3 is stabilised by an additional disulfide bond between the CDR3 loop and the CDR1 loop (common in camel and dromedary VHHs) or between CDR3 and CDR2 (which is common in llama VHHs)[6, 17, 19, 22, 24, 26, 29]. This extra disulfide bond favours the stability of a VHH in harsh conditions[29] and creates higher affinity due to the reduced flexibility of the CDR3[17, 19, 22, 30].

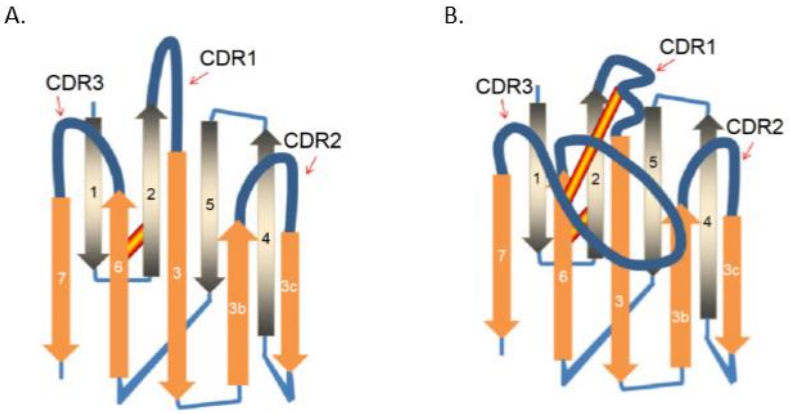

Figure 3: Structure of VH (A) and VHH (B). Those single domains have four framework regions alternated with three complement determine regions (CDR). Both, VH and VHH, are structural build-up of nine β strands, divided in two β sheets (a four-stranded and a five-stranded β sheet). Figure is adapted from Wang *et al.*[19].

1.2.2 Advantages and disadvantages of nanobodies

Because a nanobody or VHH consists of only one immunoglobulin domain, it makes a nanobody the smallest natural antigen binding fragment that retains its binding properties and affinity[17, 28]. The complete antigen binding capacity depends on only three CDRs, while a conventional antibody needs six CDRs[15, 22]. Nanobodies are known to have **high specificity** and **high affinities** in the nanomolar range, and even picomolar range[1, 15, 17, 31]. Because of the properties of this monomeric domain, nanobodies are more stable than its counterpart found in conventional antibodies[1, 17, 28]. Due to the more hydrophilic amino acids (compared to the VH), a nanobody is more **soluble in aqueous solutions** than a VH fragment[28]. Nanobodies possess high **conformational stability** and are able to unfold and refold again without the feared aggregation problems that are found for most proteins[18, 32]. Next to the conformational stability, nanobodies have high **thermal stability** and **survive harsh conditions**[32, 33]. They preserve their binding capacities after incubation at elevated temperatures and in different pH conditions[25, 33-35]. This opens possibilities as it signifies that nanobodies are still functional in the gut, and they are able to resist the acidic environment of the stomach[17, 34]. Anti-rotavirus Nbs for instance were able to reduce the morbidity of rotavirus-induced diarrhea in mice after oral administration[34]. The nanobody stability in high pH or in detergent containing environments are also useful: e.g. nanobodies against the *Malassezia furfur* cell surface protein (Malf1) have been used in shampoo to inhibit the growth of *M. furfur* which causes dandruff[35]. Because of the large sequence similarity and structural homology with the human VH gene family, nanobodies have **low toxicity** and **low immunogenity**[1, 17, 31]. As the nanobody lacks the Fc domain which is needed to activate the Fc-receptors on natural killer cells and macrophages, nanobodies on itself cannot induce antibody-dependent cell-mediated cytotoxicity (ADCC)[8, 29].

Nanobodies are **easy to modulate and to produce** in prokaryotic and eukaryotic cells[1, 30]. As mentioned above, nanobodies are able **to target challenging epitopes**. They are able to bind cryptic epitopes, unreachable for four-chain antibodies, which is a result of the extended CDR3[15, 17-19, 22, 28, 36]. Next to cryptic antigens, nanobodies have a broader range of antigens than antibodies. While the large size of antibodies can sometimes be an obstacle for certain epitopes, nanobodies have the advantage of targeting smaller biomolecules such as epitopes found on pathogenic agents like toxins, viruses, bacteria, or parasites[15, 17, 36]. This gets special attention for therapeutic purposes[17]. Nanobodies are also able to target flat surfaces in macromolecules[18] or small linear peptides[19, 37, 38], but they prefer binding to clefts[39]. The **size of a nanobody** is 2.5 nm in diameter and 4 nm in height[4, 19, 28]. However, this has both advantages and disadvantages. When a nanobody is

used to coat substrates e.g. to perform ELISA, the paratopes of the nanobodies are very close to the surface, which can obstruct the interaction with the antigen[19]. This problem can easily be undone by adding tags at the C-terminus[19].

The interstitial fluid pressure (IFP) in tumors is elevated compared to the surrounding tissues, meaning the transport of large molecules is hindered[40]. This makes tumor penetration difficult for larger proteins such as antibodies. The small size of nanobodies has the advantage to overcome this problem. As observed previously, nanobodies show a **good tumor penetration** and a more **homogenous distribution** through the tumor[19, 40]. If the nanobodies are used *in vivo*, a **fast renal clearing** is observed[1, 17, 19]. This fact can be an advantage and disadvantage simultaneously. Because of their small size, a rapid extravasation and diffusion into tissues is observed[18, 19, 28]. As such, the nanobodies give a fast renal clearing which is required for a good *in vivo* imaging agent[17]. This means that nanobodies are able to give high contrast images as early as 1h post-injection in case of positron emission tomography (PET) or single-photon emission computed tomography (SPECT)[17-19]. Another advantage is low radiation exposure for the patient, when using radionuclides[17, 18]. A major hurdle however is the accumulation of the radiolabelled nanobodies in the proximal tubuli of the kidney[18, 19]. If a more therapeutic setting is desired, a fast renal clearing would be a disadvantage. If a nanobody is coupled to a drug, the fast renal clearing could cause renal toxicity[40]. The easiness of modulating nanobodies makes it possible to conjugate a nanobody to another biomolecule, e.g. another nanobody, albumin, polyethylene glycol, sugar moieties … [1, 28, 40]. This conjugation increases the size and enlarges the circulation time of the nanobody[1, 28]. For example, CONAN1, a biparatopic anti-EGFR nanobody, against the epidermal growth factor (EGF) receptor (EGFR), when fused to an anti-albumin Nb, increased the circulation time from 1-2h to 2-3 days[8, 41]. Besides the good *in vivo* tissue penetration, nanobodies rarely penetrate the blood-brain-barrier[39].

Probably the biggest disadvantage of nanobodies, as for many other proteins, is the problem that they are not able to pass through the (cell) membrane[30, 39]. This is caused by the anionicity and hydrophobicity of the membrane itself[42] and explains why studies using nanobodies against intracellular targets are routinely performed by transduction or transfection[28, 43-48]. Since antibodies suffer from assembly and folding issues due to the reducing environment of the cytoplasm, nanobodies are preferred for intracellular targeting[6]. High glutathione concentrations tend to disrupt the disulfide bonds between antibody chains in the cytosol[6]. If recombinant protein delivery is desired, researchers are faced with a challenge. **Protein delivery** is a problem not only for nanobodies[10, 49]. Many ways have already been investigated, such as electroporation[50-52], microinjection[53-55], cell squeezing[56, 57] and virus-like particles (delivery of proteins as Gag-fusion protein or

on the surface of virus-like particles)[58]. These are only possible when a small number of cells need to be subjected to protein delivery or when the required recipient or device is used (e.g. in case of the electroporation). If recombinant nanobodies are used *in vivo* (without any adaptations), they are only able to target extracellular epitopes. Different options have already been tried to target the nanobody to the cytoplasm, i.e. by coupling cell-penetrating peptides to nanobodies (cyclic arginine-rich peptides[59] or penetratin[60, 61]), by polycationic resurfacing of a nanobody (done by changing amino acids in the frame work region to arginine or lysine)[62, 63], by making use of already existing internalization proteins on the target cell (e.g. by making use of the folate receptor specific uptake process[64] or by inducing receptor dimerization using a bivalent nanobody[39]), by transportation of the nanobodies in mesoporous silica nanoparticles[65] or by using the *Escherichia coli (E. coli)* type III secretion system[39, 66].

A more recent and more physical procedure is photoporation (Figure 4). This is shown by Liu *et al.*[67, 68]. In those experiments the nanobody is introduced into a living cell through laser light and nanoparticles such as gold nanoparticles (AuNP) or graphene quantum dots (GQD)[67, 68]. The laser light causes thermal energy transfer to the nanoparticle making it extremely hot[67, 69]. Depending on the laser intensity, two options are possible of which both result in pore formation of the cell membrane[70, 71]. This pore formation is a reversible process in which cells reseal those pores in a time range of seconds to a few minutes depending on the size of the pore[69, 70, 72]. In case of low intensity laser pulses, the pores are formed due to the increase of the temperature[70, 71]. At the heated nanoparticle, the local temperature can rise up to 100 °C[70, 71]. This causes a local phase transition in the lipid bilayer or a thermal denaturation of integral glycoproteins resulting in the pore formation[70, 71]. However, when higher laser energy is used, the heated nanoparticle leads to the evaporation of the surrounding water which result in the formation of a vapor nanobubble[69, 70]. Due to this, the mechanical force of this expanding and imploding vapour nanobubble perforate the cell membranes locally allowing a free diffusion of an external protein into the cell[67, 70, 71]. A disadvantage of the first options is that the local heat increase will diffuse throughout the cell and its environment. This can create hyperthermia-induced cell stress and a decreased cell viability[70, 71]. However, in case of the vapour nanobubbles there is no toxicity increase or no decrease in cell viability[69, 70]. This is because the diffusion of heat from the nanoparticles into the environment is negligible[69, 70]. This is the result of the extremely short (<1 μs) lifetime of a vapour nanobubble and of the conversion of almost all the energy of the irradiated nanoparticles to mechanical energy[70]. Additionally, Xiong and co-workers showed that the vapor nanobubble option was more efficient due to the larger pore size that is created compared to direct heating[70]. Both, AuNP and GQD, can create such pores after

irradiation with laser light[67]. However, while AuNPs are fragmenting after one laser pulse, the GQD are more resistant and are able to form repeated vapor nanobubbles[67]. While photoporation is not a commonly used technique, it is functional with different agents already such as phalloidin[67, 73], siRNA[74] and dextran[67, 70, 74]. It has shown to combine a good cell viability with high delivery efficiencies[67, 70, 73, 74]. Photoporation allows high throughput experiments since it is a fast technique and can be used in different cell culture substrates and devices[67, 68]. This technique is not only applicable on cultured cell lines, it is also useful for primary cells such as T-cells[71, 74].

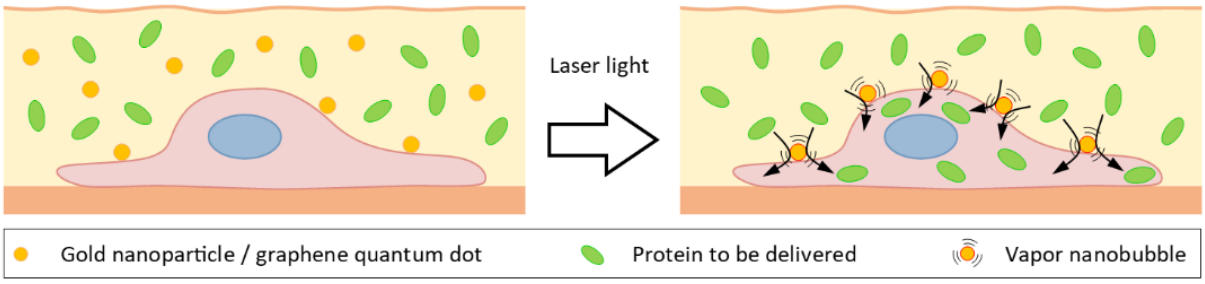

Figure 4: Schematic representation of the photoporation technique. Due to laser light, the gold nanoparticles or graphene quantum dots heighten in temperature creating a vapour nanobubble. This makes reversible pores in the cell membrane allowing other proteins to enter the cell.

Other options are possible as well; Teng and co-workers have used streptolysin O, a bacterial toxin, to create pores into the cell membrane which allows the uptake of labelled nanobodies[75]. Another strategy was used by Leduc and co-workers[76]. They used a GFP nanobody which was coated on gold nanoparticles[76]. This negatively charged GFP Nb - Au nanoparticle complex allows electroporation of the nanobodies into living cells and detection by photothermal imaging[76]. By implementing this, they were able to visualise GFP fusion proteins (e.g. GFP-kinesin fusion protein) in living and fixed cells[76]. Additionally, Ressler *et al.*[42] have shown another strategy in which it was possible to internalize a ribonuclease 1 into the cytosol of living cells (Figure 5). The esterification of the carboxyl groups of the protein (Glu and Asp) with 2-diazo-2-(p-methylphenyl)-N,N-dimethylacetamide allows the passage through the membrane. Once inside the cell, the esterases of the cell will reverse the process[42]. This means that once intracellular the internalized protein is unchanged and is able to carry out its activity as before[42]. However, before having an ideal method for all nanobodies, the search of protein delivery still continues.

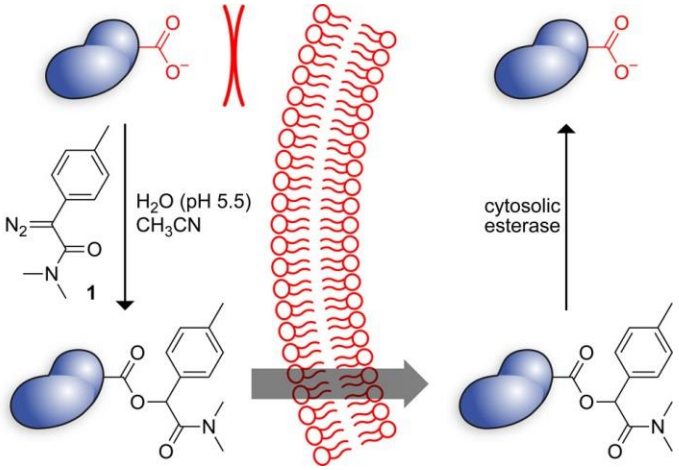

Figure 5: Protein delivery by esterification. The Glu and Asp will be coupled to 2-diazo-2-(p-methylphenyl)-N,N-dimethylacetamide in order to establish the esterification. This allows internalisation. Once inside the cell, cytosolic esterases undo the protein modification and restore the original state of the delivered protein. This figure is adapted from Ressler *et al.*[42].

1.2.3 Nanobody generation

To obtain immunoglobulin derivates such as nanobodies, animals are required to perform an immunisation to obtain nanobodies. By immunizing the animal with an antigen, the B-cells of the immune system will produce specific antibodies against the target. Afterwards, the peripheral blood lymphocytes are isolated from the immunized animal and the total RNA will be extracted (Figure 6)[4, 15, 19, 39]. Next, cDNA is synthesised via reverse transcriptase of those collected RNA. Because the nanobodies belong to the same gene family, they have homologous border sequences which makes it possible to use the cDNA for amplifying specifically only the VHH sequences[4]. For this, some methods with small differences are possible. Pardon and co-workers use two sets of primers[77]. The first set amplify the fragment between a conserved region of the CH2 for all IgG isotypes of *Camelidae* and a well-conserved region of the signal sequence of the most abundant V element family in camelids[77]. After the first polymerase chain reaction (PCR), they perform a second nested PCR by using primers at the beginning and end of the nanobody[77]. This method has been shown to be successful for dromedaries, camels, llamas and alpacas[77]. Van der Linden and co-workers used a different set of primers[78]. They amplify the fragment from the N-terminal nanobody sequence to the hinge region of each HCAb IgG isotype of all camelid species[78]. Other options exist as well, but those are in most case not applicable for all *Camelidae*[79, 80].

Once the nanobody cDNA is obtained, this product has to be transferred and cloned into a selected plasmid leading to a nanobody library[4, 15, 19]. Next, the screening can start[4]. A common way is the phage display which is based on the expression of a nanobody fused with coat proteins on the phage surface[31, 77, 81]. For this the used vector is a phage display

vector or phagemid, so the selection is performed by panning which allows a selection for binders with high affinity and for nanobodies that are expressed well in bacteria[4]. The nanobody is fused in this case with phage coat protein pIII which will bring the nanobody at the tip of phage particles[39, 81]. This is needed for a successful round of panning[39]. In such a round of panning, those phages are added to the coated and immobilised antigen followed washing steps in order to remove the unbound phages[31]. After a few rounds of panning, the best binders will remain and become more and more enriched[15, 31, 39]. The immunisation and panning together takes approximately 3 months starting from the first injection until the first experiments of the nanobodies[15, 31].

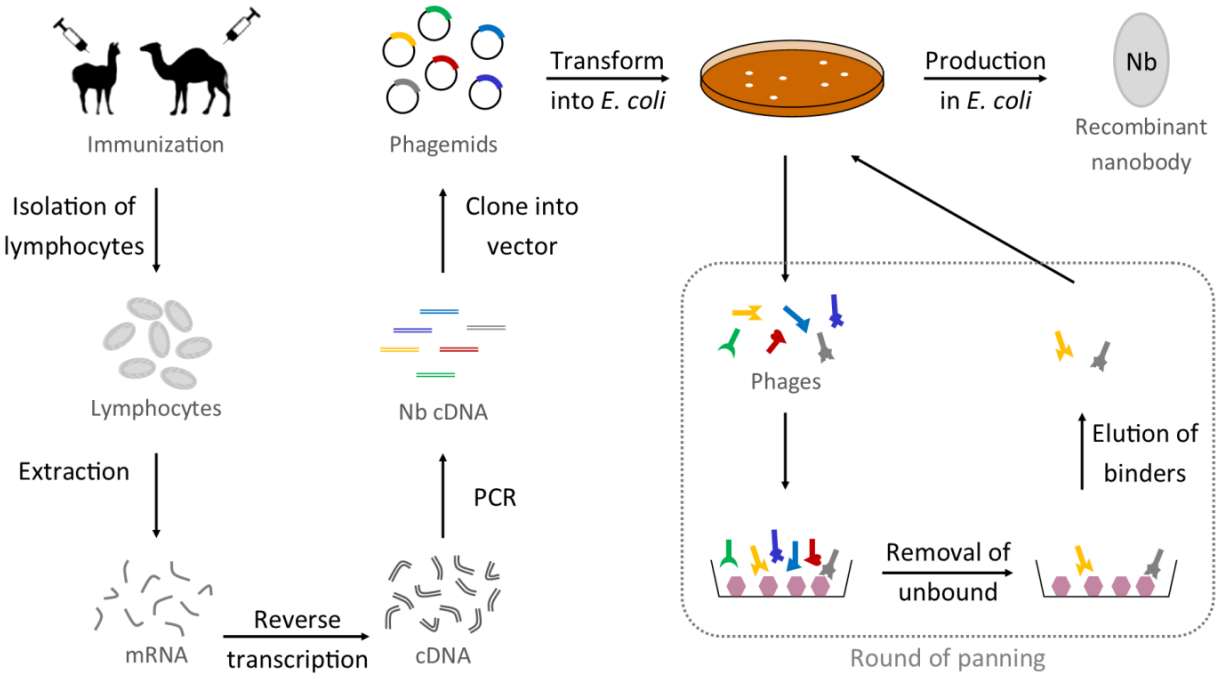

Figure 6: Generation and isolation of nanobodies through phage panning. After the immunisation in an animal of the *Camelidae* family, the mRNA is extracted from the lymphocytes. This is converted to cDNA and eventually cloned into a vector (here: phagemid) to obtain a nanobody library. The screening is performed via phage display. A nanobody is fused to a phage coat protein which allows a selection of binders through a few rounds of panning. In a round of panning, the phages are incubated with the immobilised target. The unbound phages are washed away, which leaves only the fraction of phages that contain a target-binding nanobody. The latter fraction is eluted and amplified in *E. coli* which allows another round or panning. The figure is adapted and modified from Revets et al.[4], Desmyter *et al.*[15] and Liu *et al.*[31].

However, an immunisation is not always required anymore to obtain nanobodies. Sometimes an immunisation is even not possible (in case of toxins[4, 31], non-immunogenic compounds[31, 39], lack of purified proper folded antigens[39], bloodstream stability[31] …) or unwanted, but alternatives are already available. Nanobodies can be obtained from a naïve library[15, 31]. This is a nanobody library starting from blood of non-immunized animals[15]. Once such a library is obtained, it can be used for different targets. This way of obtaining nanobodies reduces the time to approximately three weeks[15]. The only problem is found in the lack of somatic hypermutation which increases the chance on finding low affinity binders, meaning a large diversity library is needed to find high affinity nanobodies[15, 19, 31]. This requires a substantial amount of blood samples from

different individual animals and/or species[31]. Besides, synthetic or semi-synthetic libraries can offer a solution[19]. As somatic hypermutation is found in nature to obtain better affinities, synthetic or semi-synthetic libraries mimic this process to have more diversification[31]. This kind of library is based on engineering an existing library[19, 31]. While the conserved FWRs of a nanobody are kept unchanged, the CDRs are randomly changed and especially the CDR3[19, 31]. This can be achieved using different approaches, e.g. by introducing length and sequence variations using randomized CDR3 primers[19, 82], spiked mutagenesis combined with ribosome display[17] or error-prone PCR[17]. This can even lead to a library with more variation than found after immunisation[19].

1.2.4 Nanobody interference with protein functions

Nanobodies bind their target in a non-covalent way. When a nanobody is present, the targeted protein or the protein of interest and its interaction partners are likely to be disturbed. While both, the nanobody and the interaction partner are competing for the same epitope on the protein of interest, the nanobody is most likely going to win the battle since nanobodies are known to be high affinity binders. When the nanobody occupies a domain of the protein, it will mask or block that domain resulting in a disturbance of its functions[2, 83]. This is a big difference compared to RNAi, nanobodies can target and interfere with only the targeted part of the protein of interest, while RNAi targets the full-length protein[6, 84]. Koromyslova and co-workers developed a nanobody that targets the capsid protein of noroviruses[85]. Upon binding, the nanobody targeted an epitope that triggered the disassembly of the virus particle[85]. Rudolph *et al.* generated a nanobody that was able to neutralize the ricin toxin, a ribosome inactivating protein, upon binding to its enzymatic subunit[86].

If it is necessary to target the full-length protein, the nanobodies can be used to selectively bind proteins and induce protein degradation[19, 30]. This results in a functional knock-out of the protein that is targeted by the nanobodies[19, 30]. In the next section, this will be explained in more detail (1.3.1 Research purposes). However, similar outcomes can be obtained by genetically adding a localisation tag to the nanobody[2]. This results in redirecting the antigen to a new cellular compartment which is different from its normal site of action[2]. It is interesting to relocalise the protein of interest knowing that the molecular control is missing or that the endogenous modification (e.g. phosphorylation) at the redirected location is no longer achievable[83]. This can disturb its usual interaction, function and pathway[83].

Next to disturbing the proteins, nanobodies can lock the protein of interest in an (in)active conformation. Based on this phenomenon, the company Confo Therapeutics used intracellular nanobodies to stabilise a G protein-coupled receptor (GPCR) in a conformation at which they want to screen for a small molecular drug that can be active extracellularly[87].

1.3 Nanobody applications

1.3.1 Research purposes

Due to the properties of nanobodies, they have a broad capability to be used in many applications such as a research tool in basic research. Because of their high specificity and affinity, they can operate as an **alternative to conventional antibodies**. They can replace antibodies in protocols such as ELISA experiments[88-90], pull-down assays, immunoprecipitations[91, 92], affinity purifications[93], immunocytochemistry[94, 95], flow cytometry[95, 96] … . For example, Pollithy and colleagues have made a fusion protein of an RFP nanobody and the magnetosome protein MamC[92]. By expressing this construct in the magnetite-synthesizing bacterium *Magnetospirillum gryphiswaldense*, the nanobody will be found on the surface of magnetic nanoparticles (magnetosomes), from bacterial origin[92]. By using this in immunoprecipitations, nanobodies facilitate pull down of their targets[92]. BAC BV/Life Technologies has commercialised an anti-CaptureSelect C-tag VHH and a CaptureSelect C-tag, a tag of only four amino acids (EPEA or Glu – Pro – Glu – Ala)[3]. This combination leads to an efficient protein purification[3]. Nanobodies can be used in flow cytometry as has been shown by de Bruin *et al.*[97]. By staining a Vδ2-T-cell receptor specific nanobody for flow cytometry, the mean fluorescence intensity appears to be higher compared to the staining with a commercial *anti*-Vδ2 monoclonal antibody[97]. Sheng *et al*. made a nanobody-HRP (horseradish peroxidase) fusion protein for an ELISA assay to detect Newcastle disease viruses[90].

As mentioned above, nanobodies can be modified easily which increases the possibilities for nanobody applications. Nanobodies can be used as **fusion protein**. They can be fused to alkaline phosphatase to reduce the number of steps of the protocol and to made sensitivity improvements in immunoassays[98], to fluorescent proteins (like green fluorescent protein (GFP)) for tracking the antigen inside cells[99], to make antibody-drug

conjugates[36], to albumin for prolonged circulation time in the body[17, 40], to HRP as detection tool[90, 100] … .

Recently, different techniques to obtain **functional knock-outs** using nanobodies have been developed as alternative to conventional methods. Current methods without genomic modification (such as RNA interference (RNAi) and Morpholino antisense oligonucleotides (ASOs)) are able to reduce proteins expression levels. However, they suffer from off-target effects, are inefficient for depleting of long-lived proteins and require long treatments before having an outcome[84]. Persengiev and co-workers showed that one siRNA molecule can alter over a 1000 genes of diverse cellular functions[101]. Besides, RNAi does not obtain a 100% knock-out in most cases. To obtain gene knock-outs, methods like clustered regularly interspaced short palindromic repeat DNA sequences (CRISPR) / CRISPR-associated gene (Cas9) are used. Nevertheless, it is irreversible, not possible for proteins which are essential for cell survival and it causes off-target effects. Because those methods still have some disadvantages, the search continues for new alternative techniques to create specific protein degradation[19, 30]. Targeting proteins directly for degradation can lead to faster outcomes compared to e.g. RNAi. Through making adaptations to the Cullin-RING (really interesting new gene) E3 ubiquitin ligase (CRL) complex, different strategies are already being developed to directly degrade proteins (Figure 7)[30]. Caussinus *et al.* developed the deGradFP fusion protein in which a GFP Nb is fused to an F-box domain, thus recruiting the poly-ubiquitination machinery and degrading GFP fusion proteins (Figure 7B)[102]. It is functional for nuclear, cytoplasmic and transmembrane GFP-fusion proteins[102]. Another method was developed by Shin and co-workers, termed Protein interference (Protein-i)[103]. They replaced the substrate recognition domain of SPOP, an adaptor protein of the Cullin-RING E3 ubiquitin ligase complex, by a GFP Nb (Figure 7C)[103]. Due to the interaction between SPOP and the cullin3 E3 ligase complex, the GFP-fusion protein is degraded. Their technique was limited to nuclear GFP-fusion proteins[103]. Fulcher *et al.* created a third method, the affinity-directed protein missile (AdPROM)[104, 105]. They fused the GFP Nb to the von Hippel-Lindau (VHL) adaptor protein which enables the interaction of the GFP-fusion protein with the adaptor protein, Elongin B/C, to establish cytoplasmic protein degradation (Figure 7D)[104, 105]. Those three methods were able to cause a specific proteasome-dependent degradation of GFP-fusion proteins. However, the later one was also able to degrade a protein tyrosine phosphatase (SHP2) and apoptosis-associated speck-like protein (ASC) by using nanobodies targeting those two proteins[105]. Recently a fourth method has been established by Daniel *et al.*[106]. This degradation method requires the ectopic expression of TIR1, a plant F-Box protein, and a GFP Nb fused to an auxin-inducible degron (AID)[106]. A GFP-fusion protein, which is targeted by the GFP Nb -

AID fusion protein, will be recruited to the ubiquitin E3 ligases complex by TIR1 in an auxin-dependent manner (Figure 7E)[106]. An advantage of this method is the possibility to induce the degradation via auxin[106]. Daniel and co-workers were able to obtain promising results in HeLa cells and in zebrafish[106]. Since these four models are planning to knock-out proteins at the post-translational level, they can be a valuable alternative because the outcome is obtained faster compared to methods like RNAi, which are focused on gene-silencing at the post-transcriptional but pre-translational level[84].

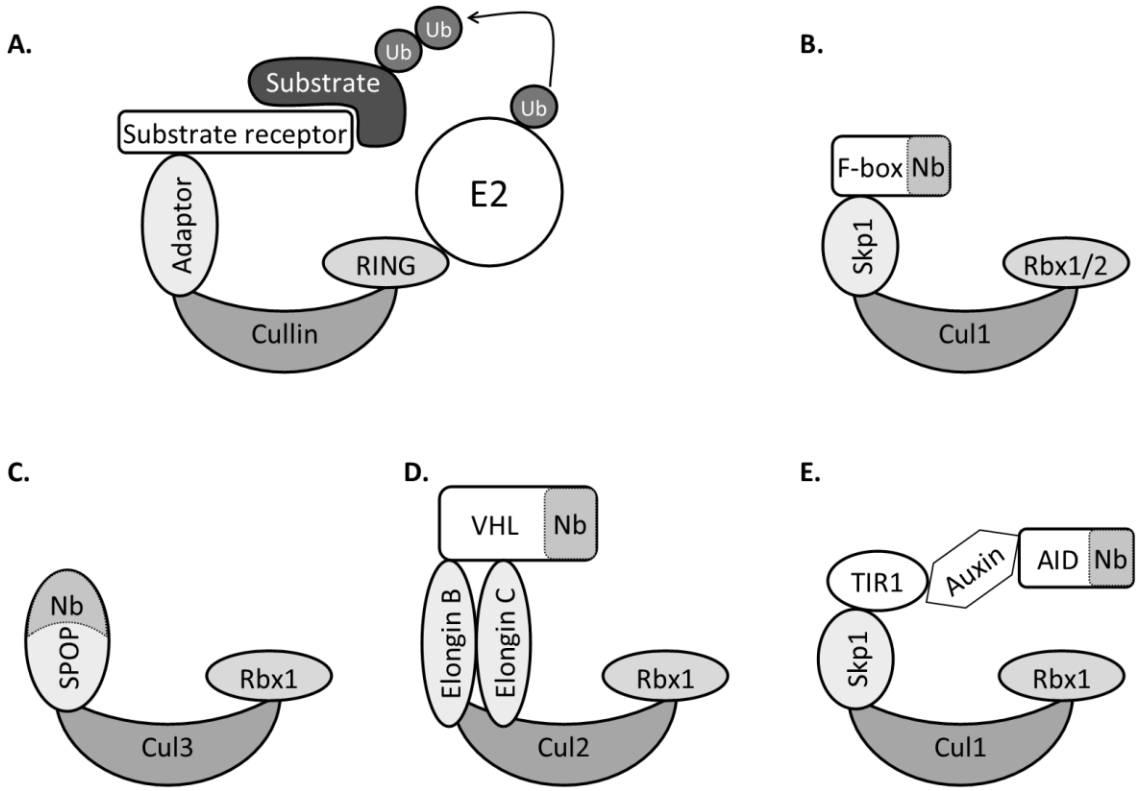

Figure 7: Nanobody-based protein degradation methods. (**A**) The Cullin-RING (really interesting new gene) E3 ubiquitin ligase complex consist of an Cullin-RING core, adaptor proteins and/or substrate receptors to enable the E2 ubiquitin-conjugating enzyme to load the substrate with ubiquitin-molecules (Ub). (**B**) The deGradFP method of Caussinus *et al.* in which an GFP Nb is fused to an F-box domain[102]. (**C**) The Protein interference (Protein-i), developed by Shin *et al.*[103]. They replaced the substrate recognition domain of SPOP, an adaptor protein, by an GFP Nb. (**D**) The affinity-directed protein missile (AdPROM) of Fulcher *et al.*[104, 105], created by fusing a GFP Nb to the von Hippel-Lindau (VHL) adaptor protein. (**E**) Daniel *et al.* fused a GFP Nb to an auxin-inducible degron (AID) and binds the E3 ligase complex through TIR1, a plant F-Box protein[106].

To study intracellular proteins using nanobodies, those nanobodies need to traverse the plasma membrane. Such delivery of a nanobody as recombinant protein, is still challenging as discussed earlier. Nanobodies are able to fold properly even in a reducing environment such as the cytosol[26]. That is why they can be properly expressed intracellularly after transfection or transduction. This is not a new idea as the expression of an antibody in *Saccharomyces cerevisiae* was first reported in 1988 by Carlson *et al.*[107]. An intracellular nanobody or **intrabody** can be useful for different goals, such as interfering with the protein conformation, with the protein localization with protein functioning[3]. This intrabody can be a fusion protein or the original nanobody[26]. Because

nanobodies can easily be modified, they can be genetically tagged with a localization tag (e.g. mitochondrial outer membrane (MOM)-tag[45, 47]). After intracellular expression, such nanobodies can be used to study the function of proteins by translocating or delocalising the protein of interest. Van Audenhove *et al.*[45] observed that fascin nanobodies were only able to reduce matrix metalloproteinase 9 (MMP9) secretion when fascin was delocalised due to a MOM-tag; without MOM-tag MMP9 secretion could not be reduced[45]. Herce *et al.* studied **protein-protein interactions** using nanobodies[108]. They used an anti-GFP nanobody to delocalise a GFP-tagged protein to a chosen location (e.g. to the nuclear lamina with GFP Nb-laminB1, to the centriole with GFP Nb-centrin or to the nucleus with GFP Nb fused to the methyl cytosine-binding domain), and the interaction partner is RFP-tagged. After transfection of the constructs, the GFP tagged protein of interest will translocate to the location of the GFP Nb. If the interaction partner (tagged with RFP) interacts, both GFP and RFP signals will be found at the relocated site confirming the interaction[108]. Because this is done in living cells, they were able to study binding interactions and the kinetics[108].

For some techniques, nanobodies can be a helpful tool to make certain experiments possible. Since it is difficult to obtain crystal structures of membrane proteins for instance, or of large molecular complexes, nanobodies can be and are used as **chaperones** to enable X-ray crystallography[109-111]. They assist the crystallisation process and improve the crystallisation behaviour by accelerating the production of high resolution diffraction crystals[3, 19, 36]. Nanobodies are able to stabilise a protein in a certain conformation and to prevent self-oligomerisation[3, 19, 36]. Next to X-ray crystallography, they can also be used as probe in nuclear magnetic resonance (NMR) spectroscopy to better understand protein structures and folding[112]. Nanobodies can offer more than only the function of a chaperone. They can **modulate or stabilise protein conformations**. Pardon and co-workers showed that nanobodies against G protein-coupled receptors (GPCR) were able to stabilise or lock the receptor in a certain conformation[87, 113]. Due to the intracellular nanobody binding to the GPCR to maintain the locked conformation, they were able to identify novel conformation-specific small molecules which bind extracellularly[87]. Kirchhofer *et al.* have shown that nanobodies can modulate the conformation of GFP and by doing so, they enhance the spectral properties[114]. This enables a higher intensity, leading to better visualisation[114]. Besides, nanobodies can be used as **imaging tool**, but this will be described further (Chapter 2 Labelling and microscopy).

1.3.2 Therapeutic and diagnostic purposes

Antibodies have already a long history as therapeutics[26]. In 1901, Emil von Behring received the first Nobel Prize in medicine for the invention of passive immune therapy to cure diphtheria, an epidemic disease in those days, while the molecular structure of an antibody was discovered nearly 50 years later[26, 115]. Until today researchers are still searching for better, more specific and more efficient therapeutics. As nanobodies are a good alternative for classical antibodies, many of the properties for a good therapeutic or diagnostic are also found in nanobodies as well. They are low immunogenic, small in size, easy to modify, robust against harsh conditions. Because of a broader range of epitopes, nanobodies can be an option for example when the large size of antibodies interferes with the access to certain epitopes[17]. This makes nanobodies an ideal tool for developing new and better alternatives than the currently available methods.

As described above, nanobodies can be used as an *in vivo* imaging agent or biosensor because of their small size, high specificity, robustness and the fast renal clearing. Nanobodies as ***in vivo* imaging agent** opens the opportunity for SPECT[116, 117] and PET scans[118], as some nanobodies are entering clinical phases[39, 119]. For example, ^{68}Ga-labeled anti-HER2 Nb can be used to screen patients using PET imaging leading to a faster decision in knowing if a patient would benefit from an anti-HER2 therapeutic treatment[119]. Additionally, a nanobody has also applications as **biosensor**. For example, due to the fusion between HIV-1 p24, an antigen of HIV, and a red blood cell-specific nanobody, a simple agglutination test can diagnose HIV in the patient[120]. As antibodies are used for diagnostic purposes in antibody-based slides or arrays, nanobodies can be used as well[19, 121].

Next to the imaging application of nanobody-radionuclide conjugates, these conjugates can offer therapeutic use as well. **Radionuclide therapy** requires a targeting moiety which causes the accumulation at the tumor, and a radionuclide which delivers the cytotoxic load[8]. Because of the high stability against harsh conditions and homogenous tumor penetration, nanobodies are an ideal candidate[8]. Since nanobodies can locally deliver the cytotoxic radiation, there will be a minimal toxicity to surrounding healthy tissues compared to conventional radiation treatments[8]. For example, ^{177}Lu-labeled anti-HER2 nanobodies were able to prevent tumor growth in HER2-positive xenografts *in vivo*, while radioactivity levels in normal organs remained low[122].

Due to the easiness of modifying nanobodies, a high variety for therapeutic purposes is available[8]. Nanobodies could easily be coupled to toxins by **genetic fusion**, e.g. the anti-CD7 nanobody fused to the truncated form of *Pseudomonas* Exotoxin A (PE38) shows

cytotoxicity in T-cell acute lymphoblastic leukaemia *in vitro* (in CD7-positive cell lines such as Jurkat, and primary T-cell acute lymphoblastic leukemia or T-ALL cells) expressing and in a preclinical mouse model *in vivo*[123, 124]. Unfortunately, this has a big drawback as it can induce a strong immune reaction against the foreign protein toxin[8]. As protein-toxin fusions have a disadvantage, fusions with non-toxic proteins such as enzymes are safer. For example, Cortez-Retamozo *et al.* were able to cure the established tumor xenografts by using nanobodies which target the carcinoembryonic antigen (CEA or CD66e)[125]. CEA is highly expressed on epithelial cancer cells and very low on healthy adult cells, making it possible to selectively target cancer cells[26, 125]. Those nanobodies were fused to a β-lactamase enzyme which is able to convert a non-toxic pro-drug into a toxic agent[125]. The combination of the nanobody targeting cancer cells selectively and the β-lactamase conversion of the pro-drug, enables the drug to be active in the direct environment of the cancer without harming healthy tissue[125]. **Nanobody-targeted nanoparticles** (<200 nm) offer the advantage to transport encapsulated drugs, that otherwise suffer from fast clearance, limited stability and/or poor solubility[8]. The nanobody covering of nanoparticles results in a decreased risk of immunogenic response to the nanoparticle, a delayed retention time and a better targeting of the nanoparticle to specific locations such as cancer cells[8]. Polymeric micelles decorated with anti-EGFR nanobodies and containing doxorubicin were internalized into the target cell resulting in inhibiting tumor growth[126].

There are already **therapeutic nanobodies** passing phase I and phase II clinical trials[127]. Because of the stability against harsh conditions (pH, temperatures …), nanobodies offer the advantage of a patient-friendly administration (oral, topical or inhalation)[17, 34]. For example: nanobodies for treatment of psoriasis, Vobarilizumab (or ALX-0061, an Ablynx Nb) targeting interleukin-6Rα[128] and ALX-0761 (another Ablynx Nb) targeting interleukin-17A and IL17A/F. ALX-0761 consist of two nanobodies (one against interleukin-17A and one against interleukin-17A/F) and human albumin which increases the half-life[128, 129]. Caplacizumab (or Cablivi) is the first nanobody that is allowed to be used for clinical use to treat patients with acute thrombotic thrombocytopenic purpura[127, 130]. It is a bivalent humanised nanobody containing two identical anti-von Willebrand factor nanobodies developed by Ablynx[127, 130, 131].

Because nanobodies are a good counterpart of conventional antibodies, they have the opportunity to be used as **antiserum** for toxins and venoms like from scorpions and snakes[17, 19]. Nowadays, blood of venom-immunized horses and sheep are used, but it has low potency and is very variable in efficacy[26, 39]. This is due to the toxin or venom itself which is small and low immunogenic[26, 39]. Nanobodies are able to target a high range of biomolecules and without the Fc region, nanobodies only neutralize the toxin. Because

of its small size and fast renal clearing, it gave a lot of benefits compared to the practices existing today[39]. First experiments in mice using nanobodies against the most toxic venom of scorpions, show better results than the existing antibody therapy[132]. A dromedary VHH against *Androctonus australis hector* AahI' toxin, a scorpion toxin, was able to neutralize the toxin and even at low Nb doses it showed better results than in case of the scFv alternative[132].

Next to medical purposes, nanobodies have their applications in other divisions as well. For example, nanobodies against caffeine are able to detect caffeine in hot and cold drinks (from coffee to coke)[133]. This was possible because nanobodies are thermally stable[133]. When developing a "dip-stick" format assay, it gives consumers a qualitative determination of caffeine[133].

1.4 **Non-immunoglobulin based molecules**

In contrary to nanobodies and antibodies in general, some non-immunoglobulin based molecules can be used as counterpart to target biomolecules similar as antibodies do (Figure 8). Those antibody alternatives are engineered to have an affinity comparable to that of antibodies[36]. Those proteins they need huge libraries where antibodies use immunisation mechanisms to obtain high-affinity binders. In contrast to nanobodies and antibody fragments, non-immunoglobulin based antigen-binding proteins benefits from the lack of a disulphide bond which allow them to be more resistant in reducing environments[134]. Monobodies, also called adnectins (Figure 8B), (± 10 kDa) are based on human fibronectin type III and are such an alternative to conventional immunoglobulin based molecules[36, 135]. Monobodies are structurally very similar to the immunoglobulin structure[36] and consist of seven β sheets and three CDR-like loops[134, 136]. Their affinities can reach nanomolar and picomolar affinity[137]. Monobodies also have high thermal (up to 80 °C) and conformational stability and are able to reversibly and rapidly unfold and refold[135, 138]. Dineen *et al.* was able to observe the preventing of tumor growth and metastasis by using monobodies targeting the vascular endothelial growth factor receptor (VEGFR-2)[139, 140]. Another possibility are affibodies (Figure 8C) (± 6.5 kDa). Those are small synthetic binders consisting of three α-helices and are based on ProteinA, a cell wall protein of *Staphylococcus aureus*[36, 141-144]. Affibodies prefer interacting with flat surfaces and resistant to high temperatures[134, 145, 146]. Affibodies already showed promising results in disturbing protein-protein interactions and as carrier for drug

delivery[142, 147]. Lindborg *et al.* was able to show specific changes in tumoral angiogenesis and not in normal blood vessels by using an affibody against the platelet-derived growth factor receptor (PDGFR)[148]. Next, anticalins (Figure 8D) (± 20 kDa) are another possibility. Those are based on lipocalins structurally containing a β-barrel and four loops[36, 137, 149]. Anticalins are low immunogenic and are beneficial binders against small molecules. A few anticalins are already in clinical phase, e.g. an anticalin which neutralise vascular endothelial growth factor (VEGF) to inhibit angiogenesis in solid tumors[137]. Last to be discussed here, designed ankyrin-repeat proteins or DARPins (Figure 8E) (± 18 kDa). Those are based on natural ankyrin repeats[36] and have high thermodynamic stability[150]. The ankyrin fold is biological of importance in mediating protein-protein interactions[134, 151]. DARPins consist of a β-turn, a pair of antiparallel α-helices and a loop of typically 33 amino acids[150, 152]. DARPins are beneficial for flat surfaces[146]. DARPins are used to selectively inhibit the c-Jun N-terminal kinases isoforms in human cells, which is important stress-induced signalling[153].

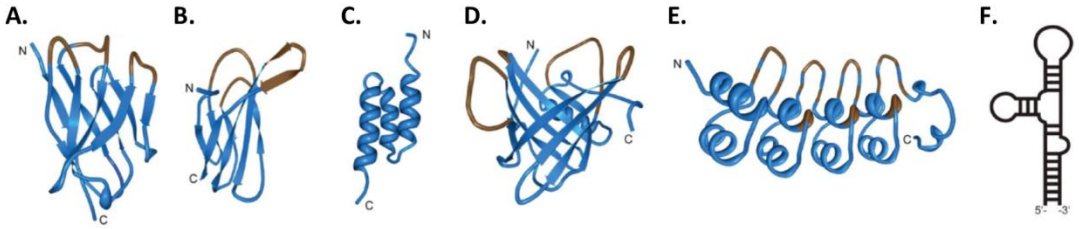

Figure 8: A nanobody and non-immunoglobulin based molecules: (**A**) a nanobody or VHH, (**B**) a monobody or adnectin, (**C**) an affibody, (**D**) an anticalin, (**E**) a DARPin and (**F**) an aptamer.

As the above mentioned molecules all are amino acid based and can be easily manufactured in *E. coli*, other alternatives to immunoglobulin molecules based on nucleotides are options as well. Aptamers (Figure 8F) were discovered in the same period as nanobodies[154-156]. They are found in nature and are single-stranded oligonucleotides which forms complex shapes. Both DNA and RNA aptamers are possible[157, 158]. This allows them to act as a scaffold which enables the targeting of a protein[159]. Aptamers are also able to interfere in the protein-protein interactions[159]. Their affinity range is similar to that of nanobodies[157]. To find high affinity binders large libraries and a selection method (systematic evolution of ligands by exponential enrichment or SELEX) are needed[157, 160, 161]. Since aptamers are nucleotide based, they suffer from nuclease activity, but are never immunogenic. Aptamers can denature and regenerate easily[160]. Aptamers also suffer from limited shelf life and are suggested to have a production cost similar to antibody production[157]. Because of the small size, they are able to access to many biological compartments[36, 159]. However, similar to nanobodies, they cannot enter the cell by itself[157, 162].

Chapter 2
Labelling and microscopy

Researchers in the field of cell biology make frequently use of microscopic techniques for their own experimental setups and purposes, but they all have a similar goal: by imaging their research, they try to illustrate their work and findings in a way that is more difficult to describe with words[163]. Not only more intuitively the results are becoming more comprehensive, it is also a primary source of data that is available to be analysed and interpreted[163].

2.1 **Fusion proteins**

To look at an intracellular protein of interest, the protein itself can be modified by coupling to a fluorescent protein, e.g. GFP. Such fusion proteins can help in studying the protein of interest. Due to the large size of fluorescent proteins (27 kDa for GFP), differences between the endogenous protein and the fusion protein in terms of functionality can be observed, as well as some unwanted effects such as artificial self-oligomerization, loss of function and mislocalization[163-170]. Next, the expression of a fusion protein leads to the presence of two pools of the protein of interest (the fluorescent fusion protein and the endogenous untagged protein). This latter one results in a pool that is not visible for analysing and probably competes with the fluorescent pool[166, 167]. Because one fraction is undetectable for microscopic purposes, this pool is undesired in the study.

As mentioned above, nanobodies are easily modified and can be used as a fusion protein, e.g. after coupling to the green fluorescent protein (GFP). In that way the unwanted effects of modifying the protein of interest are overcome and it is possible to look directly at the endogenous protein. The company ChromoTek has discovered this as well. They sell chromobodies as a plasmid in which a nanobody is genetically engineered to GFP[99, 171, 172]. These chromobodies can help to study proteins on an endogenous level *in vivo*[171, 172]. Noticeable is the fact that nanobodies have to bind the protein and can interfere in the normal binding interactions between the protein of interest and other proteins. This is wanted in case of examining the function of the protein, but in visualising the native conditions this can be a disadvantage. However, this is not always the case. It is previously seen that some nanobodies do not interfere with any interaction e.g. a survivin nanobody[47].

While the use of chromobodies or fluobodies are on the rise, a fluorescent protein fusion is not always desired depending on the kind of assay. GFP is in diameter 4 nm, but will be seen as a 400 nm blur by light microscopy[173, 174]. Especially when a high resolution is required e.g. super resolution, smaller fluorophores are desired above fluorescent proteins[175]. When considering the resolution, the diffraction of light has to be mentioned as well. The maximal resolution of a microscope is constrained by the diffraction limit of light[163]. This was found by Ernst Abbe in 1873[176]. It is the minimal distance between two objects in the same plane which are still distinguishable as separated elements[163, 174]. This depends on the wavelength of light and the numerical aperture of the lens that has been used[163]. When using a light microscope, the resolution is 200-250 nm laterally and 500-700 nm in the axial direction, meaning all signals closer together than this will be seen as one signal. This is why a normal light microscope does not always provide an accurate representation of the sample that is being visualized[174, 177]. For this reason, super resolution microscopy has been worked out. Depending on the used technique, super resolution microscopy made it already possible to gain a resolution from 200 – 250 nm to approximately 10 nm laterally[163, 177].

As mentioned above, it is preferable to choose a bright small label to increase localisation precision instead of a big fluorescent protein which will give a blur[178]. Besides, fluorescent proteins have typically a bigger spectral range compared to small chemical dyes and they also suffer from limited photostability[170]. Because of the better resolving power, sizable fluorophores undo the benefits of super resolution, but not only the fluorophores have to be taken into account. Nowadays, antibodies are used commonly to visualize the protein of interest. A big problem when using antibodies, is the 'localisation error' or 'linkage error' (Figure 9)[174, 178]. If an accurate location of the protein is desired, the size of an antibody increases the distance between the protein

and the fluorescent dye. Because one antibody has a size of around 12-15 nm (Figure 9B), the location of the dye is not entirely the same as the location of the desired biomolecule[163, 174, 175, 179]. Especially not when a secondary antibody is needed (Figure 9A), the distance between the label and the protein can even reach 24-30 nm[175, 179]. If an accurate location is required, especially when super resolution microscopy is used, this distance is of high importance to give accurate information about the location of the protein of interest[175]. As mentioned before, nanobodies are an ideal counterpart to antibodies and can represent a better alternative. The 'linkage error' of nanobodies will be decreased by a factor 4 to 7 compared to the use of the standard antibody staining (Figure 9C). In that case nanobodies have to be labelled directly, otherwise the benefits of the smaller linkage error are wasted. Indeed, nanobodies have been used before for immunostaining. However, the linkage error was not decreased since they used a labelled primary antibody targeting the nanobody, or a tag on the nanobody[180], or they used an unlabelled antibody combined with a labelled secondary antibody[94, 97].

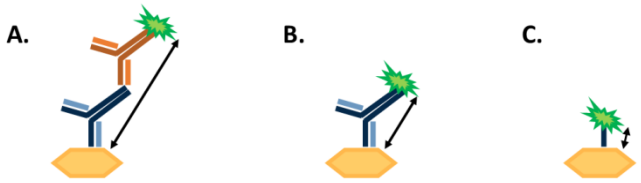

Figure 9: Linkage error. (**A**) When using a primary antibody and a labelled secondary antibody, the linkage error can reach 24-30 nm. (**B**) In case of a labelled primary antibody, the distance between the dye and the target decreases to approximately 12-15 nm. (**C**) A labelled nanobody is able to reduce the linkage error even more.

2.2 Coupling mechanisms for the labelling of nanobodies

Because of the big size of a fluorescent protein, it also heightens the size of a fusion to a nanobody by a factor 2-3 (e.g. GFP is 27 kDa). Therefore, smaller fluorophores have to be chosen of which the Alexa fluorophores are the best known. The only challenge is a specific addition of a fluorophore onto a nanobody. Many strategies were already tested, all with their own advantages and disadvantages.

2.2.1 Self-labelling enzymes

To overcome the blur of the big fluorophores and retain the easiness of fusion proteins, it is an option to fuse a nanobody to a self-labelling enzyme. Such enzymes can be fused to a protein of interest (e.g. a nanobody) with the intention to covalently attach an

exogenous synthetic ligand. If such a ligand is fluorescently modified, it enables fluorescent labelling[181-183]. The fusion protein can be expressed in cells but needs in that case a dye that is cell permeable and non-toxic (e.g. rhodamin), meaning the labelling has to occur before fixation in living cells[181]. A few self-labelling enzymes are already commercially available, such as a HaloTag[184], a SNAP-tag[182, 185] and a CLIP-tag[182, 186]. The first originated from a haloalkane dehalogenase, which removes a halide from an alkyl halide ligand[184, 187]. The SNAP-tag is from an O^6-alkylguanine-DNA-alkyltransferase, a DNA repair enzyme, which reacts with benzylguanine derivatives[185, 186]. The third one, the CLIP-tag is derived from an O^2-alkylcytosine-DNA-alkyltransferase and uses O^2-benzylcytosine ligands[186]. This method can be introduced for nanobodies as well. However, to image a protein of interest with labelled nanobodies, the cell has to express the nanobody fused to the self-labelling enzyme tag. This fusion enlarges the nanobody in size by a factor of approximately two (e.g. the SNAP-tag is 20 kDa) which also heightens the linkage error compared to a directly labelled nanobody.

2.2.2 Enzymatic recognition tags

A nanobody can easily be genetically engineered with a small tag which is recognised by an enzyme to obtain an enzymatic labelling. One such effort is performed by Schumacher and co-workers (Figure 10)[36, 188]. A GFP nanobody was provided with a C-terminal tubulin-derived recognition sequence (Tub-tag), existing of 14 amino acids (VDSVEGEGEEEGEE)[36, 188, 189]. This Tub-tag sequence is recognised by **tubulin tyrosine ligase** (TTL) which adds a small unnatural tyrosine to the Tub-tag in an ATP dependent reaction[189]. Schumacher *et al.* were able to couple a 3-formyl-L-tyrosine to the Tub-tagged anti-GFP nanobody followed by a chemical hydrazone forming reaction to couple it with an Alexa Fluor594-hydrazide dye (Figure 10A)[189]. Many functional groups can be added to the tyrosine which allows a chemical reaction of choice for the coupling of the dye. Since this is a two-step process, they further developed a one-step protocol by using a coumarin coupled amino acid or β-(1-azulenyl)-l-alanine (Figure 10B)[188]. However, the main disadvantage in this one-step method is the limitation of the fluorescent substrates that are compatible with this method[188].

Another possibility is by genetically adding a sortag to the nanobody (Figure 10C). Its consensus sequence is LPETG (Leu – Pro – Glu – Thr – Gly)[36, 190]. By engineering this sequence at the C-terminus of a nanobody, it will be recognised by **sortase A** (SrtA), a transpeptidase derived from *Staphylococcus aureus*[36]. SrtA cleaves at the sortag and coupled the nanobody to peptides starting with GGG (Gly – Gly – Gly) followed by molecules of choice[191]. The nanobody can be engineered to facilitate the purification

between a sortase labelled nanobody and an unmodified nanobody[191]. In that case, the C-terminus contains a sortag followed by a His_6-tag[191]. This allows a purification after production via immobilized metal affinity chromatography (IMAC) and an elimination of the unmodified nanobodies after SrtA-mediated cleavage[191]. Massa *et al.* developed this method to add radiolabels onto a HER2 nanobody for SPECT and PET visualization[191]. They conjugate a Cy5 fluorophore to the HER2 nanobody as well for use in fluorescence reflectance imaging (FRI)[191]. Truttmann and co-workers have conjugated a GGG-AF647 peptide onto an anti-HypE nanobody (Huntingtin-associated yeast-interacting protein E) using the SrtA method[192]. Fabricius *et al.* made use of SrtA as well[193]. They enzymatically couple a dibenzocyclooctyne-amine (DBCO) moiety on the nanobody which allows to perform a strain-promoted alkyne-azide cycloaddition (SPAAC) with an azide-modified oligonucleotide[193]. Through a DNA-PAINT method based on labelled single strand DNA oligonucleotides which are complementary to the oligonucleotide on the nanobody, they were able to visualise endogenous tubulin proteins[193]. Further, Witte and colleagues used a TAMRA labelled peptide (GGGK(N_3)K-TAMRA) to attach the dye onto a nanobody (targeting class II MHC products) through sortase[194]. As those TAMRA labelled nanobodies had their application in FACS, Witte *et al.* introduced alkyne and azide bearing peptides to obtain bivalent nanobodies through SPAAC[194]. Since those bivalent nanobodies had their application in microscopy, they were chemically labelled[194].

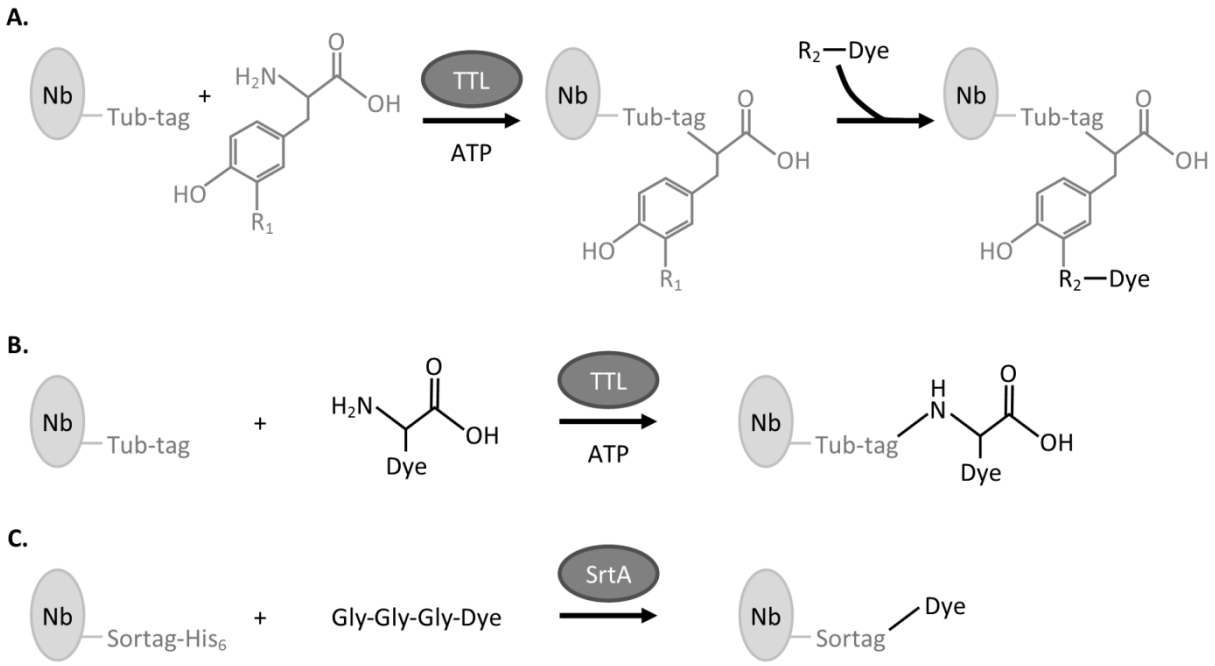

Figure 10: An enzymatic labelling method using a tubulin tyrosine ligase (TTL) or using a sortase A (SrtA). (**A**) In a two-step process, TTL added a tyrosine derivate with a reactive chemical group (such as 3-formyl-L-tyrosine) to a Tub-tag followed by a chemical coupling of the dye to the nanobody. (**B**) In the one-step process, the TTL is able to ligate dyes to the Tub-tag of the nanobody. However, the substrates for this process are rather limited. (**C**) In case of a sortase labelling, the nanobody must be engineered with the sortag (LPETG) followed by a His_6-tag. Through SrtA, the His_6-tag is cleaved and a labelled peptide (Gly-Gly-Gly-dye) is linked to the nanobody. If the SrtA enzyme is His_6-tag, the unreacted nanobody and SrtA can easily be removed from the end result.

Other enzymatic methods are published as well, but none of them have as goal to make nanobodies fluorescent. Besides, those techniques can be complementary methods. Such an alternative is found by Hudak *et al.* (Figure 11A)[195]. By incorporating a tag into a protein consisting of 5 amino acids (CxPxR or Cys – x – Pro – x – Arg), this sequence will be recognised by formylglycine-generating enzyme (FGE)[187, 195]. FGE changes the cysteine into an aldehyde-bearing residue, a formylglycine (fGly), during the protein expression[187, 195]. The aldehyde allows modification to hydrazide or aminooxy which bears e.g. an alkyne/azido functional group allowing a SPAAC reaction afterwards[195]. Again this is a multi-step process[195]. Another enzymatic option could be via transglutaminases (Figure 11B)[196]. Transglutaminases are able to site-specifically modify proteins on a glutamine residue in a highly flexible region[196], which is not common on a nanobody[36]. By genetic engineering a glutamine-containing tag at the C-terminus (e.g. myc-tag (EQKLISEEDL)), a transglutaminase will be able to modify the glutamine by coupling it to a primary amine group[196-198]. However, the separation between labelled and unlabelled nanobodies will not be that easy, because there is no cleavage of a His_6-tag as in case of sortase. Dennler *et al.* have used this to label Fabs with an ATTO-488 or TAMRA dye for microscopic purposes[198].

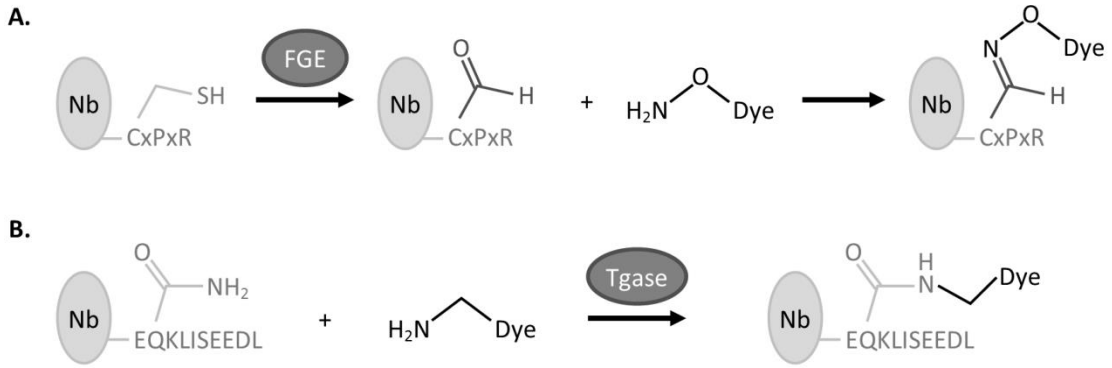

Figure 11: Enzymatic labelling methods by using a formaylglycine-generating enzyme (FGE) or a transglutaminase (Tgase). (**A**) The labelling via FGE transforms a cysteine in a short sequence (Cys – x – Pro – x – Arg) to a formylglycine. This can react with an aminooxy moiety that allows to attach a functional group to allow a chemical labelling afterwards. (**B**) The method via Tgase requires a glutamine-contacting tag (e.g. myc-tag). Tgase couples a primary amine group to the glutamine which leads to the labelling.

As these are all enzymatic processes, it has to be noticed that the reaction can be reversible, as has been shown for sortase, which is a drawback for enzymatic attachments[36].

2.2.3 Chemical ways for labelling nanobodies

Since enzymatic strategies can be reversible, chemical ways have been executed as complementary method. One of the first was the **N-hydroxysuccinimide (NHS)**

chemistry. This is based on a simple chemical reaction in which a **NHS ester dye** is coupled to a **solvent exposed lysine** onto the nanobody (Figure 12A). However, it caused some unwanted results because the abundant occurrence of lysine residues and accessibility represented a major disadvantage, because it creates a heterogeneous mixture of dense and less dense labelled nanobodies[36, 179, 191, 199]. Besides, the labelling can occur at different positions leading to a more random and unselective labelling[36, 179, 191, 199]. This could be solved by adding a poly-lysine stretch at the C-terminus which resulted in a less heterogeneous mixture[179, 200]. Additionally, a bigger problem rises because lysines are also present in the CDR regions and when these are modified, the affinity and specificity of the nanobody could be altered[28, 36, 191]. Pleiner and co-workers experienced even total loss of antigen recognition capacity after NHS labelling[179]. Ries and co-workers used the NHS chemistry to label anti-GFP nanobodies with Alexa Fluor 647 (AF647)[178]. They stained tubulin-YFP in *Potorous tridactylis* epithelial kidney cells (Ptk2) and tried to resolve the diameter of a microtubule using PALM[178]. The diameter of a microtubule is known to be 25 nm. After fixation, they found that a nanobody staining was able to resolve the diameter of the microtubule to 26.9 nm (± 3.7 nm) while a (primary and secondary) antibody staining showed a diameter of 45 nm (± 5.8 nm)[178]. This immediately shows the significant reduction in linkage error when using nanobodies[178]. Similar results were found by Mikhaylova *et al.* when using nanobodies targeting tubulin directly[201].

This C-terminal addition of a poly-lysine stretch led to further thinking. Cysteines are much less abundant than lysines[36]. When an **unpaired cysteine** was engineered at the C-terminus, another way of labelling could be performed. This site-specific conjugation was following the **maleimide chemistry** (Figure 12B)[199]. The free thiol group of the cysteine needs to be reduced to react with a **maleimide dye**[36, 190]. Because free thiol is robust, it is often difficult to achieve high conjugation efficiency[202]. The protocol is a bit challenging since the conditions and timing are important[202]. First, the cysteines have to be reduced by a strong reducing agent such as dithiothreitol (DTT)[202, 203], 2-mercaptoethylamine (2-MEA)[199] or tris[2-carboxyethyl]phosphine (TCEP)[179, 204-206]. During this reduction step, the reducing agent has to be titrated carefully to the unpaired cysteine because only the chosen cysteine residue is desired to be reduced and not the intradomain disulfide bonds[30, 179]. If this happens the stability of the nanobody will be altered and unwanted side products will be created[199]. After the reduction step and just before the labelling reaction, the reducing agent had to be removed since it can react with the maleimides itself[202]. To remove the reducing agent, a desalting is required, followed by a quantification to obtain the right stoichiometric amount for the reaction[202]. However, this has to be fast because the longer it takes, the more reoxidation of those free thiol

residues will occur resulting in a less efficient labelling[202]. However, compared to the NHS ester method, the maleimide method is more quantitative as the reaction follows more in stoichiometric fashion[179]. Besides, this strategy showed an enhanced homogeneity compared to the heterogeneous mixture when targeting lysines[36]. On the one hand the presence of an unpaired cysteine is desired, while on the other hand it is a disadvantage at the same time. An unpaired cysteine can cause dimerization and irreversible unfolding of the nanobodies, which in that case results in the lower yield after bacterial expression or even toxicity for the bacteria[30, 179, 199]. Nevertheless, Pleiner and colleagues labelled nanobodies against the nuclear pore complex with an AF647 via the NHS and the maleimide strategy, and they preferred the maleimide method as they observed a much lower background compared to the NHS ester method (using STORM microscopy)[30, 179]. Besides, they also conclude that the maleimide-labelled nanobodies recognize their target better and more consistently than in case of the NHS labelling strategy[30, 179].

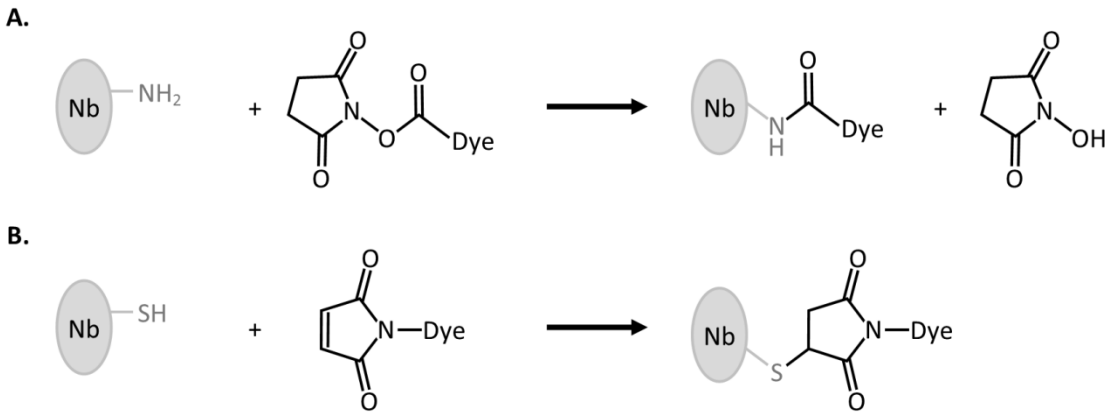

Figure 12: Chemical labelling methods. (**A**) Labelling via N-hydroxysuccinimide (NHS) chemistry needs a NHS ester dye which will be coupled onto the nanobody via a solvent exposed lysine residue. (**B**) The maleimide labelling strategy couples a maleimide linked dye to a Cys residue on a nanobody.

2.2.4 Other strategies

Finally, other ways to fluorescently label nanobodies have been performed for other purposes. Ramos-Gomes *et al.* coupled nanobodies to quantum dots[207]. This coupling ensued due to sulfosuccinimidyl-4-(*N*-maleimidomethyl)cyclohexane-1-carboxylate which cross-links the C-terminal Cys at the nanobody to an amino group at the quantum dots[207, 208]. Quantum dots are highly fluorescent homogeneous semiconductor nanocrystals. They were able to selectively conjugate four nanobodies onto one quantum dot[207]. Quantum dots are capable of emitting enough signal to be detected deeper into tissues compared to Alexa fluorophores. For this purpose, quantum dots are more preferable than Alexa fluorophores. Ramos-Gomes *et al.* showed the possibility of detecting disseminating cancer cells and micrometastasis inside tissues and organs[207].

Next, a few strategies of intracellular labelling were devised to cell-free labelling. Chen and colleagues have worked out a 'tagging-then-labelling' method to label proteins in living cells[209]. For this, they transfected the cells with a fusion protein, consisting of their protein of interest fused with an *E. coli* dihydrofolate reductase (DHFR)[209]. The latter one is a protein of 18 kDa and has a high affinity for the antibiotic trimethoprim (TMP)[209]. By chemically incorporating an azido group onto this antibiotic and adding this to the cell culture medium, they were able to tag the fusion protein with an azide[209]. Once tagged, the labelling could be performed through a strain-promoted alkyne-azide cycloaddition (SPAAC) afterwards. This method could be implemented for nanobodies as well, but this would lead to a bigger linkage error compared to a labelled nanobody since the DHFR alone is 18 kDa in size[209].

Recently, Graulus and co-workers used another mechanism to couple a peptide or molecule to a nanobody which is called intein-mediated protein ligation (IPL)[210]. Inteins are natural occurring bacterial proteins and have a protein splicing activity[210]. In this strategy, the nanobody is recombinantly expressed as fusion to intein and the chitin binding domain (CBD)[210-213]. This allows an easy purification using a chitin substrate (e.g. on column)[214]. To allow the intein-mediated protein ligation, a genetically engineered cysteine between the nanobody (or protein of choice) and intein is required. This enables the initial step, which is an N-S acyl shift leading to a thioester linkage between the nanobody and intein (Figure 13A)[210, 212, 214]. Next, a nucleophilic attack on the thioester occurs by a small chemical thiol compound (e.g. 2-mercaptoethane sulfonate sodium (MESNA) or thiophenol)[210, 211, 213, 214]. This cleaves between the nanobody and the intein (Figure 13B) and creates a new thioester at the C-terminus of the nanobody which is reactive to attack a cysteine at the N-terminus on the peptide (Figure 13C)[214]. This results in a thioester bond between the nanobody and the peptide followed by an S-N acyl shift (Figure 13D) making it a normal peptide bond (Figure 13E)[212, 214]. Besides the reaction using the small thiol compound, the peptide can also directly attack the thioester bond between the nanobody and intein[210, 214]. Graulus *et al.* used this method to add an alkyne containing peptide to the nanobody[210]. Additionally, the use of intein is found in protein purification with an inducible autocatalytic cleavage activity in presence of e.g. DTT and a chitin substrate (e.g. chitin resins)[210, 214, 215].

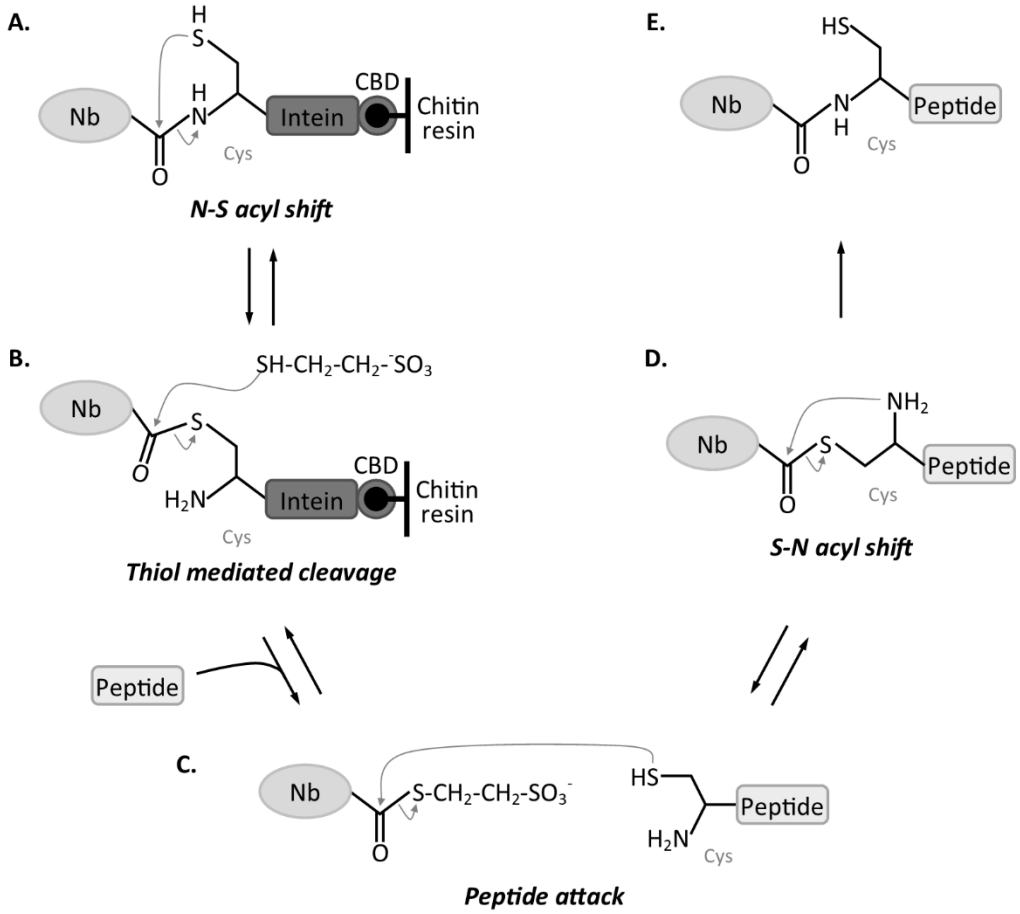

Figure 13: Intein-mediated protein ligation (IPL). By equipping the nanobody with a cysteine between the nanobody and chitin binding domain (CBD) of intein, this cysteine enables an N-S acyl shift resulting in a thioester linkage between the nanobody and intein. Next, a small thiol compound attacks the thioester in order to cleave the nanobody and the intein. This creates a new thioester at the C-terminus of the nanobody which reacts with a cysteine at the N-terminus on the peptide. This results in a thioester bond between the nanobody and the peptide followed by an S-N acyl shift. The figure is adapted and modified from Evans *et al.*[214] and Graulus *et al.*[210].

2.2.5 An alternative method: the genetic incorporation of unnatural amino acids

During translation from RNA to amino acids, 20 conical or natural amino acids are the building block to obtain a protein. With these 20 amino acids, a huge range of proteins can be created[216]. On top of the 20 canonical amino acids, biological modifications expand the range of protein functions such as glycosylation, phosphorylation and metal ions[216]. However, some archaea and eubacteria have a natural genetic code expansion since they encode for some non-canonical amino acids as well[183, 216]. Those are seleno-cysteine and pyrrolysine which can be seen as the 21st and 22nd amino acid[216, 217].

Inspired by this phenomenon, researchers have developed an expansion of the genetic code or a technique which allows site-specific unnatural amino acid incorporation (Figure 14)[217]. Their intention was to modify proteins in a way in order to gain novel chemical

and physical properties[183]. However, this requires some important needs. First, an amino acid with the desired bio-orthogonal group in its side chain has to be cell permeable and metabolically stable[216]. Secondly, the codon has to be unique, so it is only recognised by the newly engineered tRNA[183, 216]. Since only three out of 64 different triplet codons do not encode for an amino acid, these three nonsense codons or stop codons are typically used[218]: the amber stop codon (TAG), the ochre stop codon (TAA) or opal stop codon (TGA)[216-220]. The amber stop codon is most preferred since it is least found nonsense codon in an *E. coli* and it rarely terminates essential genes[218-220]. Though, these codons demand the complementary anti-codon, meaning the right corresponding tRNA[183, 216]. For instance the amber stop codon requires the corresponding amber suppressor tRNA[221]. This tRNA is found in nature in the archaea *Methanococcus jannaschii*. It does not use the amber codon as stop codon, but it actually encodes for a tyrosine[218, 222]. The last requirement is the specificity of the aminoacyl-tRNA synthetase for the chosen non-canonical amino acid[183, 216, 218, 220].

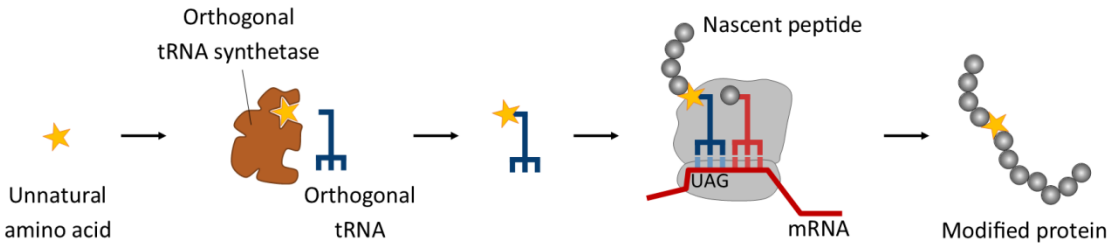

Figure 14: The incorporation of an unnatural amino acid. To efficiently incorporate an unnatural amino acid, an orthogonal tRNA/tRNA synthetase is required. The tRNA synthetase couples the non-canonical amino acid to the tRNA. Next, the tRNA will recognise the amber codon and allow the site-specific incorporation of the amino acid in the protein. The figure is adapted and modified from Chin *et al.*[221].

The most straightforward method to encode an unnatural amino acid in *E. coli* is by introducing a heterologous aminoacyl-tRNA synthetase and its tRNA pair from another species such as from archaea[216]. Based on mutagenesis, the chosen amino acid, with the desired functional side chain, and the anti-codon can be selected. The most successful combination is using the amber (TAG) codon together with the heterologous Tyr tRNA synthetase/$tRNA^{Tyr}$ (*Mj*TyrRS/*Mj*$tRNA^{Tyr}$) pair form *Methanocaldococcus jannaschii*. There are already more than 35 derivates available of this orthogonal tRNA/tRNA synthetase pair for unnatural amino acids with different bio-orthogonal groups[183, 216, 223]. Another frequently used orthogonal pair is found in the archaea *Methanosarcina mazei* in which the tRNA synthetase incorporates a pyrrolysine, the 22nd amino acid[224].

Today, many unnatural amino acids are available with different chemical functional groups such as an azide[225], an alkyne, a furan moiety[226-228], fluorescent groups[223], fluorinated residues[220, 229] … . The incorporation of such amino acids widen the processes in which a protein can participate; e.g. oxime condensation reactions[230, 231], click chemistry[225], Michael addition reactions and as redox-activereagents[232]. The

incorporation of unnatural amino acids has some interesting perspectives and a huge range of applications[183, 216, 218, 220]. For instance, this allows the incorporation of amino acids that are useful for infrared (IR)[233] and/or NMR spectroscopy[234] or the incorporation of amino acids containing heavy atoms for X-ray structure determination[235, 236].

The incorporation of unnatural amino acids is not yet used to fluorescently label nanobodies. Nevertheless, labelling of proteins by using the genetic expansion has been previously performed. Brustad and co-workers were able to incorporate a ketone bearing amino acid into a T4 lysozyme[237]. Next, they coupled it to an Alexa Fluor to use it in a single molecule fluorescence resonance energy transfer (smFRET) experiment[237]. Yanagisawa *et al.* incorporated an N^{ε}-(o-azidobenzyloxycarbonyl)-L-lysine (o-AzbK)[238] into a glutathione transferase and labelled it with a fluorescein derivative through a Staudinger ligation. Lang and co-workers used dienophile bearing amino acids to label the epidermal growth factor receptor (EGFR) with a fluorescent tetrazine conjugate[239]. Antonatou *et al.* showed promising results of coupling a furan containing amino acid to Fluorescein-5-thiosemicarbazide or to Alexa Fluor 488 hydrazide[227]. As these are only a few examples, it immediately shows the variety of options that can be created using unnatural amino acid incorporation.

2.2.5.1 Non-canonical amino acid options

To obtain fluorescent labelled nanobodies, it is possible to use fluorescent amino acids (Figure 15A), e.g. 3-(6-acetylnaphthalen-2-ylamino)-2-aminopropanoic acid (Anap)[223, 240], (S)-1-carboxy-3-(7-hydroxy-2-oxo-2H-chromen-4-yl)propan-1-aminium (CouAA)[241, 242] and 2-amino-3-(5-(dimethylamino)naphthalene-1-sulfonamide)propanoic acid (dansyl-alanine)[243]. Those amino acids have been incorporated previously in prokaryotic[223, 241, 242] and eukaryotic proteins[240, 243]. The direct incorporation of a fluorescent amino acid means a low linkage error and is unlikely to interfere with the functionality of the protein because it introduces only minimal perturbations to the protein structure[183]. While the amino acid is already fluorescent, it minimises the risks of functional disruptions in case a chemical labelling was needed[217]. However, the incorporation of fluorescent amino acids suffers from low production yields[217], as has been observed for dansylalanin[243] and CouAA[244]. Additionally, those fluorescent amino acids require only short wavelengths which is not ideal for *in vivo* imaging[183]. To enlarge the fluorescent amino acid derivates, the limiting factor is to find or to engineer a good working orthogonal aminoacyl-tRNA synthetase[217], as this is the same for any other non-canonical amino acid.

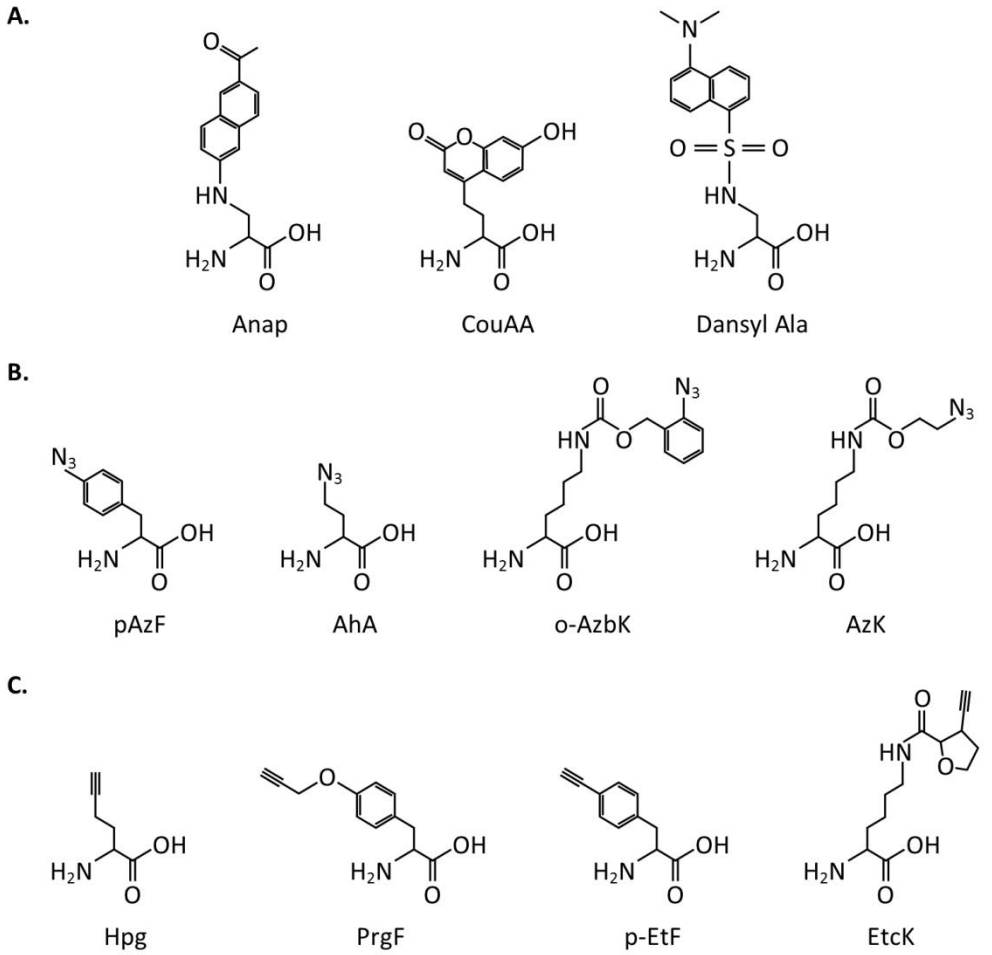

Figure 15: Unnatural amino acids. (**A**) Fluorescent amino acids. Anap, 3-(6-acetylnaphthalen-2-ylamino)-2-aminopropanoic acid; CouAA, (S)-1-carboxy-3-(7-hydroxy-2-oxo-2H-chromen-4-yl)propan-1-aminium; Dansyl Ala, dansylalanine or 2-amino-3-(5-(dimethylamino)naphthalene-1-sulfonamide)propanoic acid. (**B**) Amino acids containing an azido group: pAzF, para-azido phenylalanine; AhA, azidohomoalanine; o-AzbK, N^{ε}-(o-azidobenzyloxycarbonyl)-L-lysine; AzK, N^{ε}-(2-azidoethoxy) carbonyl-L-lysine. (**C**) Alkyne bearing amino acids: Hpg, homopropargylglycine; PrgF, p-propargyloxy-L-phenylalanine; p-EtF, p-ethinylphenylalanine; EtcK, N^{ε}-(3-ethynyltetrahydrofuran-2-carbonyl)-L-lysine.

To obtain fluorescent nanobodies, the nanobody would benefit to use other amino acids than those fluorescent amino acids. Although the incorporation of a fluorescent amino acid will reduce the linkage error, a non-fluorescent amino acid will require some additional steps after nanobody production to make the nanobody fluorescent. As mentioned before, many unnatural amino acids with different functional groups are already available. Importantly, a labelling method has to be chosen in which the risks of functional disruptions and additional side reactions is minimised. Here, only a few azido and alkyne bearing amino acids are mentioned. An azide is a chemical group that is reactive to an alkyne and for those are already many complementary fluorescent dyes commercially available. Such non-canonical amino acids that bears an azide (Figure 15) are para-azido phenylalanine (pAzF)[225], azidohomoalanine (AhA)[183], N^{ε}-(ortho-azido benzyloxycarbonyl)-L-lysine (o-AzbK)[183, 238] and N^{ε}-(2-azidoethoxy) carbonyl-L-lysine (AzK)[183]. Since alkyne is more stable than azide, it would be convenient to use an alkyne bearing amino acid. Regarding such amino acids, a few are already known (Figure 15): a

tyrosine analogue homopropargylglycine (Hpg)[183], p-propargyloxy-L-phenylalanine (PrgF)[245], p-ethinyl phenyl alanine (p-EtF)[183] and N^{ε}-(3-ethynyltetrahydrofuran-2-carbonyl)-L-lysine (EtcK)[183]. There is only one big issue: the water solubility of such alkyne bearing amino acids is limited which results in a lower cellular uptake making the incorporation more challenging[245].

2.2.5.2 Optional chemical reactions after the incorporation of an unnatural amino acid

As mentioned above, an azido or alkyne bearing amino acid can be incorporated. When this is the case, a copper catalysed azido-alkyne click chemistry or CuAAC reaction can be performed. The copper ions enhance the region-selectivity of the reaction, since it predominantly creates 1,4-disubstitued 1,2,3-triazoles (Figure 16A)[183]. Next, a Cu-independent alternative of CuAAC is already known as well and is called strain promoted azide–alkyne click reaction (SPAAC) (Figure 16B). This reaction is based on strained cyclooctynes, which are highly strained alkynes[246]. This means that the alkyne is located in a ring structure, while in case of CuAAC the alkyne is a terminal group. Since the SPAAC reaction does not require a catalysing metal, the reaction (± 2 x 10^{-3} M^{-1} s^{-1}) is a factor 10 – 100 times slower compared to CuAAC (± 3 M^{-1} s^{-1})[217, 247].

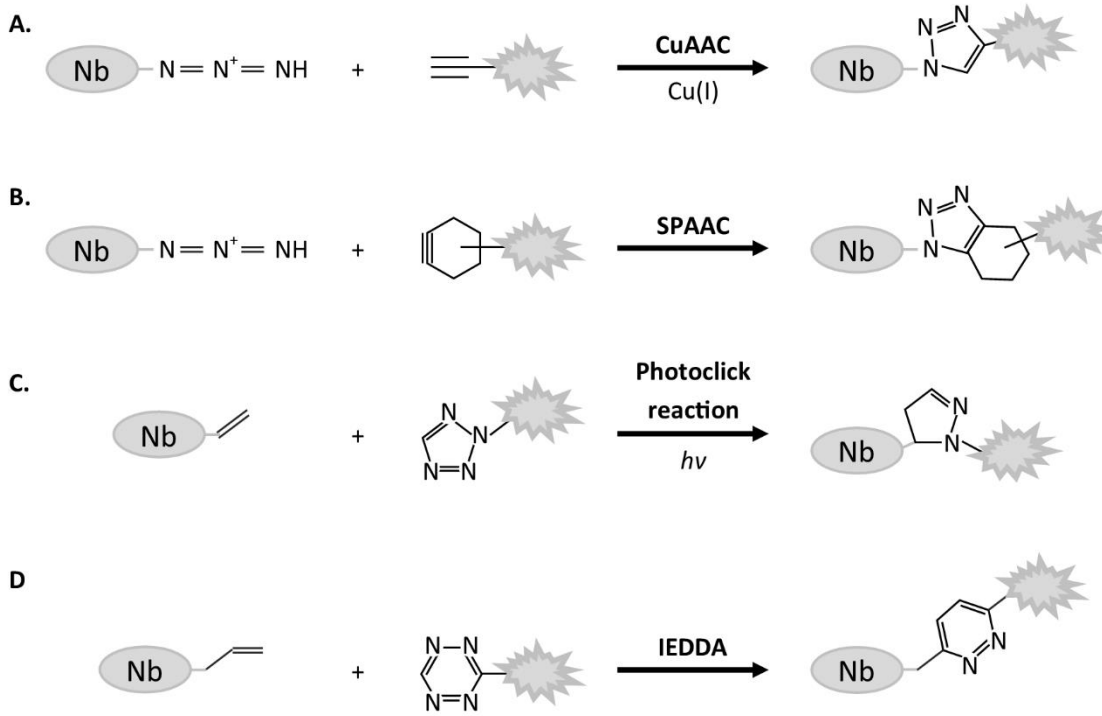

Figure 16: Chemical labelling reactions. (**A**) The CuAAC reaction which requires an azido and alkyne group. This reaction is copper dependent. (**B**) The strain promoted azide–alkyne click reaction (SPAAC) is a Cu-independent alternative of CuAAC and is a reaction between an azide and strained cyclooctynes. (**C**) The Cu-independent the photoclick reaction is and photo-dependent chemical reaction between an alkene and a nitrile imine. (**D**) The inverse electron-demand Diels–Alder cycloadditions (IEDDA) is a fast chemical reaction in which a dienophile reacts with a diene. This figure is adapted and modified from Lee *et al.*[217].

Another alternative is a photo-inducible dipolar cycloaddition or photoclick reaction. This reaction requires a low-power UV lamp, LED or laser beam which is less harmless compared to metal ligands[217, 248]. Yu *et al.* showed that this photoclick reaction could be executed by using a nitrile imine and an alkene in a mammalian cell (Figure 16C)[217, 248]. They incorporated an alkene bearing amino acid into a protein with a tRNA/tRNA synthetase orthologous pair and after using the photoclick reaction they were able to obtain a fluorescent signal onto that protein[248].

Next, the inverse electron-demand Diels–Alder cycloadditions (IEDDA) can be an interesting alternative to CuAAC since no catalyst or reagent is required for the conjugation and is highly specific[217]. IEDDA causes a cycloaddition between a dienophile and a diene (Figure 16D)[217, 249]. Additionally, this reaction is very fast (± 10^6 M^{-1} s^{-1}) compared to a CuAAC reaction[217].

2.2.6 A label-free strategy

The above mentioned methods introduce a fluorophore onto the nanobody which will eventually require fluorescent light microscopy. However, the use of fluorescent signal goes together with photobleaching, phototoxicity, blinking and saturation which all have an influence on the brightness[250]. Additionally, when using fluorescent microscopy, researchers image the fluorescent dye or fluorophore as projection of their protein of interest. Nevertheless, some microscopic techniques already allow label-free imaging to visualise the protein directly. A label-free method has the advantage that the cell does not need any pre-treatments since no label had to be added[251]. This also ensures no modulation of protein functions because no dye or fluorescent molecule is needed in close proximity of the protein of interest[251]. Another benefit is that a label-free method is a non-destructive strategy that allows to image living cells and after, those cells can be used in further experiments[252]. The downside of looking label-free is that the resolution is similar to a normal light microscopy (around 200 nm)[253].

A way to look label-free at cells, is by imaging the cellular autofluorescence via using the blue and UV spectrum[253, 254]. This allows to observe changes in the morphological and the physiological state of the cell[254]. The majority of the autofluorescence is originated from the mitochondria and lysosomes[254]. Most of the time, the autofluorescent signal is caused by the aromatic amino acids in proteins[254], the reduced form of pyridine nucleotides (nicotinamide adenine dinucleotide phosphate or NAD(P)H)[254, 255], flavin coenzymes[254, 256] and lipopigments[257]. Fuerst and co-workers were able to visualise eosinophils based on autofluorescence[258].

Raman spectroscopy is another example to image in a label-free manner. Raman spectroscopy operates by laser light and detects Raman scattering light[252, 259, 260]. This Raman scattering light is inelastic scattering light and is originated from a wavelength shift that corresponds to the energy of a molecular vibration (Figure 17)[251]. During this process, the photons from the laser transfer their energy to molecules as vibrational energy which depends on the chemical composition of the sample[259]. This creates a vibrational fingerprint of the cell and is generated from the functional groups of proteins, nucleic acids, lipids, phospholipids, and carbohydrates[259, 261]. The vibrational spectra is obtained by using infrared or laser light[261]. However, the efficiency of the Raman scattering is very low[251, 259]. Approximately only one in 10^8 incident photons will be inelastic scattering[251, 259]. This requires a high concentration of the biomolecules inside living cells which is ideal for RNA, DNA and proteins[259]. A challenge for Raman spectroscopy is to study proteins in the intracellular environment because of the strong background of other proteins that are present in the close neighbourhood of the protein of interest[259]. Since the strongest Raman signal of a protein is derived from the protein backbone, it is very difficult to discriminate between proteins with similar secondary structures[259]. Similar to the autofluorescence method, Raman is ideal to use when looking at the biochemical changes of the cell[251, 261]. Raman spectroscopy is a good technique to visualise cell organelles such as the nucleus, chromatin, mitochondria and lipid bodies[252, 261, 262]. Puppels and co-workers were the first to describe Raman microscopy in living cells to visualise the nucleus[262]. Klein *et al.* was able to clearly visualise Golgi apparatus and mitochondria[252]. Complementary to Raman spectroscopy is the label-free method via infra-red microscopy. However, it is not recommended using it in aqueous environments[251, 263].

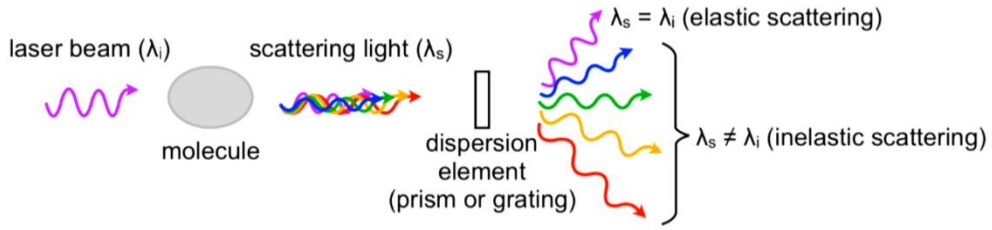

Figure 17: Raman scattering. Raman or inelastic scattering light is the result of a wavelength shift that corresponds to the energy of a molecular vibration. The figure is adapted and modified from Kumamoto *et al.*[251].

Chapter 3
Cancer, metastasis and cellular protrusions

3.1 Cancer and metastasis

Cancer is one of the main causes of death in developed countries. A few cancers are already treatable, particularly when the cancer is diagnosed in the early stages (e.g. breast cancer). If it is detected in later stages, the probability of surviving decreases dramatically. In those later stages metastasis is found in many cases. Once metastasis has started, the perspectives for cure and recovery diminish exponentially because metastasis is the most common cause of cancer-associated mortality[264]. The process of metastasis is linked to a series of steps (Figure 18). In order to establish metastasis, some cells of a primary tumor acquire malignant properties (e.g. formation of protrusions and extracellular matrix (ECM) degradation). However, not all cancer cells will metastasize, only the most malignant ones. Those cells undergo an epithelial–mesenchymal transition (EMT) which is a biological process that converts the cancer cell into a more motile cell[265, 266]. Once this happens, such a malignant cancer cell interrupts its contact with other cells and becomes resistant to apoptosis[264, 267-269]. Additionally, it starts to degrade the extracellular matrix in order to break through the basement membrane, the physical barrier that keep tissues separated, leading to the invasion of the surrounding tissues[264, 267-269]. Once escaped from the primary tumor, that cell is able to degrade the extracellular matrix to make their path and to enable the dissemination throughout the body[267]. This can be via different potential routes. On the one hand the haematogenous or lymphogenous route is an option. It starts with an intravasation, meaning that the cancer cell goes through the blood/lymphatic vessels into the lumina where it is free to flow through the whole body[264, 267, 268]. Another option is through transcoelomic spread such as dissemination across the peritoneal cavity[267]. At a certain point, extravasation

takes place and the cancer cell locally leaves the vessel in order to colonize new sites to form a secondary tumor[264, 268, 269]. However, fewer than 1 in 10 000 cells that survive the escape from the primary tumor, is able to form a secondary tumor[270]. When such cells arrive at a new site, it still must be able to multiply without any surrounding identical cell and be able to adhere to the new cell types. This process is the opposite process of EMT and is called mesenchymal to epithelial transition (MET)[266]. Once a cell establishes this, it has to supply itself for nutrients by recruiting new blood vessels, as well as the other requirements similar to the growth of a primary tumor.

Cellular migration and invasion is not only found in cancer development, they both are dynamic and complex processes which play a vital role in different other cell mechanisms such as embryonic development, wound healing and immune response[269, 271]. Cancer cells will mimic those innocent processes and hijack certain molecular components which enables them to degrade the extracellular matrix (ECM) and disseminate throughout the body[269]. For instance, the metastasis is enhanced due to cancer cells that mimic actin rich protrusions found in immune cells which will be discussed in the next paragraphs.

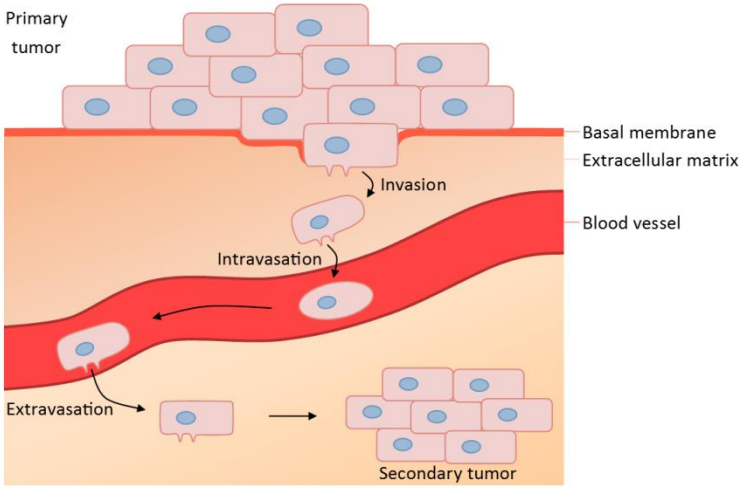

Figure 18: Schematic visualization of metastasis. When cells from a primary tumor are getting more malignant and undergo the epithelial–mesenchymal transition, those cells will degrade the surrounding extracellular matrix and basal membranes. This results in an escape of the cancer cell and in the invasion of the surrounding tissue. Eventually, intravasation of the cancer cell takes place through the blood vessel. Once the cell is found in the blood stream, it can easily disseminate throughout the body until extravasation occurs. This can lead to the formation of a secondary tumor at a new site in the body at which the cell becomes less motile via the mesenchymal to epithelial transition.

3.2 The actin cytoskeleton

The cytoskeleton is the key to control the mechanical properties of the cell, to transport cargo molecules and to maintain cell shape[272, 273]. The basic structure of the cytoskeleton

is composed of three main components (Figure 19): microtubules, intermediate filaments and actin filaments, each of them with their own function and purpose[272, 274].

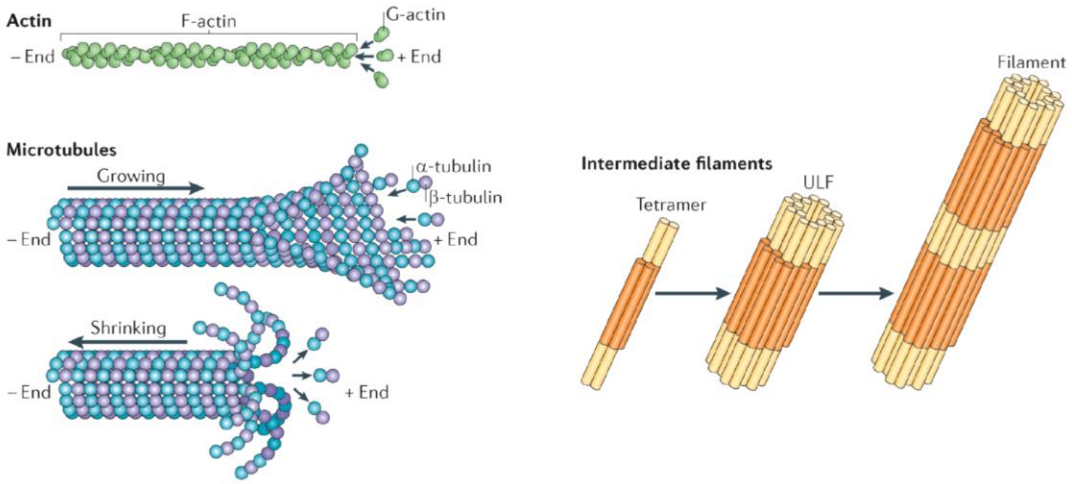

Figure 19: The main components of the cytoskeleton: actin filaments, microtubules and intermediate filaments. Actin filaments are composed of actin monomers which forms a structure of two helices. The microtubules are a polymer of α and β tubulin, which forms a hollow cylinder. The intermediate filaments are rods constructed with two parallel α-helices. The figure is adapted from Finkenstaedt-Quinn *et al.*[272].

The microtubule structure consists of a polymer of α and β tubulin and is organized as a hollow cylinder[272, 273, 275]. They play an important role in intracellular transport, positioning of organelles and in the formation of the mitotic spindle[272, 273]. The intermediate filaments are a family of about 70 different proteins with vimentin as the most common one[273]. The composition of the intermediate filaments is much more variable depending on the tissue and cellular environment[272]. However, it concerns similar structures: a rod, composed of two parallel α-helices, with variable head and tail domains[272]. This part of the cytoskeleton functions in maintaining the cellular shape and acting on cellular stress[272, 273]. The intermediate filaments are more stable than the other two cytoskeleton components[273].

The third part is the actin cytoskeleton. It plays a role in maintaining the cell morphology, in assembling protrusions, in cellular movement, in endocytosis and exocytosis, in facilitating transport in cells, in cell-cell and cell-matrix junctions, in cell signalling, in cell contractility, in tension and in motility of the cell[272-274, 276]. Its basic structure is the monomeric actin (G-actin), a globular protein of 42 kDa in size[272, 276-278]. The actin protein can be the product of different genes located on different chromosomes[273, 274]. This results in six different mammalian actin isoforms of which four are predominant in muscle cells (α-cardiac, α-skeletal, α-smooth muscle and γ-smooth muscle actin) and two non-muscle isoforms (β- and γ-actin)[274, 276, 279]. Based on small differences in isoelectric points (5.40, 5.42 and 5.44), they are divided in three groups (α-, β- and γ-actin)[273, 274, 276]. The actin monomers form filaments (F-actin) which are polar structures existing of two helices of ADP-P_i- and ADP-bound actin[272, 275, 277, 280-282]. The actin structures are very

dynamic and undergo constant remodelling[283]. The filaments have a 'plus' or 'barbed' end which is important for assembling, while their 'minus' or 'pointed' end has its importance in disassembly[271]. Not only actin filaments, but also microtubules have a polarity[275]. At both structures the polymerization takes place at the plus end, while depolymerisation occurs at their minus end[275]. During the actin polymerisation, ATP is required[281]. ATP-bound actin leads to the polymerisation. After assembly, ATP is hydrolysed and an ADP-P_i-actin remains in the actin filaments. Structurally ATP-actin and ADP-P_i-actin are very similar[284]. Once the P_i is released, a conformation change occurs which destabilise the actin filament and trigger its disassembly[284, 285]. In presence of ATP, G-actin is able to polymerize to more complex actin structures such as a branched, a cross-linked, a parallel bundled and an antiparallel bundled actin network[277, 278]. Two types of the actin cytoskeleton are abundant in protrusions: a branched, diagonal or dendritic actin network and a parallel bundled network[286]. The actin structure is a complex network that is assembled into a complex, three-dimensional structure by more than 100 different actin associated proteins[283].

As the actin cytoskeleton is involved in a wide range of processes, it is associated with a variety of diseases in case of malfunction, ranging from muscle diseases, over Alzheimer's disease[278, 287, 288] and atherosclerosis[278, 289] to immune diseases[273, 290, 291]. The cytoskeleton is also hijacked to stimulate cancer malignancy[286, 288, 292]. In this case, the cancer cells appropriate actin cytoskeleton proteins for migration and invasion[286, 288, 292]. Moreover, different pathogens are also able to hijack the actin cytoskeleton to move through the cytoplasm and to increase their infectivity and virulence[278]. This is observed for bacteria such as *Listeria monocytogenes*, *Shigella flexneri* and *Ricketssia coronii*, as well as for viruses like *Vaccinia virus*[278].

3.3 **Actin-based protrusions, a way to move the cell**

Dynamic cells make use of specialised structures to enable them to be motile and to degrade the surrounding area (e.g. in the case of immune cells). Usually, these structures are actin based protrusions which can be found at different places and in different formats throughout the cell. The protrusions are grouped depending on their function and occurrence. This will be described in the next paragraph.

3.3.1 Lamellipodia and filopodia

Lamellipodia and filopodia are the main components that drive migration (Figure 20)[283]. They also command the direction of migration[283]. Lamellipodia are flat, sheet-like plasma membrane extensions which give protrusive force to the two-dimensional cell motility (Figure 20)[269, 293, 294]. The cytoskeleton inside a lamellipodium is a branched actin network[269, 294], which is established by actin polymerisation factors like actin-related protein 2/3 (Arp2/3)[292, 294] and mDia2[292, 295]. mDia2, a formin protein, creates 'mother' filaments, whereas Arp2/3 creates a branched network starting on those existing filaments[292, 294, 295]. The combination of both branched and filamentous actin generates a force that is able to drive the cell migration[283, 292, 295]. Other important proteins for actin polymerisation in lamellipodium formation are WAVE1-2 and Rac1[292-294].

Filopodia differ from lamellipodia in size and shape as they are thinner, needle-like protrusions (Figure 20)[269, 292, 293]. Filopodia are not the major force behind the cell motility, but their role is found mostly in sensing the chemical and physical composition and properties of the environment, making them a guide in forming protrusions and showing the direction to migrate[269, 283, 292-294]. They are often found extending from the actin network of a lamellipodium[269]. The actin cytoskeleton consists of long parallel bundles of F-actin giving a high stiffness to a filopodium[269, 292, 294, 295]. The actin associated proteins that are important in the filopodium formation are Neural Wiskott-Aldrich syndrome protein (N-WASp), cell division cycle 42 (Cdc42), Arp2/3 and formins[292-294].

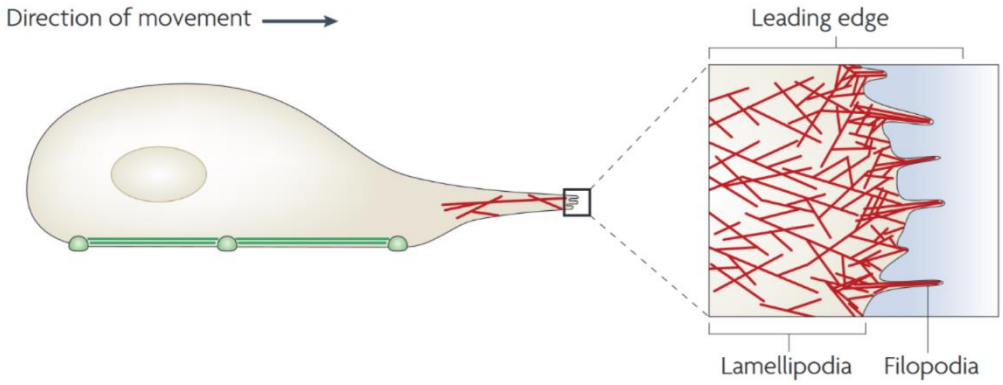

Figure 20: Lamellipodia and filopodia. Lamellipodia are flat, sheet-like plasma membrane protrusions that causes the force for cell movements, while filopodia are thinner and needle-like protrusions that are important for the direction of the movement. This figure is adapted and modified from Matilla *et al.*[296].

3.3.2 Invadosomes: podosomes and invadopodia

Invadosomes is a term compromising podosomes and invadopodia without making a distinction (Figure 21)[297]. Podosome comes from the Greek words "podos" (ποδος),

meaning feet, and "soma" (σομα), meaning body, making podosomes the 'bodies' or structures that works as 'cellular feet'[289, 298]. This immediately clarifies their function. In 1989, Chen *et al.* described for the first time invadopodia which were formed by Rous sarcoma virus transformed chicken embryonic fibroblasts[267, 299]. Those cells were seeded on a degradable ECM substrate and were termed as 'invading podosomes' which later on became the word 'invadopodium'[299]. A podosome and an invadopodium are quite similar, but a distinction is sometimes made. While invadopodia are used to name those protrusions in invasive cancer cells, podosomes refer to the structures in non-cancer cells such as typically monocytic cells (e.g. monocytes, macrophages, dendritic cells and osteoclasts), endothelial cells and smooth muscle cells[300]. Invadosomes, so both podosomes and invadopodia, make use of physical and chemical mechanisms for cell movement through actin polymerization and ECM degradation[289, 301]. Invadosomes act as micro sensors by sensing the extracellular environment to determine the best direction to invade followed by a degradation of the ECM[298].

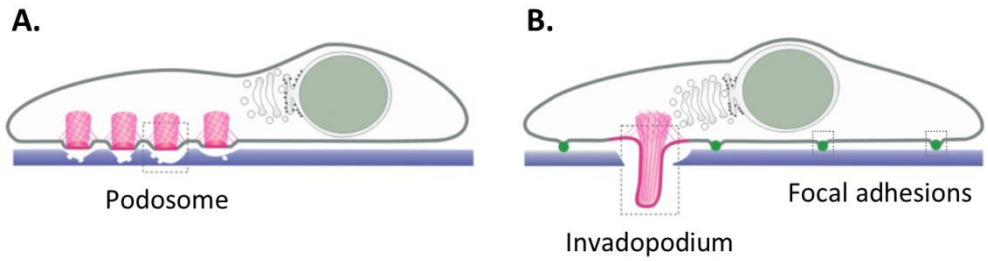

Figure 21: Invadosomes (podosomes and invadopodia) and focal adhesions. Podosomes (**A**) are found in monocytes, endothelial and smooth muscle cells. Invadopodia (**B**) are the counterpart of podosomes and are typically found in malignant cancer cells. Invadosomes are known to be the 'feet' of the cell that are able to degrade the extracellular matrix in order to enhance migration of the cell. Podosomes are usually found in higher numbers per cell compared to the amount of invadopodia. Focal adhesions are visible as green dots (**B**) and are streak-like protrusions that are able to degrade the ECM in only low amounts. This figure is adapted and modified from Spuul *et al.*[298].

The formation of invadopodia is suggested to be one of the first steps in tumor dissemination[271]. It could be said that cancer cells hijack the process of podosome formation to generate invadopodia[269]. However, some distinctions can be observed. In case of podosomes, cells form a great number of podosomes (often more than 100 per cell), while only relatively few invadopodia are found in cancer cells (approximately 10 per cell depending on cell type)[300, 301]. Invadopodia typically have a longer protrusive length (> 2 µm) compared to podosomes (0.5 - 2 µm), which make them able to protrude deeper into the ECM[300-303]. Besides, invadopodia are more persistent as they can be stable for over an hour, while podosomes are more dynamic and have a lifetime of several minutes[300-302, 304]. This makes the degradation pattern of an invadopodium deeper and more focused than in case of a podosome[269, 301].

The metastasis of malignant cancer cells has a striking similarity to some extent to embryonic development where similar protrusive cytoskeletal structures are previously

observed in e.g. *Drosophila*, *Caenorhabditis elegans* and *Danio rerio* (zebrafish)[301]. Altogether, invadosomes play a part in physiological or pathological processes such as development, inflammation and cancer.

3.3.3 Focal adhesions

Other actin based protrusions have been found that show more similarity to invadosomes than expected, while their nanoarchitecture is very different[304]. Those structures are called focal adhesions and are streak-like adhesion structures which link the actin cytoskeleton to the ECM (Figure 21B)[292, 305]. Focal adhesions are found at the end of stress fibres where they are connected to adhesion molecules such as integrins[278, 305]. They function as signalling and attachment sites to the ECM[269] and they are able to degrade the ECM to some degree[300, 305]. Focal adhesions have been suggested to be a precursor of invadosomes[298, 304, 306].

The focal adhesion kinase (FAK) is a cytoplasmic cytoskeleton-associated tyrosine kinase and it is mostly found at focal adhesions[300, 301, 307]. Although FAK does not localize to invadopodia, it still has an important role in its formation[301, 308]. FAK keeps the tyrosine phosphorylation in balance between invadopodia and focal adhesions[301, 308]. The depletion of FAK in focal adhesions acts as a switch from focal adhesion to invadopodium initiation by causing an increase of the phosphorylation levels of invadopodium-associated proteins (such as tyrosine kinase substrate with five SH3 domains (Tks5))[289, 301, 308]. Due to the depletion of FAK and to the change in phosphorylation levels, adjustments in the membrane will occur leading to the accumulation of phosphatidylinositol-(3,4)-biphosphate ($PI(3,4)P_2$) which is found to recruit the N-WASp:Arp2/3 invadosome precursor[293, 298].

3.3.4 Formation of an invadopodium

Invadopodia are estimated to contain approximately 129 different invadopodium key proteins[283, 309, 310]. These are all necessary in a proper formation of invadopodia, including signalling proteins, membrane remodelling proteins, actin and actin-regulatory proteins, adhesion proteins and matrix degrading proteins[303, 310, 311]. Some of those proteins and the formation of an invadopodium will be discussed in the next paragraphs.

3.3.4.1 Initiation

Invadopodia can be induced through different stimuli which rely on the activation of the GTPases of the Rho family[298]. Mostly it does not depend on only one stimulus, but a combination of the below described stimuli. The origin of the stimuli can be extracellular and/or intracellular.

3.3.4.1.1 Growth factors

Soluble growth factors are an important extracellular factor that can initiate the invadopodium formation. Once a growth factor is sensed, a signal cascade will be triggered as this is the case for epidermal growth factor (EGF) and its receptor (EGFR)[312, 313]. This pathway will recruit Src, leading to the phosphorylation of Arg (Abl-related gene), an Abl-family kinase, resulting in the initiation of the cascade[314]. Other growth factors are possible as well, e.g. transforming growth factor β (TGFβ), hepatocyte growth factor (HGF), platelet derived growth factor (PDGF)[269, 315, 316] and vascular endothelial growth factor (VEGF)[269].

3.3.4.1.2 Oncogene expression

Oncogene expression can also play a role in the initiation, such as proteins of the Src family kinases[293]. The primary role of cellular Src kinase (c-Src) is believed to regulate cell adhesion, invasion, and motility[306]. Scientists already concluded that c-Src is a possible master switch for invadosome formation for three reasons[298, 300]. First, the Src family kinases are activated by PDGF and EGF[289, 315]. Second, they are able to mediate integrin signals to the actin cytoskeleton[289] and lastly, they phosphorylate important proteins that are necessary for the formation of invadosomes (e.g. cortactin and Tks5)[289, 317].

3.3.4.1.3 Extracellular matrix properties

The extracellular matrix (ECM) consists of different components such as collagen, laminin and fibronectin[271]. The amount of matrix cross-linking, which is related to matrix rigidity, is supposed to regulate the formation of an invadopodium[269, 271]. In addition, a lower pH[269, 271] (caused by cortactin and the sodium hydrogen exchanger NHE1) and the presence of matrix metalloproteinase (MMP) activity[315] can further induce invadopodium formation[318]. Next, integrins are adhesion receptors for ECM components[271, 315, 319]. They function as a bridging molecule as they are able to translate an extracellular signal to an intracellular one and vice versa[289, 300]. When a surface integrin interacts with substrate components, this results in the initiation of invadopodium formation[312]. The kind of integrins responsible for the start depends on

the cell type[312]. Mostly, a β1 integrin is responsible for the initiation of the invadopodium formation pathway[316, 320].

3.3.4.1.4 Focal adhesion kinases

While FAK is mostly found in focal adhesions, it binds to β1 and β3 integrins as well as to Src[300]. FAK is known to be an important regulator of Src[301]. As mentioned before, FAK does not localize to an invadopodium but it has an important role in invadopodium formation[301, 308]. Phosphorylated FAK (Y397) recruits active Src to focal adhesions to mediate localized tyrosine phosphorylation[289, 301, 308]. This limits the invadopodium formation[308]. However, when FAK is depleted, active Src is released which increases the phosphorylation of invadopodium-associated proteins (such as Tks5) and enhances the invadopodium formation[289, 301, 308, 321]. The depletion of FAK induces a switch from focal adhesion to invadopodium initiation[308].

3.3.4.1.5 Phosphoinositides

Phosphoinositides are phospholipids found in the cell membrane. Depending on an extracellular signal, they are able to initiate the invadopodium formation pathway[306]. It is known that phosphoinositide(3)-kinase (PI3K) is activated through the Src-FAK pathway[306]. This PI3K creates products such as phosphoinositol-(3,4,5)-triphosphate ($PI(3,4,5)P_3$) which is available in negligible amounts under normal circumstances[293, 306]. Due to its increase in concentration, several cytosolic proteins are recruited to the membrane[306]. The newly formed $PI(3,4,5)P_3$ will bind to the pleckstrin homology (PH) domain of guanine nucleotide exchange factors (GEFs)[306]. Through those GEFs, $PI(3,4,5)P_3$ is able to modulate the functions of GTPases of the Rho family (such as Cdc42), which takes part in the invadopodium formation precursor[306].

The higher amount of $PI(3,4,5)P_3$ results also in higher amounts of $PI(3,4)P_2$, which is also rarely present in normal circumstances[293, 306]. This is due to the dephosphorylation of $PI(3,4,5)P_3$ by $PI(3,4,5)P_3$ 5-phosphatases (such as synaptojanin2)[306]. $PI(3,4)P_2$ recruits Tks5 to the membrane which is important to form the invadopodium formation precursor[293, 306].

3.3.4.2 Overview of the initiation

As mentioned above, there are different options to begin the cascade of the invadopodium formation. Mostly it is a combination. A possible pathway is described here as an overview (Figure 22).

Due to ECM components and their properties, the cytoplasmic tail of β1 integrin will bind to the non-receptor tyrosine kinase Arg[289, 315]. This interaction unmasks the Y272 of Arg leading to Arg autophosphorylation and activation[320, 322]. Once EGF is sensed by its receptor EGFR, it can recruit the oncogene c-Src by its SH2 domain[289, 313]. Next, the recruited c-Src will perform a last phosphorylation on Arg Y439, leading to a fully activated Arg[314, 320]. In its turn, the fully active Arg will phosphorylate cortactin on Y421 and Y466[314].

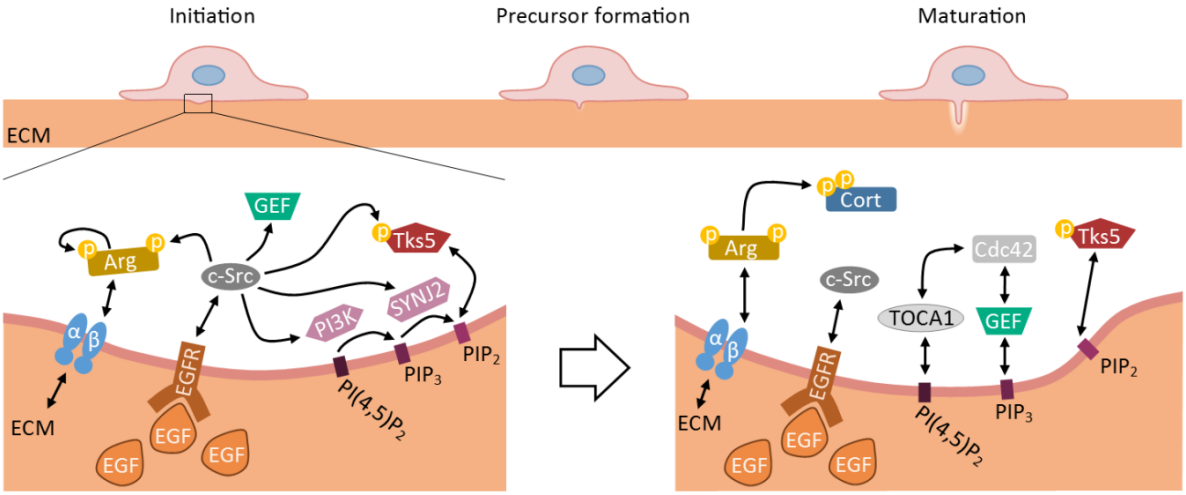

Figure 22: Schematic visualisation of the invadopodium formation pathway: the initiation. Extracellular signals, such as ECM and EGF, can trigger the start of the invadopodium formation by interacting respectively with integrins (αβ) and EGFR. While integrin binds Arg causing autophosphorylation, EGFR recruit c-Src. Next, c-Src will initiate different responses. c-Src phosphorylates Arg which eventually leads to cortactin phosphorylation. It also recruits PI3K which increase the $PI(3,4,5)P_3$ levels and triggers synaptojanin2 to creates more $PI(3,4)P_2$. The later leads to recruitment of Tks5 which will be phosphorylated by c-Src as well. Additionally, c-Src activates GEFs which creates activated GTPases such as Cdc42. Cdc42 interacts on its turn with TOCA1 that is able to cause membrane curvature. (Arg, Abl-related gene; αβ, α unit and β unit of an integrin; Cdc42, cell division cycle 42; Cort, cortactin; ECM, extracellular matrix; EGF, epidermal growth factor; EGFR, epidermal growth factor receptor; GEF, guanine nucleotide exchange factor; PI3K, phosphoinositide 3-kinase; PIP_2, phosphatidylinositol-(3,4)-biphosphate; $PI(4,5)P_2$, phosphatidylinositol-(4,5)-biphosphate; PIP_3, phosphoinositol-(3,4,5)-triphosphate; c-Src, cellular Src kinase; SYNJ2, synaptojanin2; Tks5, tyrosine kinase substrate with five SH3 domains; TOCA1, transducer of Cdc42-dependent actin assembly protein 1)

Src also activates guanine nucleotide exchange factors (GEFs), which stabilize the active state or the GTP-bound state of GTPases[315, 323]. At the same time, activated c-Src recruits PI3K which creates an increased $PI(3,4,5)P_3$ level. $PI(3,4,5)P_3$ binds GEFs[306]. In their turn, these GEFs bind to and activate GTPase Cdc42[298, 306]. This locates Cdc42 at the membrane which will cause a recruitment of the transducer of Cdc42-dependent actin assembly protein 1 (TOCA1), an F-BAR protein[323, 324]. TOCA1 binds to phosphatidylinositol-(4,5)-biphosphate ($PI(4,5)P_2$) and Cdc42[324]. TOCA1 is known to cause the membrane curvature[325].

Because of the elevated levels of $PI(3,4,5)P_3$ and because of Src phosphorylation of the phosphatase synaptojanin2, dephosphorylation of $PI(3,4,5)P_3$ will occur, thus creating $PI(3,4)P_2$ which leads to the recruitment of Tks5[306, 326]. The activated c-Src phosphorylates Tks5 at Y558[317].

3.3.4.3 The initiation leads to the invadopodium precursor

For the formation of an invadopodium, a nucleation complex or precursor must be formed. This precursor will contain actin nucleators to perform the actual actin polymerization, and actin nucleation promoting factors (NPF) which are required to aid the actin nucleator to create a more efficient actin polymerisation[301]. In this first polymerization step, a branched actin network is generated. The actin nucleator responsible here is the actin related protein 2/3 (Arp2/3). Arp2/3 consists of seven subunits of which only two are actin associated, Arp2 and Arp3[327]. The branched actin network is created by adding actin polymers at a 70° angle to the existing mother filament (Figure 23)[273]. Arp2/3 in itself is not able to cause rapid actin polymerisation, it needs the aid of NPFs. Those NPFs trigger a conformational change in the Arp2/3 complex to reposition the Arp2 and Arp3 subunits into a filament-like conformation[327]. This change enables the Arp2/3:NPF complex to induce actin polymerisation at the barbed ends of actin filaments[327]. NPFs promote also the binding of the Arp2/3:NPF complex and the newly formed filament branch to the pre-existing mother filament[327]. A known nucleation promoting factor for invadopodia is N-WASp due to its important VCA domain (verprolin-homology (V), cofilin-homology or central (C) and acidic (A) region). It contains even a duplication of the V part, also known as WASp homology (WH2) domain, which binds directly to actin monomers and delivers it to Arp2 and Arp3[327]. The second part of the VCA domain, the CA part, interacts directly to Arp2/3 which is needed to fully activate Arp2/3[328].

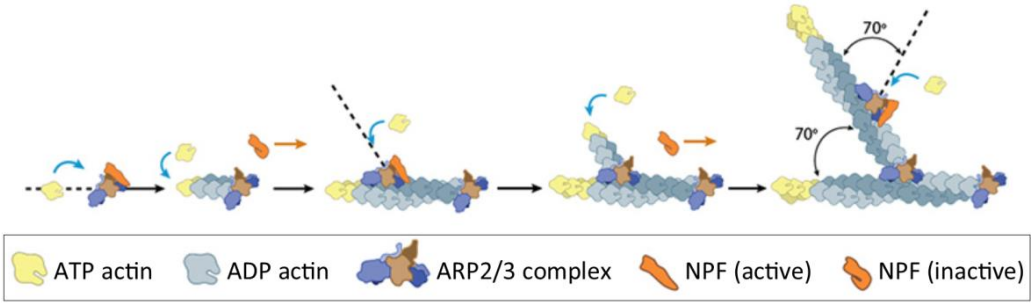

Figure 23: Actin polymerisation via Arp2/3. The actin nucleator Arp2/3 creates a branched actin network by adding actin polymers at a 70° angle to the existing mother filament. Actin nucleation promoting factors (NPF) are required for enhancing the actin polymerisation. While they trigger a conformational change of Arp2/3 causing a more active Arp2/3, they also promote the binding of the Arp2/3:NPF complex and of the newly formed filament branch to the pre-existing mother filament. A known nucleation promoting factor for invadopodia is N-WASp. Figure is adapted and modified from mechanobio.info.

Since cortactin is phosphorylated (see 3.3.4.2 Overview of the initiation), the activated cortactin will recruit Nck1, an adapter protein (Figure 24, left panel)[314, 329]. Besides, the phosphorylated Tks5 is also able to recruit Nck1 to the membrane[317, 329]. Due to the interaction between WASp-interacting protein (WIP) and Nck1, N-WASp is recruited to the invadopodium site[268, 317, 329, 330]. Nck1 binds N-WASp to facilitate Arp2/3 activation[330]. Once N-WASp is located at the invadopodial site, a WIP release and TOCA1 binding will

happen simultaneously[323, 324]. TOCA1 increases the affinity of N-WASp for Cdc42 which leads to the interaction of the GTP-bound Cdc42 to N-WASp causing a conformational change of N-WASp (Figure 24, left panel)[271, 298, 323, 324, 331]. This change leads to the activation of N-WASp[298, 323]. In the open conformation, N-WASp activates Arp2/3 by binding to the CA part of its VCA domain[301]. This process is enhanced by cortactin because cortactin acts as a scaffold to bring Arp2/3 and N-WASp together[329]. The N-WASp binding to Arp2/3 causes a conformational change in the Arp2/3 complex[332]. In that case, Arp2 and Arp3 are in closer proximity and form a 'pseudo actin dimer' which is necessary to enable the rapid actin polymerisation[332]. Now that the precursor consists of cortactin:N-WASp:Arp2/3, cofilin will interact with cortactin as well (Figure 24, middle panel)[329]. Cofilin is also called an actin depolymerizing factor (ADF) and severs actin filaments in order to create a pool of actin monomers and free barbed ends[301]. However, when cofilin is bound to the precursor, it inhibits its severing function[329]. Due to a phosphorylation on cortactin, cofilin can be released[329, 333] which allows cofilin to sever actin filaments resulting in the creation of free barbed ends (Figure 24, right panel)[313, 334, 335]. Arp2/3 is able to occupy these free barbed sites on which actin polymerization will start leading to the creation of a branched actin network[301]. Because the actin polymerisation must happen at the membrane of the invadopodial site, many proteins try to ensure this by anchoring the precursor at the membrane such as Tks5, TOCA1, Cdc42 and PI(4,5)P_2[326, 336, 337].

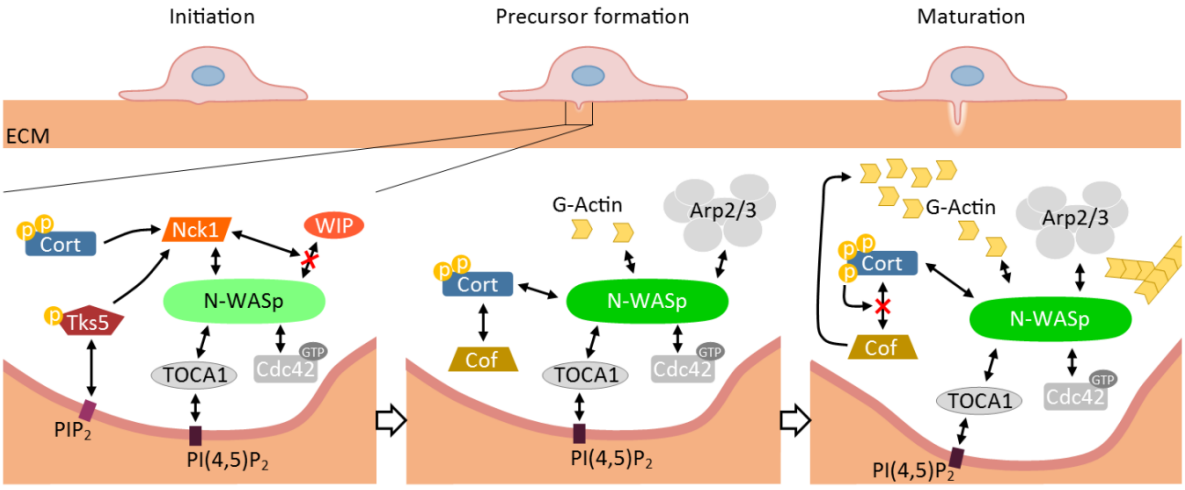

Figure 24: Schematic visualisation of the invadopodium formation pathway: the precursor formation. Phosphorylated cortactin and phosphorylated Tks5 recruit Nck1 (left panel). Due to the interaction between WIP, Nck1 and N-WASp, N-WASp will be activated. This results in the formation of the precursor in which N-WASp, Arp2/3, actin, cortactin, TOCA1, Cdc42 and cofilin participate (middle panel). Due to a phosphorylation on cortactin, the cofilin interaction is interrupted. This results in the severing activity of cofilin which creates actin monomers and free barbed ends on which the precursor will start the actin polymerisation leading to a branched network (right panel). (Arp2/3, actin-related protein 2/3; Cdc42, cell division cycle 42; Cof, cofilin; Cort, cortactin; ECM, extracellular matrix; G-actin, globular actin or actin monomers; GTP, guanosine triphosphate; PIP_2, phosphatidylinositol-(3,4)-biphosphate; PI(4,5)P_2, phosphatidylinositol-(4,5)-biphosphate; Tks5, tyrosine kinase substrate with five SH3 domains; TOCA1, transducer of Cdc42-dependent actin assembly protein 1; Nck1, non-catalytic region of tyrosine kinase adaptor protein 1; N-WASp, neural Wiskott-Aldrich syndrome protein; WIP, WASp-interacting protein)

3.3.4.4 Maturation and ECM degradation

Active N-WASp is found at the base of invadopodia which implies that the N-WASp:Arp2/3 complex is creating a dense branched actin network at the base of the invadopodium[298, 338]. However, to push the membrane deeper into the ECM, maturation of the invadopodium has to occur. This happens by elongating the invadopodium which requires the stabilisation of the branched actin network and the creation of a filamentous structure[295, 298]. Steadying the branched network is established by stabilising the precursor through restoring the binding between cofilin to cortactin (Figure 25, left panel)[301]. This inhibits the severing capacity of cofilin resulting in a lower concentration of actin monomers which stops the fast actin polymerisation[301]. Starting from the branched actin network, actin filaments will grow to create an actin filamentous actin structure that forces the membrane deeper into the ECM (Figure 25, right panel)[295, 298]. The proteins responsible for this actin polymerisation are the actin nucleators of the Diaphanous-related formin (DRF) / mDia family[298, 316]. To strengthen this actin filamentous core structure, cross-linking or F-actin bundling proteins such as α-actinin and fascin are found to be important in this stage (Figure 25, right panel)[293, 298].

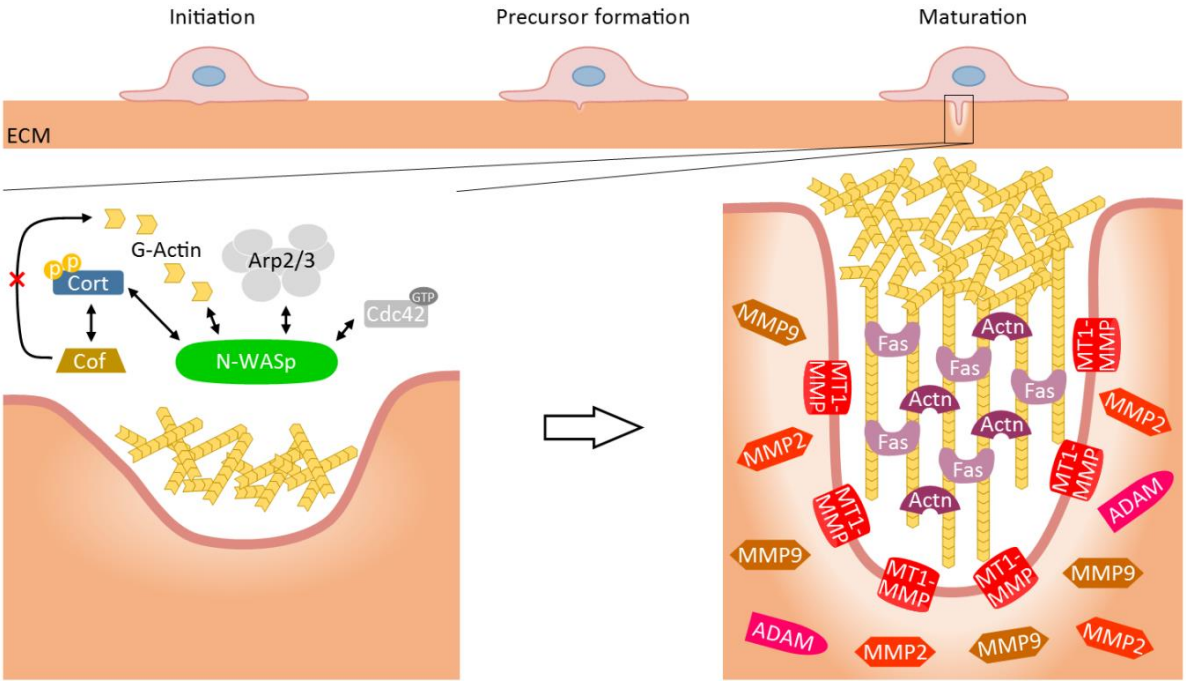

Figure 25: Schematic visualisation of the invadopodium formation pathway: the maturation. Once a branched network is formed, the invadopodium needs to be pushed deeper into the ECM. At this point the precursor stabilise by rebinding of cofilin (left panel). From the branched network, formins create a filamentous actin structure to elongate the invadopodium (right panel). F-actin bundling proteins, actinin and fascin, stabilise and strengthen this filamentous bundled actin structure. Next to the elongation, the ECM degradation is occurring as well through membrane bound (e.g. MT1-MMP) and soluble proteases (e.g. MMP2, MMP9 and ADAM). (Actn, actinin; ADAM, a disintegrin and metalloprotease; Arp2/3, actin-related protein 2/3; Cdc42, cell division cycle 42; Cof, cofilin; Cort, cortactin; ECM, extracellular matrix; Fas, Fascin; G-actin, globular actin or actin monomers; GTP, guanosine triphosphate; MMP, matrix metalloproteinase; MT1-MMP, membrane type I matrix metalloproteinase; N-WASp, neural Wiskott-Aldrich syndrome protein).

The maturation also includes a recruitment of proteases which will be released extracellularly to enable the ECM degradation (Figure 25, right panel). Three main classes of proteases were detected around invadosomes[269]. The first are zinc-regulated metallo-proteases such as matrix metalloproteinases (MMPs)[339, 340] and 'a disintegrin and metalloprotease' (ADAM) family proteases[341]. The other two classes are cysteine proteases (e.g. cathepsin) and serine proteases (e.g. seprase)[269, 289, 316]. Besides, the most prominent proteases at invadosomal sites are the MMPs. The membrane type I matrix metalloproteinases (MT1-MMP, also known as MMP14) is seen as master switch since MT1-MMP activates other soluble MMPs[269, 339]. MT1-MMP is capable of cleaving an N-terminal pro-domain from pro-MMP2 to gain the activated MMP2, while pro-MMP9 needs MT1-MMP, MMP2 and MMP3 to be activated[342, 343].

At the invadopodium, the MT1-MMP is anchored through its 20 amino acid cytoplasmic tail by a dense actin network limiting its mobility (Figure 26E), while high dynamics and high internalisation rates were detected when it is found at non-invadosome membranes[316]. The fixed positioning of MT1-MMP in invadopodia allows a more optimised ECM degradation functioning[344]. The actin network that stabilise the MT1-MMP at its cytoplasmic tail is mediated by e.g. N-WASp:Arp2/3[344, 345]. An accumulation of MT1-MMP at the membrane is important for the invasive character of the invadopodium[316]. This occurs through different ways. It was previously observed that invadopodia are formed proximal to the Golgi apparatus[299, 346]. One of the ways to accumulate MT1-MMPs is through newly synthesized MT1-MMPs transported from Golgi to the plasma membrane (Figure 26A). This is controlled by exocyst complex[347, 348] which is an octameric complex consisting of six vesicle-associated proteins and of two plasma membrane-associated proteins[302, 316]. Once arrived at the membrane, this complex functions as tethering complex which enhances the exocytosis by keeping the vesicle close to the membrane until the SNARE-fusion machinery acts[349, 350]. This is also controlled by Cdc42 and RhoA[298, 347]. Additionally, soluble MMPs are mainly secreted via secretory vesicles from Golgi to the membrane (Figure 26B)[351, 352]. However, the exocyst complex is not suggested causing the MMP2/9 transport, but Rab40b is supposed to achieve this[351]. Next, another way to have an accumulation of MT1-MMP is through recycling processes like clathrin- and caveolae-mediated endocytosis (Figure 26C)[344, 353, 354]. Through the cytoplasmic tail of MT1-MMP, a direct interaction takes place with the clathrin adaptor complex[344]. The Cdc42-interacting protein 4 (CIP4) is an F-BAR protein that helps in the formation of endocytic vesicles, while it also interacts with N-WASp, Cdc42 and dynamin[331]. In this way, CIP4 promotes the curvature and the scission of the budding vesicles and it forms a link between the membrane curvature and the localised actin remodelling[331]. Because of the interaction with N-WASp, it is possible to activate

the actin polymerisation process (cortactin:N-WASp:Arp2/3) in proximity of the endocytic vesicles and to form a branched actin network[331, 353]. This creates a driving force to reshape the membrane and to facilitate the pinching off of the endosome[331, 353, 355].

The vesicular transport is important to recruit MMPs to the invadopodial site. It is previously observed that the vesicular transport is enhanced by actin comet tails (Figure 26D)[356, 357]. Those comet tails give a propelling force to enhance the movement of the vesicles through e.g. an invadopodium[357, 358]. Also here, an association of the MMP pathway and N-WASp:Arp2/3 actin polymerisation pathway is found to create those actin comet tails[359-361].

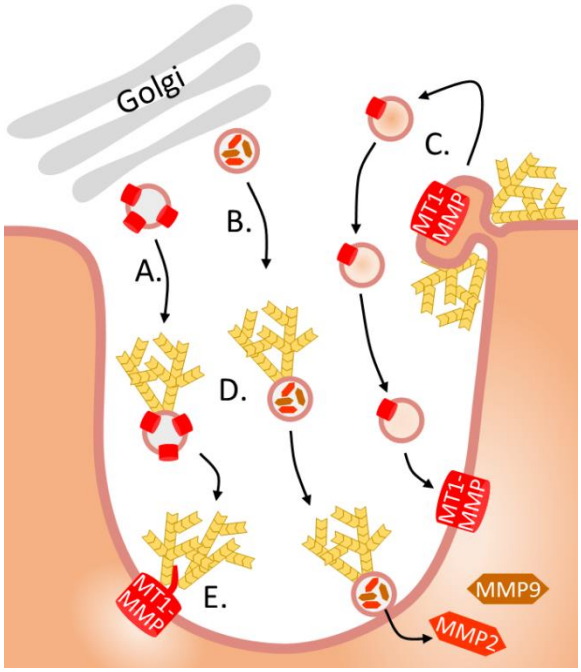

Figure 26: Schematic visualisation of the invadopodium formation pathway: the accumulation of MMPs. At the Golgi, vesicles with newly synthesized MMPs are transported to the membrane at invadopodial sites. This depends on two systems; the exocyst complex for MT1-MMP (**A**) and Rab40b for the soluble MMP2 and MMP9 (**B**). (**C**) The recycling process (e.g. clathrin- and caveolae-mediated endocytosis) helps in the accumulation of MT1-MMP as well. The actin cytoskeleton facilitates the budding of vesicles. (**D**) The transport of MMP containing vesicles through the invadopodium is enhanced by the actin polymerisation by creating comet tails. (**E**) A branched actin network at the intracellular tail of MT1-MMP promotes a better ECM degradation. (MMP, matrix metalloproteinase; MT1-MMP, membrane type I matrix metalloproteinase)

3.4 Neural Wiskott-Aldrich syndrome protein or N-WASp

3.4.1 Wiskott-Aldrich syndrome

In 1937, Alfred Wiskott described three brothers who were affected by an innate thrombocytopenia (a decreased number of small platelets)[362, 363]. They all suffered from bloody diarrhea, eczema and recurrent infections which led to their death[363]. In that time, the cause was still not known. These patients were the first to be described to have the Wiskott-Aldrich syndrome (WAS)[362]. In 1954, Robert Aldrich studied a family which suffered from an X-linked recessive thrombocytopenic purpura[364]. Later on, the discovery of the *WAS* gene clarified that the mutants of its corresponding Wiskott-Aldrich syndrome protein (WASp) seemed to be responsible for those phenotypes which were a result from defected podosome formation in macrophages[298, 365]. Since then, those patients were identified to have the WAS disease[362]. WAS is a rare X-linked recessive immunodeficiency disorder which affects approximately 1 out of 250 000 Europeans[298, 366]. It is characterised by immunodeficiency, eczema, autoimmunity and/or micro-thrombocytopenia[366]. The syndrome is caused by gene mutations which can be highly variable, going from nonsense to missense mutations[269, 366]. This can result in the expression of the full-length WASp with changes in the amino acid sequence, a shortened protein or even no expression[366]. The cause of suffering for WAS patients, is found in the loss of podosomes in the cells of the hematopoietic lineage[269]. Early studies clearly show a defective podosome formation in macrophages of WAS patients[269]. The severity of the syndrome depends on the kind of mutation and the residual expression that is left[362, 366]. The worst scenario is the one of the classical WAS patients. They suffer from a loss-of-function mutation meaning the WASp expression is fully disabled[362]. Another group with a milder form of WAS are the X-linked thrombocytopenia (XLT) patients[357, 362]. These patients have a partial WASp expression and suffer from low platelets and minimal immunodeficiency[362]. In those patients the mutations is mostly found in the VCA domain[367]. When the mutations lead to a constitutively active form of WASp, this causes X-linked neutropenia[357].

3.4.2 Wiskott-Aldrich syndrome protein family

The discovery of the syndrome introduced a new protein family as well, the Wiskott-Aldrich syndrome (WAS) protein family. The WAS protein family proteins are known to be effectors of the Rho family GTPases and are able to induce rapid actin polymerisation

underneath the membrane[293]. This protein family has a wide variety of functions of this family, from physiological to pathological processes. They play a role in the immune response, tissue morphogenesis, synaptogenesis, pathogen infection, cancer invasion and metastasis[293]. Members of this family can either enhance or suppress cancer malignancies depending on the cell type and pathological state of the cancer[293].

Proteins of the WAS protein family are all characterized by two important domains. The first is a proline rich or poly-proline region[293, 357]. The second is a VCA domain which can be divided into three subdomains. The first is a V or verprolin-homology region which is able to directly bind to actin[294, 357]. The other two are a C and an A region which stands for cofilin-homology or central region and acidic region, respectively[293, 357]. This CA region directly binds to Arp2/3[294].

The WASp protein was the first member of the WAS protein family. It is a protein of 502 amino acids[362]. N-WASp or neural Wiskott-Aldrich syndrome protein has the highest homology with WASp (approximately 50% of the overall identity)[368]. Next to WASp and N-WASp, this protein family contains 'WASP family verprolin-homologous' protein (WAVE) or 'suppressor of cAR' (SCAR), 'WASp and SCAR homologue' protein (WASH), 'WASp homologue associated with actin, membranes, and microtubules' protein (WHAMM), 'junction-mediating and regulatory' protein (JMY), 'WASP and missing-in-metastasis like' protein (WAML) and 'WASp without WH1 domain' protein (WAWH)[293, 357, 369].

3.4.3 N-WASp

N-WASp or neural Wiskott-Aldrich syndrome protein is the expressed product from the *WASL* gene[370]. It is a scaffold protein consisting of 505 amino acids[370]. N-WASp is an actin nucleation promoting factor. By binding actin nucleation factors such as Arp2/3, N-WASp enhances the formation of a branched actin network. It is an important factor in enhancing the metastasis by assisting in the formation of invadopodia in cancer cells.

Since migration is also found in embryonic development, it is suggested that N-WASp plays a role in it as well[291]. Next to migration and degradation processes, N-WASp is supposed to stabilize podocyte foot processes in kidneys by maintaining the actin cytoskeleton[371, 372]. When making an N-WASp knock-out mouse model, total loss of N-WASp caused embryonic lethality[291]. While conditional knock-outs in brain or muscle cells were lethal, mice with a knock-out in epidermal keratinocytes of the skin are viable, but result in complications such as growth defects[291]. Gligorijevic *et al.*, who showed the first invadopodia *in vivo*, used a xenograft model containing N-WASp knockdown cells[373].

They observed a significant decrease of invadopodium formation, intravasation and metastasis using intravital imaging[301, 373]. When performing RNAi or expression of dominant negative N-WASp, it is observed that the ability to invade decreases[344, 374] and a nearly complete disruption of invadopodia is detected[293, 316]. Contrary, overexpression of N-WASp stimulates migration and invasion while the cell apoptosis is decreased[375].

WASp and N-WASp are very similar and show almost 50% sequence identity[362]. While WASp is expressed in only non-erythroid hematopoietic cells, N-WASp is ubiquitously expressed[357, 368]. Podosome formation is ascribed to WASp activity, but Isaac and colleagues observed that in WASp-deficient macrophages N-WASp could functionally compensate for WASp loss[283, 376]. After the activation of WASp-deficient macrophages, they detected an increased N-WASp level and an increase in the macrophage functionality[376]. However, the matrix degradation capability was less efficient compared to when WASp is available[376]. Still, this leads to the acceptation that N-WASp could partially replace WASp[283, 376].

3.4.3.1 The domains of WASp and N-WASp

Starting at the N-terminus, the first domain is the WASp homology 1 (WH1) domain, also known as the Ena-VASP homology 1 (EVH1) domain (Figure 27)[357]. This domain is important in keeping the (N-)WASp in an auto-inhibited state by interacting with the WASp-interacting protein (WIP)[377, 378]. Once (N-)WASp is activated, the WH1/EVH1 domain assists in the recruitment of (N-)WASp via Nck to the membrane[379].

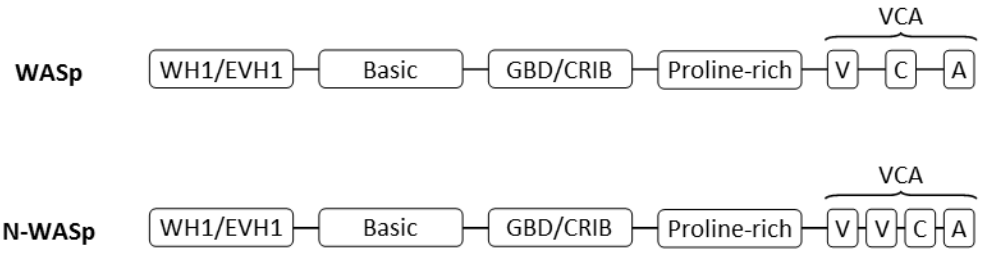

Figure 27: Schematic representation of the domains of WASp and N-WASp. Starting from the N-terminus, the WASp homology 1/Ena-VASP homology 1 (WH1/EVH1) domain is the first domain, followed by a basic domain. The third domain is a Cdc42- and Rac-interactive binding region or GTPase binding domain (CRIB/GBD). Next a proline-rich domain is found. At last, the VCA domain is most important in de actin polymerisation and is divided in three sub domains: the verprolin-homology (V) region, the C (cofilin-homology or central) region and the A (acidic) region.

The following domain is the basic region as there are multiple lysine and arginine residues[357, 380]. This domain can directly bind to $PI(4,5)P_2$ which partially activates (N-)WASp[380]. The C-terminal neighbouring domain of this basic region is the Cdc42- and Rac-interactive binding region (CRIB) or GTPase binding domain (GBD) (Figure 27). This CRIB/GBD domain binds the active form of the GTPase Cdc42 which also activates

(N-)WASp[293]. By the cooperation of the basic and the CRIB/GBD region, the (N-)WASp protein will be activated synergistically[362, 367].

As mentioned before, the next domains are typical for the WAS family: a proline-rich domain and a VCA domain (Figure 27). The proline-rich or poly-proline domain interacts with SH3 containing proteins and has a localisation and signalling function[357]. It is able to interact with the non-catalytic region of tyrosine kinase adaptor protein 1 (Nck1), Cdc42-interacting protein 4 (CIP4), profilin and others[366]. The poly-proline domain is able to accelerate the polymerisation activity by providing a pool of monomeric actin[367, 381]. This is caused by the binding with profilin-actin complexes which shuttles the actin monomers to the following domain, the V region of the VCA domain[367, 381]. This part of the VCA domain is also called verprolin-homology or WASP homology 2 (WH2) region and is able to bind actin[327, 357, 381]. The other two regions of the VCA domain are the C (cofilin-homology or central) and A (acidic) region. They interact directly with Arp2/3[294, 382]. The VCA domain is the most important part for actin polymerisation. A noticeable difference between WASp and N-WASp is found in the VCA domain. N-WASp contains a duplication of the V region, while WASp only has one V region[357]. This tandem array of the V region is supposed to promote the actin nucleation, due to a more efficient actin delivery to Arp2/3, and to localize N-WASp between the membrane and the barbed ends more efficiently compared to a single V region[357].

3.4.3.2 From an auto-inhibition state to an activated protein

N-WASp and WASp are found in two conformations (Figure 28). In normal cells they are found in the cytosol in an auto-inhibited resting state (Figure 28A)[293, 362]. In this conformation, the VCA domain is shielded and is unable to bind actin or Arp2/3. The basic domain and the CRIB/GBD domain are causing the inactive closed conformation by interacting with the A region and the VC region respectively[366, 383, 384]. To maintain the inhibited state, the WH1/EVH1 domain is bound to WIP[362, 366].

When WIP is released, the F-BAR protein TOCA1 binds to N-WASp[323, 324]. This protein is important for increasing affinity of N-WASp for Cdc42 and is important for the curvature of the membrane in the invadopodium initiation[324]. While WIP helps in maintaining the closed conformation, guanosine triphosphate (GTP)-bound Cdc42 disrupts the inactive state[362]. When GTP-bound Cdc42 binds to the CRIB/GBD domain of N-WASp, it will open its conformation (Figure 28B)[362, 366]. Besides, the basic domain participates also in the activation by binding to phosphatidylinositol-4,5-biphosphate ($PI(4,5)P_2$)[362, 366]. Together, they have a synergetic effect on the activation of (N-)WASp[362]. Once in the open conformation, the proline-rich region is available for binding SH3 domain containing

proteins[362]. It even can bind Src, which can phosphorylate WASp on Y291 or N-WASp on Y256[293, 331, 362]. This phosphorylation will only happen when (N-)WASp is in the open conformation and creates a kind of 'memory' mechanism that reminds (N-)WASp of its activated state even long after the initiating signals were present[331]. Not only the poly-proline region is accessible, also the VCA domain is available. After the activation, the V region can bind monomeric actin, where the CA region will bind Arp2/3 leading to the initiation of actin polymerisation to create a branched actin network[293, 362].

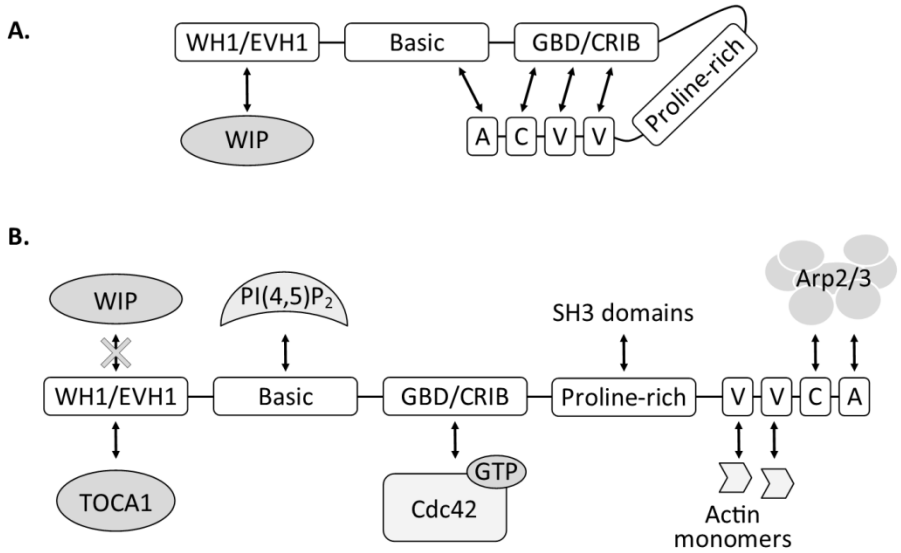

Figure 28: Conformations of N-WASp, from auto-inhibited to activated state. (**A**) Due to the auto-inhibition state, VCA is not available to induce the actin polymerisation. The basic domain and the CRIB/GBD domain are bound to the A region and the VC region respectively. The WASp-interacting protein (WIP) interacts with WH1/EVH1 to maintain the inhibited state. (**B**) In the active conformation, the WIP interaction is replaced by TOCA1, leading to an increased affinity of the CRIB/GBD domain for GTP-bound Cdc42. While the VCA domain is no longer shielded, it interacts with actin monomers and Arp2/3. The basic domain will interact with $PI(4,5)P_2$ at the plasma membrane and the proline-rich domain is available for binding SH3 domain containing proteins such as Src, cortactin … .

Part II

Scope

Chapter 4
Scope

One of the hallmarks of cancer is metastasis[264]. It is known that this is the most common cause of cancer deaths. Patients suffering from metastasis are likely to experience cancer-treatment failure which indicates the importance to search for new and better therapies to suppress the metastatic process[385, 386]. During metastasis and invasion, cancer cells gain more motility by hijacking normal cellular functions for their own purposes. For instance, they mimic the actin-based protrusions which are found in macrophages, to promote their invasiveness. These invadopodia are also known to enhance the spreading of such malignant cancer cells. However, it is only recently observed *in vivo* and accepted that invadopodia are important in this pathway[373, 387]. Buccione *et al.* were previously convinced that the disruption of invadopodia results in information which can lead to a better therapeutic development than the existing therapies[312]. Inside an invadopodium, many proteins are present and most of them are scaffold proteins, which makes it more challenging investigating since they lack an enzymatic activity. In the first part of this thesis, the VCA domain of the scaffold protein N-WASp is studied, since it is a suggested key domain to enhance the actin polymerisation during the invadopodium pathway. Our goal is to examine the role of this domain by using nanobodies and to unravel the mechanism of an invadopodium. The nanobody technology is used here as an alternative method to study intracellular proteins. An advantage of using this technology here, is that only a part of the protein is targeted, while methods like RNAi and CRISPR/Cas deplete the full length protein[6, 84, 388]. This allows us to study the importance of only a small part or a domain of a protein without altering its other interactions much. This way is ideal to examine only the VCA domain.

In the second part, the goal was to establish an efficient and broadly applicable protocol to create nanobodies bearing a fluorophore. Current methods to visualise biomolecules

in a microscope are susceptible to improvement and suffer from a problem known as linkage error. Frequently, a primary and a labelled secondary antibody or a directly labelled primary antibody are used. These large antibodies introduce a space between the dye and the protein, leading to an inaccurate visualisation of the localisation of the protein of interest. Another commonly used method is by using fluorescent protein-fusion proteins. This potentially alters the normal functioning of the protein or can trigger the same drawbacks as seen by overexpressed proteins. As nanobodies are a good equivalent of antibodies, they can be utilised to target endogenous proteins and visualise them, causing the linkage error to decrease. Next to the linkage error, a small size of the dye has beneficial effects on the imaging. The combination of a dye that is smaller compared to fluorescent proteins, and a nanobody that is smaller than an immunoglobulin, results in a higher resolution when used in fluorescence imaging. Due to these benefits, nanobodies can be a complementary tool to the existing visualisation methods. Different strategies to label nanobodies have been tested before, and they all have their own complications. We chose to incorporate an alkyne/azide moiety which allows chemical addition of a dye to the nanobody through the copper catalysed azido-alkyne click chemistry (CuAAC) reaction. Two strategies were expounded in the second part of this thesis. In the first strategy an enzymatic coupling of a nanobody with an alkyne bearing peptide was used, while the second strategy incorporates a non-canonical amino acid in the nanobody sequence itself. For this project, nanobodies were selected which already were characterised before. Those nanobodies can be used for further analysing the architecture of an invadopodium by using super resolution microscopy thereby providing higher precision.

Part III

Results

Chapter 5
VCA nanobodies target N-WASp to reduce invadopodium formation and functioning

Tim Hebbrecht[a], Isabel Van Audenhove[a], Olivier Zwaenepoel[a], Adriaan Verhelle[a] and Jan Gettemans[a]

5.1 Introduction

In this chapter, our goal was to characterize N-WASp nanobodies and to investigate the function of N-WASp in the invadopodium pathway. The nanobodies were generated in alpacas against the C-terminal domain of N-WASp, the VCA domain (verprolin-homology, cofilin-like and acidic region). It is known that N-WASp participates in invadopodium precursor formation to enhance the actin polymerization. Invadopodia are degrading structures formed by cancer cells, which promote cancer cell metastasis. The VCA domain of N-WASp is able to directly interact with actin and Arp2/3[294, 381, 382], making it an important domain for actin polymerization. By using nanobody technology, we seek to determine the contribution of the VCA domain to actin polymerization and invadopodium formation.

[a] Department of Biomolecular Medicine (former department of Biochemistry), Faculty of Medicine and Health Sciences, Ghent University, B-9000 Ghent, Belgium

The N-WASp nanobodies highlight the importance of the VCA domain because the number of invadopodia is significantly reduced in cancer cells expressing one of these VCA nanobodies. Extracellular matrix degradation by cancer cells is also countered in the study. The results of this study lead to the conclusion that VCA nanobodies perturb the functioning of endogenous N-WASp in the cancer cells. However, the effect of the VCA nanobodies shows that the role of the VCA domain during the invadopodium formation is more prominent than during the ECM degradation process.

5.2 **Research paper**

The paper[389] is published in PlosOne after a peer revision on September 22nd, 2017.

5.2.1 Abstract

Invasive cancer cells develop small actin-based protrusions called invadopodia, which perform a primordial role in metastasis and extracellular matrix remodelling. Neural Wiskott-Aldrich syndrome protein (N-WASp) is a scaffold protein which can directly bind to actin monomers and Arp2/3 and is a crucial player in the formation of an invadopodium precursor. Expression modulation has pointed to an important role for N-WASp in invadopodium formation but the role of its C-terminal VCA domain in this process remains unknown. In this study, we generated alpaca nanobodies against the N-WASp VCA domain and investigated if these nanobodies affect invadopodium formation. By using this approach, we were able to study functions of a selected functional/structural N-WASp protein domain in living cells, without requiring overexpression, dominant negative mutants or siRNAs which target the gene, and hence the entire protein. When expressed as intrabodies, the VCA nanobodies significantly reduced invadopodium formation in both MDA-MB-231 breast cancer and HNSCC61 head and neck squamous cancer cells. Furthermore, expression of distinct VCA Nbs (VCA Nb7 and VCA Nb14) in PC-3 prostate cancer cells resulted in reduced overall matrix degradation without affecting MMP9 secretion/activation or MT1-MMP localisation at invadopodial membranes. From these results, we conclude that we have generated nanobodies targeting N-WASp which reduce invadopodium formation and functioning, most likely via regulation of N-WASp – Arp2/3 complex interaction, indicating that this region of N-WASp plays an important role in these processes.

5.2.2 Introduction

Metastasis is the primary cause of cancer associated deaths. In this process cancer cells leave a primary tumour to disseminate through the entire body[390]. In doing so, these cancer cells are able to create secondary tumours throughout the body, a lethal process for the cancer patient in almost all cases[390]. In order to leave the primary tumour, cancer cells create small actin-based protrusions to facilitate their spreading[391]. Invadopodia are such malignant specialized structures known to enable cancer cells to invade through natural barriers[387, 391]. Invadopodium formation is found in highly invasive cancer cell lines[374] and has been evinced *in vivo*[387]. A mature invadopodium displays considerable proteolytic activity. More specifically, invadopodium-related degradation of the extracellular matrix (ECM) has been linked to extravasation and metastasis *in vivo*[392]. Inside an invadopodium, approximately 129 different proteins can be found[310]. They contribute to the aggressive nature of invadopodia in cancer. Before an invadopodium can be formed, assembly of a precursor is required. This precursor will kick-start actin polymerisation towards the plasma membrane and invadopodia will arise[329, 337, 344, 393].

Activation of the Arp2/3 – N-WASp pathway, found to be important in invadopodium formation, has been observed in a broad spectrum of cancers[394]. Arp2/3 (actin related protein) is a protein complex existing of seven subunits, of which Arp2 and Arp3 are the only two proteins of the complex that are actin-related[395]. Once Arp2/3 is activated, those two subproteins will mimic two actin monomers to boost the actin polymerisation[332, 395].

The neural variant of WASp (N-WASp) is a ubiquitously expressed member of the Wiskott-Aldrich syndrome protein (WASP) family[344, 396, 397]. This family is known as nucleation-promoting factors of the Arp2/3 complex[357] and fills the gap between reorganisation of the actin cytoskeleton and signalling molecules[373, 398]. Because N-WASp is a scaffold protein, it has several domains through which it interacts with interaction partners[344, 396, 397]. Using its C-terminal VCA domain, N-WASp can directly interact with actin monomers and the Arp2/3 complex. The VCA domain consists of a verprolin-homology (V) domain (a.k.a. WASp homology 2 (WH2) domain), a cofilin-like or central (C) domain and an acidic (A) domain[399]. While the V domain is a binding site for actin monomers, the Arp2/3 complex binds the latter two parts (C and A domains)[357, 397, 399-401]. It has been shown *in vitro* that N-WASps VCA domain is needed during the formation of the invadopodium precursor[336, 337, 373, 402]. Moreover, by bringing actin monomers and Arp2/3 closer together, N-WASp stimulates and enhances the actin polymerisation[383].

We generated alpaca nanobodies against the VCA domain of N-WASp (VCA Nb) to investigate the role of this region in formation of cancer cell invadopodia. Nanobodies are single-domain antibody fragments or, more specifically, the variable part of the heavy chain of Camelid heavy chain antibodies[16]. A nanobody is the smallest, natural, antigen binding fragment that completely retains its original binding affinity and specificity. Contrary to RNAi, intracellularly expressed nanobodies or so-called intrabodies can interfere with protein functions without silencing the whole protein. Moreover, intracellular nanobodies render the need for overexpression, siRNA or dominant negative mutants superfluous, which makes it able to study functions of endogenous proteins. By using VCA Nbs, we study the influence of N-WASps VCA domain in invadopodium formation and extracellular matrix degradation. Using breast, prostate and head and neck cancer cell lines that inducibly express these VCA nanobodies, we show that this N-WASp region indeed contributes to invadopodium formation and extracellular matrix remodelling, suggesting that it is involved in invadopodium based spreading of cancer cells.

5.2.3 Results

5.2.3.1 N-WASp recognising of VCA nanobodies

Initially, 16 different nanobodies were identified through phage display following immunization with chemically synthesized N-WASp VCA domain (human N-WASp K420-D505), lymphocyte collection and library construction. Based on their amino acid sequence, 10 different groups could be discerned. One nanobody was chosen from each group for biochemical characterisation. To detect antigen-nanobody binding *in vitro*, recombinant HA-tagged nanobodies were used in a pull down assay. MDA-MB-231 breast cancer cell lysate was used as a source of endogenous N-WASp. Seven nanobodies out of 10 bound with the endogenous N-WASp (Figure 29).

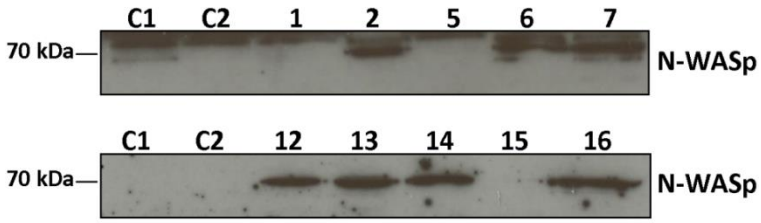

Figure 29: VCA nanobody - N-WASp binding. Pull down assay of endogenous N-WASp from MDA-MB-231 breast cancer cell lysate with HA-tagged VCA Nb (1, 2, 5, 6, 7 and 12, 13, 14, 15, 16) by means of anti-HA agarose beads. Two negative controls were included, anti-HA agarose beads were incubated with no nanobody (C1) or with a cortactin NTA nanobody against the N-terminal acidic (NTA) region of cortactin (C2). N-WASp was blotted and detected by anti-N-WASp antibody. To see the pull down of the 4 selected VCA Nbs using HNSCC61 cancer cells, which express EGFP-tagged VCA Nbs, see Figure 30.

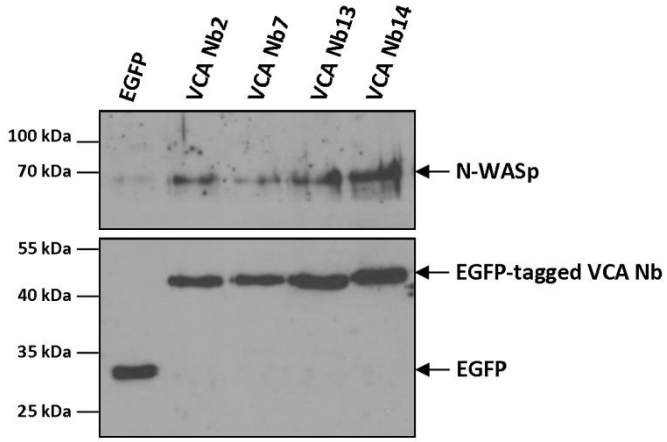

Figure 30: VCA nanobody—N-WASp binding in EGFP-tagged VCA Nb expressing HNSCC61. The EGFP-tagged VCA Nbs were pulled down using a GFP Ab and Protein G Sepharose beads. N-WASp is detected by N-WASp antibody and the VCA-Nbs by GFP Ab.

5.2.3.2 Mitochondrial outer membrane anchoring and intracellular displacement of N-WASp

To investigate whether the nanobodies would still bind their target in the reducing environment of the cytosol, we performed a MOM (mitochondrial outer membrane) delocalisation assay. In this experiment, the nanobodies were equipped with a MOM- and V5-tag at their N-terminus. The MOM-tag originates from yeast TOM70[403] and redirects the tagged nanobodies to the mitochondrial outer membrane, which can confirm the intracellular binding capacity of VCA Nb to endogenous N-WASp. If N-WASp binds to the VCA Nbs, N-WASp will be found at the mitochondrial outer membrane which does not correspond with its natural subcellular localization. The effectiveness of the MOM-tag is first analysed by performing immunofluorescent assays visualising the mitochondria with MitoTracker Orange (Figure 31). This confirmed that the MOM-tagged nanobody patterns are similar to the mitochondrial patterns. Further, we will only look at the nanobody patterns as it stands for the mitochondrial patterns. Secondly, the N-WASp co-localisation is performed by visualising the VCA Nbs and N-WASp at the same time. In MOM-tagged EGFP Nb expressing control cells, no mitochondria-like pattern for N-WASp could be found (Figure 32, upper panel). The same was observed in MOM-VCA Nb1, 5 and 15 expressing cells. These are the same 3 nanobodies which did not bind N-WASp in pull down experiments. All other MOM-VCA nanobodies resulted in a mitochondrial-like N-WASp distribution pattern. This was most obvious in MOM-VCA Nb2, 7, 13 and 14 expressing cells (Figure 32, lower panels). The intensity plots were determined as well to quantify the co-localisation (Figure 32, at the right). In conclusion, the nanobodies which were able to bind N-WASp *in vitro* (Figure 29) are also able to efficiently capture endogenous N-WASp in the dense intracellular environment, demonstrating their *in vivo* interaction with the target.

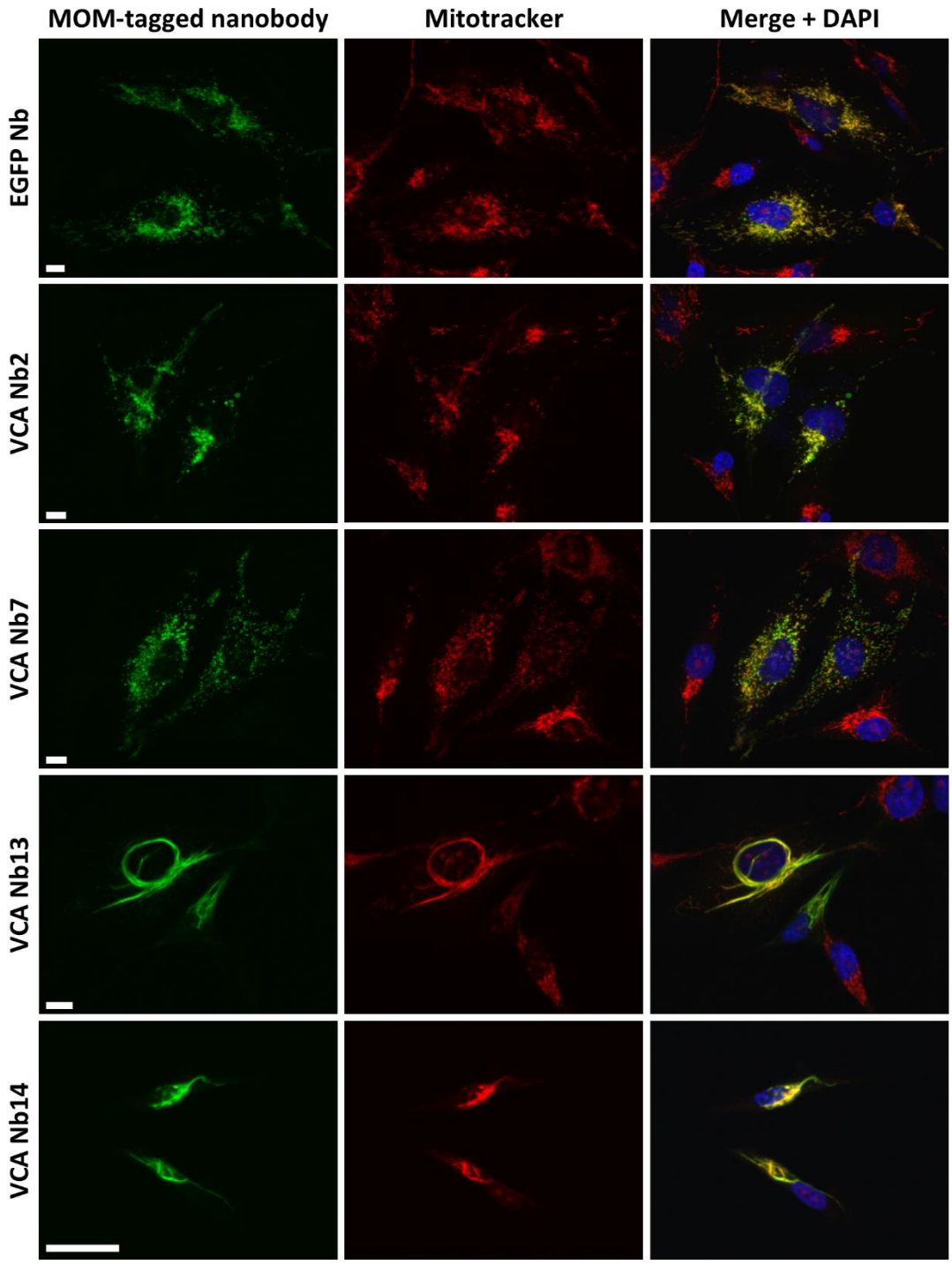

Figure 31: Mitochondrial pattern in MDA-MB-231 breast cancer cells which transiently express a VCA Nb equipped with a MOM-tag. Representative epifluorescence images showing the mitochondrial patterns indicating that the MOM-tag directs the nanobody to the mitochondrial outer membrane (compare with the MitoTracker channel). MOM-tagged EGFP nanobody was used as a negative control (upper panel). Nuclei were visualized with DAPI (blue), nanobodies with anti-V5 antibody (green) and the mitochondria with MitoTracker Orange (red). (Scale bar = 10 µm)

The mitochondrial patterns of the MOM-tagged VCA Nb13 and VCA Nb14 show a dissimilar pattern compared to the control and the other VCA Nb conditions (VCA Nb2 and VCA Nb7) (Figure 31 and Figure 32). These patterns were only found with the MOM-tag which is used here to demonstrate binding. In all subsequent experiments this tag was not included and under these conditions the mitochondrial pattern looks the same for all nanobodies (Figure 33).

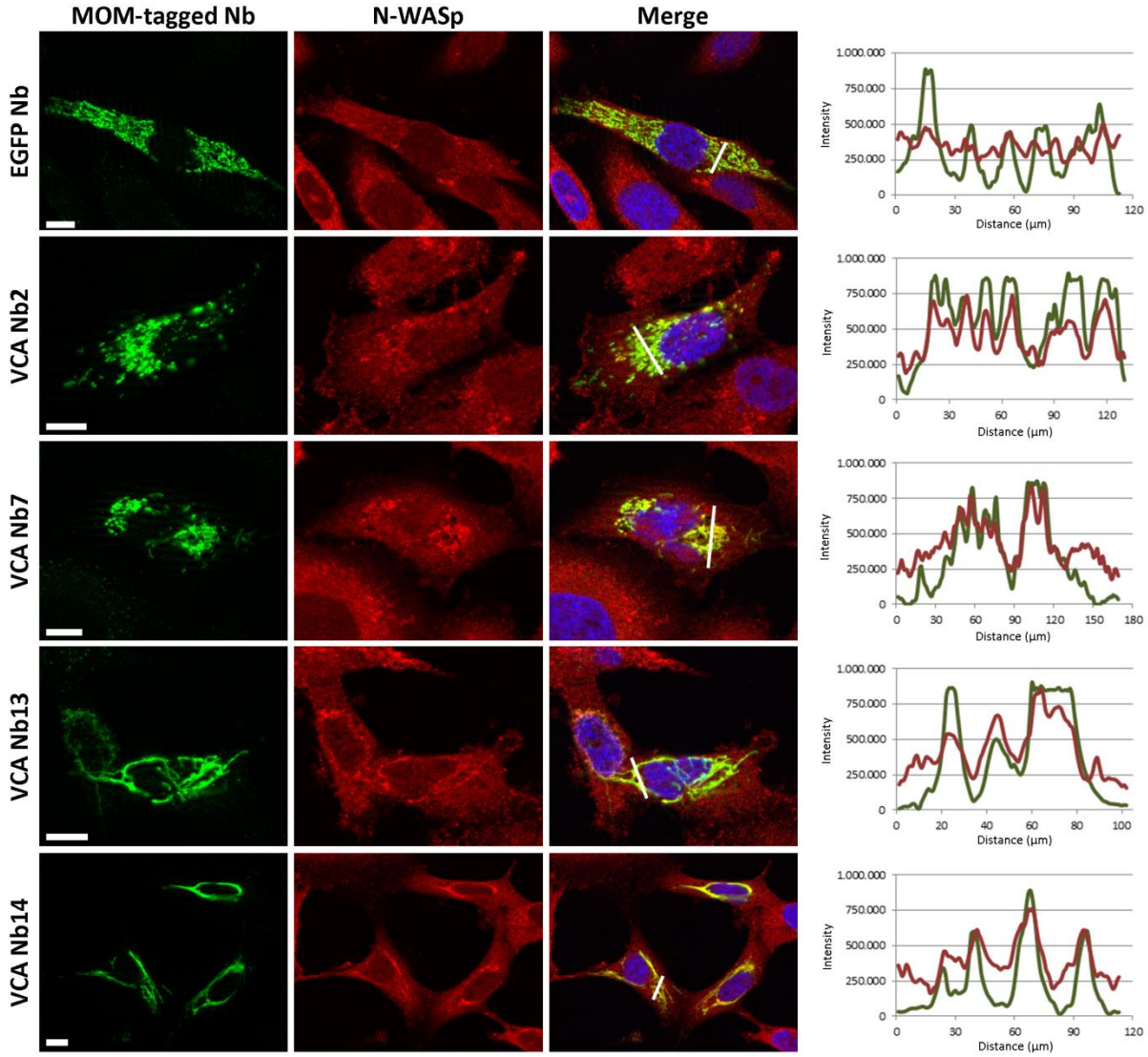

Figure 32: VCA Nb2, 7, 13 and 14 capture endogenous N-WASp at mitochondria. Representative epifluorescence images of MDA-MB-231 breast cancer cells transiently expressing VCA Nbs equipped with a MOM-tag. MOM-tagged EGFP nanobody was used as a negative control (upper panel). Nuclei were visualized with DAPI (blue), nanobodies with anti-V5 antibody (green) and N-WASp with anti-N-WASp antibody (red). Right: the intensity profiles for N-WASp (red) and MOM-tagged nanobodies (green) are very similar, indicative of co-localisation, except for the EGFP nanobody (negative control). (Scale bar = 10 µm)

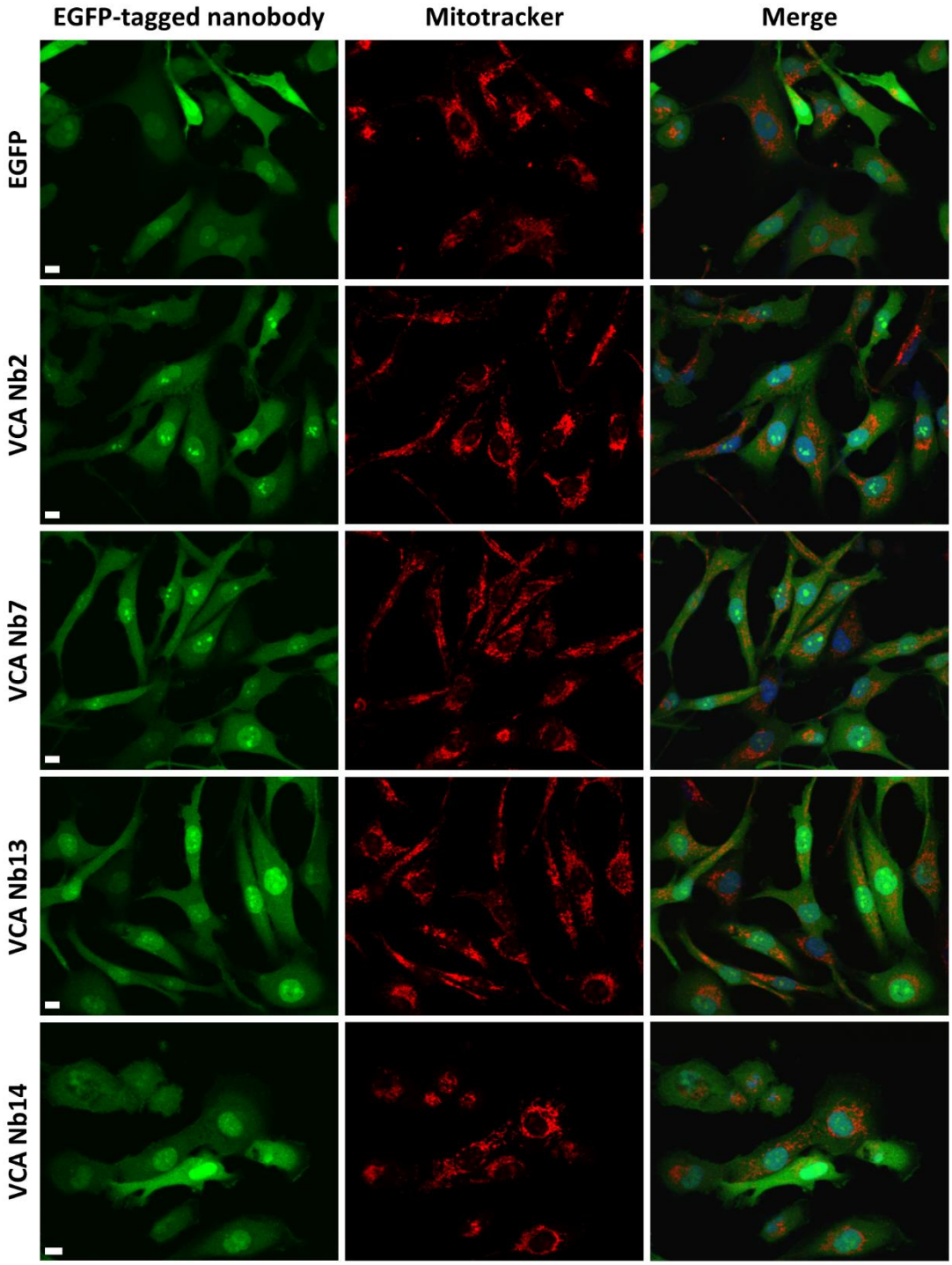

Figure 33: Mitochondrial pattern in MDA-MB-231 breast cancer cells in which EGFP-tagged VCA Nbs inducibly are expressed. Representative epifluorescence images showing the mitochondrial patterns. Nuclei were visualized with DAPI (blue) and the mitochondria with MitoTracker Orange (red). (Scale bar = 10 µm)

5.2.3.3 Affinity and stoichiometry of 4 selected VCA Nbs

Based on the pull down and MOM delocalisation criteria, we determined the binding affinity and stoichiometric properties of 4 nanobodies; VCA Nb2, 7, 13 and 14. Isothermal titration calorimetry (ITC) was performed at physiological pH by using recombinant VCA Nbs (Figure 34). As these nanobodies were generated against a domain of N-WASp, we used chemically synthesized pure VCA peptide. The K_d values were determined at 0.699 ± 0.154 µM for VCA Nb2, 0.820 ± 0.201 µM for VCA Nb7, 0.685 ± 0.133 µM for VCA Nb13 and 1.597 ± 0.249 µM for VCA Nb14 (Table 1 and Figure 34). These results showed that VCA Nb2, 7, 13 and 14 have a submicromolar affinity for the VCA peptide. This submicromolar affinity proved to be sufficient as the VCA nanobodies were able to relocate N-WASp to the outer membrane of mitochondria (Figure 32).

Parameters	VCA Nb2	VCA Nb7	VCA Nb13	VCA Nb14
N[#]	0.912 ± 0.037	0.905 ± 0.037	0.757 ± 0.035	0.780 ± 0.031
ΔH (cal/mol)	-4657 ± 254	-4686 ± 258	-6967 ± 433	-3194 ± 165
ΔS (cal/mol)	12.8	12.4	5.2	16.0
K_d (µM)	0.699 ± 0.154	0.820 ± 0.201	0.685 ± 0.133	1.597 ± 0.249

[#]Stoichiometry

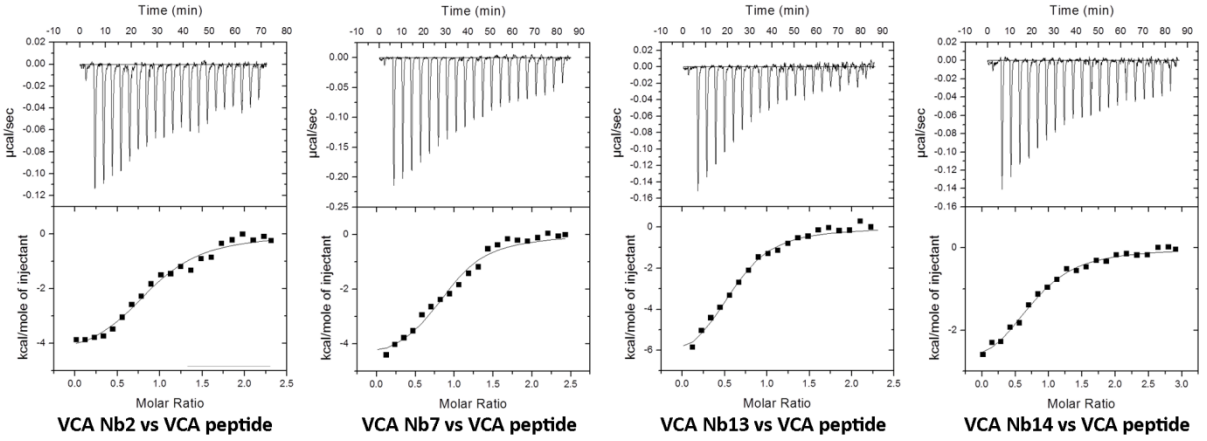

Figure 34: Affinity study of VCA Nbs. ITC profiles of recombinant HA-tagged VCA Nbs with synthetic VCA peptide of human N-WASp. VCA peptide was titrated once with VCA Nb7 and once with VCA Nb14. VCA Nb2 and VCA Nb13 were titrated with VCA peptide. The upper panel shows the raw data of heat release in function of time, while the lower panel shows the fitted binding curve of total heat release per injection as a function of the molar ratio.

Table 1: Thermodynamic parameters (and respectively standard deviations) of HA-tagged VCA nanobodies interacting with synthetic VCA peptide, determined by ITC. ([#], molar ratio or stoichiometry; [*], ΔG = ΔH – T * ΔS with T = 303.15 K)

Parameters	VCA Nb2	VCA Nb7	VCA Nb13	VCA Nb14
N[#]	0.912 ± 0.037	0.905 ± 0.037	0.757 ± 0.035	0.780 ± 0.031
ΔH (cal/mol)	-4657 ± 254	-4686 ± 258	-6967 ± 433	-3194 ± 165
ΔS (cal/mol)	12.8	12.4	5.2	16.0
ΔG (cal/mol)[*]	-8537.45	-8445.18	-8551.53	-8044.56
K_d (µM)	0.699 ± 0.154	0.820 ± 0.201	0.685 ± 0.133	1.597 ± 0.249

5.2.3.4 The VCA Nbs interfere in the binding between N-WASp and its direct interaction partner Arp2/3, but not actin

N-WASps VCA domain can directly interact with actin monomers via its V region and with Arp2/3 via its CA regions. To analyse if the VCA Nbs are able to interfere with the binding between N-WASp and either actin or Arp2/3, a pull down assay was performed by adding a concentration range of VCA Nb2, 7, 13 or 14 together with biotinylated VCA peptide and STREPTactin beads. As an Arp2/3 and actin source, we used MDA-MB-231 cell lysate (Figure 35). Via Western blotting, the amount of bound Arp2/3 and actin was quantified. A quadruplicate of this experiment was analysed with a Kruskal-Wallis test and Dunns post tests. Four different concentrations of each VCA Nb were added, based on the stoichiometry of VCA Nb to the VCA domain. The results show a dose dependent decrease of Arp2/3 binding with increasing concentrations of VCA Nb. While only VCA Nb2 and VCA Nb13 were able to show significant differences, the decreasing trend was found in all four VCA Nbs. This reduction in binding was not observed for actin, meaning that VCA Nbs do not disturb the interaction between N-WASp and actin and VCA Nbs do not interfere at the V region of the VCA domain.

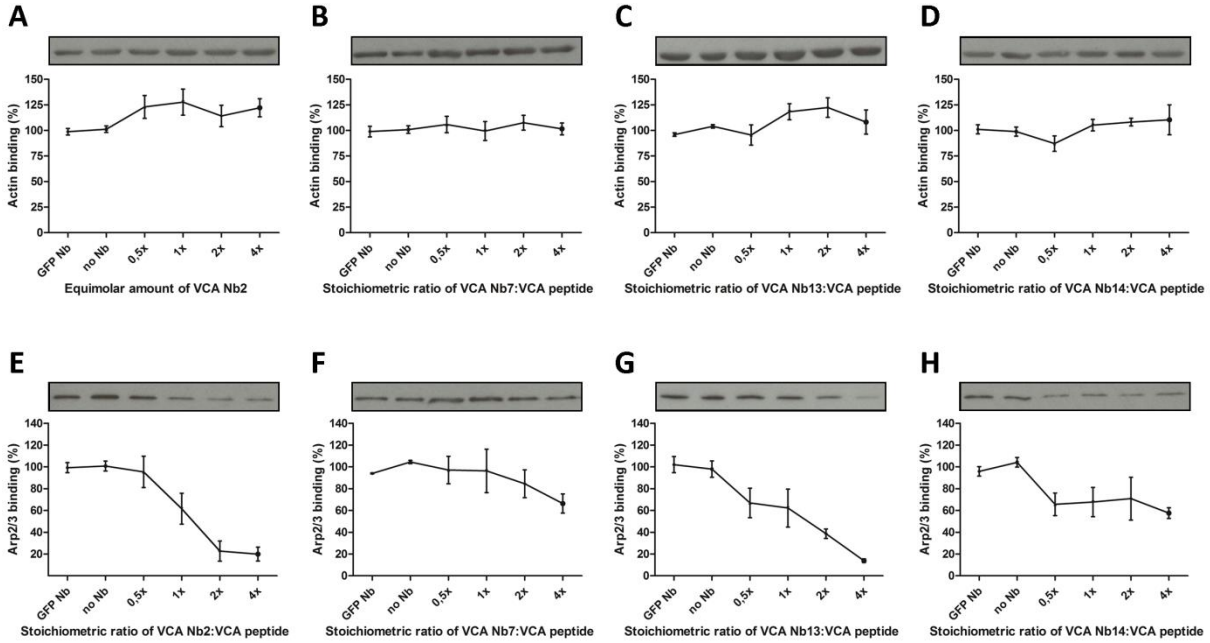

Figure 35: **VCA Nb effect on actin or Arp2/3 binding to N-WASp using a nanobody concentration range.** Pull down was performed by using biotin-tagged VCA peptide, MDA-MB-231 breast cancer cell lysate, recombinant VCA Nbs and STREPTactin beads. The two controls (no nanobody (No Nb) or EGFP Nb) show maximal Arp2/3 binding. A concentration range was used (VCA Nb : VCA domain stoichiometry of 0.5x, 1x, 2x, 4x). For each repeat, actin as well as Arp2/3 were analysed on western blot and quantification was done using ImageJ (bars represent mean and SEM, n=3). Kruskal-Wallis and Duns post test was performed. On top the influence of each VCA Nb on actin – N-WASp binding (**A-D**) is shown and at the bottom the effect of each VCA Nb on Arp2/3 – N-WASp binding (**E-H**) is shown.

5.2.3.5 VCA nanobodies reduce cancer cell invadopodium formation

Before a fully mature invadopodium can be formed, an invadopodium precursor has to be created. N-WASp plays an important role in the latter[344, 393, 394]. The VCA domain of N-WASp brings Arp2/3 and actin monomers in close proximity to enhance actin polymerisation. This polymerisation creates actin-based protrusions, which in cancer cells may develop into invadopodia. To visualise N-WASp in invadopodia, a staining was performed of invadopodia markers (actin and cortactin) (Figure 36). Our findings clearly revealed N-WASp concentrated at invadopodium sites, which confirms previous research[383, 394].

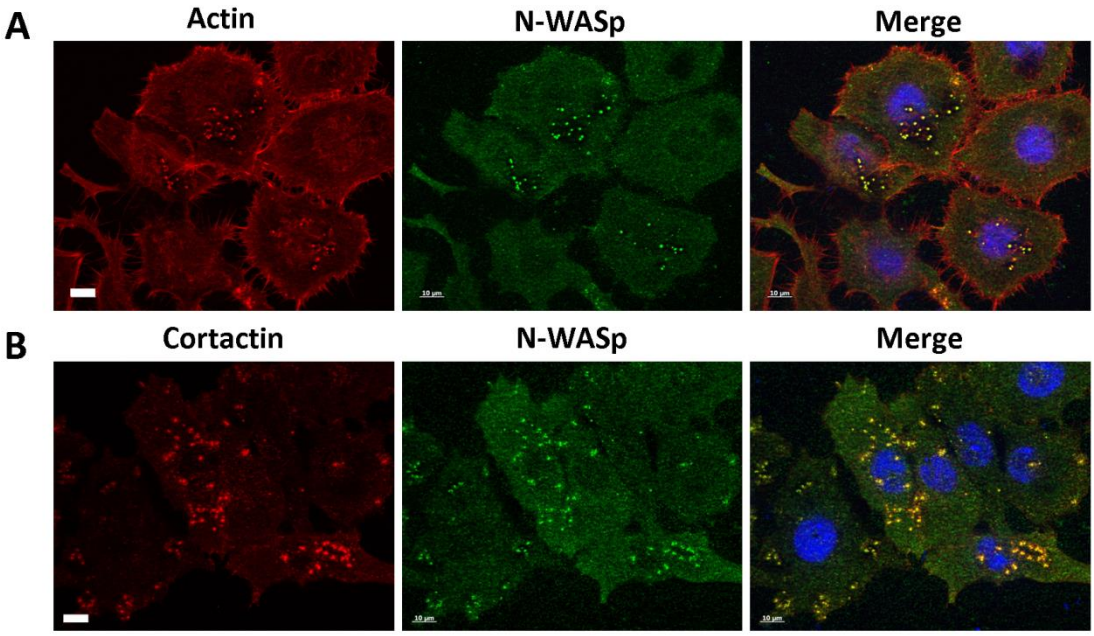

Figure 36: N-WASp colocalizes with invadopodia markers. Representative epifluorescence images of HNSCC61 head and neck squamous cancer cells. Nuclei were visualized with DAPI (blue) and N-WASp (green) with anti-N-WASp antibody. Invadopodia were visualized by using an invadopodium marker; (**A**) actin (red) with Alexa Fluor labelled phalloidin and (**B**) cortactin (red) with anti-cortactin antibody. (Scale bar = 10 µm)

To analyse if the VCA Nbs could influence invadopodium formation in different cancer cells, lentiviral, stable doxycycline-inducible MDA-MB-231 breast and HNSCC61 head and neck squamous cancer cell lines were made in which EGFP-tagged VCA Nbs are expressed as intrabodies. As a control, an EGFP-only expressing stable cell line was made. After nanobody induction overnight, the cells were fixed with paraformaldehyde and stained with phalloidin. When VCA Nb2, 7, 13 and 14 were expressed a significant reduction in invadopodia numbers was observed in both MDA-MB-231 and HNSCC61 cancer cells (Figure 37).

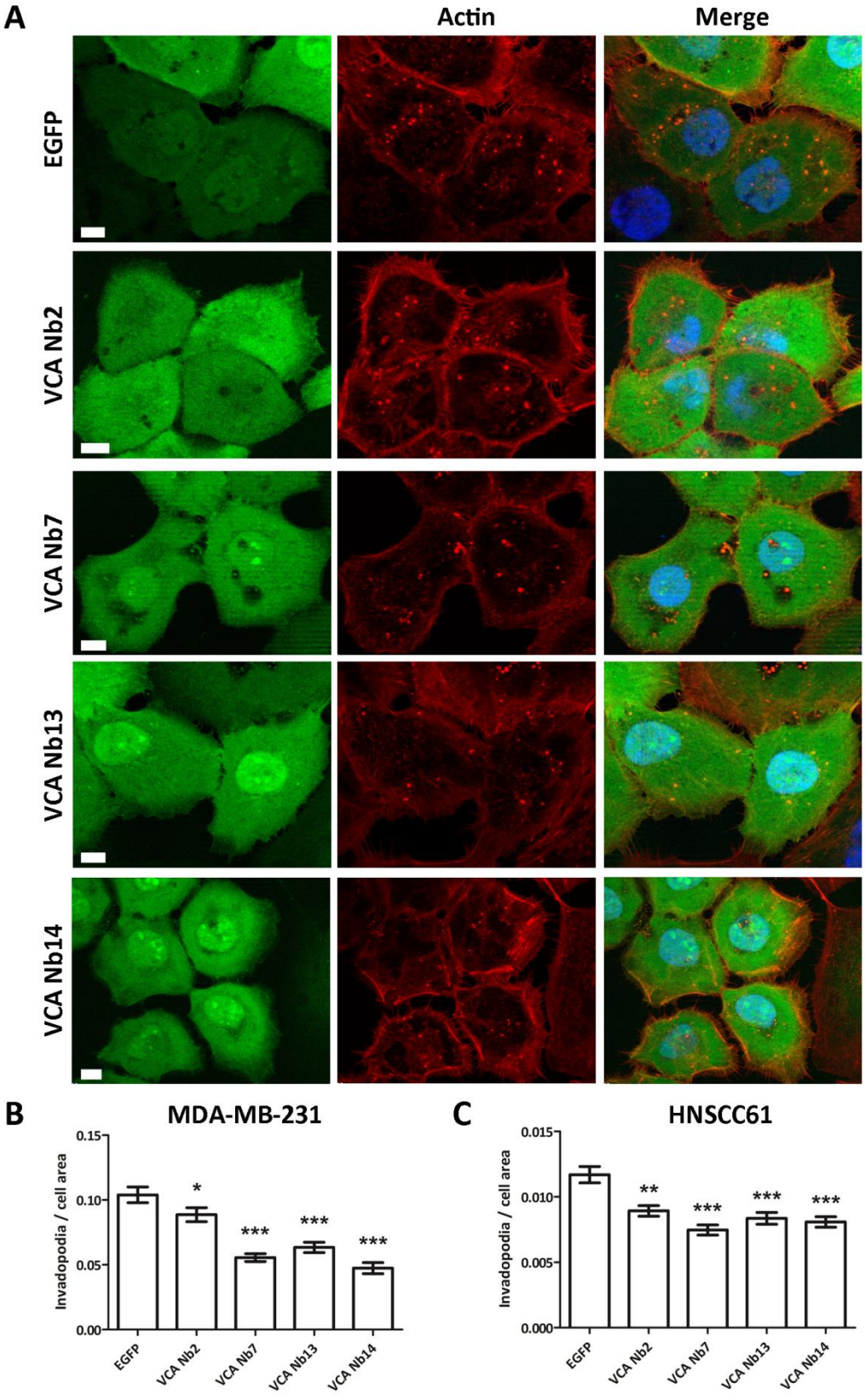

Figure 37: Expression of VCA Nbs in cancer cells reduces invadopodia number. Representative epifluorescence images of HNSCC61 head and neck squamous cancer cells which express EGFP-tagged VCA Nbs (green) (**A**). Nuclei were visualized with DAPI (blue) and actin (red) with phalloidin. Bar plots of MDA-MB-231 breast (**B**) and HNSCC61 head and neck squamous (**C**) cancer cells, which inducible express EGFP- tagged VCA Nbs, were used to count invadopodia per cell. Quantification was done using ImageJ and Kruskal-Wallis and Dunns post tests were performed. As negative control EGFP-only expressing stable cells were used. (* $p < 5\%$, ** $p < 1\%$, *** $p < 0.01\%$)

5.2.3.6 The VCA Nbs reduce overall matrix degradation

A conspicuous and important link to metastasis is the proteolytic activity of a mature invadopodium[392]. Once this structure is formed, matrix remodelling follows, underlining the importance of matrix metalloproteinases (MMPs). MMPs are zinc-containing endopeptidases[296, 309, 344, 391]. The gelatinases MMP2 and MMP9 and the membrane bound collagenase MT1-MMP (also known as MMP14) are the most abundant MMPs. The latter is important since it acts as a master switch to activate other MMPs[296, 309, 391, 404]. To analyse the effect of N-WASp nanobodies on matrix degradation, stable doxycycline-inducible PC-3 prostate cancer cell lines were constructed in which the EGFP-tagged VCA Nbs are expressed as an intrabody after adding doxycycline. As a control, an EGFP-only expressing stable cell line was made. In earlier studies we have used a similar approach[45, 46, 48, 405-407]. The cells were seeded on a Cy3-gelatin matrix and overnight induced with doxycycline (Figure 38A). Analysis was done with ImageJ[45, 408] and a Kruskal-Wallis test and Dunns post tests were performed. First, the degradation index was determined. This parameter can be interpreted as the normalised difference between the mean grey value of the background (here the red fluorescent labelled gelatin matrix) and of the cell area. For two out of four VCA Nbs (VCA Nb7 and Nb14), significant less degradation was found (Figure 38B). The second parameter 'degradation area per cell' revealed significantly less degradation per cell for the same two VCA Nbs (Figure 38C). Thirdly, the ratio of 'degradation area to total cell area' was determined. This parameter gives only for VCA Nb14 a significant reduction in degradation per cell area (Figure 38D). In conclusion, only expression of VCA Nb7 and Nb14 in PC-3 cells resulted in reduced matrix degradation.

Matrix remodelling is caused by proteolytic activity of invadopodia[344, 392]. The MMPs need to be transported through the invadopodia before they can perform their function extracellularly. N-WASp is suggested to form actin comet tails at vesicles, which brings the MMPs to the membrane[356]. These actin tails will give the vesicles a propelling force to help their movement. To study this, the secretion and activity in the medium of the most abundant MMP was analysed by zymography experiments with PC-3 prostate cancer cells. Initially, the purpose was to study either MMP2 and MMP9, but no MMP2 activity was observed after 20 h of incubation, not even in the control experiment. We could observe a small decrease of MMP9 secretion/activity between the induced and the non-induced VCA Nb-EGFP expressing cell lines but these proved to be not statistically significant (Figure 39). Furthermore, another proposed function of N-WASp involves proper localisation of MT1-MMP[344]. The potential effect of the VCA Nbs on MT1-MMP positioning was analysed in HNSCC61 cells by counting MT1-MMP containing invadopodia when MT1-MMP positive dots overlapped with F-actin dots. However, no

difference in MT1-MMP localisation was observed (Figure 40). In conclusion, VCA Nb7 and VCA Nb14 reduce the degrading properties of PC-3 cells, but without significant effects on MMP9 secretion/activity or on MT1-MMP localisation.

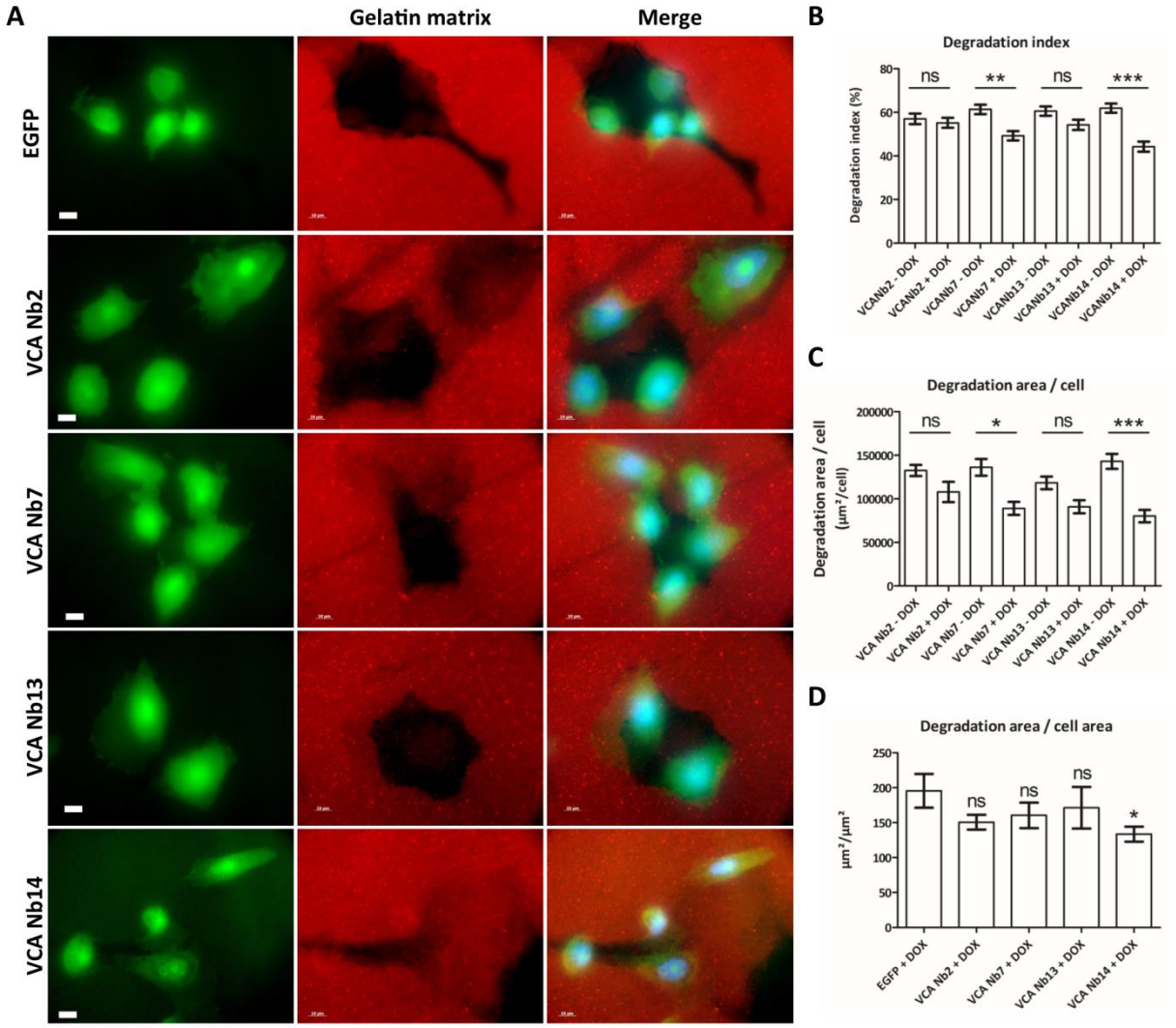

Figure 38: Effects of VCA intrabodies on matrix degradation. (**A**) Representative epifluorescence images of PC-3 prostate cancer cells, which inducibly express EGFP-tagged VCA Nbs, were seeded on Cy3-gelatin matrix (scale bar = 10 µm). As negative control EGFP-only expressing stable cells were used. Quantification was done using ImageJ and Kruskal-Wallis test and Dunns post tests were performed. Degrading capacity of PC-3 cells was analyzed by 3 parameters. For the first parameter 'degradation index' (**B**) and the second parameter 'degradation area per cell' (**C**), a comparison between 'not induced' and 'doxycycline induced' was made for each stable cell line. The third parameter 'degradation area per total cell area' (**D**) was compared to the EGFP-only cell line. (ns = not significant, * $p < 5\%$, ** $p < 1\%$, *** $p < 0.01\%$)

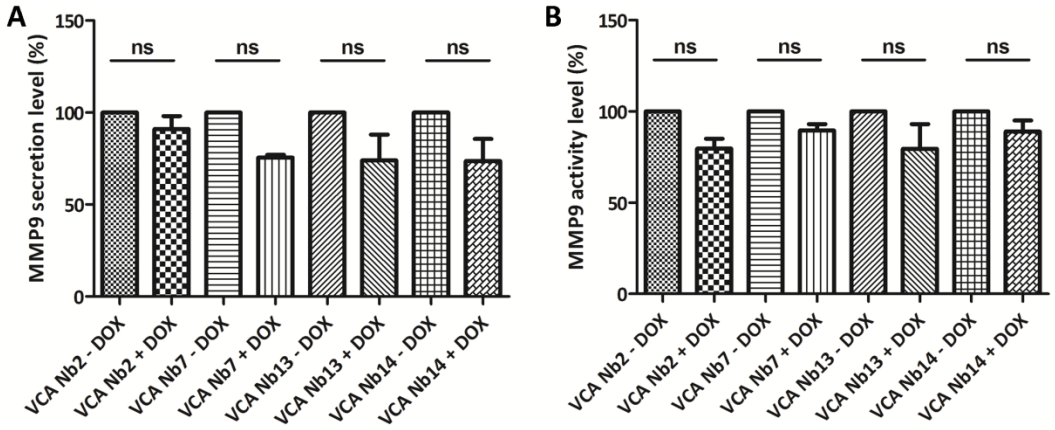

Figure 39: Effects of VCA Nbs on MMP9 secretion and activity levels. (A) Quantification of MMP9 levels in medium was determined using ImageJ after SDS-PAGE and Western blotting. As control the uninduced cell line was used. (B) Activity was obtained after digestion in 0.1% gelatin gel. Quantification was performed using ImageJ and a Kruskal-Wallis and Dunns post tests were performed. The bars represent mean and SEM (n = 3). (ns, not significant)

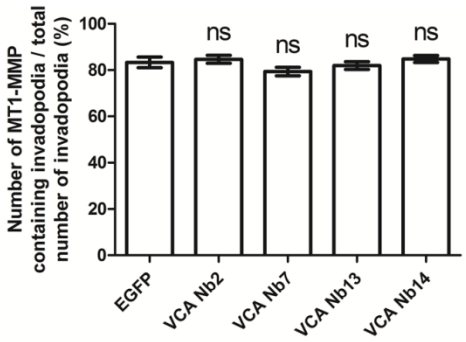

Figure 40: Effects of VCA Nbs on MT1-MMP positioning. MT1-MMP containing invadopodia were counted when MT1-MMP dots were overlapping with F-actin dots in HNSCC61 cells, in which VCA Nbs expression could be induced. The number of MT1-MMP containing invadopodia was divided by the total amount of invadopodia for each cell and Kruskal-Wallis and Dunns post tests were used. The bar plot represents mean and SEM (n = 3). (ns, not significant)

5.2.4 Discussion

In this study, nanobodies were generated against the VCA domain of N-WASp, an actin and Arp2/3 interaction partner. Out of all binders, four VCA nanobodies (VCA Nb2, 7, 13 and 14) were selected and expressed in 3 different cancer cell lines. Pull down experiments and immunofluorescence revealed their ability to bind endogenous N-WASp. Their submicromolar affinity for the VCA peptide was determined with ITC. Previous studies found actin binding affinities to the VCA domain of WASP family proteins ranging from 50 to 250 nM, also using ITC[409, 410]. The affinity between VCA and Arp2/3 complex is more difficult to determine and expected to be lower[382, 411-414]. Depending on the techniques used, previous research suggested a binding of one Arp2/3 complex to two N-WASp molecules[411-413]. These previously determined affinities cover a

broad range, but almost all conclude that the affinity differences between those two binding sites differs by one or two order of magnitude[411-413]. As we observed a delocalization of N-WASp using the MOM-tagged VCA nanobodies (Figure 32), a decreased binding of Arp2/3 to VCA in the presence of the VCA Nbs (Figure 35), a significant disturbance of invadopodium formation (Figure 37) and a decrease in the overall matrix degradation (Figure 38), we conclude that VCA nanobodies indeed perturb several functions of endogenous N-WASp in these cancer cells.

N-WASp participates in the formation of an invadopodium precursor which activates the actin polymerisation process. It was previously demonstrated that N-WASp is a key player in invadopodium genesis[289]. The cancer cell receives a signal (i.e. EGF) which activates a cascade leading to invadopodium formation. In this cascade, the RhoGTPase Cdc42 is activated and will change the conformation of N-WASp from the inactive to the active state[384, 397]. Only in the active state will the VCA domain of N-WASp bind Arp2/3 and actin and stimulate actin polymerisation at the pre-invadopodium site. Next, Arp3 binds to cortactin and after the activated N-WASp comes in, the Arp2/3 complex will interact with N-WASp, leading to a higher activation of Arp2/3 and initiation of actin polymerisation[395]. N-WASp interacts with Arp2/3 through the central or cofilin-like (C) and acidic (A) regions of the VCA domain. Of the seven subunits of the Arp2/3 complex, only Arp2 and Arp3 bind to the VCA domain of N-WASp[332, 395]. This double interaction differs in properties and functions[402, 415]. The first interaction occurs at the acidic (A) region of the VCA domain and is important for the affinity between N-WASp and the Arp2/3 complex, but is not essential for Arp2/3 activation. The second interaction involves the central (C) region, which binds Arp2/3 with lower affinity, but it is indispensable for Arp2/3 activation. Our observations show that the VCA nanobodies are able to interfere with this process. The Arp2/3 and actin binding experiments reveal that the VCA Nbs have no effect on actin binding, but the VCA Nbs all show a reduction in Arp2/3 interaction with VCA. Moreover, we observed a significant reduction in the number of invadopodia, both in MDA-MB-231 and HNSCC61 cells, when VCA Nbs were expressed as intrabody (Figure 37), highlighting the importance of the VCA domain of N-WASp in invadopodium formation[336, 337, 373, 402]. Because VCA Nb2 and VCA Nb13 show a significant reduction in Arp2/3 interaction, we suggest that these nanobodies interrupt the interactions via binding to the acidic (A) region of the VCA domain. In contrast, VCA Nb7 and VCA Nb14 elicit only a slight reduction in Arp2/3 interaction, but display a significant effect in the degradation properties of PC-3 cells. We suggest that VCA Nb7 and VCA Nb14 bind the central (C) region of the VCA domain, where they do not disturb the Arp2/3 interaction that much, but more specifically affect Arp2/3 activation. Because VCA Nb2 and VCA Nb13 do not show an effect on overall degradation, we hypothesize

that the interference with the acidic (A) part of the VCA domain is enough to significantly reduce the number of invadopodia but not sufficient to show effects in the following degradation step.

After invadopodium maturation, matrix remodelling will follow. Our results revealed that VCA Nb7 and 14 were able to significantly reduce the overall degradation (Figure 38). Presumably, these nanobodies lead to invadopodia that are defective in protrusion through interfering with N-WASp - Arp2/3 interaction. When there are less protrusive invadopodia, the overall degrading properties of cells will decrease because actin polymerisation is what drives invadopodium growth through the matrix, followed by matrix degradation.

The properties of N-WASp in this pathway may also be related to the transportation of vesicles[356-358]. To elicit matrix degradation, the MMPs must traverse the invadopodium to the extracellular space, where they can exert their function[358]. N-WASp is expected to activate actin polymerisation via Arp2/3 to form actin comet tails at vesicles[356, 358]. This will give a propelling force to enhance the movement of these vesicles through an invadopodium[357, 358]. To study this further, we analysed MMP9 secretion and activity in VCA nanobody expressing cancer cells. However, in PC-3 cells no effects were found (Figure 39). This is contrary to what we observed for cortactin[48]. Indeed, cortactin nanobodies targeting its C-terminal SH3 or the N-terminal NTA domains significantly reduced MMP9 secretion and activity. FasNb5 however, which blocks the actin bundling activity of the actin bundling protein fascin that is also present in invadopodia, did not[45, 48]. Alternatively, the degrading properties of N-WASp can be attributed to MT1-MMP as suggested previously[344]. Yu *et al.* concluded that N-WASp plays a role in matrix degradation by optimising the organisation and positioning of MT1-MMP, the master switch of other MMPs. At the cytoplasmic tail of MT1-MMP, N-WASp creates an actin network to specifically stabilize MT1-MMP to increase the effectiveness of degradation[344]. Moreover, no difference in MT1-MMP localisation was observed in HNSCC61 cells (Figure 40). Currently, we suggest that the reduction in overall matrix degradation is due to the reduction in Arp2/3 complex binding to N-WASp leading to defective invadopodia. When the VCA Nbs reduce the number of invadopodia per cell, the overall degradation properties will also be lower per cell. Less invadopodia implies less available MT1-MMP (enriched in invadopodia) for degradation. We therefore propose that the effect of N-WASp in matrix remodelling is caused by its regulation of invadopodium formation.

Recently, Fulcher *et al.* succeeded in eradicating endogenous proteins via the proteasome degradation pathway using nanobodies and monobodies[105]. If this approach

proves to be efficient for a broad variety of targets (providing that a nano/monobody can be generated or is available), it would be an important new tool to study protein function, one that parallels the advent of RNAi in mammalian cells nearly two decades ago[416]. In this respect, Shaefer *et al.* very recently demonstrated that CRISPR/Cas9 genome editing can trigger hundreds of unintended mutations and deletions in the genome[417]. It is therefore incumbent to continue developing new methodologies aimed at studying protein function in cells and organisms and we expect that proteasome-induced protein knock out represents a valuable and important new technological approach towards this end.

In conclusion, nanobodies against the VCA domain of N-WASp affect invadopodium formation and overall matrix degradation, most likely via regulation of N-WASp – Arp2/3 complex interaction, indicating that this region of N-WASp critically contributes to these processes.

5.2.5 Materials and methods

5.2.5.1 Antibodies and reagents

Rabbit polyclonal anti-N-WASp (H100) was obtained from Sigma (St. Louis, MO, USA) and Santa Cruz Biotechnology (Santa Cruz, CA, USA). Mouse monoclonal anti-actin clone C4 (0869100) was obtained from MP Biomedicals (Santa Ana, CA, USA). Rabbit monoclonal anti-ARPC2 antibody (ab133315) and anti-MMP14 (ab51074) were obtained from Abcam (Cambridge, UK). Rabbit monoclonal anti-MMP9 was obtained from Epitomics (Burlingame, CA, USA). Alexa Fluor-labeled secondary goat anti-rabbit or anti-mouse IgG antibodies were obtained from Molecular Probes (Eugene, OR, USA). Mouse monoclonal anti-V5 antibody, Alexa Fluor labeled phalloidin and MitoTracker Orange were purchased from Invitrogen (Merelbeke, Belgium). The synthetic VCA – hN-WASp peptide biotin-Ahx-^{420}KKVEQNSRPVSCSGRDALLDQIRQGIQLKSVADGQESTPPTPAPTSGIVGALMEVMQKRSKAIHS SDEDEDEDDEEDFEDDDEWED^{505}-NH_2, used for raising nanobodies (see further), was chemically synthesized by Caslo (Denmark).

5.2.5.2 Generation of VCA Nbs

Nbs were obtained in collaboration with the Vlaams Instituut voor Biotechnologie (VIB) Nanobody Service Facility (NSF). All animal work was performed by the VIB NSF and has PHS approved animal welfare assurance from OLAW (F16-00131(A5593-01)). Briefly, two alpacas were immunized by a subcutaneous injection of human VCA-N-WASp peptide on days 0, 7, 14, 21, 28 and 35. On day 39, anticoagulated blood was collected for

lymphocyte preparation. A nanobody library was constructed by extracting total RNA from peripheral blood lymphocytes and screened for the presence of antigen-specific nanobodies. The obtained Nbs were subcloned into the phagemid vector pMECS. In order to isolate N-WASp nanobodies, several rounds of phage panning were performed. These experiments suggested that the phage population was enriched for antigen-specific phages from round 3 panning onwards. In total, 380 colonies from 3rd and 4th rounds were randomly selected and analyzed by ELISA for the presence of antigen-specific nanobodies in their periplasmic extracts. The positives ones were sequenced. Based on those sequence data, the positive colonies represented 5 different groups of nanobodies in each of the two alpacas.

5.2.5.3 cDNA cloning

Nbs were cloned into mitochondrial outer membrane (MOM) V5 pcDNA3.1 His_6 and pEGFP-N1 vectors (Clontech, Mountain View, CA, USA), as described before[45, 406, 418]. The nanobodies were subcloned by means of a Cold Fusion Cloning Kit (System Biosciences, Mountain View, CA, USA). The first subcloning was performed into V5 pcDNA3.1 His_6 vector by using the following primers: forward 5'-TCGATTCTACGCGTACCGGTGCCCAGGT GCAGCTGCAGGAG-3' and reverse 5'-GGTGATGATGACCGGCTAGCTGGAGACGGTGACCTG-3'. Cloning of the Nbs in the pEGFP-N1 vector was done using the following primers: forward 5'-CGAGCTCAAGCTTCGGCCACCATGCAGGTGCAGCTGCAGGAG-3' and reverse 5'-GGCGACCGGTGGATCCTTGCTGGAGACGGTGACCTG-3'.

To obtain inducible Nb expressing cells, a third cloning of the EGFP-tagged VCA Nbs into the pLVX-TP vector (Clontech) was done using following primers: Forward 5'-TGGAGAAG GATCCGCGGCCGCGCCACCATGGCCCAGGTGCAGCTGCAGGAGTCTGGG-3' and reverse 5'-CTACCCGGTAGAATTCTTACTTGTACAGCTCGTCCATGCC-3'.

5.2.5.4 Recombinant nanobody and N-WASp production

BL21 cells were transformed with VCA Nbs in pMECS vector or N-WASp in pTrcHis TOPO. They were grown in TB (with 100 µg/ml ampicillin) at 37 °C. After induction with 1 mM IPTG, incubation was performed at 28 °C (overnight for nanobody production or 4 h for N-WASp production).

Nanobodies were extracted from the periplasm, where they are located due to an N-terminal PelB signal, by means of an osmotic burst of the outer membrane using TES buffer (0.2 M Tris, 0.5 mM EDTA, 0.5 M sucrose, pH 8.0). Next an IMAC and/or gel filtration was performed for a higher purification, as described before[47].

To extract recombinant N-WASp, pelleted cells were dissolved in lysis buffer (1% Triton, 20 mM Tris-HCl, 150 mM NaCl, 1 mM PMSF and 1 mM protease inhibitor, pH 7.5) supplemented with 200 µg/ml lysozyme and incubated during 30 min at room temperature. After sonication and pelleting, IMAC purification was performed.

5.2.5.5 Cell culture, transfection and transduction

MDA-MB-231 (ATCC HTB-26), PC-3 (ATCC CRL-1435) and HEK293T (ATCC CRL-11268) cells were maintained at 37 °C in a humidified 10% CO_2 incubator, HNSCC61 cells were grown at 5% CO_2. All cells (except PC-3) were grown in DMEM. We obtained the HNSCC61 cells from Prof. Dr. Weaver[419] (Vanderbilt University) in August 2011, who obtained the cells from Prof. Dr. Yarbrough[420-422]. PC-3 cells were grown in RPMI. All media (from Gibco Life Technologies (Grand Island, NY, USA) were supplemented with 10% foetal bovine serum, 10 µg/mL streptomycin and 10 IU/mL penicillin. As an exception, HNSCC61 required 20% fetal bovine serum and an extra addition of 0.4 µg/mL hydrocortisone (Sigma-Aldrich, St. Louis, MO, USA).

JetPrime (Polyplus Transfection Inc., New York, NY, USA) was used to perform transient expression according to the manufacturer's protocol. For virus production HEK293T cells were transfected using the calcium phosphate method as described before[45]. Inducible stable cell lines were obtained by transduction of the VCA Nbs in the pLVXTP vector, making use of the Lenti-X Tet-On advanced system (Clontech, Mountain View, CA, USA) according to the manufacturer's protocol. Expression was induced by addition of 500 ng/mL doxycycline.

5.2.5.6 Pull down assays, immunoprecipitations and binding assay

Cells were lysed with ice-cold lysis buffer (1% Triton, 20 mM Tris-HCl, 150 mM NaCl, 1 mM PMSF and 1 mM protease inhibitor, pH 7.5)[406]. Protein concentrations were determined using the Bradford assay (Bio-Rad Laboratories, Hercules, CA, USA).

In the pull down assays to analyse binding between N-WASp and the 10 VCA Nbs, recombinant HA-tagged nanobodies were immobilized onto HA-agarose beads (Sigma-Aldrich, St. Louis, MO, USA) (1.5 h at 4 °C). Next, 650 µg crude cell lysate was added and followed by incubation (1.5 h at 4 °C).

In the pull down to analyse binding between N-WASp and VCA Nbs using EGFP-tagged VCA Nb expressing cancer cells, we performed overnight incubation of cell lysate with anti-GFP antibody (at 4 °C), followed by an incubation with Protein G Sepharose beads (GE Healthcare) (1.5 h at 4 °C).

In the binding assay, recombinant HA-tagged VCA Nbs, in a concentration range, were incubated with the synthetic biotin-tagged VCA domain (1.5 h at 4 °C). Next, 550 µg crude MDA-MB-231 cell lysate was added, as source for Arp2/3 and actin, and an incubation was followed (1.5 h at 4 °C). Last, an immobilization on STREPTactin beads (IBA, Göttingen, Germany) was performed (1h at 4 °C).

After washing steps, elution of the beads was obtained by boiling for 5 minutes in Laemmli SDS sample buffer (65 mM Tris-HCl, 20% glycerol, 5% SDS, 0.2% bromophenol blue, 5% β-mercaptoethanol in Milli-Q, pH 6.8). This was followed by SDS-PAGE and Western blot analysis. The H100 N-WASp antibody from Santa Cruz Biotechnology was used to detect N-WASp on blot.

5.2.5.7 Isothermal titration calorimetry

Isothermal titration calorimetry (ITC) was performed as described before[45, 47, 406]. Binding of VCA Nbs to VCA peptide was measured by ITC using a MicroCal VP-ITC MicroCalorimeter and MICROCAL ORIGIN software (Malvern Instruments Ltd, Malvern, UK). The recombinant VCA Nbs were dialyzed against 20 mM Tris buffer and 150 mM NaCl at pH 7,5. Briefly, 8,6 µM biotinylated VCA peptide was titrated once with 108 µM VCA Nb7 and once with 88 µM VCA Nb14. 46,91 µM VCA Nb2 and 5,6 µM VCA Nb13 was titrated with 46,91 µM and 56 µM biotinylated VCA peptide, respectively. The obtained values are expressed with the standard deviation.

5.2.5.8 Immunofluorescence and microscopy

Cells were seeded on a 100 µg/ml gelatin (Sigma-Aldrich, St. Louis, MO, USA) or 50 µg/ml rat tail type I collagen (BD Biosciences, Franklin Lakes, NJ, USA) coated coverslip. Cells were fixed using 3% paraformaldehyde, permeabilized using 0.1% Triton for 5 min and neutralized in 0.75% glycin for 20 min. Next, a blocking step was performed using 1% bovine serum albumin (Sigma-Aldrich), followed by an incubation with primary antibodies (1 h at 37 °C) and Alexa Fluor-conjugated secondary antibodies (30 min at room temperature). DAPI (0.4 µg/ml; Sigma) and Alexa Fluor labeled phalloidin (Invitrogen) were used to stain nuclei and actin filaments, respectively. Cells were mounted using VectaShield (Vector Laboratories, Burlingame, CA, USA). For imaging, a Zeiss Axiovert 200 M Apotome epifluorescence microscope equipped with a cooled CCD Axiocam camera (Zeiss x63 1.4-NA Oil Plan-Apochromat objective; Carl Zeiss, Oberkochen, Germany) and Axiovision 4.5 software (Zeiss) was used at room temperature.

5.2.5.9 Matrix degradation

In matrix degradation assays, coverslips were coated with Cy3-labeled gelatin according to the manufacturer's protocol (QCM Gelatin Invadopodia Kit, Millipore, Billerica, MA, USA). 24h after induction with doxycycline, cells were seeded and allowed to degrade the matrix for another 24h. Degradation is found on the places where black holes were present in the matrix underneath the cells. Two parameters were used to analyze the degradation. The parameter 'degraded area per cell area' was obtained by dividing the total degraded area by the total cell area per picture. The second parameter 'degradation area per cell' is determined by the total degradation area divided by the amount of cells per picture.

5.2.5.10 Gelatin zymography

24 h after induction with 500 ng/ml doxycycline, cells were seeded in a 1 mg/ml collagen matrix which was allowed to polymerize for 1 h at 37 °C. After approximately 20 h incubation in serum-free medium, equal amounts of conditioned medium proteins were analyzed on 10% SDS-PAGE without (for secretion levels) or with 0.1% gelatin (for activity). In the SDS-PAGE containing 0.1% gelatin, proteins were enabled to renature by removing SDS with 2% Triton X-100 washing buffer. To analyse the activity, digestion was allowed during an overnight incubation in MMP buffer (50 mM Tris and 10 mM $CaCl_2$, pH 7.5). Band intensities were analyzed with ImageJ.

5.2.5.11 MT1-MMP localization

Nanobody expression was induced 24 h before cells were seeded on a 100 µg/ml gelatin matrix. They were fixed, stained and imaged as described above. MT1-MMP containing invadopodia were count when MT1-MMP dots were overlapping F-actin dots. To analyse MT1-MMP, the amount MT1-MMP containing invadopodia was divided by the total amount of invadopodia for each cell.

5.2.5.12 Image and statistical analysis

Image analysis (protein intensities, intensity profiles, quantifications) was performed with ImageJ (National Institutes of Health, Bethesda, MD, USA). Statistical analysis was performed with GraphPad Prism (GraphPad Software Inc., San Diego, CA, USA) using Kruskal-Wallis test and Dunns post tests with p=0.05. Bar plots were made using mean and SEM.

5.2.6 Acknowledgments

This work was supported by grants from the Research Foundation Flanders (Fonds Wetenschappelijk Onderzoek (FWO) Vlaanderen) and Ghent University (BOF13/GOA/010). T.H. is supported by Ghent University (BOF PhD fellowship) and an Emmanuel van der Schueren grant of the Flemish League against Cancer (VLK). A.V. is supported by the Agency for Innovation by Science and Technology in Flanders (IWT). I.V.A. is supported by the Research Foundation Flanders (Fonds Wetenschappelijk Onderzoek (FWO) Vlaanderen).

The authors thank Dr. Gholamreza Hassanzadeh-Ghassabeh (Nanobody Service Facility, Vlaams Instituut voor Biotechnologie (VIB), Brussels, Belgium) for the generation and isolation of VCA-specific nanobodies. We thank Dr. A. Weaver (Department of Cancer Biology, Vanderbilt University Medical Center, Nashville, TN) for the gift of HNSCC61 cells, Prof. Dr. Marc Bracke (Experimental Cancer Research, Ghent University, Belgium) for the gift of MDA-MB-231 cells and Prof. Dr. Sven Eyckerman (VIB-UGent Center for Medical Biotechnology, Ghent University, Belgium) for the gift of HEK293T cells.

Chapter 6

Nanobody click chemistry for convenient site specific fluorescent labelling, single step immunocytochemistry and delivery into living cells by photoporation and live cell imaging

Tim Hebbrecht[a], Jing Liu[b], Olivier Zwaenepoel[a], Gaëlle Boddin[a], Chloé Van Leene[a], Klaas Decoene[c], Annemieke Madder[c], Kevin Braeckmans[b, d] and Jan Gettemans[a]

6.1 Introduction

In this chapter, we intended to obtain fluorescent and site specifically labelled nanobodies for microscopic use. The strategy uses the Cu-dependent chemical reaction, the Cu(I)-catalyzed Azide-Alkyne Click Chemistry (CuAAC) or click chemistry. This reaction requires an alkyne and an azide moiety[423-425]. However, these are not naturally occurring

[a] Department of Biomolecular Medicine, Faculty of Medicine and Health Sciences, Ghent University, Ghent B-9000, Belgium
[b] Laboratory of General Biochemistry and Physical Pharmacy, Department of Pharmaceutics, Faculty of Pharmaceutical Sciences, Ghent University, Ghent B-9000, Belgium
[c] Department of Organic and Macromolecular Chemistry, Faculty of Sciences, Ghent University, Ghent B-9000, Belgium
[d] Center for Advanced Light Microscopy, Ghent University, Ghent B-9000, Belgium

in a nanobody or any other protein. To incorporate such a chemically reactive group, two methods were used. While in the first strategy an alkyne bearing peptide was ligated to the nanobody through an enzymatic sortase reaction, the second method was based on genetic engineering of the nanobody to allow incorporating of a non-canonical amino acid which contains an azide moiety. Afterwards, the CuAAC reaction covalently coupled an AlexaFluor488 to the nanobody.

Once fluorescent labelled nanobodies (or fluobodies) were obtained, they could be used to visualize their target. The original goal was to use those fluorescent nanobodies in a conventional immunocytochemistry protocol. Because the nanobodies contain a fluorophore, such a staining procedure is reduced to a single-step immunocytochemistry. In this study, two nanobodies were used. The first is a nanobody against the SH3 domain of cortactin[45]. Cortactin assists the actin polymerisation process, plays a role in the invadopodium dynamics and stabilizes actin filaments[48, 329]. The second nanobody targets the C-terminal part of β-catenin. β-Catenin is a structural protein in adherens junctions and has a role as transcriptional activator in the Wnt signal transduction pathway[426, 427].

Special attention has to go to the fixation and/or permeabilisation of cells, since this can cause loss of antibody (here: nanobody) immunoreactivity to its target[163]. In this study, a solution is proposed by using the photoporation technique to deliver recombinant fluorescent nanobodies in living cells[69, 73]. This allows the nanobody to bind its target in its native conditions prior to fixation and permeabilisation. The positive effect of this approach is clearly shown using β-catenin Nb86.

6.2 **Research paper**

The paper[428] is published in New Biotechnology after a peer revision on June, 2020.

6.2.1 Abstract

While conventional antibodies have been an instrument of choice in immunocytochemistry for some time, their small counterparts known as nanobodies have been much less frequently used for this purpose. In this study we took advantage of the availability of nanobody cDNAs to site-specifically introduce a non-standard amino acid carrying an azide/alkyne moiety, allowing subsequent Cu(I)-catalyzed Azide-Alkyne

Click Chemistry (CuAAC). This generated a fluorescently labelled nanobody that can be used in single step immunocytochemistry as compared to conventional two step immunocytochemistry. Two strategies were explored to fluorescently label nanobodies with Alexa Fluor 488. The first method involved enzymatic addition of an alkyne containing peptide to nanobodies using sortase A, while the second consisted of incorporating para-azido phenylalanine at the nanobody C-terminus. Through these approaches, the fluorophore was covalently and site-specifically attached. It was demonstrated that cortactin and β-catenin, cytoskeletal and adherens junction proteins respectively, can be imaged in cells in this manner through single step immunocytochemistry. However, fixation and permeabilisation of cells can alter native protein structure and form a dense cross-linked protein network, encumbering antibody binding. It is shown that photoporation prior to fixation not only allows delivery of nanobodies into living cells, but also facilitates β-catenin Nb86 imaging of its target, which was not possible in fixed cells. Pharmacological inhibitors are lacking for many non-enzymatic proteins, and it is therefore expected that new biological information will be obtained through photoporation of fluorescent nanobodies which allows the study of short term effects, independent of gene-dependent (intrabody) expression.

6.2.2 Introduction

An important aspect of cell biology is visualization of proteins of interest at high resolution. Not only does visualization help in comprehending results more intuitively, it also results in a primary source of data available for analysis and interpretation[163]. The most commonly used techniques for imaging of biomolecules are immunofluorescence assays using a primary and secondary antibody or fusions with a fluorescent protein. Nanobodies can simplify this process. They are single-domain antibody fragments originating from the variable part of the heavy chain of camelid heavy chain antibodies (VHH)[16]. A nanobody is the smallest, natural antigen-binding fragment that retains its original affinity and specificity[16, 17]. Because of its small size (2.5 nm diameter and 4 nm height[429]), the 'linkage error' (space between the dye and the protein) will be reduced 4-7-fold compared to the use of conventional antibodies. Nanobodies are easier to manipulate because their cDNAs are available, allowing site-specific derivatization. REFERENCE Previously, different routes to link small fluorophores to nanobodies have been tested, e.g. N-hydroxysuccinimide (NHS) chemistry has been used to covalently link a small fluorophore to a nanobody[178]. However, random labelling of lysine residues is difficult to avoid (including in CDR regions), resulting in heterogeneously labelled nanobodies[430]. Alternatively, the use of maleimide chemistry requires unpaired

cysteines, with problems of dimerization or irreversible unfolding of the nanobody due to harsh reaction conditions[179].

In this study, we present an alternative nanobody labelling approach that circumvents these problems. We here demonstrate site specific covalent labelling of nanobodies with a fluorophore through click chemistry reaction. The reactive alkyne or azido group is introduced at the C-terminus of a nanobody in a sortase A mediated manner (enzymatic) (Figure 41A) or by modifying the nanobody cDNA sequence at the 3' end (non-enzymatic), thus encoding a non-standard para-azido phenylalanine (pAzF) residue at the carboxy terminus of the nanobody primary structure (Figure 41B).

Nanobodies labelled in this fashion can be used for immunocytochemistry, as demonstrated here by specifically targeting cortactin and β-catenin in cells with nanobodies raised against the respective proteins. Because the nanobodies contain a dye, such a staining procedure is time beneficial since it is reduced to a single step. It is further shown that photoporation is an efficient and convenient way to circumvent problems related with immunocytochemistry when the epitope is occluded in a dense and inaccessible cross-linked protein network, due to chemical permeabilization and fixation. Photoporation is a laser-induced transfection-type approach to overcome the cell membrane barrier for delivery of biomolecules (including nanobodies) into living cells[67, 431]. Since nanobodies are the small counterpart of antibodies, it is easier to insert them through the membrane barrier. This photoporation strategy allows live cell labelling with exogenous labels that can be used for microscopic analysis and in vivo imaging[67, 431]. Through this approach, the nanobody can bind its target under native conditions before the cells are fixed. In addition, direct delivery of a (fluorescent) nanobody into the cytoplasm creates the possibility of studying short term effects on target perturbation, whereas intrabody expression is dependent on a relatively slow process of gene expression after transfection or transduction of DNA.

6.2.3 Results

Prior to subsequent derivatization with organic compounds or larger moieties, introduction of new functional groups into a nanobody is preferably at the C-terminus, to avoid interference with the binding capacity of the nanobody to its target[432]. Two different strategies leading to a nanobody carrying a C-terminal azido or alkyne group were exploited: an enzymatic sortase ligation procedure (Figure 41A) or incorporation of a non-canonical amino acid directly into the encoding sequence of the nanobody (Figure 41B). (For more experimental detail, see 6.2.6 Supplementary information.) Once the

nanobody contains such a group, it can be used in a CuAAC click reaction to covalently add a moiety of interest to the nanobody.

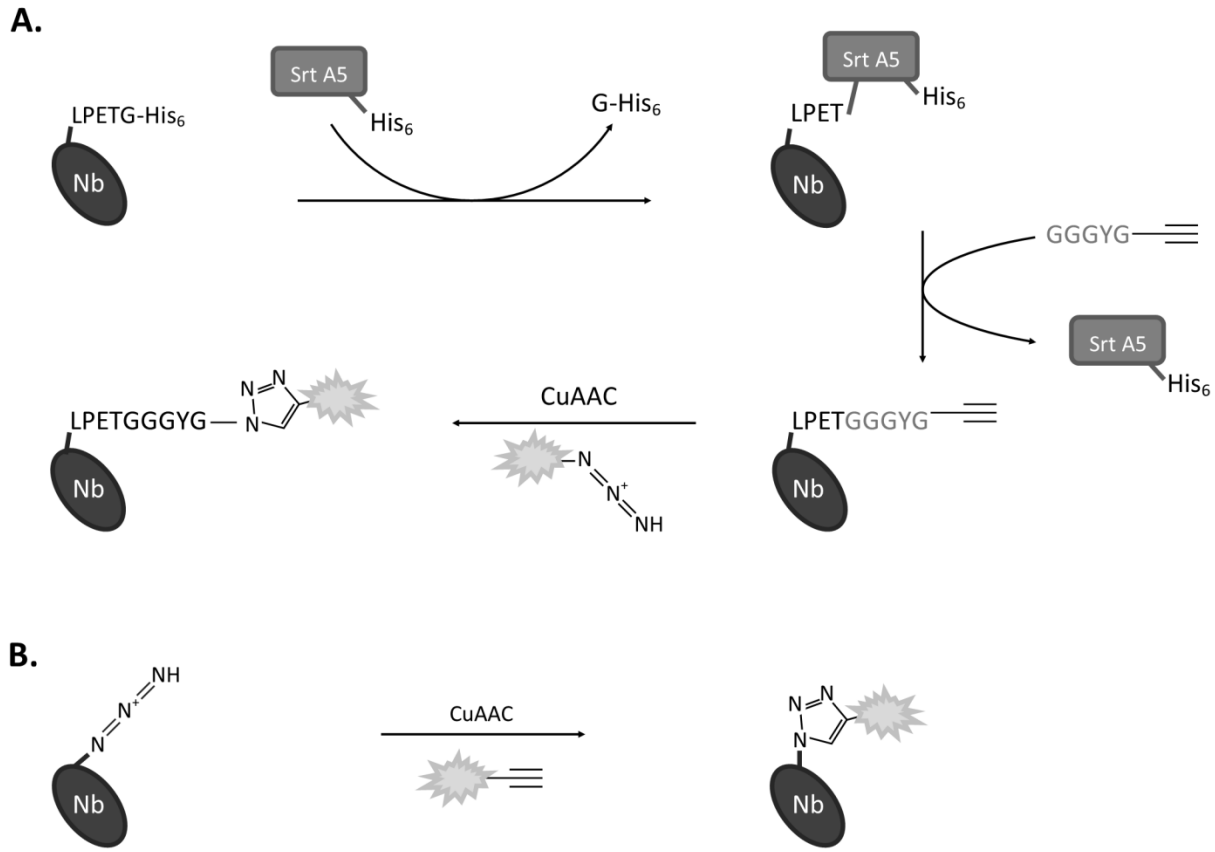

Figure 41: Schematic visualization of labelling strategies in this study. (**A**) Schematic visualization of the enzymatic SrtA labelling process, a recombinant nanobody containing the sortag (LPETG), is coupled to a peptide with an alkyne. Then, CuAAC can be completed to obtain a labelled nanobody. (**B**) Schematic visualization of the labelling process via a pAzF incorporation into the recombinant nanobody by using CuAAC.

6.2.3.1 CuAAC reaction

The test CuAAC reaction was performed on cortactin Nb2[45, 46, 48, 433], a nanobody that interacts with the cortactin SH3 domain. (For additional information about the test experiment, see 6.2.6 Supplementary information). Alexa Fluor 488 (AF488) was chosen in these test experiments, as a bright and commonly used fluorophore known to be stable for longer time periods and available with both the azide or alkyne reactive moieties. Figure 42A shows the result of the CuAAC reaction when the purified alkyne-nanobody was used directly after the sortase reaction. Because the sortase reaction buffer (50 mM Tris-HCl, 150 mM NaCl, 10 mM CaCl2) contained a high concentration of Cl^- ions, it was possible that the CuAAC reaction was suboptimal[424]. By changing the buffer to 10 mM HEPES, the reaction proved to be more efficient (Figure 42B), confirming previous observations that a lower concentration or absence of Cl^- ions is preferable for the CuAAC reaction[434, 435], since high Cl^- ion concentrations compete for copper, leading to lower efficiency[434]. Regarding the buffer effect, the range of THPTA

and sodium ascorbate can be adjusted according to[436]. The experiment was further optimized by comparing the effect of both compounds on the click reaction. The CuAAC reaction was performed once with the initial concentrations (Buffer 1 in Table 2), once with elevated THPTA (Buffer 2 in Table 2) and once with elevated sodium ascorbate (Buffer 3 in Table 2). The addition of sodium ascorbate showed the greatest impact on the CuAAC reaction as shown in Figure 42C. From these experiments, a low concentration of THPTA and increased sodium ascorbate was the best choice. Since sodium ascorbate reduces the Cu(II) to Cu(I), using a higher concentration of sodium ascorbate and lower concentrations of THPTA created a higher risk of hydrolysis due to radicals and/or peroxides as noted in[437, 438]. The selected concentrations for the CuAAC were set at 0.1 mM $CuSO_4$, 1 mM THTPA and 7.5 mM sodium ascorbate.

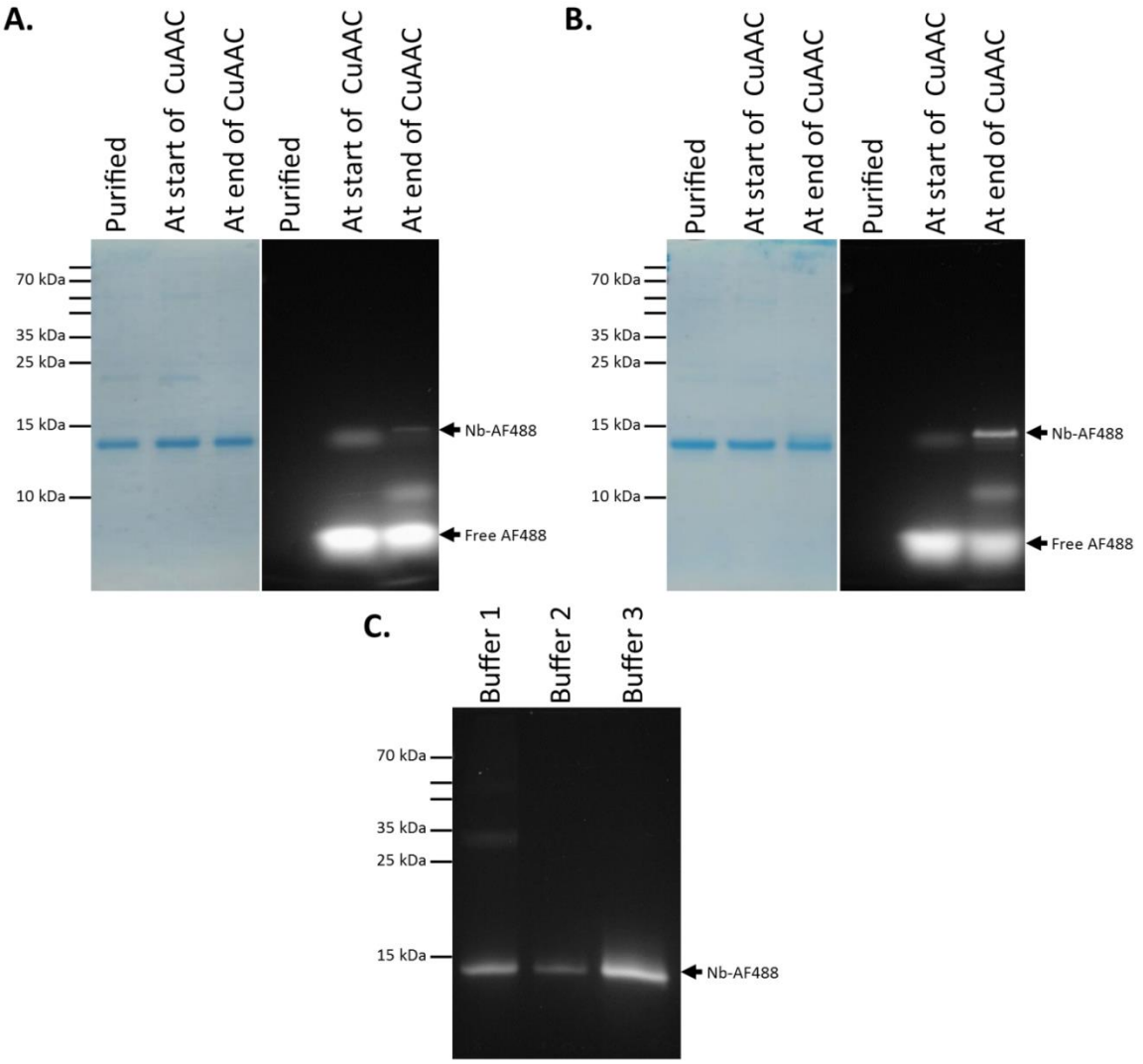

Figure 42: Optimization of the labelling of cortactin nanobody 2 - sortag. CuAAC labelling was less efficient when the sortase reaction mixture was used directly for CuAAC (**A**) compared to dialysis into HEPES buffer before the CuAAC reaction (**B**). These results were obtained by using the buffer 1 composition (Table 2). Each lane corresponds to 6 µl of the CuAAC reaction mixture. The lowest fluorescent band is free labelled peptide/free fluorophore. (**C**) Elevated levels of THPTA (Buffer 2 (Table 2)) or Na Ascorbate (Buffer 3 (Table 2)): only an elevated Na Ascorbate concentration showed better labelling efficiency compared to the initial test reaction (Buffer 1 (Table 2)). Each lane corresponds to 6 µl of the CuAAC reaction mixture.

Table 2: Buffer composition overview. Buffer 1-3 were used to determine optimal buffer concentrations for the CuAAC reaction for nanobody labelling.

Buffer 1	Buffer 2	Buffer 3
10 mM HEPES-NaOH	10 mM HEPES-NaOH	10 mM HEPES-NaOH
0.1 mM $CuSO_4$	0.1 mM $CuSO_4$	0.1 mM $CuSO_4$
0.5 mM THPTA	2.5 mM THPTA	0.5 mM THPTA
5 mM sodium ascorbate	5 mM sodium ascorbate	10 mM sodium ascorbate
pH 7.4	pH 7.4	pH 7.4

To monitor the optimal duration of the CuAAC reaction, a sample was taken after 0, 5, 15, 20, 30, 45, 60 and 75 min. As show in Figure 43, the reaction proceeded very rapidly, with a fluorescent band being observed within a few minutes and most of the reaction completed after 1h.

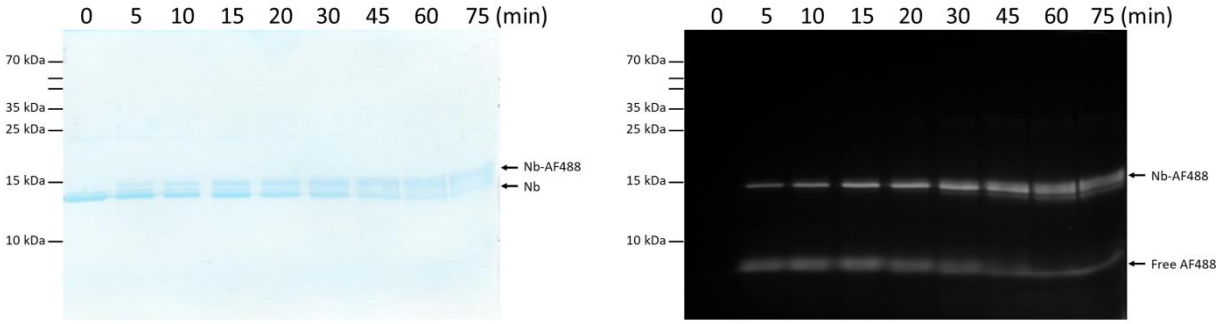

Figure 43: CuAAC reaction time course after incorporation of a para-azido phenylalanine (pAzF). After nanobody production, the nanobodies were dialysed against a HEPES buffer to remove imidazole. This was followed directly by the CuAAC reaction resulting in fluorescently labelled nanobodies. CuAAC reaction time course using cortactin Nb2-pAzF (Nb-pAzF). Coomassie stained gel on the left and corresponding fluorescent signal on the right. The reaction proceeded fast and at 45-60 minutes, saturation was reached. Each lane corresponds to 3 µl of the reaction mixture.

Eluting the nanobodies with the incorporated C-terminal pAzF directly into a compatible buffer can speed up the protocol. The standard buffer used for nanobody purifications[215, 389] contains too high a level of Cl^- ions to be followed by the CuAAC reaction; therefore others used a potassium phosphate buffer[434], or preferred a HEPES buffer[436]. Both are compatible as elution buffers and as buffers for CuAAC[434, 438]. For the elutions, there is almost no difference using those two buffers as they gave similar yield. When performing CuAAC using these two buffers, similar results were found as shown in Figure 44. As precipitate was observed in some cases after the CuAAC using the potassium phosphate buffer, HEPES was preferred as elution buffer during IMAC purification and as buffer in CuAAC reaction. After CuAAC, an Amicon Ultra-0.5 Centrifugal Filter Unit was used to remove copper ions. This step decreases free AF488, as can be observed in

Figure 44. In a final step, free fluorophore was removed by size exclusion chromatography (SEC) using a PD Spintrap™ G-25.

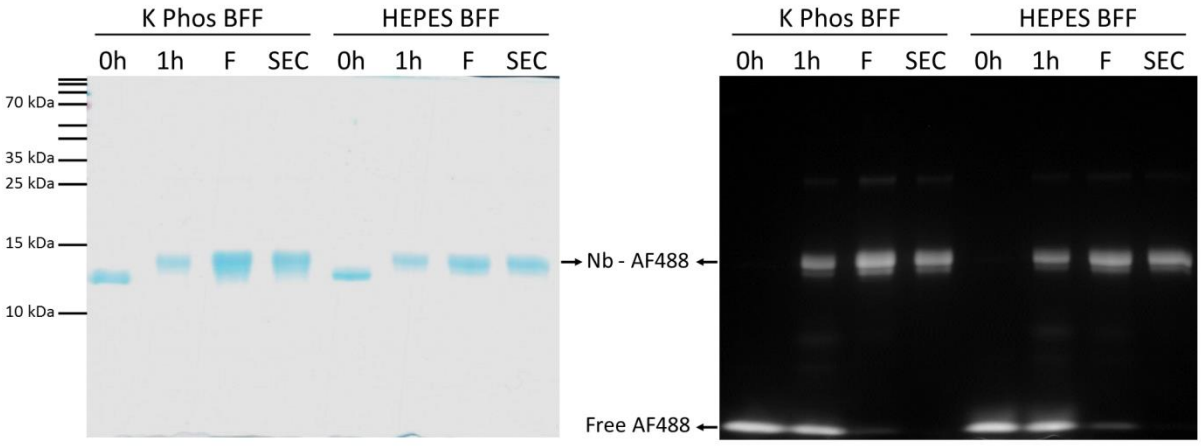

Figure 44: Purifying Alexa Fluor 488-labeled nanobody. Comparison between CuAAC after using different elution buffers for β-catenin Nb77 (K Phos BFF = potassium phosphate elution buffer, HEPES BFF = HEPES elution buffer). CuAAC was performed for 1h (0h = before CuAAC reaction, 1h = after CuAAC reaction) followed by the removal of copper using an amicon centrifugal filter device (F) and the removal of free AF488 through SEC (PD Spintrap™ G-25). Free AF488 was efficiently removed. (Each lane was loaded with 3 µl of the mixture, making the bands not entirely quantitative due to differences in elution volume.)

To compare the sortase A strategy to the incorporation of pAzF, the quantities of labelled nanobody per L bacterial growth culture is reported in Table 3 and Table 4. The efficiency of each step was similar, but the SrtA method required one additional step (the enzymatic sortase reaction followed by the CuAAC) than the pAzF incorporation method (only CuAAC). The extra step caused a higher reduction in yield compared to the pAzF method.

Table 3: Quantification of purified nanobody obtained per L of bacterial culture via the sortase A labeling method. (*Cortactin nanobody 2 expresses significantly below average compared to other nanobodies.)

Nanobody yield through the sortase A method			
Nanobody	**After production**	**After sortase reaction**	**After CuAAC**
Cortactin Nb2*	1.7 mg Nb / L culture	0.8 mg Nb / L culture	0.2 mg Nb / L culture

Table 4: Quantification of purified nanobody obtained per L of bacterial culture following pAzF incorporation method. (*Cortactin nanobody 2 expresses significantly below average compared to other nanobodies.)

Nanobody yield through the pAzF incorporation method		
Nanobody	**After production**	**After CuAAC**
Cortactin Nb2*	1,4 mg Nb / L culture	0,7 mg Nb / L culture
B-catenin Nb77	13,9 mg Nb / L culture	9,1 mg Nb / L culture
B-catenin Nb86	8,9 mg Nb / L culture	5,6 mg Nb / L culture

6.2.3.2 Single step immunocytochemistry with click chemistry labelled cortactin and β-catenin nanobodies.

Fluorescent nanobodies were next used in immunocytochemistry. The first experiments were performed on 4% PFA fixed head and neck squamous cell carcinoma cells (HNSCC61). The nanobody concentrations used for staining ranged from 1-10 µg/ml, similar to the use of conventional antibodies and to previous instances when nanobody staining has been performed[95, 189, 439-442]. It should be noted that, unlike IgG, nanobodies are monovalent.

Cortactin is an actin cytoskeleton associated protein and assists the Arp2/3 complex in actin polymerization, which is required in a variety of processes such as invadopodium formation and cell motility[310]. Cortactin is used as marker of these cancer cell invadopodia, ventral protrusions of the plasma membrane supported by actin polymerization and which are involved in matrix degradation. The Cort Nb2 targets the SH3 domain and diminishes invadopodia numbers, matrix degradation, MMP9 secretion and the invasive capacity of MDA-MB-231 and HNSCC61 cells[45, 46, 48, 433]. When using cortactin Nb2-AF488, generated through the sortase reaction followed by CuAAC, cortactin was difficult to visualize in HNSCC61 invadopodia (Figure 45, second panel). Staining with cortactin Nb2-AF488, through labelling after the pAzF incorporation, was more successful (Figure 45, third panel). The cortactin Nb2-AF488 staining pattern at 1 µg/ml (Figure 45, third panel) was similar to a commercial cortactin antibody (anti-cortactin antibody clone 4F11) (Figure 45, top). As a control, another cortactin nanobody was used (Figure 45, bottom), namely FHP Nb11, which was generated to a cortactin fragment consisting of the F-actin, the helical and the proline rich domain[433]. FHP Nb11 did not show any co-localisation with the actin cytoskeleton in PFA fixed cells, confirming that cortactin Nb2 recognised cortactin selectively. An additional control, a dual staining of cortactin Nb2-AF488 (labelled via pAzF strategy) was performed together with the commercial antibody (Figure 46A) and showed good co-localisation between the nanobody and the antibody.

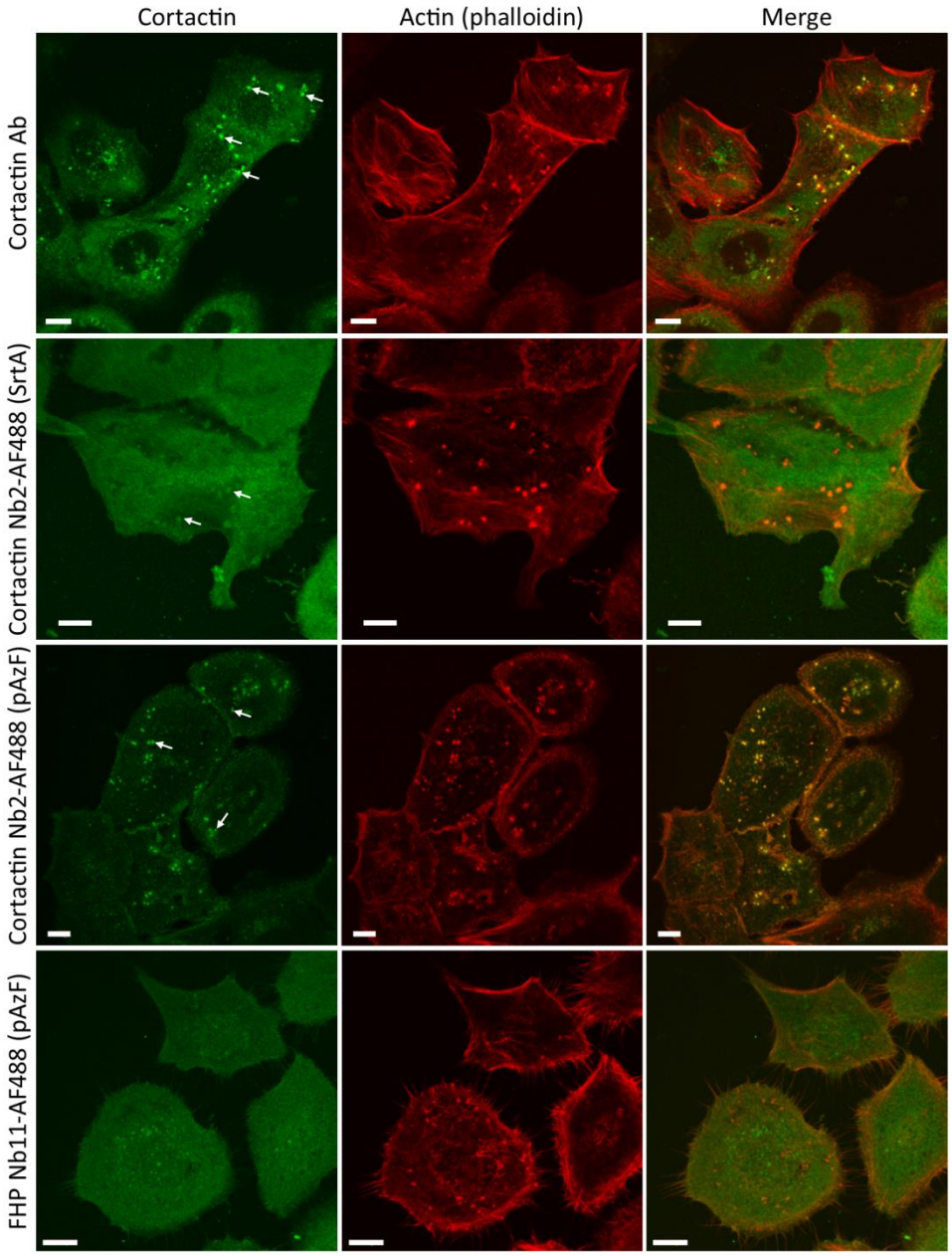

Figure 45: Comparison of cortactin staining in HNSCC61 cells. The cells were seeded on a gelatine coating. Since cortactin is a known invadopodial marker, invadopodia are visible (some are indicated by arrows). Top, cortactin was visualized by a commercial anti-cortactin Ab (a mouse monoclonal anti-cortactin antibody clone 4F11). A clear co-localisation between the antibody and invadopodia (actin rich structures) was observed. Second panel, cortactin localization using cortactin Nb2-AF488 (5 µg/ml) which was labelled through SrtA and CUAAC. Third panel, cortactin Nb2-AF488 (1 µg/ml) obtained through the incorporation of pAzF followed by CuAAC, revealed a pattern highly reminiscent of the top panel. At the bottom panel, an FHP nanobody 11, which was generated against another region of cortactin (a fragment consisting of F-actin-helical-proline rich domain of cortactin) was used as control[433] and did not show co-localisation with the actin cytoskeleton in PFA fixed cells. (Scale bar = 10 µm)

A second nanobody used used similarly was raised against human β-catenin. β-catenin Nb77 targets the C-terminal part of human β-catenin (a fragment from Ser389 to Leu781 was used for immunization). A dual staining was performed using a commercial antibody (anti-β-catenin antibody (ab32572)) and the β-catenin Nb77-AF488 (5 µg/ml), labelled via pAzF and CuAAC. β-catenin is important for cell-cell interactions and both antibody

and nanobody stained cell-cell contacts, showing similar patterns (Figure 46B), attesting to the ability of the nanobody to bind catenin in PFA fixed cells.

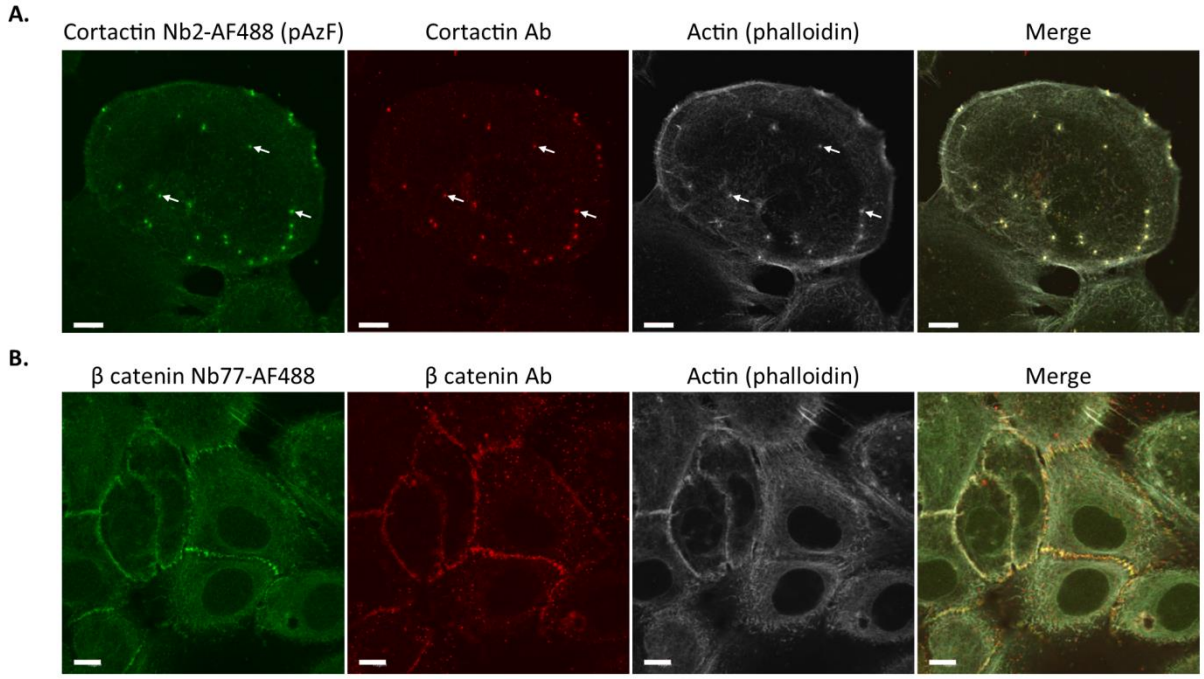

Figure 46: Dual staining using a nanobody and a commercial antibody to visualise cortactin and β-catenin in 4% PFA fixed HNSCC61 cells, seeded on collagen coating. (**A**) The imaging of cortactin by the cortactin Nb2-AF488 (1 µg/ml), labelled through the pAzF method, and a commercial antibody (a mouse monoclonal anti-cortactin clone 4F11) (red channel) showed co-localisation. As additional confirmation, the actin staining (far red channel) showed the invadopodia on the same spot. A few invadopodia arrowed. (**B**) A commercial antibody (a rabbit monoclonal anti-β-catenin antibody (ab32572)) was used to localize β-catenin (red channel) together with the AF488 labelled β-catenin Nb77 (5 µg/ml), labelled through the pAzF method. Both showed heightened intensity at the cell-cell contacts. Phalloidin was used to visualize the actin cytoskeleton (far red channel). (Scale bar = 10 µm)

6.2.3.3 Delivering a fluo-nanobody in living cells by photoporation improves the applicability of nanobodies in immunocytochemistry.

In the course of the study it became clear that not every nanobody is suitable for immunocytochemistry, which also applies to conventional antibodies. For instance, β-catenin Nb86 (another nanobody against human β-catenin obtained after immunization with the same β-catenin fragment from Ser389 to Leu781), labelled through pAzF, yielded poor results in a conventional staining protocol on permeabilized and PFA fixed cells (Figure 47A, cf. Figure 46B). With methanol fixation, β-catenin Nb86 was able to visualize β-catenin (Figure 47A, bottom). It was hypothesized that this could be due to cross-linking by para-formaldehyde and that delivery of the nanobody into living cells would allow it to bind its target under native conditions, prior to cross-linking. Crossing the plasma membrane, however, remains a major hurdle for nanobodies. A recently developed transfection technique termed photoporation has been reported to accomplish this[67]. This is an upcoming flexible and safe physical transfection method that can deliver a wide variety of molecules into a broad range of cells. Cells are first

incubated with photothermal nanoparticles, such as graphene quantum dots used here, which can bind to the cell membrane. After washing, pulsed laser irradiation is applied rendering the cell membrane temporarily permeabilized by photothermal effects induced locally by the graphene quantum dots. Compounds in the cell medium, including labelled nanobodies, can then diffuse into the cell cytoplasm until the cell membrane is resealed.

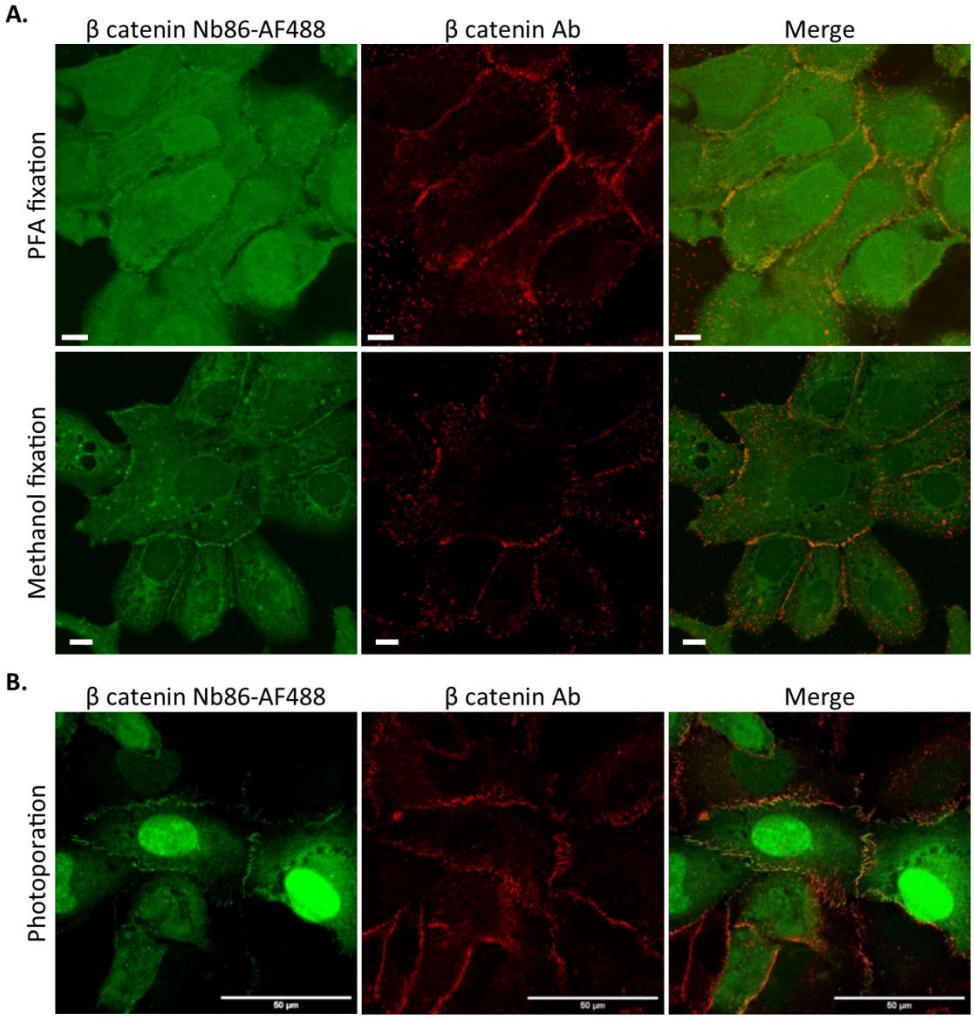

Figure 47: β-catenin visualization using β-catenin Nb86-AF488 and the commercial antibody (a rabbit monoclonal anti-β-catenin antibody (ab32572)). The nanobody was labelled through the pAzF method. (**A**) Top, the β-catenin Nb86-AF488 was used in 4% PFA fixed HNSCC61 cells in single step immunocytochemistry and did not show a specific β-catenin signal. Bottom, methanol fixation on HNSCC61 cells was performed and the same β-catenin Nb86-AF488 staining performed, showing heightened intensity at the cell-cell contacts. (Scale bar = 10 µM). (**B**) The β-cat Nb86-AF488 was photoporated into HeLa cells and then fixed. As a control, a conventional staining was performed with a commercial anti-β-catenin antibody (a rabbit monoclonal anti-β-catenin antibody (ab32572)) (in red, middle panel). (Scale bar = 50 µM)

β-catenin Nb86-AF488 was delivered into living cells by photoporation and the cells fixed thereafter. It was observed that β-catenin became clearly discernible at cell-cell contacts (Figure 47B). In a photoporation time lapse experiment, it was possible to observe β-catenin at cell-cell contacts (e.g. time frame between 5h50 and 9h35 indicated with an arrow in **Video 1**; **Video 2** is as control showing a fascin nanobody in photoporation). It was concluded that β-catenin Nb86 bound to its epitope in living cells but failed to do so

subsequent to cell fixation. Hence, photoporation may represent a new avenue for introduction of nanobodies into living cells, allowing the study of short and medium range (24h) dynamic cellular processes and the immediate effects of protein binders on their targets.

Video 1: HeLa cells photoporated with β-catenin Nb86-AF488 (labelled through the pAzF method). An image was taken every 25 min over 12h30. The arrows highlight visualization of β-catenin at cell contact site during 2 cells passing by (e.g. time frame between 5h50 and 9h35). (Scale bar = 50 μM)

Video 2: HeLa cells photoporated with fascin Nb2-AF488 (labelled through the pAzF method). An image was taken every 25 min over 12h30. Since fascin is an F-actin bundling protein, fascin Nb2-AF488 visualizes filopodia and microspikes. This video is to be considered as a control for the β-catenin Nb86-AF488 photoporation. (Scale bar = 50 μM)

In view of these findings, cortactin Nb2, similar to β-catenin Nb86, was photoporated and the cells then fixed. Phalloidin-AF647 was added to the medium in order to co-stain F-actin with cortactin in invadopodia of HNSCC61 cells. Comparison with Figure 45 shows that a slightly better contrast was obtained and that invadopodia were highlighted by photoporation of cortactin nanobody 2-AF488 and phalloidin-AF647, as well as by the commercial cortactin antibody (anti-cortactin antibody clone 4F11) (Figure 48).

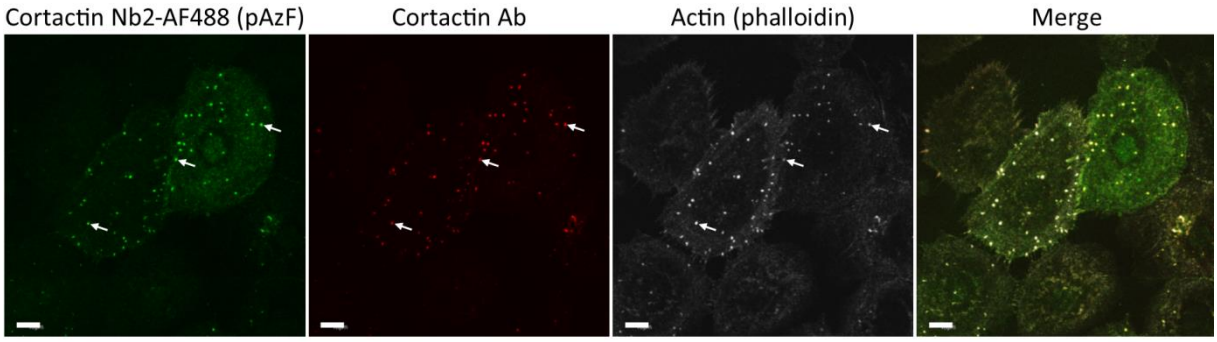

Figure 48: Cortactin Nb2 photoporation in HNSCC61 cells. A few invadopodia are arrowed. The cells were photoporated with cortactin Nb2-AF488 and phalloidin-AF647, followed by a fixation with 4% PFA and a commercial cortactin Ab staining (a mouse monoclonal anti-cortactin antibody clone 4F11). (Scale bar = 10 μM)

6.2.4 Discussion

This work compares two possibilities for incorporation of an alkyne/azido group into a nanobody, an enzymatic method in which sortase A adds an alkyne containing peptide and another in which an azido containing amino acid is incorporated at the nanobody C-terminus. The click chemistry or CuAAC reaction led to the most promising results when incorporating the unnatural para-azido Phe (pAzF) C-terminal to a nanobody. The procedure is straightforward, reliable, relatively fast and has a higher yield when start and end are taken into account. It may become broadly applicable as it can be used for

different nanobodies and coupling to a variety of moieties e.g. different fluorophores, magnetic beads, quantum dots, gold nanoparticles. The use of fluorescently-labelled nanobodies and the new avenue of introducing them into living cells by photoporation will allow study of short and medium range (24h) dynamic cellular processes targeting a broad range of proteins. Moreover, this technique reduces linkage error and will enable the imaging of endogenous proteins at higher resolution and can be of interest for super resolution microscopy. The present study used a CuAAC reaction which has the advantage of site selectivity. Unlike the maleimide method, the presence of a reactive moiety in this case depends on the incorporation of the alkyne/azido carrying amino acid through sortase or through pAzF. As there is only one sortag or one amber stop codon present, the stoichiometry is 1:1. It is known that alkyne and azido groups are highly specific towards each other and that they remain inert to other chemical groups present in proteins[443]. Hence, labelling will be near stoichiometric as only one reactive group is present on the nanobody to react in the CuAAC reaction. The method also has the advantage that no obvious decrease in yield of the purified pAzF carrying nanobody was observed compared to the unmodified nanobody or to the nanobody with sortag (which is also produced without non-natural amino acids). Recently the CuAAC reaction was used after incorporating an alkyne/azido group into a nanobody[444]. An alkyne containing peptide was employed in combination with the intein-mediated protein ligation (IPL) technique. By equipping the nanobody with a Cys residue between the nanobody and intein sequences, an N-S shift leading to a thioester linkage was facilitated. By using an alkyne bearing cysteine derivative, an on-column cleavage was performed, resulting in an alkynated nanobody.

The incorporation of an alkyne/azido group can also offer several other opportunities. Previously nanobodies have been used to couple other moieties than fluorophores. They have been coupled to quantum dots and four nanobodies were selectively conjugated onto one quantum dot[207]. This was achieved by means of sulfosuccinimidyl-4-(N-maleimidomethyl)cyclohexane-1-carboxylate which crosslinks the C-terminal Cys of the nanobody to an amino group on the quantum dots[207, 208]. Quantum dots are capable of emitting enough signal to be detected deeper in tissues than Alexa fluorophores and are therefore preferred. This can easily be performed as well using the CuAAC principle. Non-fluorescent moieties are also possible. A linear polyethylene glycol (PEG) molecule was coupled to nanobodies using maleimide chemistry in order to prolong the in vivo circulation time and to study the changes in pharmacokinetics[203]. As discussed above, biotin added to GFP nanobodies enabled immunoprecipitation of GFP fusion proteins[189]. Through maleimide chemistry, EGFR nanobodies were conjugated to liposomes in order to induce receptor internalization in cancer cells resulting in an inhibition of tumor cell

proliferation[445, 446]. As these are examples of the potential of nanobodies, these can all be obtained using the CuAAC reaction as well. The alkyne-azido functionality can be further exploited as for example in Western blotting.

Others produced a green fluorescent protein (GFP) nanobody with a C-terminal tubulin-derived recognition sequence (Tub-tag), consisting of 14 amino acids (VDSVEGEGEEEGEE)[188, 189, 430]. By using a tubulin tyrosine ligase (TTL), small unnatural tyrosine derivatives were attached to the Tub-tag[189]. The authors were able to couple a 3-formyl-L-tyrosine to a Tub-tagged anti-GFP nanobody, followed by chemical labelling with Alexa Fluor 594-hydrazide. This was further reduced to a one-step protocol using a coumarin-coupled amino acid or β-(1-azulenyl)-l-alanine[188]. However, the fluorescent substrates allowed in this one-step process are limited.

The sortase time course experiment in the present study showed reversibility of the amide-bond formation between the nanobody and GGGY-PAG peptide, resulting in a need for higher substrate concentrations[430]. Another disadvantage of sortase is that peptides used are not readily available[179]. In addition to TTL and sortase coupling, other methods include the bacterial biotin ligase (BirA) method which is limited to biotinylation[430], the use of transglutaminases to couple moieties on glutamines[198] or the lipoic acid ligase (lplA) method, which couples moieties to lysines in a lipoic acid acceptor peptide tag[447]. Others have used SrtA and butelase-1, which is believed to have a much higher turnover number compared to SrtA[448, 449].

Nanobodies are already used as a counterpart to antibodies, resulting in improved imaging resolution. NHS chemistry was employed for AF647 labelling of anti-tubulin nanobodies[164] and it was observed that the AF647-nanobody resolved microtubules much better than a conventional (directly labelled) anti-tubulin antibody using single molecule localization microscopy (SMLM). Others were able to visualize the nuclear pore complex with AF647-labelled nanobodies at high resolution using stochastic optical reconstruction microscopy (STORM) microscopy[179]. The nanobodies were labelled using both NHS and maleimide. Endogenous tubulin has been targeted with labelled nanobodies by using the DNA-PAINT (DNA point accumulation for imaging in nanoscale topography) method based on sortase coupling[450]. Thus nanobodies may further develop into excellent tools for future super resolution microscopy in which high precision and accuracy is desired. For this it is important to minimize the linkage error, a result not only of the size of the protein moiety (the nanobody) but also of the size of the fluorescent molecule. The smaller a fluorophore, the more accuracy and resolution can be gained. If resolution at the level of tens of nm is not required, GFP fusion nanobodies can nevertheless yield interesting data as shown for protein-protein interactions[108].

For entry into cells, chemical permeabilization and fixation is one method, but this kills the cells and may cause blockage of the binding site or alter protein structure[272]. Moreover, permeabilisation can also be disadvantageous as it can cause loss of proteins or even promote their relocalisation[272]. As shown in Figure 47, β-catenin Nb86 was ineffective in reaching its target in 4% PFA fixed cells, but this could be circumvented by first delivering the nanobody by photoporation. This illustrates the effect of fixation and the advantage of addressing living cells. Introduction of recombinant nanobodies into living cells, and target binding under native conditions, combined with live cell imaging, could solve problems of fixation and permeabilisation, although the delivery of proteins is challenging[272]. Coupling of cell-penetrating peptides (such as cyclic arginine-rich peptides[59] or penetratin[60, 451]) to nanobodies, transportation of nanobodies in mesoporous silica nanoparticles[65] or using an *E. coli* type III secretion system[39, 66] have been employed previously to address this issue. Another option is the use of streptolysin O to create pores into the cell membrane to allow diffusion of nanobodies from the cell medium into the cytosol[50]. Photoporation is a recent technique which has major advantages compared to other protein delivery techniques. It allows targeting of many cells (>80%), with low toxicity (< 2%) and a broad range of cells, even primary cells[67, 68, 70, 71, 74]. A comparative experiment was performed in which FITC-Dextran-10kDa was delivered into HeLa cells using photoporation or electroporation, as a standard transfection method[67]. It was observed that cell viability was higher with photoporation. Electroporation resulted in more (>90%) positive cells, but the amount of FITC-Dextran-10kDa was lower in each cell compared to photoporation. Another advantage of photoporation is the ability to use a recipient of choice and compatibility with optical microscopy, while electroporation only allows use of non-adherent cells in a specific electroporation recipient[67]. Photoporation was also compared to the commercial protein transfection (PULSin) reported to be efficient for cytosolic delivery of proteins and peptides such as antibodies and nanobodies[68]. An inhomogeneous intracellular staining pattern of histone nanobodies was observed with this method together with toxicity which was not observed when using photoporation.

In conclusion, we propose that the combination of fluorescent nanobodies and photoporation may develop into a new method for studying protein behavior and function in mammalian cells. As pharmacological inhibitors are lacking for many cytoplasmic proteins that, by virtue of their properties, do not display catalytic activity, it is expected that new biological information will be obtained through photoporation of nanobodies.

6.2.5 Material & methods

6.2.5.1 Antibodies and reagents

Rabbit monoclonal anti-β-catenin (ab32572) was obtained from Abcam (Cambridge, UK), the mouse monoclonal anti-cortactin clone 4F11 from Millipore (Billerica, MA, USA). Alexa Fluor-labelled secondary goat anti-rabbit or anti-mouse IgG antibodies were obtained from Molecular Probes (Eugene, OR, USA). Alexa Fluor-labelled phalloidin was from Invitrogen (Merelbeke, Belgium). The synthetic peptide GGGY-propargylglycine (GGGY-PAG) was chemically synthesized by Peptide Specialty Laboratories GmbH (Heidelberg, Germany). pEVOL-pAzF was a gift from Prof. Dr. Peter Schultz (Scripps Research Institute, Cincinnati, OH, USA) (Addgene plasmid #31186; http://n2t.net/addgene:31186; RRID:Addgene_31186)[225]. Sortase A pentamutant in pET29 was a gift from Prof. Dr. David Liu (Harvard University, Cambridge, MA, USA) (Addgene plasmid #75144; http://n2t.net/addgene:75144; RRID:Addgene_75144)[452].

6.2.5.2 cDNA cloning

Nanobodies were cloned into a pMECS or pHEN6 vector, as described before[47, 215]. The nanobodies were subcloned by means of a Cold Fusion Cloning Kit (System Biosciences, Mountain View, CA, USA). To add the sortag to a nanobody, the first subcloning was performed into pMECS vector by using the following primers: forward 5'-GATGTGCAGCT GCAGGAGTCTGGAGGAGG-3' and reverse 5'-CTAGTGCGGCCGCGCCACCGGTTTCCGGAAGC GCGCTGCCTGAGGAGACGGTGACCTGGGT-3'. For amber stop codon introduction, cloning of the nanobodies in the pHEN6 vector was done using the following primers: forward pHEN6 5'-CCAGGTGCAGCTGCAGGAGTCTGGGGGAGGATT-3' and reverse pHEN6 5'-GTCAC CGTCTCCTCAGGAGGAAGCGGTGGCTAGACCGGTCATCATCACCATC-3'.

6.2.5.3 Recombinant nanobody and sortase A pentamutant production

The production and purification of the nanobodies, was performed as described previously[47]. *E. coli* WK6 cells were transformed with nanobodies in pMECS/pHEN6 vector. They were grown at 37 °C in TB with 100 µg/ml ampicillin (Duchefa, Haarlem, the Netherlands) and if the pEVOL-pAzF was co-transformed, with 34 µg/ml chloramphenicol (Duchefa) and 1 mM pAzF. After induction with 0.2% (w/v) arabinose (Sigma-Aldrich, St. Louis, MO, USA) and 1 mM IPTG (Biosynth, Staad, Switzerland), incubation was performed at 28 °C overnight. French press was used to obtain total cell lysis followed by short sonication. Next, an IMAC purification was performed as described before[47]. Briefly, the recombinant His_6-tagged nanobodies were purified from *E. coli* WK6 cells by

binding to Co^{2+}-chelating resins (Takara Bio Inc., France) and were recovered from the beads with standard elution buffer (50 mM NaH_2PO_4, 500 mM NaCl, 250 mM imidazol, pH 8.0), the potassium phosphate elution buffer (100 mM potassium phosphate, 100 mM KCl, 250 mM imidazole, pH 7.4) or the HEPES elution buffer (50 mM HEPES (Duchefa), 50 mM NaCl (Duchefa), 250 mM imidazole, pH 8.0).

Sortase A pentamutant in pET29 was transformed in *E. Coli* BL21 cells and grown at 37 °C in LB with kanamycin. After induction with IPTG, they were incubated at 20 °C overnight. French press was used to obtain total lysis followed by short sonication. Next an IMAC purification was performed as mentioned above.

6.2.5.4 Sortase A reaction

The nanobodies were dialyzed into a sortase compatible buffer (50 mM Tris-HCl (Duchefa Biochemie, Haarlem, The Netherlands), 150 mM NaCl, pH 8.0). Subsequently, the sortase reaction was performed at 30 °C for 90 min. The reaction mixture (total volume 100 µl) consists of 50 µM peptide, 4 µM sortase A pentamutant, 20 µM nanobody in sortase reaction buffer (50 mM Tris-HCl, 150 mM NaCl and 10 mM CaCl2 (Sigma-Aldrich, St. Louis, MO, USA), pH 8.0). Thereafter, immobilized metal affinity chromatography (IMAC) purification was used to remove His_6-tagged proteins still present in the mixture.

6.2.5.5 CuAAC after sortase: test experiment for optimisation – benefit of HEPES

After sortase reaction, the nanobodies were used directly or were diafiltered through an Amicon Ultra-0.5 Centrifugal Filter Unit (MWCO 3kDa) (Sigma-Aldrich) according to the manufacturer's instructions, into a buffer with lower Cl^- ions concentration (10 mM HEPES-NaOH, 50 mM NaCl, pH 8). Subsequently, Cu(I)-catalyzed Azide-Alkyne Click Chemistry (CuAAC) was performed. Two tubes were prepared of which the first tube contained $CuSO_4$ (20 mM stock solution) (Merck, Overijse, Belgium), tris(3-hydroxypropyltriazolylmethyl)amine (THTPA) (50 mM stock solution) (Sigma-Aldrich) and sodium ascorbate (100 mM stock solution) (Sigma-Aldrich) and the second contained HEPES (100 mM stock solution), an alkyne-bearing nanobody and an azide-Alexa Fluor AF488 (5 mM stock solution) (Jena Bioscience, Jena, Germany). Bringing the content of both tubes together, the final concentrations (Buffer 1 at Table 2) were 0.1 mM $CuSO_4$, 0.5 mM THTPA, 5 mM sodium ascorbate, 10 mM HEPES-NaOH, 3 µM nanobody and 6 µM azide-AF488. This was incubated overnight at 33 °C and analysed on sodium dodecyl

sulphate – polyacrylamide gel electrophoresis (SDS-PAGE) and with a FastGene FAS-digi Geldoc device (NIPPON genetics, Dueren, Germany).

6.2.5.6 CuAAC after sortase: test experiment for optimisation – benefit of THPTA or sodium ascorbate

After sortase reaction, the nanobodies were diafiltered through an Amicon Ultra-0.5 Centrifugal Filter Unit (MWCO 3kDa) (Sigma-Aldrich) according to the manufacturer's instructions into a low Cl^- ions solution (10 mM HEPES-NaOH, 50 mM NaCl, pH 8). Subsequently, CuAAC was performed. Two tubes were prepared of which the first tube contained $CuSO_4$ (20 mM stock solution) (Merck), THTPA (50 mM stock solution) (Sigma-Aldrich) and sodium ascorbate (100 mM stock solution) (Sigma-Aldrich) and the second contained HEPES (100 mM stock solution), an alkyne-bearing nanobody and an azide-AF488 (5 mM stock solution) (Jena Bioscience). Bringing the content of both tubes together started the reaction. The end concentration in this mixture was determined by the conditions in the experiment. For the following compounds, the final concentrations remained constant at 0.1 mM $CuSO_4$, 50 mM HEPES-NaOH, 5 µM nanobody and 10 µM azide-AF488. THTPA and sodium ascorbate were different in the different conditions as can be seen in Table 2. The mixtures were incubated overnight at 33 °C and analysed by SDS-PAGE and with a FastGene FAS-digi Geldoc device (NIPPON genetics).

6.2.5.7 CuAAC after pAzF incorporation: test experiment for optimisation – time point determination

After the pAzF incorporation (see supplementary material), nanobodies were dialyzed against a HEPES buffer (50 mM HEPES-NaOH, 50 mM NaCl, pH 7.4) to make them compatible with the CuAAC reaction. Two tubes were prepared (one with $CuSO_4$ (20 mM stock solution), THTPA (50 mM stock solution) and sodium ascorbate (100 mM stock solution), the other with HEPES (100 mM stock solution), pAzF containing nanobody and alkyne-AF488 (5 mM stock solution) (Jena Bioscience)) and mixed gently to obtain final concentrations of 0.1 mM $CuSO_4$, 1 mM THTPA, 7.5 mM sodium ascorbate, 50 mM HEPES-NaOH, 30 µM nanobody and 60 µM alkyne-AF488. At each time point (0, 5, 15, 20, 30, 45, 60 and 75 min) during the CuAAC reaction, a 3 µl sample out of the total reaction mixture volume of 400 µl was removed and analysed by SDS-PAGE and with a FastGene FAS-digi Geldoc device (NIPPON genetics).

6.2.5.8 CuAAC to obtain fluorescently labelled nanobodies - final protocol

After the pAzF incorporation, nanobodies were dialyzed against HEPES buffer (50 mM HEPES-NaOH, 50 mM NaCl, pH 7.4) to make them compatible with the CuAAC reaction. Before the start of CuAAC, two tubes were prepared. The first tube contains $CuSO_4$ (20 mM stock solution) (Merck), THTPA (50 mM stock solution) (Sigma-Aldrich) and sodium ascorbate (100 mM stock solution) (Sigma-Aldrich), while the second tube contained HEPES (100 mM stock solution), a pAzF containing nanobody and an alkyne-AF488 (5 mM stock solution) (Jena Bioscience). After mixing both tubes, the final concentrations in this mixture are 0.1 mM $CuSO_4$, 1 mM THTPA, 7.5 mM sodium ascorbate, 50 mM HEPES-NaOH, 30 µM nanobody and 60 µM alkyne-AF488. This was incubated for 60 min at 33 °C. Thereafter, an EDTA solution (20 mM HEPES-NaOH, 500 µM EDTA (Sigma-Aldrich), pH 7.4) was used to complex the Cu^{2+} ions. Their removal from the mixture was achieved by diafiltration using an Amicon Ultra-0.5 Centrifugal Filter Unit (MWCO 3kDa) (Sigma-Aldrich). At least 3 times the reaction volume of the EDTA solution was used during the diafiltration. This was followed by a PD Spintrap™ G-25 (Sigma-Aldrich) used according to the manufacturer's instructions. The product was analysed by SDS-PAGE and a FastGene FAS-digi Geldoc device(NIPPON genetics), and protein concentrations were determined using the Bradford assay (Bio-Rad Laboratories, Hercules, CA, USA).

6.2.5.9 Immunocytochemistry and microscopy

The immunocytochemistry was performed as described before[389]. Cells were seeded on a 100 µg/ml gelatine (Sigma-Aldrich) or 50 µg/ml rat tail type I collagen (BD Biosciences, Franklin Lakes, NJ, USA) coated coverslip. In case of a 4% paraformaldehyde (PFA) fixation, cells were fixed using 4% PFA, permeabilized using 0.2% TritonX-100 (Sigma-Aldrich) for 5 minutes and neutralized and blocked in 20 mM glycine (Sigma-Aldrich) for 20 minutes. In case of a methanol fixation, cells were fixed and permeabilised with 100% ice-cold methanol for 5 minutes and blocked in 20 mM glycine (Sigma-Aldrich) for 60 minutes. After the blocking steps, an incubation with primary antibodies or labelled nanobody (1 h at 37 °C) was performed and if necessary followed by Alexa Fluor-conjugated secondary antibodies (30 min at room temperature). DAPI (0.4 µg/ml; Sigma) and Alexa Fluor labelled phalloidin (Invitrogen) were used to stain nuclei and actin filaments, respectively. Cells were mounted using VectaShield (Vector Laboratories, Burlingame, CA, USA). For imaging, an Olympus IX81 FluoView 1000 confocal laser scanning microscope (UPlanSApo x60 1.35-NA UplanSApo objective; Olympus, Tokyo, Japan) with FluoView FV1000 software (Olympus) was used at room temperature.

6.2.5.10 Photoporation

The photoporation was performed as described in more detail elsewhere[67]. Briefly, a µ-slide (µ-Slide Angiogenesis, ibidi, Beloeil, Belgium) was seeded with 5000 HeLa cells per well one day in advance. Before laser treatment, cells were incubated with graphene quantum dots-PEG suspended in cell culture medium for 30 min. The fluorescently labelled nanobody was dispersed in Dulbecco's phosphate-buffered saline (DPBS) at a concentration of approximately 40 µg/mL. 10 µL nanobody solution was added into each well before the photoporation laser treatment. The sample was scanned through the photoporation laser beam (20 Hz pulse frequency) using an electronic microscope stage (HLD117, Prior Scientific, USA). The scanning speed was 2.1 mm/s, and the distance between subsequent lines was 0.1 mm to ensure that each cell received a single laser pulse. The total scanning time per well was 2 min. The fluorophore solution was then removed and the cells were gently washed with DPBS and supplemented with fresh cell culture medium. Samples were analysed using a spinning disk confocal microscope (Nikon eclipse Ti-e inverted microscope, Nikon, Japan) equipped with an MLC 400 B laser box (Agilent technologies, Santa Clara, CA, USA), a Yokogawa CSU-22 Spinning Disk scanner (Andor Technology, Belfast, UK) and an iXon ultra EMCCD camera (Andor). A 60×/1.4 oil immersion objective lens (CFI Plan Apo VC 60 × oil, Nikon, Japan) was used for imaging.

6.2.5.11 Cell culture

HNSCC61 and HeLa cells were maintained at 37 °C in a humidified 5% CO_2 incubator. All were grown in Dulbecco's Modified Eagle Medium (DMEM) (Gibco Life Technologies, Grand Island, NY, USA) supplemented with 10% fetal bovine serum, 10 µg/mL streptomycin and 10 IU/mL penicillin. In case of HNSCC61 cells, an extra 0.4 µg/mL hydrocortisone (Sigma-Aldrich) was added and 20% fetal bovine serum was used.

6.2.5.12 Generation of β-catenin nanobodies

A cDNA fragment covering the C-terminal half of human catenin (amino acids 398-end) was cloned into the pTYB12 prokaryotic expression vector and expression/purification was done as described for other constructs described above. A llama was immunized with this protein fragment by a subcutaneous injection on days 0, 14, 28 and 35. Anticoagulated blood was collected on day 39 for lymphocyte preparation. By extracting total RNA from peripheral blood lymphocytes, a nanobody library was constructed and screened for the presence of antigen-specific nanobodies by phage panning. The

obtained nanobodies were subcloned into the phagemid vector pMECS. They are currently licensed to *Gulliver Biomed* (www.gulliverbiomed.com).

6.2.6 Supplementary information

6.2.6.1 Incorporation of an azido/alkyne functional group into a nanobody

Sortase A (SrtA) is a transpeptidase that recognizes the specific amino acid sequence LPETG (Leu – Pro – Glu – Tyr – Gly). This sequence was genetically incorporated at the C-terminus of the cortactin nanobody 2 by PCR, resulting in a nanobody sequence that is C-terminally followed by a GSA linker sequence and the LPETG sortag sequence followed by a His_6-tag. This cortactin Nb2 was shown to diminish invadopodium numbers, matrix degradation, MMP9 secretion and invasive capacity in invasive MDA-MB-231 and HNSCC61 cells[45, 46, 48, 433]. The modified cortactin nanobody was expressed and purified from bacteria following a procedure similar to standard nanobody production as performed before[47, 215, 406]. As described earlier[191], SrtA cleaves the nanobody at Gly residue of the sortag sequence, removing this residue in addition to the His_6-tag (Figure 41A). This creates a nanobody-SrtA intermediate. Next, sortase A couples the donor peptide Gly-Gly-Gly-Tyr-Propargylglycine (GGGY-PAG) onto the acceptor nanobody (Figure 41A), which as a result of this reaction process acquires an alkyne group. Since sortase A also carries a His_6-tag as well as the unmodified nanobody, all nanobody molecules which have not taken part in the sortase reaction together with sortase A itself can be easily removed by Ni^{2+} or Co^{2+} IMAC. In the final reaction, 50 µM peptide : 4 µM sortase A : 20 µM nanobody was used. As expected, the nanobody is cleaved at the sortag sequence and the donor peptide is coupled. After a few consecutive Co^{2+} IMAC incubation steps, the remaining protein band corresponds to the new nanobody derivative that contains the alkyne group.

Next to an enzymatic way to incorporate an alkyne moiety, a second method was explored based on the incorporation of an unnatural amino acid bearing an azido group (Figure 41B). For this purpose, para-azido phenylalanine was used. As pAzF is a non-canonical amino acid, an amber stop codon (TAG) was genetically engineered at the C-terminus of the nanobody, before the His_6-tag. By using the correct tRNA/tRNA synthetase orthogonal pair (pEVOL-pAzF (Addgene plasmid #31186)), pAzF is specifically and site-selectively incorporated at the amber stop codon in the nanobody sequence[225]. By engineering this construct, all purified nanobodies are expected to contain the azido group, because if they do not incorporate the pAzF, the resulting nanobody will not carry a His_6-tag and thus cannot be purified by IMAC. Moreover, the tRNA synthetase from

Methanococcus jannaschiityrosyl used in this study does not aminoacylate any endogenous *E. coli* tRNAs, but only the mutant tyrosine amber suppressor ($mutRNA_{CUA}$) [225, 453].

6.2.6.2 Additional information for CuAAC

Once a nanobody bearing an alkyne/azido group was generated, the Cu(I)-catalysed Azide-Alkyne Click Chemistry (CuAAC) reaction can be performed. The catalytic component is a Cu(I)-source which is a copper(II) sulfate ($CuSO_4$) salt in combination with sodium ascorbate to reduce Cu(II) to Cu(I), and tris(3-hydroxypropyltriazolylmethyl) amine (THPTA) which stabilizes Cu(I). THPTA addition is important as this ligand blocks the bioavailability of Cu(I) and prevents potential toxic effects[425]. Based on the findings of Presolski and Hong *et al.*[423-425], a test protocol was developed. The azido-fluorophore and the alkynylated cortactin nanobody 2[45, 46, 48, 433] were incubated overnight in a 2:1 ratio with 0.1 mM $CuSO_4$, 0.5 mM THTPA, 5 mM sodium ascorbate, 10 mM HEPES buffer at 33 °C. Different fluorophores are commercially available and are suitable to label alkyne/azido-derivatized nanobodies in this manner.

6.2.7 Acknowledgments

This work was supported by grants from the Research Foundation Flanders (Fonds Wetenschappelijk Onderzoek (FWO) Vlaanderen) and Ghent University (BOF13/GOA/010). T.H. is supported by Ghent University (BOF PhD fellowship). K.B. acknowledges financial support from the European Research Council (ERC) under the European Union's Horizon 2020 research and innovation program (grant agreement No 648124) and from the Ghent University Special Research Fund (01B04912) with gratitude. J.L. gratefully acknowledges the financial support from the China Scholarship Council (CSC) (201506750012) and the Special Research Fund from Ghent University (01SC1416). We thank Serge Muyldermans and Maxine Crauwels from the VUB (Free University Brussels) for insightful discussions.

Part IV

General discussion & conclusions

Chapter 7 General discussion and conclusions

This work showed the use of nanobodies in research for studying protein functions and for imaging of proteins. This was shown separately, but in future experiments these two projects can be brought together to establish a new research purposes and obtaining new insights in the biological mechanisms. In following paragraphs, both projects are discussed separately as the targeted proteins in both projects were different as well.

7.1 VCA nanobodies, a tool to study N-WASp functioning in the invadopodium pathway

Different strategies are available to study a protein of interest. It can be obtained through knockdown or knockout techniques. A frequently used method is RNA interference (RNAi). This method causes gene silencing at a post-transcriptional level[84, 388]. It is a straightforward technique but it is limited in its specificity[84]. A variant to RNAi is the antisense oligonucleotide method (ASOs) in which the RNA is degraded by RNase H[388]. Further, a more recent and well-known knockout strategy is the CRISPR/Cas9 genome editing method[388, 454]. This is a method in which a bacterial endonuclease enzyme targets a desired site in the genome[388]. This enables the removal or replacement of the gene of interest[388]. While CRISPR/Cas9 is an easy-to-use and affordable strategy for gene editing, it has some not negligible off-target effects resulting in the deletion or modification of the wrong genes and/or genomic instability[417, 454, 455]. Since those are all strategies aimed at the DNA level, the nanobody technology used here, enables to study a protein of interest at a post-translational level. The big difference to the above mentioned methods is found in the way nanobodies create a knockout of protein functions[84] meaning that nanobodies enable to investigate the function of only a part or

a domain of the protein of interest, while the other domains still can interact with their usual interaction partners. This was observed previously for fascin Nb5. If the nanobody was present, it reduced the invasiveness of cancer cells via a reduced invadopodia density and a decreased elongation and lifetime of invadopodia[45]. Moreover, the nanobody can also be used to relocate the protein and in that case the nanobody technology can introduce other outcomes. When the same fascin Nb5 was used but tagged with a mitochondrial outer membrane (MOM) delocalisation tag, an additionally reduced secretion and activity of MMPs could be observed[45]. In this case, not only the domain is 'silenced', fascin cannot interact similar to native conditions due to the delocalisation to the mitochondrial outer membrane.

Adding to the advantage of selectively studying protein function, nanobody technology enables to analyse the target protein at an endogenous level, which avoids possible effects that could be introduced by overexpression. Those overexpression effects can differ from the ones with expression levels that are found in healthy cells or maybe even cancer cells. Indeed, changes in expression levels for many proteins have been observed previously to enhance the cancer pathway. By performing overexpression, there is a risk of activating other processes to keep the cell balanced. Similar to GFP fusion proteins, by inserting an exogenous gene into the cell, two populations are found: the endogenous protein and the extra inserted exogenous gene translated product[456]. If the inserted protein is tagged or labelled, it can result in different interactions than with other proteins as compared to the endogenous protein. This can be caused by steric hindrance of the tag or label, and/or the presence of the endogenous protein that is still able to interact as well[456]. An additional advantage of using the nanobody technology for protein studies, is the longer active half-life of a nanobody (compared to RNA based methods)[84].

Here, VCA nanobodies were used to study N-WASp. In this case, only the VCA domain was targeted, while the other domains of N-WASp still can interact as usual. Previously, it was observed that N-WASp is important in embryonic development since total loss of N-WASp caused embryonic lethality[291]. This shows that studies through knockout mice were not an option. However, an N-WASp – knockout in keratinocytes of the skin proved to be possible, although it introduced some other defects as well such as growth problems and body weight reduction[291]. Furthermore, other techniques were used for N-WASp studies as well, such as overexpression of the full length N-WASp[457] or through the expression of a dominant negative N-WASp. The latter can be an N-WASp variant with a deletion of a domain[458] or a deletion of only a few amino acids[336, 337, 373, 394, 459]. However, a deletion or change in amino acid sequence can introduce differences in the conformation of the protein compared to the native structure. In contrast, instead of modifying the native N-WASp, here we used the nanobody technology which enables to

investigate N-WASp in its native conformation and location without silencing the whole protein.

First, a characterisation was done to select the nanobodies that were able to bind N-WASp. Eventually, we selected four nanobodies which were used in the experiments. To confirm the binding capacity of the nanobodies in the cytoplasm, a MOM tag was used to relocate the nanobodies and N-WASp to mitochondria. After the characterisation, the VCA nanobodies were used for further examination of N-WASp functions. As the N-WASp nanobodies target its C-terminal VCA domain, they were found to interfere with the Arp2/3 interaction (Figure 49). They were able to perturb the N-WASp function and affect actin polymerisation in three cell lines, breast cancer cells (MDA-MB-231), head and neck squamous carcinoma cells (HNSCC61) and prostate cancer cells (PC-3). This resulted in the reduction of invadopodium numbers and in the disturbance of the overall matrix degradation (Table 5). The effects on the number of invadopodia indicated clearly that N-WASp is involved in the formation pathway.

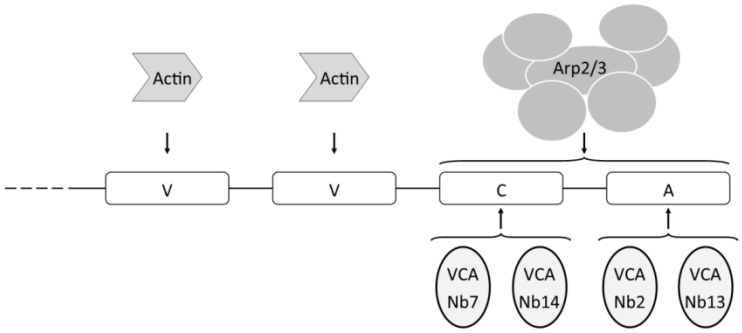

Figure 49: VCA Nbs binding on VCA domain of N-WASp. While the verprolin-homology (V) region of N-WASp interacts with actin, the cofilin-like (C) and acidic (A) part binds to Arp2 and Arp3 of the Arp2/3 complex. Since the immunoprecipitation of the VCA domain with the nanobodies resulted in only a decrease of Arp2/3, the VCA nanobodies interact with the CA part of N-WASp. Since N-WASp made a double interaction with Arp2/3, each binding has another influence on the activation of the N-WASp:Arp2/3 complex. The first interaction occurs at the A region which is important for the affinity between N-WASp and the Arp2/3 complex while the second interaction with the C region does not need high affinity but is required for a better Arp2/3 activation. Since VCA Nb7 and VCA Nb14 have a bigger influence on the degradation and a lower influence on the Arp2/3 binding, we hypothesised that those VCA nanobodies interfere the Arp2/3 – C region interaction, while VCA Nb2 and VCA Nb13 disturb the Arp2/3 – A region interaction.

Table 5: Overview of the effects on the invadopodium pathway due to the VCA nanobodies. The binding assay showed that the VCA nanobodies were able to decrease the binding between N-WASp and Arp2/3 and they did not have any effect on the actin – N-WASp interaction. The invadopodia amounts were significantly decreased in the presence of the VCA nanobodies as intrabodies in two different cancer cell lines (MDA-MB-231 breast cancer cells and HNSCC61 head and neck squamous carcinoma cells). Next, only two nanobodies were able to cause significant reduction of the overall ECM degradation (PC-3 prostate cancer cells). The values in this table are based on the 'degradation index' which is the parameter that is the normalised difference between the mean grey value of the background (here the red fluorescent labelled gelatin matrix) and the mean grey value of the cell area. (* $p < 5\%$, ** $p < 1\%$, *** $p < 0.01\%$)

		VCA Nb2	VCA Nb7	VCA Nb13	VCA Nb14
Binding assay: Arp2/3 –N-WASp		↓↓	↓	↓↓	↓
Invadopodia	MDA-MB-231	*	***	***	***
	HNSCC61	**	***	***	***
Overall ECM degradation (PC-3)			**		***

Due to inhibitory effect on invadopodium formation, defects in the invadopodia may result in a decreased degradation capacity. Only two of the four nanobodies (VCA Nb7 and VCA Nb14) were able to show a significant effect on the overall ECM degradation, but small non-significant changes in MMP9 secretion and activity were found for all four VCA nanobodies (Figure 39). As described previously, N-WASp is involved in the matrix degradation pathway as well. MMP degradation is based on both membrane bound MMPs (such as MT1-MMP) and soluble MMPs (e.g. MMP2 and MMP9). The association of N-WASp with the MMP pathway is reflected in MMP delivery by vesicular transport[356, 358]. As discussed before (3.3.4.4 Maturation and ECM degradation), different pathways exist to deliver MMPs to invadopodial sites[302]. In endocytosis, N-WASp is suggested to create a branched actin network resulting in a force that is able to reshape the membrane leading to vesicle invagination[331, 344, 353-355]. This means that the actin cytoskeleton causes the driving force for pinching off the endosome[355]. Additionally, N-WASp helps in the establishment of actin comet tails to endosome vesicles[356-358]. This creates a propelling force that enhances the transport of the endosome through the invadopodium[358]. Besides the transport, N-WASp is supposed to stabilise and fix MT1-MMP at invadopodial locations[344]. By doing this, the functionality of MT1-MMP is enhanced[344]. Since we were not able to detect MMP2, we checked MMP9 and MT1-MMP in this study, as those are the most abundant MMPs. By using the VCA Nbs, we observed small non-significant changes in MMP9 secretion and activity. When we checked the master switch MT1-MMP, we did not observe changes using the VCA nanobodies as intrabody (Figure 39). We conclude that our VCA nanobodies were able to interfere in the invadopodium formation, while the degradation effects were a result of the invadopodium defective structure. So, the role of the VCA domain of N-WASp is mainly important in the initial steps of the invadopodium pathway. This confirms the findings of Castro-Castro *et al.*[316] and Gomez *et al.*[460]. They indicated that another member of the WASp protein family, the Wiskott–Aldrich syndrome protein and Scar homologue (WASH), is involved in these processes instead of N-WASp. WASH has been found to be important for exocytosis to transport MMP bearing vesicles from Golgi to the invadopodium membrane[316]. Gomez suggested that WASH was required for endosomal and lysosomal networks in mammalian cells[292, 460]. As WASH is found in the endosomal, lysosomal and exocyst pathways, this can explain why the influence of the VCA nanobodies on the MMP9 secretion and degradation is minimal or even not existing. However, Jacob and co-workers have found that the delivery of MT1-MMP differs from the delivery routes of MMP2 and MMP9[351, 352]. MT1-MMP transport is a balance between exocytosis and endocytosis[352], while the secretion of MMP2 and MMP9 will rely on the delivery in Rab40 bearing secretory vesicles from the Golgi to the membrane[351]. Another possible explanation is that the VCA domain is not important for the ECM

degradation, but another domain of N-WASp is. In that case, it can explain why our VCA Nbs are not able to cause huge reductions in the ECM degradation. Benesch and co-workers observed that the WH1 domain and the poly-proline domain contributed to the interaction of the vesicle surface and the actin comet tail formation. This would suggest that N-WASp still can play a role in the MMP recruitment[359].

Since N-WASp interacts directly with cortactin, this could lead to the suggestion that nanobodies targeting cortactin and the VCA nanobodies would have a similar influence on the MMP9 secretion and activity[48]. However, our earlier studies on cortactin significantly reduced the MMP9 secretion and activity by using nanobodies targeting its C-terminal SH3 or the N-terminal NTA domains[48]. Hence, by using nanobodies we can attribute specific roles of cytoskeletal proteins in cancer cell invadopodium formation and functioning. This information can be very instrumental for the generation of future protein domain-selective compounds and therapeutic targeting of tumor cell motility.

7.2 Fluorescent nanobodies, an emerging tool for microscopic purposes in fixed and living cells

The enthusiasm for smaller fluorescent imaging tools is heightened in the last years, congruent with increasing resolution of microscopic techniques. In this case, nanobodies are receiving more and more attention since they are a good alternative to antibodies. Since the linkage error is relatively large when using antibodies, the nanobodies offer benefits in techniques where a high resolution is required. Recently, some companies (e.g. ChromoTek[461] and NanoTag Biotechnologies[462]) started to offer nanobodies for super resolution purposes. However, the commercially available labelled nanobodies are limited to a small range of targets[463]. In most cases, they target fluorescent proteins (e.g. GFP and RFP). This will indeed minimise the linkage error to the fluorescent protein[463]. Nevertheless, the benefits of small linkage error and high resolution are contradictory to the size of the fluorescent protein that is coupled to the protein of interest, which also can include possible side effects compared to the case of the endogenous protein (such as loss of function, multimerization or mislocalization)[166]. In other words, the localisation of the fluorescent protein is more precise and accurate than in case of using an antibody, but the benefits of using nanobodies for super resolution are partially undone by the use of a fluorescent protein fused to the protein of interest. This leads to a resolving power that is not fully used. Therefore, it would be beneficial to use nanobodies against the

protein directly. In our study, the nanobodies do target the endogenous protein which is cortactin and β-catenin. This enables the visualisation of the protein in its native conditions. The visualisation of the protein of interest with a fluorescent nanobody results in a detected signal that can be converted into a more accurate position compared to the observed intensities when detecting the fluorescent protein fused to the protein of interest. Besides, by targeting the protein of interest directly, the risks and problems which are possible due to the fusion protein, are avoided. It is therefore beneficial to have nanobodies targeting the endogenous protein.

Companies such as ChromoTek offer nanobodies tagged with a fluorescent protein, which they call chromobodies. These are delivered by plasmids that have to be transfected into the cells to allow the nanobody to target the protein of interest. This immediately shows the differences in visualisation we propose in our work. First, the use of a fluorophore such as GFP will be detected as a bigger, more blurred position than when a high-quality small dye is used. Additionally, fluorescent proteins suffer from a limited photostability, spectral range and brightness[170]. A smaller dye offers benefits in higher resolution microscopic techniques. As such, labelled nanobodies with a small chemical dye are difficult to be expressed or delivered in living cells. This indicates the second problem that is also found with the commercial chromobodies: nanobodies cannot breach the cell membrane as recombinant protein. As mentioned above, chromobodies avoid this problem by entering the cells as DNA. Initially, the labelled nanobodies used in our work have found their application in standard immunocytochemistry.

In this study, two strategies were compared to obtain labelled nanobodies. Our first labelling strategy used sortase A as basic instrument. For this, a two-step process was executed in which the SrtA enzyme first couples a peptide onto a nanobody followed by the CuAAC reaction. While SrtA is versatile in respect to the moieties that can be coupled to a nanobody[464], the commercial substrates are rather limited. However, other groups have already performed the sortase reaction as a one-step method by using a fluorescent peptide. Massa *et al.*[191] used a Cy5 labelled peptide (GGGYK-Cy5) for this. Since their goal was to use those nanobodies for visualisation in living animals through fluorescence reflectance imaging (FRI)[191], no confocal or super resolution microscopy was executed. In our hands, the one step sortase method using the GGGYK-Cy5 peptide resulted in a very low intensity signal for confocal microscopy purposes (unpublished data). In another study, Truttmann and co-workers attached a GGG-AF647 peptide into an anti-HypE nanobody (Huntingtin-associated yeast-interacting protein E) via the sortase reaction for visualisation on confocal microscopy[192]. They also observed low

intensity and suggested that this was caused by the ratio of a single dye to one nanobody[192].

The sortase A enzyme, and other similar enzymes probably as well, catalyse reversible reactions[36]. Hence, a peptide that was previously coupled onto a nanobody or another cargo can be released again. This results in a lower yield of the fluorescently labelled protein. Such enzymatic reactions can be avoided by incorporating an unnatural amino acid into a nanobody as part of its primary structure. This was also implemented in our second labelling strategy. Compared to our first strategy (with sortase A), the non-canonical amino acid incorporation is a one step process. After the nanobody production, the click chemistry can follow directly. In this study, a pAzF is incorporated into the nanobody with a tRNA/tRNA synthetase orthogonal pair which was already available. Next, a copper catalysed chemical reaction was used, called copper catalysed azido-alkyne click chemistry or CuAAC. For this reaction already many fluorophores (AF488, AF546, AF555, AF594, AF647, Cy5, Cy7 …) are commercially available. Because some studies indicated that Cu ions may cause toxicity, it is advised to keep the Cu ions at a low level. In order to reduce the amounts of Cu(I) and so the ROS level, some water-soluble ligands can be used, such as tris-(3-hydroxypropyltriazolylmethyl)-amine (THPTA), tris-(benzyltriazolylmethyl)amine (TBTA), bis(L-histidine), 2-[4-((bis[(1-tertbutyl-1H-1,2,3-triazol-4-yl)methyl]amino)-methyl)-1H-1,2,3-triazol-1-yl]ethyl hydrogen sulfate (BTTES) and 2-[4-((bis[(1-tert-butyl-1H-1,2,3-triazol-4-yl)methyl]amino)methyl)-1H-1,2,3-triazol-1-yl]acetic acid (BTTAA)[183, 217, 247]. Nevertheless, reactions without metals or other ligands can be taken into consideration. A Cu-independent alternative of CuAAC is known as strain promoted azide–alkyne click reaction (SPAAC). When performing the SPAAC reaction, other fluorescent moieties are required than in case of CuAAC which are commercially available already; e.g. DBCO, difluorocyclooctyne (DIFO) derivatives, dibenzocyclooctynes (DIBO) and biarylazacyclooctynone compounds (BARAC)[183].

Labelled nanobodies can have different purposes such as Western blotting but in this work they were used for microscopic goals. Only recently, the benefits of nanobodies for super resolution are becoming clear. The most important one is the reduction in linkage error which allows an improvement of the accuracy and precision of the image. Yet, there are only few studies which have used nanobodies for super resolution microscopy (Table 6). Due to the recent and successful imaging studies, it indicates that the use of a directly labelled nanobody in microscopic applications is still a relatively young research tool and will likely attract more attention in the future, as up till now mostly GFP Nbs were used. At the time we performed our first labelling method (through sortase), we implemented cortactin Nb2-AF488 for super resolution microscopy (Airyscan and PALM/TIRF) in collaboration with the group of Prof. Dr. Alessandra Cambi (Radboud

University, Faculty of Medical Sciences, Nijmegen, the Netherlands). However, the invadopodia were not as clear as in case of labelling through the pAzF method (as judged by confocal microscopy (Figure 45)). Although, using cortactin Nb2-AF488 (labelled through sortase reaction), it was possible to detect a low signal for podosomes in dendritic cells (Hebbrecht and Joosten *et al.*, unpublished data).

Table 6: The use of labelled nanobodies for super resolution microscopy. (CuAAC, Cu(I)-catalyzed Azide-Alkyne Click Chemistry; DNA-PAINT, DNA point accumulation for imaging in nanoscale topography; GFP, green fluorescent protein; NHS, N-hydroxysuccinimide; NPC, nuclear pore complex; pAzF, para-azido phenylalanin; SIM, structured illumination microscopy; SMLM, single molecule localization microscopy; SPAAC, strain-promoted alkyne-azide cycloaddition; STED, stimulated emission depletion microscopy; STORM, stochastic optical reconstruction microscopy; TIRF, total internal reflection fluorescence; TTL, tubulin tyrosine ligase; *, unknown since it was bought from ChromoTek GmbH; **, unknown since it was bought from NanoTag Biotechnologies GmbH)

Nanobody	Labelling strategy	Microscope	References
GFP Nb	NHS	PALM	Ries *et al.*[178]
GFP Nb	TTL	3D-SIM super resolution microscopy	Schumacher *et al.*[189]
NPC Nb	NHS / maleimide	STORM	Pleiner *et al.*[179]
Tubulin Nb	NHS	SMLM	Mikhaylova *et al.*[201]
Nbs against a short linear epitope of β-catenin	Sortase	STORM	Virant *et al.*[165]
Tubulin Nb	Sortase + SPAAC + DNA-PAINT	SMLM	Fabricius *et al.*[193]
GFP Nb RFP Nb	*	STED	Cramer *et al.*[461]
GFP Nb mCherry Nb mTagBFP Nb	Maleimide + SPAAC + DNA-PAINT	TIRF	Sograte-Idrissi *et al.*[463]
Fascin Nb2	pAzF incorporation + CuAAC	Airyscan super resolution microscopy and TIRF	Liu *et al.*[68]
GFP Nb	**	STED	Seitz *et al.*[462]

As suggested, the use of nanobodies for microscopic intents likely will increase. However, nanobodies still suffer from crossing of the cell membrane, one of their major disadvantages. This means that the cells first need to be fixed and permeabilised before nanobodies can enter the cell. During fixation, proteins and cellular content are immobilised[163]. However, it was noticed previously that fixation can alter the epitopes resulting in total loss of antibody immunoreactivity[163]. After the fixation, permeabilisation is followed to allow an enhanced antibody entering into the cell[465]. Together, those processes can alter the normal appearance of the protein of interest[163, 272]. While fixation can block the binding site or even alter the protein structure, permeabilisation can cause the loss of proteins via extraction or relocalization[163, 272]. This means that compared to living cells, a protein in fixed cells can be modified in shape,

interaction sites, location and its abundance[163]. Taking this into account, a choice of different fixatives and detergents are available. A fixation is typically performed by using paraformaldehyde (PFA) or glutaraldehyde (GA) or a combination of PFA and GA[163]. Both have their advantages and disadvantages. PFA is a faster fixation strategy than GA and it causes fewer changes in epitope immunoreactivity compared to GA[163, 465, 466]. However, both PFA and GA cause morphological changes[163, 467]. GA is a stronger fixative resulting in a superior structural preservation due to higher cross-linking level[466, 467], while PFA is not able to fully immobilize all cellular structures[163]. The latter can result in a movement after fixation leading to artefacts such as mislocalizations[163]. Using a combination of PFA and GA, the fixation profits from fast PFA fixation properties and the fully immobilization due to GA[163]. Additionally, alcohol-based fixations are used as well (e.g. ice-cold methanol). This results in a stable fixation for only a few cellular structures and a poor morphological preservation[467]. Methanol typically causes changes in tertiary structures due to protein denaturation[466]. Additionally, a dialdehyde fixative, glyoxal, can be used which is complementary to PFA or GA. As a matter of fact, it is only recently rediscovered as Sabatini and co-workers already used it in 1963[467, 468]. It is a faster fixative than PFA and since it is a dialdehyde, it cross-links proteins more effectively and more accurate which results in an improved immobilisation and preservation of the cellular morphology[467]. As it is a stronger fixative than PFA, it does not induce reduction in epitope immunoreactivity as observed for GA[467]. An advantage of glyoxal fixation is the typically brighter results or, in other words, less background[467]. Besides, glyoxal is safer to work with, since it is less harmful by inhalation than PFA[465-467]. For cortactin Nb2-AF488, we executed an immunofluorescence assay on HNSCC61 cells through PFA and glyoxal fixation. The results show the lower background and more intense signal for the cortactin Nb2-AF488 in case of glyoxal compared to PFA (unpublished data, figure added in addendum (Figure 51)). As detergent, Triton X-100 was used. This is a non-ionic, mild detergent and is used to improve penetration of antibodies and nanobodies which is supposed not to change epitope immunoreactivity[465]. Other mild detergents can be used as well since they generally do not denature proteins: Tween 20, digitonin and saponin[163, 469, 470]. The biggest impact of Triton X-100 is found after an incomplete immobilization, which leads to the loss of cytosolic elements[163].

When using conventional imaging techniques, the changes due to the fixation are most of the time negligable[163]. However, in case of super resolution techniques, such changes can be a huge problem due to the high resolution. Otherwise, the proper and correct interpretation of the data can be doubtfull[163]. As we know our in-house characterised nanobodies are able to find their cytoplasmic target and are able to interfere in the functionality of the protein, they work perfectly on the native structure. Since the

fixation can alter the protein its native conformation, it is not always certain the same nanobodies can find their target in these fixed cells. To circumvent this problem, a nanobody delivery is required. Here, we used the photoporation technique that allows the nanobodies to enter living cells. In that way it enables the nanobodies to interact with their target in its native form. By using the β-catenin nanobodies, we came across this problem. β-Catenin Nb77 is able to bind β-catenin after the cells are fixed and permeabilised. However, β-catenin Nb86, which was found from the same immunisation, was not. While the fluorescently labelled nanobodies may create a faster immunocytochemistry protocol, they face the same problems as antibodies. Nevertheless, Liu *et al.* have shown the possibility to bring exogenous proteins into cells via photoporation[67]. By photoporating the β-catenin Nb86 in living cells, β-catenin Nb86 showed its capacity to target β-catenin. Photoporation has important advantages compared to other techniques that were used for protein delivery. It allows exogenous protein delivery without the need to escape from endosomes and it can be performed in standard recipients for cell growth[67]. It only needs a short optimisation depending on cell line and growth conditions (e.g. coating). Since we have other in-house nanobodies, of which we know that they are able to bind their target in its native form, those nanobodies can be used for photoporation as well. In the collaboration with Liu and co-workers, we have used our fascin Nb2 for this purpose[68] and in this study we have shown it for cortactin Nb2 and β-catenin Nb86 as well. A possible drawback has to be mentioned. In case of staining fixed cells, it is possible to wash out the unbound nanobody fraction. When using the photoporation, this is not possible which introduces the risk of unintended fluorescent background. Those unbound nanobodies will be present in the cell but does not correspond to specific signal. To circumvent this problem, the concentration for each nanobody has to be optimised (which is a standard procedure in case of fixation as well). Next to the determination of the concentration, the time between photoporation and imaging can be prolonged in order to let the cell remove the overshoot of nanobody. However, the latter is not the most recommended option, since this can create stress on the cells which possibly can introduce small change the proper cell functioning.

It has been noticed that using the photoporation during this work showed some accumulation in the nucleus of the fluorescent nanobodies. This is most clear in case of the β-catenin nanobodies (Figure 47B). A possible explanation is that β-catenin also has transcriptional activity in the WNT signal transduction pathway and so can be found in the nucleus[427]. However, this phenomenon is also present in case of the other nanobodies as well (cortactin Nb2 and fascin Nb2[68]) but only slightly. As mentioned above, if accumulation is observed in the nucleus, this can be reduced by incubating the

cells (longer) between photoporation and imaging (Liu J., Hebbrecht T. and Van Leene C. *et al.*, unpublished results).

Additionally, the photoporation does not only allow delivery of nanobodies to target the native form of a protein, it also enables to investigate follow up of processes in real time. By performing life-cell imaging, Liu *et al.* have used fascin Nb2 and histone Nb which still allows to visualise their target 24h and even 72h after photoporation[68]. As we observed, β-catenin Nb86 enabled us to follow β-catenin interaction in the adherens junctions between two cells. The combination of fluorescent labelled nanobodies and the photoporation technique enables the study of long and/or short term processes which can be followed through time. Important to mention here, if one desires to study a protein purely by tracing it, the nanobody must not interfere with the function of the protein of interest. For instance, Fascin Nb2 interact with fascin without hindering its actin bundling function, while fascin Nb5 decreases invadopodium elongation, a shorter invadopodium lifetime and less ECM degradation[45]. For β-catenin Nb86, this is not yet clear and requires further investigation.

Moreover, when more nanobodies against other targets are available in fluorescent format, the possibility to study processes and pathways will expand due to the enabling of the visualisation in living cells. It has been shown before that nanobodies are an ideal tool to study fast (and so short term) processes. Seitz and co-workers have used GFP nanobodies for the investigation of post-exocytosis events in neurons (Figure 50)[462]. After the expression of exocytosis vesicle proteins fused to GFP, they incubated the neurons with non-fluorescent GFP Nbs to block the extracellular vesicle proteins which are already present on the membrane[462]. Next, they added the fluorescent GFP Nbs which will target newly-exocytosed vesicle proteins[462]. After a ten seconds incubation with the fluorescent GFP Nb, they were able to visualise newly-exocytosed vesicle proteins at synaptic sites of neurons which indicates that using nanobodies allow to investigate processes that happen in a matter of seconds[462].

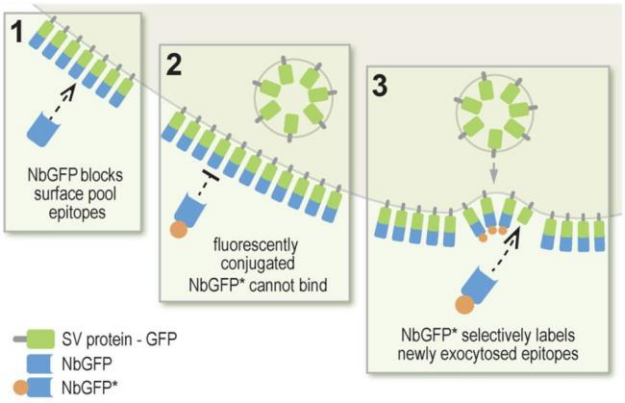

Figure 50: GFP nanobodies enable the selective labelling of newly-exocytosed vesicle proteins. The neuron cells in the study of Seitz and co-workers express a GFP fused synaptic vesicle (SV) proteins. (**1**) During an incubation with non-fluorescent GFP Nbs (NbGFP), (1) the extracellular vesicle proteins will be targeted. (**2**) This makes them inaccessible to fluorescently-conjugated nanobodies (NbGFP*). (**3**) When a new vesicle protein is exposed on the plasma membrane due to a newly-exocytosed vesicle, it interacts with the fluorescent GFP Nb (NbGFP*) which reveals its position. The figure is adapted and modified from Seitz *et al.*[462].

7.3 Conclusion and future perspectives

N-WASp plays a key role in the invadopodium pathway. As the VCA nanobodies indicated, N-WASp is important in the formation, but not in the ECM degradation step. However, those nanobodies could be used to further study N-WASp and the role between the VCA domain and Arp2/3. The VCA domain is the most important domain of N-WASp due to participation in the invadopodium precursor and its direct interaction with actin and Arp2/3 for actin polymerisation. As the results were found by expressing the EGFP-tagged VCA nanobodies through transfection, photoporation and labelled nanobodies can be used as well in additional experiments to explore the role of VCA domain further (e.g. determining the lifetime of invadopodium, unravelling the invadopodium architecture …). Next to the VCA domain, the generation of nanobodies against other domains of N-WASp can have an additional value in evaluating the role of N-WASp in the invadopodium pathway. Nanobodies against almost every domain would have their own special interest; e.g. the remaining of N-WASp in its inactive state or the disturbance in binding to the membrane.

As published before, when using a nanobody against an invadopodium protein (e.g. fascin and cortactin[45, 48, 407, 433]), the proper functioning of invadopodia is hindered. Each time, only one protein is targeted in the study resulting in a partial disappearance of invadopodia. Since N-WASp and cortactin are found in the same invadopodium precursor, it can be interesting to introduce both nanobodies together to analyse if the effect enlarges. Preliminary data already indicated an additive effect of the VCA Nb14 in combination with cortactin Nb2 (Van Audenhove *et al.*, unpublished data). This result suggests that other important processes must be happening besides the invadopodium precursor. However, further investigation is necessary to draw definite conclusions. A combination of nanobodies is not only interesting to evaluate the biological changes, the use of photoporated fluorescent nanobodies against different targets can aid in unravelling the invadopodium structure. If that is accomplished in combination with super resolution imaging, a more accurate localization can be found. While only AF488 is used in this study, a plethora of fluorophores is already available which makes it possible to obtain nanobodies with different fluorophores rapidly. Since invadopodia closely resemble podosomes, it is interesting to compare those two structures. As have been noticed before, invadopodia and podosomes are not entirely the same. For example, the location of fascin in podosomes is the opposite of that in invadopodia[46]. By exploiting the fluorescent nanobodies, other differences can be discovered since nanobodies can allow

a more precise localization via super resolution techniques. Together with the photoporation, this can provide new biological information.

As mentioned before, nanobodies will be important in the future for super resolution microscopy as an alternative for antibodies due to the smaller linkage error. As we have tried the cortactin Nb2-AF488 (labelled via sortase) for TIRF/PALM, we obtained only low intensity signals to visualise podosomes in dendritic cells (Hebbrecht and Joosten et al., unpublished data). Due to time restrictions, we did not check the cortactin Nb2-AF488 (labelled via pAzF) using super resolution microscopy yet, but the results are supposed to be promising since the labelling via pAzF showed much better results (Figure 45). However, not only cortactin Nb2-AF488 will be interesting to check on the super resolution microscope, also other invadopodium proteins can be implemented. This can eventually lead to a better understanding of the invadopodium architecture.

As mentioned earlier, nanobodies are a powerful tool, but their biggest bottleneck was the delivery into living cells. As we have shown here, photoporation creates alternative opportunities. The delivery via photoporation is a step towards a better and more precise method to clarify the importance of proteins (or their domains) in certain pathways. Current studies to examine protein functions (e.g. RNAi and CRISPR/CAS9) are genetically based methods or use chemical inhibitors. By photoporating nanobodies, the target does not disappear from the cell and can be imaged at the same time through the labelled nanobodies. Due to the fast delivery of nanobodies, photoporation enables to notice the effects almost instantly[67, 68]. This allows much faster examination compared to e.g. RNAi[84]. In this study, the role of N-WASp is examined by transfecting the cDNA which is also an alternative to the current strategies. However, the photoporation of nanobodies is even a more valuable alternative which can be expanded for any nanobody that provokes inhibitory effects on their target and for any experiment in which nanobodies are inserted into the cell through transfection. The additional advantage of the photoporation is that it allows perturbing processes and pathways via the photoporated nanobodies for any chosen time with high precision, which is more difficult to control through conventional nanobody cDNA transfection. In other words, photoporation allows to examine the effects at a pre-determined time or even through time.

In this study, the preferred method to label nanobodies was through the incorporation of pAzF followed by the CuAAC reaction. However, the presence of a reactive group such as an azide (or an alkyne) allows the use for other purposes. This can be a coupling to quantum dots, to PEG, to biotin, to agarose/magnetic beads … . Fortunately, those components are already commercially available. The protocol to obtain labelled

nanobodies can be easily adapted to use for those other purposes. Additionally, the labelled nanobodies can have other applications than microscopy as well, such as Western blotting, ELISA … .

As for pharmaceutical interest, the intracellular delivery of a nanobody is still not an option in organisms. It would be a great discovery when nanobody intracellular delivery would be enabled in living organisms, as it can be used as pharmacological inhibitor in case when there are not yet ones available or when there are already available, as complementary therapy. Since nanobodies are still only an ideal research tool for intracellular proteins, it is therefore expected to provide new biological information which can be useful for further engineering of pharmaceutical drugs against intracellular targets rather than becoming a pharmaceutical drug in the near future. In other words, nanobodies can be the stepping stone to focus the search in finding good pharmaceuticals. Since we have used the nanobody technology as research tool here, we therefore hope that this work will contribute to develop new applications with nanobodies, thereby helping to unlock their full potential as research instruments in cell biology.

Addendum

Addendum

- Supplementary for “Nanobody click chemistry for convenient site specific fluorescent labelling, single step immunocytochemistry and delivery into living cells by photoporation and live cell imaging”
    - Video 1
    - Video 2
- Unpublished result of a staining using cortactin Nb2-AF488 (labelled through the pAzF method) in HNSCC61.

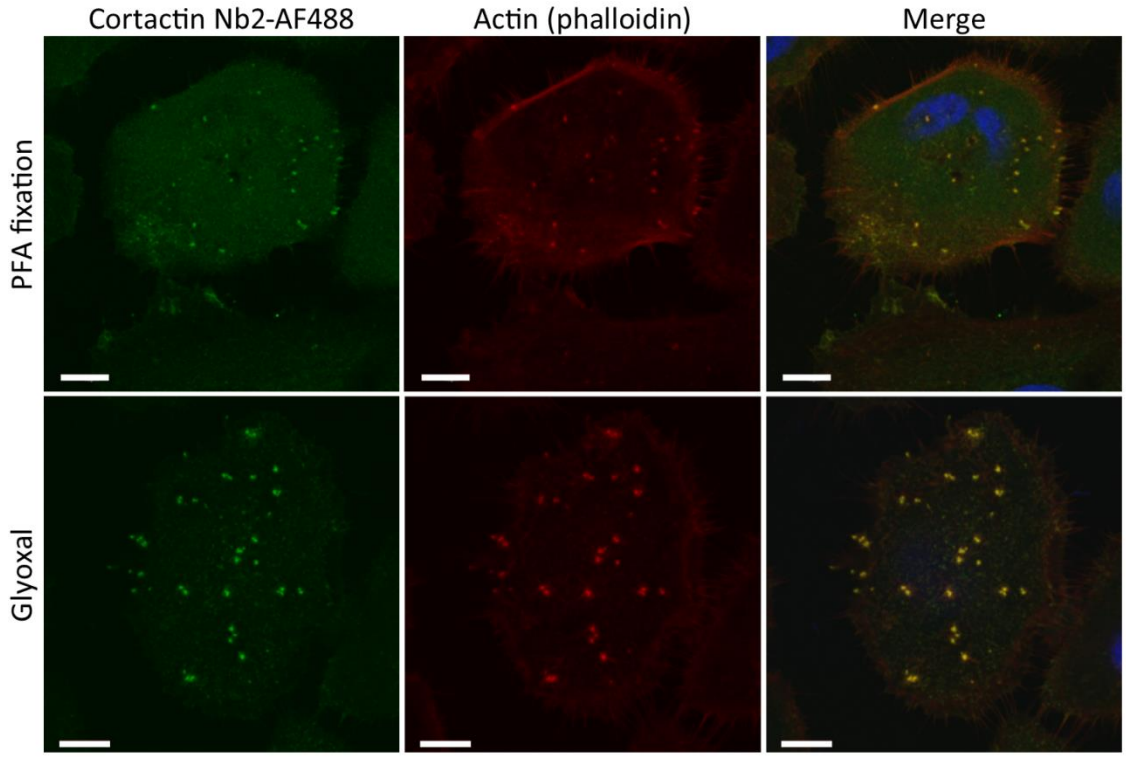

Figure 51: Comparison of PFA and glyoxal fixation of a cortactin Nb2-AF488 staining in HNSCC61. Nuclei were visualized with DAPI (blue) and actin (red) with phalloidin-AF594. (Scale bar = 10 µm)

Curriculum Vitae

Curriculum vitae

Personal information

Name:	Tim Hebbrecht
Current address:	Renning 17
	B-9950 Lievegem (Waarschoot)
Email:	hebbrecht_tim@hotmail.com
	tim.hebbrecht@ugent.be
Date of birth:	February 24th, 1992
Place of birth:	Eeklo

Education

2013 - 2015 **Master of Science in Bioscience Engineering: Cell and Gene Biotechnology**

Master dissertation: N-WASp targeting in invadopodia by using nanobodies: karakterisation & functional research.
Department of Biochemistry, Faculty of Medicine & Health Sciences
Ghent University
Promotor: Prof. dr. Jan Gettemans, Prof. dr. Els Van Damme
Tutor: Dr. ir. Isabel Van Audenhove

2014 - 2015 **Laboratory animal science, FELASA categorie C**

Ghent University

2013 **Intensive program: iGEM**

Lab experience in InBio-Lab
Department of Biotechnology, Faculty of Bioscience Engineering
Ghent University
Promotor: Prof. dr. ir. Marjan De Mey

2010-2013 **Bachelor of Science in Bioscience Engineering: Cell and Gene Biotechnology**

Bachelor dissertation: The iGEM competition: Synthetic biology based on standard parts. A new model for stabilised gene duplication
Department of Biotechnology, Faculty of Bioscience Engineering
Ghent University
Promotor: Prof. dr. ir. Marjan De Mey

Research skills

- **DNA/RNA based techniques**
  PCR, cloning (through ligase or ColdFusion), primer design, plasmid purifications, DNA electrophoresis …

- **Protein based techniques**
  Protein production and purification (Ni/Co/intein/GST), nanobody production with unnatural amino acids, dialysis, SDS-PAGE, Western blotting, pull-down assays, immunoprecipitations, gelatin zymography, isothermal titration calorimetry (ITC), bio layer interferometry (BLI) …

- **Cell based techniques**
  Mammalian cell cultivation (MDA-MB-321, PC-3, HNSCC61, HeLa, HEK293T, MCF7, THP-1), transfection (JetPrime/PEI/$CaPO_4$), RNAi, virus production, transduction and generation of inducible stable cell lines, 2D migration assays, matrix degradation assays, photoporation experiments (with LumiPore), immunocytochemistry assays, cell fixation methods (PFA, GA, methanol, glyoxal) …

- **Microscopic skills**
  Bright field, epifluorescence microscopy, laser scanning confocal microscopy, Z-stack imaging, spinning disc microscopy …

Scientific output

- **Hebbrecht T.**, Liu J., Zwaenepoel O., Boddin G., Van Leene C., Decoene K., Madder A., Braeckmans K., Gettemans J. (2020). Nanobody click chemistry for convenient site specific fluorescent labelling, single step immunocytochemistry and delivery into living cells by photoporation and live cell imaging. *New Biotechnology*

- Liu J., **Hebbrecht T.**, Brans T., Parthoens E., Lippens S., Li C., De Keersmaecker H., De Vos W., De Smedt S., Boukherroub R., Gettemans J., Xiong R., Braeckmans K. (2020). Long-term live-cell microscopy with labeled nanobodies delivered by laser-induced photoporation, *Nano Research*, 1-11.

- Gunnoo S., Vannecke W., Decoene K., **Hebbrecht T.**, Gettemans J., Laga M., Loverix S., Lasters I., & Madder A. (2018) Reviving Old Protecting Group Chemistry for Site-Selective Peptide-Protein Conjugation. *Chemical Communications* 2018, 54(84):11929-11932.

- Bertier L., **Hebbrecht T.**, Mettepenningen E., De Wit N., Zwaenepoel O., Verhelle A., & Gettemans J. (2018). Nanobodies targeting cortactin proline rich, helical and actin binding regions downregulate invadopodium formation and matrix degradation in SCC-61 cancer cells. *Biomedicine & Pharmacotherapy*, 102, 230-241.

- **Hebbrecht T.**, Van Audenhove I., Zwaenepoel O., Verhelle A., & Gettemans J. (2017). VCA nanobodies target N-WASp to reduce invadopodium formation and functioning. *PLOS ONE*, 12(9).

Scientific communications

- **Hebbrecht, T.**, Zwaenepoel, O. & Gettemans, J. (2018). Nanobody technology to study metastasis caused by malignant actin protrusions, called invadopodia. European Cytoskeletal Forum (ECF) – Biology and pathology of cytoskeleton: the crossroads of three cytoskeletal systems. Prague, Czech Republic. Poster presentation.

- **Hebbrecht T.**, Van Audenhove, I. & Gettemans, J. (2017). N-WASp VCA domain targeting nanobodies to study metastasis caused by malignant actin protrusions, called invadopodia. European Cytoskeletal Forum (ECF) – Cytoskeleton: Mechanical Coupling from the Plasma Membrane to Nucleus. Helsinki, Finland. Poster presentation.

Supervision of master dissertations (as tutor)

- Development of *Camelidae* antibodies (nanobodies) as diagnostic and therapeutic tool with applications in cancer (Chloé Van Leene, Master Bioscience engineering, 2019-2020)

- Selection and characterisation of nanobodies and para-azido phenylalanine coupling (Gaëlle Boddin, bachelor agro- en biotechnology, VIVES hogeschool, 2018-2019)

- Molecular and physiological anatomy of cancer cell invadopodia using nanobody technology (Emma Van Heuverswyn, Master Biomedical science, 2018-2019)

- Protein interference in cancer cells by means of nanobody technology (Brian De Dobbelaer, Master Bioscience engineering, 2017-2018)

- Nanobody technology, an ideal research tool (Hanne Mahieu, bachelor agro- en biotechnology, VIVES hogeschool, 2016-2017)

Professional memberships

- Membership of the Belgian Society of Biochemistry and Molecular Biology (BSBMB)

- Membership of Cancer Research Institute Ghent (CRIG)

- ORCiD iD: https://orcid.org/0000-0002-2811-5702

Bibliography

Bibliography

[1] Steeland, S., Vandenbroucke, R. E., and Libert, C. (2016) Nanobodies as therapeutics: big opportunities for small antibodies, *Drug Discov. Today 21*, 1076-1113.

[2] Lo, A.-Y., Zhu, Q., and Marasco, W. (2008) Intracellular antibodies (intrabodies) and their therapeutic potential, In *Therapeutic Antibodies*, pp 343-373, Springer.

[3] De Meyer, T., Muyldermans, S., and Depicker, A. (2014) Nanobody-based products as research and diagnostic tools, *Trends Biotechnol. 32*, 263-270.

[4] Revets, H., De Baetselier, P., and Muyldermans, S. (2005) Nanobodies as novel agents for cancer therapy, *Expert Opin Biol Ther 5*, 111-124.

[5] Hust, M., Jostock, T., Menzel, C., Voedisch, B., Mohr, A., Brenneis, M., Kirsch, M. I., Meier, D., and Dubel, S. (2007) Single chain Fab (scFab) fragment, *BMC Biotechnol. 7*, 14.

[6] Ingram, J. R., Schmidt, F. I., and Ploegh, H. L. (2018) Exploiting Nanobodies' Singular Traits, *Annu. Rev. Immunol. 36*, 695-715.

[7] Perez-Martinez, D., Tanaka, T., and Rabbitts, T. H. (2010) Intracellular antibodies and cancer: new technologies offer therapeutic opportunities, *Bioessays 32*, 589-598.

[8] Bannas, P., Hambach, J., and Koch-Nolte, F. (2017) Nanobodies and Nanobody-Based Human Heavy Chain Antibodies As Antitumor Therapeutics, *Front Immunol 8*, 1603.

[9] Pastan, I., Hassan, R., Fitzgerald, D. J., and Kreitman, R. J. (2006) Immunotoxin therapy of cancer, *Nat. Rev. Cancer 6*, 559-565.

[10] Slastnikova, T. A., Ulasov, A. V., Rosenkranz, A. A., and Sobolev, A. S. (2018) Targeted Intracellular Delivery of Antibodies: The State of the Art, *Front Pharmacol 9*, 1208.

[11] Zhu, Q., Zeng, C., Huhalov, A., Yao, J., Turi, T. G., Danley, D., Hynes, T., Cong, Y., DiMattia, D., Kennedy, S., Daumy, G., Schaeffer, E., Marasco, W. A., and Huston, J. S. (1999) Extended half-life and elevated steady-state level of a single-chain Fv intrabody are critical for specific intracellular retargeting of its antigen, caspase-7, *J. Immunol. Methods 231*, 207-222.

[12] Matz, H., and Dooley, H. (2019) Shark IgNAR-derived binding domains as potential diagnostic and therapeutic agents, *Dev. Comp. Immunol. 90*, 100-107.

[13] Ward, E. S., Gussow, D., Griffiths, A. D., Jones, P. T., and Winter, G. (1989) Binding activities of a repertoire of single immunoglobulin variable domains secreted from Escherichia coli, *Nature 341*, 544-546.

[14] Borrebaeck, C. A. K., Malmborg, A.-C., Furebring, C., Michaelsson, A., Ward, S., Danielsson, L., and Ohlin, M. (1992) Kinetic analysis of recombinant antibody–antigen interactions: relation between structural domains and antigen binding, *Bio/technology 10*, 697.

[15] Desmyter, A., Spinelli, S., Roussel, A., and Cambillau, C. (2015) Camelid nanobodies: killing two birds with one stone, *Curr. Opin. Struct. Biol. 32*, 1-8.

[16] Hamers-Casterman, C., Atarhouch, T., Muyldermans, S., Robinson, G., Hamers, C., Songa, E. B., Bendahman, N., and Hamers, R. (1993) Naturally occurring antibodies devoid of light chains, *Nature 363*, 446-448.

[17] Muyldermans, S. (2013) Nanobodies: natural single-domain antibodies, *Annu. Rev. Biochem. 82*, 775-797.

[18] Gonzalez-Sapienza, G., Rossotti, M. A., and Tabares-da Rosa, S. (2017) Single-Domain Antibodies As Versatile Affinity Reagents for Analytical and Diagnostic Applications, *Front Immunol 8*, 977.

[19] Wang, Y., Fan, Z., Shao, L., Kong, X., Hou, X., Tian, D., Sun, Y., Xiao, Y., and Yu, L. (2016) Nanobody-derived nanobiotechnology tool kits for diverse biomedical and biotechnology applications, *Int J Nanomedicine 11*, 3287-3303.
[20] Greenberg, A. S., Avila, D., Hughes, M., Hughes, A., McKinney, E. C., and Flajnik, M. F. (1995) A new antigen receptor gene family that undergoes rearrangement and extensive somatic diversification in sharks, *Nature 374*, 168-173.
[21] Feige, M. J., Grawert, M. A., Marcinowski, M., Hennig, J., Behnke, J., Auslander, D., Herold, E. M., Peschek, J., Castro, C. D., Flajnik, M., Hendershot, L. M., Sattler, M., Groll, M., and Buchner, J. (2014) The structural analysis of shark IgNAR antibodies reveals evolutionary principles of immunoglobulins, *Proc Natl Acad Sci U S A 111*, 8155-8160.
[22] Zavrtanik, U., Lukan, J., Loris, R., Lah, J., and Hadzi, S. (2018) Structural Basis of Epitope Recognition by Heavy-Chain Camelid Antibodies, *J. Mol. Biol. 430*, 4369-4386.
[23] Mitchell, L. S., and Colwell, L. J. (2018) Analysis of nanobody paratopes reveals greater diversity than classical antibodies, *Protein Eng. Des. Sel. 31*, 267-275.
[24] Muyldermans, S., Atarhouch, T., Saldanha, J., Barbosa, J. A., and Hamers, R. (1994) Sequence and structure of VH domain from naturally occurring camel heavy chain immunoglobulins lacking light chains, *Protein Eng 7*, 1129-1135.
[25] Ewert, S., Cambillau, C., Conrath, K., and Plückthun, A. (2002) Biophysical properties of camelid VHH domains compared to those of human VH3 domains, *Biochemistry 41*, 3628-3636.
[26] Wesolowski, J., Alzogaray, V., Reyelt, J., Unger, M., Juarez, K., Urrutia, M., Cauerhff, A., Danquah, W., Rissiek, B., Scheuplein, F., Schwarz, N., Adriouch, S., Boyer, O., Seman, M., Licea, A., Serreze, D. V., Goldbaum, F. A., Haag, F., and Koch-Nolte, F. (2009) Single domain antibodies: promising experimental and therapeutic tools in infection and immunity, *Med. Microbiol. Immunol. 198*, 157-174.
[27] Vu, K. B., Ghahroudi, M. A., Wyns, L., and Muyldermans, S. (1997) Comparison of llama VH sequences from conventional and heavy chain antibodies, *Mol. Immunol. 34*, 1121-1131.
[28] Hu, Y., Liu, C., and Muyldermans, S. (2017) Nanobody-Based Delivery Systems for Diagnosis and Targeted Tumor Therapy, *Front Immunol 8*, 1442.
[29] Arezumand, R., Alibakhshi, A., Ranjbari, J., Ramazani, A., and Muyldermans, S. (2017) Nanobodies As Novel Agents for Targeting Angiogenesis in Solid Cancers, *Front Immunol 8*, 1746.
[30] Beghein, E., and Gettemans, J. (2017) Nanobody Technology: A Versatile Toolkit for Microscopic Imaging, Protein-Protein Interaction Analysis, and Protein Function Exploration, *Front Immunol 8*, 771.
[31] Liu, W., Song, H., Chen, Q., Yu, J., Xian, M., Nian, R., and Feng, D. (2018) Recent advances in the selection and identification of antigen-specific nanobodies, *Mol. Immunol. 96*, 37-47.
[32] Dumoulin, M., Conrath, K., Van Meirhaeghe, A., Meersman, F., Heremans, K., Frenken, L. G., Muyldermans, S., Wyns, L., and Matagne, A. (2002) Single-domain antibody fragments with high conformational stability, *Protein Sci 11*, 500-515.
[33] van der Linden, R. H., Frenken, L. G., de Geus, B., Harmsen, M. M., Ruuls, R. C., Stok, W., de Ron, L., Wilson, S., Davis, P., and Verrips, C. T. (1999) Comparison of physical chemical properties of llama VHH antibody fragments and mouse monoclonal antibodies, *Biochim Biophys Acta 1431*, 37-46.
[34] van der Vaart, J. M., Pant, N., Wolvers, D., Bezemer, S., Hermans, P. W., Bellamy, K., Sarker, S. A., van der Logt, C. P., Svensson, L., Verrips, C. T., Hammarstrom, L., and van Klinken, B. J. (2006) Reduction in morbidity of rotavirus induced diarrhoea in mice by yeast produced monovalent llama-derived antibody fragments, *Vaccine 24*, 4130-4137.
[35] Dolk, E., van der Vaart, M., Lutje Hulsik, D., Vriend, G., de Haard, H., Spinelli, S., Cambillau, C., Frenken, L., and Verrips, T. (2005) Isolation of llama antibody fragments for prevention of dandruff by phage display in shampoo, *Appl. Environ. Microbiol. 71*, 442-450.
[36] Schumacher, D., Helma, J., Schneider, A. F. L., Leonhardt, H., and Hackenberger, C. P. R. (2018) Nanobodies: Chemical Functionalization Strategies and Intracellular Applications, *Angew Chem Int Ed Engl 57*, 2314-2333.
[37] Braun, M. B., Traenkle, B., Koch, P. A., Emele, F., Weiss, F., Poetz, O., Stehle, T., and Rothbauer, U. (2016) Peptides in headlock–a novel high-affinity and versatile peptide-binding nanobody for proteomics and microscopy, *Scientific reports 6*, 19211.
[38] Ling, J., Cheloha, R. W., McCaul, N., Sun, Z. J., Wagner, G., and Ploegh, H. L. (2019) A nanobody that recognizes a 14-residue peptide epitope in the E2 ubiquitin-conjugating enzyme UBC6e modulates its activity, *Mol. Immunol. 114*, 513-523.
[39] Hassanzadeh-Ghassabeh, G., Devoogdt, N., De Pauw, P., Vincke, C., and Muyldermans, S. (2013) Nanobodies and their potential applications, *Nanomedicine (Lond) 8*, 1013-1026.

[40] Kijanka, M., Dorresteijn, B., Oliveira, S., and van Bergen en Henegouwen, P. M. (2015) Nanobody-based cancer therapy of solid tumors, *Nanomedicine (Lond) 10*, 161-174.
[41] Roovers, R. C., Vosjan, M. J., Laeremans, T., el Khoulati, R., de Bruin, R. C., Ferguson, K. M., Verkleij, A. J., van Dongen, G. A., and van Bergen en Henegouwen, P. M. (2011) A biparatopic anti-EGFR nanobody efficiently inhibits solid tumour growth, *Int. J. Cancer 129*, 2013-2024.
[42] Ressler, V. T., Mix, K. A., and Raines, R. T. (2019) Esterification Delivers a Functional Enzyme into a Human Cell, *ACS Chem Biol 14*, 599-602.
[43] Van Impe, K., Bethuyne, J., Cool, S., Impens, F., Ruano-Gallego, D., De Wever, O., Vanloo, B., Van Troys, M., Lambein, K., Boucherie, C., Martens, E., Zwaenepoel, O., Hassanzadeh-Ghassabeh, G., Vandekerckhove, J., Gevaert, K., Fernandez, L. A., Sanders, N. N., and Gettemans, J. (2013) A nanobody targeting the F-actin capping protein CapG restrains breast cancer metastasis, *Breast Cancer Res 15*, R116.
[44] De Clercq, S., Zwaenepoel, O., Martens, E., Vandekerckhove, J., Guillabert, A., and Gettemans, J. (2013) Nanobody-induced perturbation of LFA-1/L-plastin phosphorylation impairs MTOC docking, immune synapse formation and T cell activation, *Cell. Mol. Life Sci. 70*, 909-922.
[45] Van Audenhove, I., Boucherie, C., Pieters, L., Zwaenepoel, O., Vanloo, B., Martens, E., Verbrugge, C., Hassanzadeh-Ghassabeh, G., Vandekerckhove, J., Cornelissen, M., De Ganck, A., and Gettemans, J. (2014) Stratifying fascin and cortactin function in invadopodium formation using inhibitory nanobodies and targeted subcellular delocalization, *FASEB J. 28*, 1805-1818.
[46] Van Audenhove, I., Debeuf, N., Boucherie, C., and Gettemans, J. (2015) Fascin actin bundling controls podosome turnover and disassembly while cortactin is involved in podosome assembly by its SH3 domain in THP-1 macrophages and dendritic cells, *Biochim Biophys Acta 1853*, 940-952.
[47] Beghein, E., Van Audenhove, I., Zwaenepoel, O., Verhelle, A., De Ganck, A., and Gettemans, J. (2016) A new survivin tracer tracks, delocalizes and captures endogenous survivin at different subcellular locations and in distinct organelles, *Sci Rep 6*, 31177.
[48] Bertier, L., Boucherie, C., Zwaenepoel, O., Vanloo, B., Van Troys, M., Van Audenhove, I., and Gettemans, J. (2017) Inhibitory cortactin nanobodies delineate the role of NTA- and SH3-domain-specific functions during invadopodium formation and cancer cell invasion, *FASEB J. 31*, 2460-2476.
[49] Miersch, S., and Sidhu, S. S. (2016) Intracellular targeting with engineered proteins, *F1000Res 5*.
[50] Chakrabarti, R., Wylie, D. E., and Schuster, S. M. (1989) Transfer of monoclonal antibodies into mammalian cells by electroporation, *Journal of Biological Chemistry 264*, 15494-15500.
[51] Marrero, M. B., Schieffer, B., Paxton, W. G., Schieffer, E., and Bernstein, K. E. (1995) Electroporation of pp60c− src Antibodies Inhibits the Angiotensin II Activation of Phospholipase C-γ1 in Rat Aortic Smooth Muscle Cells, *Journal of Biological Chemistry 270*, 15734-15738.
[52] Conic, S., Desplancq, D., Ferrand, A., Fischer, V., Heyer, V., Reina San Martin, B., Pontabry, J., Oulad-Abdelghani, M., Babu N, K., and Wright, G. D. (2018) Imaging of native transcription factors and histone phosphorylation at high resolution in live cells, *Journal of Cell Biology 217*, 1537-1552.
[53] Dixon, C. R., Platani, M., Makarov, A. A., and Schirmer, E. C. (2017) Microinjection of Antibodies Targeting the Lamin A/C Histone-Binding Site Blocks Mitotic Entry and Reveals Separate Chromatin Interactions with HP1, CenpB and PML, *Cells 6*, 9.
[54] Gire, V., and Wynford-Thomas, D. (1998) Reinitiation of DNA synthesis and cell division in senescent human fibroblasts by microinjection of anti-p53 antibodies, *Mol. Cell. Biol. 18*, 1611-1621.
[55] Lessman, C. A., Wang, T., Gard, D. L., and Woods, C. W. (1997) Microinjection of anti-alpha-tubulin antibody (DM1A) inhibits progesterone-induced meiotic maturation and deranges the microtubule array in follicle-enclosed oocytes of the frog, Rana pipiens, *Zygote 5*, 83-95.
[56] Kollmannsperger, A., Sharei, A., Raulf, A., Heilemann, M., Langer, R., Jensen, K. F., Wieneke, R., and Tampe, R. (2016) Live-cell protein labelling with nanometre precision by cell squeezing, *Nat Commun 7*, 10372.
[57] Klein, A., Hank, S., Raulf, A., Joest, E. F., Tissen, F., Heilemann, M., Wieneke, R., and Tampe, R. (2018) Live-cell labeling of endogenous proteins with nanometer precision by transduced nanobodies, *Chem Sci 9*, 7835-7842.
[58] Kaczmarczyk, S. J., Sitaraman, K., Young, H. A., Hughes, S. H., and Chatterjee, D. K. (2011) Protein delivery using engineered virus-like particles, *Proc Natl Acad Sci U S A 108*, 16998-17003.
[59] Herce, H. D., Schumacher, D., Schneider, A. F. L., Ludwig, A. K., Mann, F. A., Fillies, M., Kasper, M. A., Reinke, S., Krause, E., Leonhardt, H., Cardoso, M. C., and Hackenberger, C. P. R. (2017) Cell-permeable nanobodies for targeted immunolabelling and antigen manipulation in living cells, *Nat Chem 9*, 762-771.

[60] Glab-Ampai, K., Malik, A. A., Chulanetra, M., Thanongsaksrikul, J., Thueng-In, K., Srimanote, P., Tongtawe, P., and Chaicumpa, W. (2016) Inhibition of HCV replication by humanized-single domain transbodies to NS4B, *Biochem. Biophys. Res. Commun. 476*, 654-664.

[61] Thueng-in, K., Thanongsaksrikul, J., Srimanote, P., Bangphoomi, K., Poungpair, O., Maneewatch, S., Choowongkomon, K., and Chaicumpa, W. (2012) Cell penetrable humanized-VH/V(H)H that inhibit RNA dependent RNA polymerase (NS5B) of HCV, *PLoS One 7*, e49254.

[62] Bruce, V. J., Lopez-Islas, M., and McNaughton, B. R. (2016) Resurfaced cell-penetrating nanobodies: A potentially general scaffold for intracellularly targeted protein discovery, *Protein Sci 25*, 1129-1137.

[63] Bruce, V. J., and McNaughton, B. R. (2017) Inside Job: Methods for Delivering Proteins to the Interior of Mammalian Cells, *Cell Chem Biol 24*, 924-934.

[64] Roder, R., Helma, J., Preiss, T., Radler, J. O., Leonhardt, H., and Wagner, E. (2017) Intracellular Delivery of Nanobodies for Imaging of Target Proteins in Live Cells, *Pharm Res 34*, 161-174.

[65] Chiu, H. Y., Deng, W., Engelke, H., Helma, J., Leonhardt, H., and Bein, T. (2016) Intracellular chromobody delivery by mesoporous silica nanoparticles for antigen targeting and visualization in real time, *Sci Rep 6*, 25019.

[66] Blanco-Toribio, A., Muyldermans, S., Frankel, G., and Fernandez, L. A. (2010) Direct injection of functional single-domain antibodies from E. coli into human cells, *PLoS One 5*, e15227.

[67] Liu, J., Xiong, R., Brans, T., Lippens, S., Parthoens, E., Zanacchi, F. C., Magrassi, R., Singh, S. K., Kurungot, S., Szunerits, S., Bove, H., Ameloot, M., Fraire, J. C., Teirlinck, E., Samal, S. K., Rycke, R., Houthaeve, G., De Smedt, S. C., Boukherroub, R., and Braeckmans, K. (2018) Repeated photoporation with graphene quantum dots enables homogeneous labeling of live cells with extrinsic markers for fluorescence microscopy, *Light Sci Appl 7*, 47.

[68] Liu, J., Hebbrecht, T., Brans, T., Parthoens, E., Lippens, S., Li, C., De Keersmaecker, H., De Vos, W. H., De Smedt, S. C., and Boukherroub, R. Long-term live-cell microscopy with labeled nanobodies delivered by laser-induced photoporation, *Nano Research*, 1-11.

[69] Xiong, R., Samal, S. K., Demeester, J., Skirtach, A. G., De Smedt, S. C., and Braeckmans, K. (2016) Laser-assisted photoporation: fundamentals, technological advances and applications, *Advances in Physics: X 1*, 596-620.

[70] Xiong, R., Raemdonck, K., Peynshaert, K., Lentacker, I., De Cock, I., Demeester, J., De Smedt, S. C., Skirtach, A. G., and Braeckmans, K. (2014) Comparison of gold nanoparticle mediated photoporation: vapor nanobubbles outperform direct heating for delivering macromolecules in live cells, *ACS Nano 8*, 6288-6296.

[71] Delcea, M., Sternberg, N., Yashchenok, A. M., Georgieva, R., Baumler, H., Mohwald, H., and Skirtach, A. G. (2012) Nanoplasmonics for dual-molecule release through nanopores in the membrane of red blood cells, *ACS Nano 6*, 4169-4180.

[72] Yamane, D., Wu, Y. C., Wu, T. H., Toshiyoshi, H., Teitell, M. A., and Chiou, P. Y. (2014) Electrical impedance monitoring of photothermal porated mammalian cells, *J Lab Autom 19*, 50-59.

[73] Xiong, R., Verstraelen, P., Demeester, J., Skirtach, A. G., Timmermans, J. P., De Smedt, S. C., De Vos, W. H., and Braeckmans, K. (2018) Selective Labeling of Individual Neurons in Dense Cultured Networks With Nanoparticle-Enhanced Photoporation, *Front Cell Neurosci 12*, 80.

[74] Wayteck, L., Xiong, R., Braeckmans, K., De Smedt, S. C., and Raemdonck, K. (2017) Comparing photoporation and nucleofection for delivery of small interfering RNA to cytotoxic T cells, *J Control Release 267*, 154-162.

[75] Teng, K. W., Ishitsuka, Y., Ren, P., Youn, Y., Deng, X., Ge, P., Lee, S. H., Belmont, A. S., and Selvin, P. R. (2016) Labeling proteins inside living cells using external fluorophores for microscopy, *Elife 5*, e20378.

[76] Leduc, C., Si, S., Gautier, J., Soto-Ribeiro, M., Wehrle-Haller, B., Gautreau, A., Giannone, G., Cognet, L., and Lounis, B. (2013) A highly specific gold nanoprobe for live-cell single-molecule imaging, *Nano Lett. 13*, 1489-1494.

[77] Pardon, E., Laeremans, T., Triest, S., Rasmussen, S. G., Wohlkonig, A., Ruf, A., Muyldermans, S., Hol, W. G., Kobilka, B. K., and Steyaert, J. (2014) A general protocol for the generation of Nanobodies for structural biology, *Nat Protoc 9*, 674-693.

[78] van der Linden, R., de Geus, B., Stok, W., Bos, W., van Wassenaar, D., Verrips, T., and Frenken, L. (2000) Induction of immune responses and molecular cloning of the heavy chain antibody repertoire of Lama glama, *J. Immunol. Methods 240*, 185-195.

[79] Maass, D. R., Sepulveda, J., Pernthaner, A., and Shoemaker, C. B. (2007) Alpaca (Lama pacos) as a convenient source of recombinant camelid heavy chain antibodies (VHHs), *J. Immunol. Methods 324*, 13-25.

[80] Kastelic, D., Frkovic-Grazio, S., Baty, D., Truan, G., Komel, R., and Pompon, D. (2009) A single-step procedure of recombinant library construction for the selection of efficiently produced llama VH binders directed against cancer markers, *J. Immunol. Methods 350*, 54-62.

[81] Hoogenboom, H. R. (2005) Selecting and screening recombinant antibody libraries, *Nat. Biotechnol. 23*, 1105-1116.

[82] Yan, J., Li, G., Hu, Y., Ou, W., and Wan, Y. (2014) Construction of a synthetic phage-displayed Nanobody library with CDR3 regions randomized by trinucleotide cassettes for diagnostic applications, *J Transl Med 12*, 343.

[83] Harmansa, S., and Affolter, M. (2018) Protein binders and their applications in developmental biology, *Development 145*, dev148874.

[84] Cao, T., and Heng, B. C. (2005) Intracellular antibodies (intrabodies) versus RNA interference for therapeutic applications, *Ann Clin Lab Sci 35*, 227-229.

[85] Koromyslova, A. D., and Hansman, G. S. (2015) Nanobody binding to a conserved epitope promotes norovirus particle disassembly, *J. Virol. 89*, 2718-2730.

[86] Rudolph, M. J., Vance, D. J., Cassidy, M. S., Rong, Y., Shoemaker, C. B., and Mantis, N. J. (2016) Structural analysis of nested neutralizing and non-neutralizing B cell epitopes on ricin toxin's enzymatic subunit, *Proteins 84*, 1162-1172.

[87] Pardon, E., Betti, C., Laeremans, T., Chevillard, F., Guillemyn, K., Kolb, P., Ballet, S., and Steyaert, J. (2018) Nanobody-Enabled Reverse Pharmacology on G-Protein-Coupled Receptors, *Angew Chem Int Ed Engl 57*, 5292-5295.

[88] Morales-Yanez, F. J., Sariego, I., Vincke, C., Hassanzadeh-Ghassabeh, G., Polman, K., and Muyldermans, S. (2019) An innovative approach in the detection of Toxocara canis excretory/secretory antigens using specific nanobodies, *International journal for parasitology 49*, 635-645.

[89] Gelkop, S., Sobarzo, A., Brangel, P., Vincke, C., Romao, E., Fedida-Metula, S., Strom, N., Ataliba, I., Mwiine, F. N., Ochwo, S., Velazquez-Salinas, L., McKendry, R. A., Muyldermans, S., Lutwama, J. J., Rieder, E., Yavelsky, V., and Lobel, L. (2018) The Development and Validation of a Novel Nanobody-Based Competitive ELISA for the Detection of Foot and Mouth Disease 3ABC Antibodies in Cattle, *Front Vet Sci 5*, 250.

[90] Sheng, Y., Wang, K., Lu, Q., Ji, P., Liu, B., Zhu, J., Liu, Q., Sun, Y., Zhang, J., Zhou, E. M., and Zhao, Q. (2019) Nanobody-horseradish peroxidase fusion protein as an ultrasensitive probe to detect antibodies against Newcastle disease virus in the immunoassay, *J Nanobiotechnology 17*, 35.

[91] Katoh, Y., Nakamura, K., and Nakayama, K. (2018) Visible immunoprecipitation (VIP) assay: a simple and versatile method for visual detection of protein-protein interactions, *Bio Protoc. 8*, 2687e.

[92] Pollithy, A., Romer, T., Lang, C., Muller, F. D., Helma, J., Leonhardt, H., Rothbauer, U., and Schuler, D. (2011) Magnetosome expression of functional camelid antibody fragments (nanobodies) in Magnetospirillum gryphiswaldense, *Appl. Environ. Microbiol. 77*, 6165-6171.

[93] Klooster, R., Maassen, B. T., Stam, J. C., Hermans, P. W., Ten Haaft, M. R., Detmers, F. J., de Haard, H. J., Post, J. A., and Theo Verrips, C. (2007) Improved anti-IgG and HSA affinity ligands: clinical application of VHH antibody technology, *J. Immunol. Methods 324*, 1-12.

[94] Jullien, D., Vignard, J., Fedor, Y., Bery, N., Olichon, A., Crozatier, M., Erard, M., Cassard, H., Ducommun, B., Salles, B., and Mirey, G. (2016) Chromatibody, a novel non-invasive molecular tool to explore and manipulate chromatin in living cells, *J Cell Sci 129*, 2673-2683.

[95] de Bruin, R. C. G., Lougheed, S. M., van der Kruk, L., Stam, A. G., Hooijberg, E., Roovers, R. C., van Bergen En Henegouwen, P. M. P., Verheul, H. M. W., de Gruijl, T. D., and van der Vliet, H. J. (2016) Highly specific and potently activating Vgamma9Vdelta2-T cell specific nanobodies for diagnostic and therapeutic applications, *Clin Immunol 169*, 128-138.

[96] Tang, J. C. Y., Drokhlyansky, E., Etemad, B., Rudolph, S., Guo, B., Wang, S., Ellis, E. G., Li, J. Z., and Cepko, C. L. (2016) Detection and manipulation of live antigen-expressing cells using conditionally stable nanobodies, *Elife 5*, e15312.

[97] de Bruin, R. C., Lougheed, S. M., van der Kruk, L., Stam, A. G., Hooijberg, E., Roovers, R. C., en Henegouwen, P. M. v. B., Verheul, H. M., de Gruijl, T. D., and van der Vliet, H. J. (2016) Highly specific and potently activating Vγ9Vδ2-T cell specific nanobodies for diagnostic and therapeutic applications, *Clinical Immunology 169*, 128-138.

[98] Wang, J., Majkova, Z., Bever, C. R., Yang, J., Gee, S. J., Li, J., Xu, T., and Hammock, B. D. (2015) One-step immunoassay for Tetrabromobisphenol A using a camelid single domain antibody–alkaline phosphatase fusion protein, *Analytical chemistry 87*, 4741-4748.

[99] Rothbauer, U., Zolghadr, K., Tillib, S., Nowak, D., Schermelleh, L., Gahl, A., Backmann, N., Conrath, K., Muyldermans, S., Cardoso, M. C., and Leonhardt, H. (2006) Targeting and tracing antigens in live cells with fluorescent nanobodies, *Nat. Methods 3*, 887-889.

[100] Yamagata, M., and Sanes, J. R. (2018) Reporter–nanobody fusions (RANbodies) as versatile, small, sensitive immunohistochemical reagents, *Proceedings of the National Academy of Sciences 115*, 2126-2131.

[101] Persengiev, S. P., Zhu, X., and Green, M. R. (2004) Nonspecific, concentration-dependent stimulation and repression of mammalian gene expression by small interfering RNAs (siRNAs), *RNA 10*, 12-18.

[102] Caussinus, E., Kanca, O., and Affolter, M. (2011) Fluorescent fusion protein knockout mediated by anti-GFP nanobody, *Nat. Struct. Mol. Biol. 19*, 117-121.

[103] Shin, Y. J., Park, S. K., Jung, Y. J., Kim, Y. N., Kim, K. S., Park, O. K., Kwon, S. H., Jeon, S. H., Trinh le, A., Fraser, S. E., Kee, Y., and Hwang, B. J. (2015) Nanobody-targeted E3-ubiquitin ligase complex degrades nuclear proteins, *Sci Rep 5*, 14269.

[104] Fulcher, L. J., Macartney, T., Bozatzi, P., Hornberger, A., Rojas-Fernandez, A., and Sapkota, G. P. (2016) An affinity-directed protein missile system for targeted proteolysis, *Open Biol 6*, 160255.

[105] Fulcher, L. J., Hutchinson, L. D., Macartney, T. J., Turnbull, C., and Sapkota, G. P. (2017) Targeting endogenous proteins for degradation through the affinity-directed protein missile system, *Open Biol 7*, 170066.

[106] Daniel, K., Icha, J., Horenburg, C., Muller, D., Norden, C., and Mansfeld, J. (2018) Conditional control of fluorescent protein degradation by an auxin-dependent nanobody, *Nat Commun 9*, 3297.

[107] Carlson, J. R. (1988) A new means of inducibly inactivating a cellular protein, *Mol. Cell. Biol. 8*, 2638-2646.

[108] Herce, H. D., Deng, W., Helma, J., Leonhardt, H., and Cardoso, M. C. (2013) Visualization and targeted disruption of protein interactions in living cells, *Nat Commun 4*, 2660.

[109] Chaikuad, A., Keates, T., Vincke, C., Kaufholz, M., Zenn, M., Zimmermann, B., Gutierrez, C., Zhang, R. G., Hatzos-Skintges, C., Joachimiak, A., Muyldermans, S., Herberg, F. W., Knapp, S., and Muller, S. (2014) Structure of cyclin G-associated kinase (GAK) trapped in different conformations using nanobodies, *Biochem. J. 459*, 59-69.

[110] Rasmussen, S. G., Choi, H. J., Fung, J. J., Pardon, E., Casarosa, P., Chae, P. S., Devree, B. T., Rosenbaum, D. M., Thian, F. S., Kobilka, T. S., Schnapp, A., Konetzki, I., Sunahara, R. K., Gellman, S. H., Pautsch, A., Steyaert, J., Weis, W. I., and Kobilka, B. K. (2011) Structure of a nanobody-stabilized active state of the beta(2) adrenoceptor, *Nature 469*, 175-180.

[111] Abskharon, R. N., Giachin, G., Wohlkonig, A., Soror, S. H., Pardon, E., Legname, G., and Steyaert, J. (2014) Probing the N-terminal beta-sheet conversion in the crystal structure of the human prion protein bound to a nanobody, *J Am Chem Soc 136*, 937-944.

[112] De Genst, E., Chan, P. H., Pardon, E., Hsu, S. D., Kumita, J. R., Christodoulou, J., Menzer, L., Chirgadze, D. Y., Robinson, C. V., Muyldermans, S., Matagne, A., Wyns, L., Dobson, C. M., and Dumoulin, M. (2013) A nanobody binding to non-amyloidogenic regions of the protein human lysozyme enhances partial unfolding but inhibits amyloid fibril formation, *J Phys Chem B 117*, 13245-13258.

[113] Heukers, R., De Groof, T. W. M., and Smit, M. J. (2019) Nanobodies detecting and modulating GPCRs outside in and inside out, *Curr. Opin. Cell Biol. 57*, 115-122.

[114] Kirchhofer, A., Helma, J., Schmidthals, K., Frauer, C., Cui, S., Karcher, A., Pellis, M., Muyldermans, S., Casas-Delucchi, C. S., Cardoso, M. C., Leonhardt, H., Hopfner, K. P., and Rothbauer, U. (2010) Modulation of protein properties in living cells using nanobodies, *Nat. Struct. Mol. Biol. 17*, 133-138.

[115] von Behring, E., and Kitasato, S. (1890) The mechanism of immunity in animals to diphtheria and tetanus, *Deutsche Med. Wochenschr*.

[116] Vaneycken, I., Govaert, J., Vincke, C., Caveliers, V., Lahoutte, T., De Baetselier, P., Raes, G., Bossuyt, A., Muyldermans, S., and Devoogdt, N. (2010) In vitro analysis and in vivo tumor targeting of a humanized, grafted nanobody in mice using pinhole SPECT/micro-CT, *Journal of Nuclear Medicine 51*, 1099-1106.

[117] Huang, L., Gainkam, L. O. T., Caveliers, V., Vanhove, C., Keyaerts, M., De Baetselier, P., Bossuyt, A., Revets, H., and Lahoutte, T. (2008) SPECT imaging with 99m Tc-labeled EGFR-specific nanobody for in vivo monitoring of EGFR expression, *Molecular imaging and biology 10*, 167-175.

[118] Vosjan, M. J. W. D., Perk, L. R., Roovers, R. C., Visser, G. W. M., Stigter-van Walsum, M., en Henegouwen, P. M. P. v. B., and van Dongen, G. A. M. S. (2011) Facile labelling of an anti-epidermal growth factor receptor Nanobody with 68 Ga via a novel bifunctional desferal chelate for immuno-PET, *European journal of nuclear medicine and molecular imaging 38*, 753-763.

[119] Iezzi, M. E., Policastro, L., Werbajh, S., Podhajcer, O., and Canziani, G. A. (2018) Single-Domain Antibodies and the Promise of Modular Targeting in Cancer Imaging and Treatment, *Front Immunol 9*, 273.
[120] Habib, I., Smolarek, D., Hattab, C., Grodecka, M., Hassanzadeh-Ghassabeh, G., Muyldermans, S., Sagan, S., Gutiérrez, C., Laperche, S., and Le-Van-Kim, C. (2013) VHH (nanobody) directed against human glycophorin A: A tool for autologous red cell agglutination assays, *Analytical biochemistry 438*, 82-89.
[121] Even-Desrumeaux, K., Baty, D., and Chames, P. (2010) Strong and oriented immobilization of single domain antibodies from crude bacterial lysates for high-throughput compatible cost-effective antibody array generation, *Mol Biosyst 6*, 2241-2248.
[122] D'Huyvetter, M., Vincke, C., Xavier, C., Aerts, A., Impens, N., Baatout, S., De Raeve, H., Muyldermans, S., Caveliers, V., Devoogdt, N., and Lahoutte, T. (2014) Targeted radionuclide therapy with A 177Lu-labeled anti-HER2 nanobody, *Theranostics 4*, 708-720.
[123] Tang, J., Li, J., Zhu, X., Yu, Y., Chen, D., Yuan, L., Gu, Z., Zhang, X., Qi, L., Gong, Z., Jiang, P., Yu, J., Meng, H., An, G., Zheng, H., and Yang, L. (2016) Novel CD7-specific nanobody-based immunotoxins potently enhanced apoptosis of CD7-positive malignant cells, *Oncotarget 7*, 34070-34083.
[124] Yu, Y., Li, J., Zhu, X., Tang, X., Bao, Y., Sun, X., Huang, Y., Tian, F., Liu, X., and Yang, L. (2017) Humanized CD7 nanobody-based immunotoxins exhibit promising anti-T-cell acute lymphoblastic leukemia potential, *Int J Nanomedicine 12*, 1969-1983.
[125] Cortez-Retamozo, V., Backmann, N., Senter, P. D., Wernery, U., De Baetselier, P., Muyldermans, S., and Revets, H. (2004) Efficient cancer therapy with a nanobody-based conjugate, *Cancer Res. 64*, 2853-2857.
[126] Talelli, M., Oliveira, S., Rijcken, C. J., Pieters, E. H., Etrych, T., Ulbrich, K., van Nostrum, R. C., Storm, G., Hennink, W. E., and Lammers, T. (2013) Intrinsically active nanobody-modified polymeric micelles for tumor-targeted combination therapy, *Biomaterials 34*, 1255-1260.
[127] Holz, J. B. (2012) The TITAN trial--assessing the efficacy and safety of an anti-von Willebrand factor Nanobody in patients with acquired thrombotic thrombocytopenic purpura, *Transfus Apher Sci 46*, 343-346.
[128] Dumet, C., Pottier, J., Gouilleux, V., and Watier, H. (2018) New structural formats of therapeutic antibodies for rheumatology, *Joint Bone Spine 85*, 47-52.
[129] Chen, Y., and Xu, Y. (2017) Pharmacokinetics of Bispecific Antibody, *Current Pharmacology Reports 3*, 126-137.
[130] Peyvandi, F., Scully, M., Kremer Hovinga, J. A., Cataland, S., Knöbl, P., Wu, H., Artoni, A., Westwood, J.-P., Mansouri Taleghani, M., and Jilma, B. (2016) Caplacizumab for acquired thrombotic thrombocytopenic purpura, *New Engl. J. Med. 374*, 511-522.
[131] Callewaert, F., Roodt, J., Ulrichts, H., Stohr, T., van Rensburg, W. J., Lamprecht, S., Rossenu, S., Priem, S., Willems, W., and Holz, J. B. (2012) Evaluation of efficacy and safety of the anti-VWF Nanobody ALX-0681 in a preclinical baboon model of acquired thrombotic thrombocytopenic purpura, *Blood 120*, 3603-3610.
[132] Hmila, I., Abdallah, R. B., Saerens, D., Benlasfar, Z., Conrath, K., Ayeb, M. E., Muyldermans, S., and Bouhaouala-Zahar, B. (2008) VHH, bivalent domains and chimeric Heavy chain-only antibodies with high neutralizing efficacy for scorpion toxin AahI', *Mol. Immunol. 45*, 3847-3856.
[133] Ladenson, R. C., Crimmins, D. L., Landt, Y., and Ladenson, J. H. (2006) Isolation and characterization of a thermally stable recombinant anti-caffeine heavy-chain antibody fragment, *Anal Chem 78*, 4501-4508.
[134] Helma, J., Cardoso, M. C., Muyldermans, S., and Leonhardt, H. (2015) Nanobodies and recombinant binders in cell biology, *J Cell Biol 209*, 633-644.
[135] Koide, S., Koide, A., and Lipovšek, D. (2012) Target-binding proteins based on the 10th human fibronectin type III domain (10Fn3), In *Methods Enzymol.*, pp 135-156, Elsevier.
[136] Koide, A., Bailey, C. W., Huang, X., and Koide, S. (1998) The fibronectin type III domain as a scaffold for novel binding proteins, *J. Mol. Biol. 284*, 1141-1151.
[137] Lofblom, J., Frejd, F. Y., and Stahl, S. (2011) Non-immunoglobulin based protein scaffolds, *Curr. Opin. Biotechnol. 22*, 843-848.
[138] Plaxco, K. W., Spitzfaden, C., Campbell, I. D., and Dobson, C. M. (1996) Rapid refolding of a proline-rich all-beta-sheet fibronectin type III module, *Proc Natl Acad Sci U S A 93*, 10703-10706.
[139] Dineen, S. P., Sullivan, L. A., Beck, A. W., Miller, A. F., Carbon, J. G., Mamluk, R., Wong, H., and Brekken, R. A. (2008) The Adnectin CT-322 is a novel VEGF receptor 2 inhibitor that decreases tumor burden in an orthotopic mouse model of pancreatic cancer, *BMC Cancer 8*, 352.
[140] Tolcher, A. W., Sweeney, C. J., Papadopoulos, K., Patnaik, A., Chiorean, E. G., Mita, A. C., Sankhala, K., Furfine, E., Gokemeijer, J., Iacono, L., Eaton, C., Silver, B. A., and Mita, M. (2011) Phase I and

pharmacokinetic study of CT-322 (BMS-844203), a targeted Adnectin inhibitor of VEGFR-2 based on a domain of human fibronectin, *Clin. Cancer. Res. 17*, 363-371.
[141] Sha, F., Salzman, G., Gupta, A., and Koide, S. (2017) Monobodies and other synthetic binding proteins for expanding protein science, *Protein Sci 26*, 910-924.
[142] Lofblom, J., Feldwisch, J., Tolmachev, V., Carlsson, J., Stahl, S., and Frejd, F. Y. (2010) Affibody molecules: engineered proteins for therapeutic, diagnostic and biotechnological applications, *FEBS Lett. 584*, 2670-2680.
[143] Nord, K., Gunneriusson, E., Ringdahl, J., Stahl, S., Uhlen, M., and Nygren, P. A. (1997) Binding proteins selected from combinatorial libraries of an alpha-helical bacterial receptor domain, *Nat. Biotechnol. 15*, 772-777.
[144] Wikman, M., Steffen, A. C., Gunneriusson, E., Tolmachev, V., Adams, G. P., Carlsson, J., and Stahl, S. (2004) Selection and characterization of HER2/neu-binding affibody ligands, *Protein Eng. Des. Sel. 17*, 455-462.
[145] Feldwisch, J., Tolmachev, V., Lendel, C., Herne, N., Sjoberg, A., Larsson, B., Rosik, D., Lindqvist, E., Fant, G., Hoiden-Guthenberg, I., Galli, J., Jonasson, P., and Abrahmsen, L. (2010) Design of an optimized scaffold for affibody molecules, *J. Mol. Biol. 398*, 232-247.
[146] Binz, H. K., Amstutz, P., and Pluckthun, A. (2005) Engineering novel binding proteins from nonimmunoglobulin domains, *Nat. Biotechnol. 23*, 1257-1268.
[147] Baum, R. P., Prasad, V., Müller, D., Schuchardt, C., Orlova, A., Wennborg, A., Tolmachev, V., and Feldwisch, J. (2010) Molecular imaging of HER2-expressing malignant tumors in breast cancer patients using synthetic 111In-or 68Ga-labeled affibody molecules, *Journal of nuclear medicine 51*, 892-897.
[148] Lindborg, M., Cortez, E., Hoiden-Guthenberg, I., Gunneriusson, E., von Hage, E., Syud, F., Morrison, M., Abrahmsen, L., Herne, N., Pietras, K., and Frejd, F. Y. (2011) Engineered high-affinity affibody molecules targeting platelet-derived growth factor receptor beta in vivo, *J. Mol. Biol. 407*, 298-315.
[149] Beste, G., Schmidt, F. S., Stibora, T., and Skerra, A. (1999) Small antibody-like proteins with prescribed ligand specificities derived from the lipocalin fold, *Proc Natl Acad Sci U S A 96*, 1898-1903.
[150] Binz, H. K., Stumpp, M. T., Forrer, P., Amstutz, P., and Pluckthun, A. (2003) Designing repeat proteins: well-expressed, soluble and stable proteins from combinatorial libraries of consensus ankyrin repeat proteins, *J. Mol. Biol. 332*, 489-503.
[151] Li, J., Mahajan, A., and Tsai, M. D. (2006) Ankyrin repeat: a unique motif mediating protein-protein interactions, *Biochemistry 45*, 15168-15178.
[152] Kohl, A., Binz, H. K., Forrer, P., Stumpp, M. T., Pluckthun, A., and Grutter, M. G. (2003) Designed to be stable: crystal structure of a consensus ankyrin repeat protein, *Proc Natl Acad Sci U S A 100*, 1700-1705.
[153] Parizek, P., Kummer, L., Rube, P., Prinz, A., Herberg, F. W., and Pluckthun, A. (2012) Designed ankyrin repeat proteins (DARPins) as novel isoform-specific intracellular inhibitors of c-Jun N-terminal kinases, *ACS Chem Biol 7*, 1356-1366.
[154] Robertson, D. L., and Joyce, G. F. (1990) Selection in vitro of an RNA enzyme that specifically cleaves single-stranded DNA, *Nature 344*, 467-468.
[155] Tuerk, C., and Gold, L. (1990) Systematic evolution of ligands by exponential enrichment: RNA ligands to bacteriophage T4 DNA polymerase, *Science 249*, 505-510.
[156] Ellington, A. D., and Szostak, J. W. (1990) In vitro selection of RNA molecules that bind specific ligands, *Nature 346*, 818-822.
[157] Proske, D., Blank, M., Buhmann, R., and Resch, A. (2005) Aptamers—basic research, drug development, and clinical applications, *Appl. Microbiol. Biotechnol. 69*, 367-374.
[158] Wolter, O., and Mayer, G. (2017) Aptamers as Valuable Molecular Tools in Neurosciences, *J. Neurosci. 37*, 2517-2523.
[159] Keefe, A. D., Pai, S., and Ellington, A. (2010) Aptamers as therapeutics, *Nature reviews Drug discovery 9*, 537-550.
[160] Jayasena, S. D. (1999) Aptamers: An emerging class of molecules that rival antibodies in diagnostics, *Clin. Chem. 45*, 1628-1650.
[161] Ganji, A., Islami, M., Ejtehadifar, M., Zarei-Mehrvarz, E., and Darvish, M. (2019) Nanobody and aptamer as targeting moiety against bacterial toxins, *Rev. Med. Microbiol. 30*, 183-190.
[162] Opalinska, J. B., and Gewirtz, A. M. (2002) Nucleic-acid therapeutics: basic principles and recent applications, *Nat. Rev. Drug Discov. 1*, 503-514.
[163] Fornasiero, E. F., and Opazo, F. (2015) Super-resolution imaging for cell biologists: concepts, applications, current challenges and developments, *Bioessays 37*, 436-451.

[164] Mikhaylova, M., Cloin, B. M. C., Finan, K., van den Berg, R., Teeuw, J., Kijanka, M. M., Sokolowski, M., Katrukha, E. A., Maidorn, M., Opazo, F., Moutel, S., Vantard, M., Perez, F., Henegouwen, P. M. P. V. E., Hoogenraad, C. C., Ewers, H., and Kapitein, L. C. (2015) Resolving bundled microtubules using anti-tubulin nanobodies, *Nature Communications 6*, 7933.
[165] Virant, D., Traenkle, B., Maier, J., Kaiser, P. D., Bodenhofer, M., Schmees, C., Vojnovic, I., Pisak-Lukats, B., Endesfelder, U., and Rothbauer, U. (2018) A peptide tag-specific nanobody enables high-quality labeling for dSTORM imaging, *Nat Commun 9*, 930.
[166] Opazo, F., Levy, M., Byrom, M., Schafer, C., Geisler, C., Groemer, T. W., Ellington, A. D., and Rizzoli, S. O. (2012) Aptamers as potential tools for super-resolution microscopy, *Nat. Methods 9*, 938-939.
[167] Stadler, C., Rexhepaj, E., Singan, V. R., Murphy, R. F., Pepperkok, R., Uhlén, M., Simpson, J. C., and Lundberg, E. (2013) Immunofluorescence and fluorescent-protein tagging show high correlation for protein localization in mammalian cells, *Nature methods 10*, 315.
[168] Margolin, W. (2012) The price of tags in protein localization studies, *J Bacteriol 194*, 6369-6371.
[169] Jain, R. K., Joyce, P. B., Molinete, M., Halban, P. A., and Gorr, S. U. (2001) Oligomerization of green fluorescent protein in the secretory pathway of endocrine cells, *Biochem. J. 360*, 645-649.
[170] Snapp, E. L. (2009) Fluorescent proteins: a cell biologist's user guide, *Trends Cell Biol 19*, 649-655.
[171] Panza, P., Maier, J., Schmees, C., Rothbauer, U., and Söllner, C. (2015) Live imaging of endogenous protein dynamics in zebrafish using chromobodies, *Development 142*, 1879-1884.
[172] Zolghadr, K., Gregor, J., Leonhardt, H., and Rothbauer, U. (2012) Case study on live cell apoptosis-assay using lamin-chromobody cell-lines for high-content analysis, In *Single Domain Antibodies*, pp 569-575, Springer.
[173] Ahmed, S. (2011) Nanoscopy of cell architecture: The actin-membrane interface, *Bioarchitecture 1*, 32-38.
[174] Thorley, J. A., Pike, J., and Rappoport, J. Z. (2014) Super-resolution microscopy: A comparison of commercially available options, pp 199-212, Elsevier.
[175] Huang, B., Bates, M., and Zhuang, X. (2009) Super-resolution fluorescence microscopy, *Annu. Rev. Biochem. 78*, 993-1016.
[176] Abbe, E. (1873) Beiträge zur Theorie des Mikroskops und der mikroskopischen Wahrnehmung, *Archiv für mikroskopische Anatomie 9*, 413-418.
[177] Schermelleh, L., Heintzmann, R., and Leonhardt, H. (2010) A guide to super-resolution fluorescence microscopy, *J Cell Biol 190*, 165-175.
[178] Ries, J., Kaplan, C., Platonova, E., Eghlidi, H., and Ewers, H. (2012) A simple, versatile method for GFP-based super-resolution microscopy via nanobodies, *Nat. Methods 9*, 582-584.
[179] Pleiner, T., Bates, M., Trakhanov, S., Lee, C. T., Schliep, J. E., Chug, H., Bohning, M., Stark, H., Urlaub, H., and Gorlich, D. (2015) Nanobodies: site-specific labeling for super-resolution imaging, rapid epitope-mapping and native protein complex isolation, *Elife 4*, e11349.
[180] Peyrassol, X., Laeremans, T., Gouwy, M., Lahura, V., Debulpaep, M., Van Damme, J., Steyaert, J., Parmentier, M., and Langer, I. (2016) Development by Genetic Immunization of Monovalent Antibodies (Nanobodies) Behaving as Antagonists of the Human ChemR23 Receptor, *J. Immunol. 196*, 2893-2901.
[181] Liss, V., Barlag, B., Nietschke, M., and Hensel, M. (2015) Self-labelling enzymes as universal tags for fluorescence microscopy, super-resolution microscopy and electron microscopy, *Sci Rep 5*, 17740.
[182] Hinner, M. J., and Johnsson, K. (2010) How to obtain labeled proteins and what to do with them, *Curr. Opin. Biotechnol. 21*, 766-776.
[183] Lang, K., and Chin, J. W. (2014) Cellular incorporation of unnatural amino acids and bioorthogonal labeling of proteins, *Chem Rev 114*, 4764-4806.
[184] Los, G. V., Encell, L. P., McDougall, M. G., Hartzell, D. D., Karassina, N., Zimprich, C., Wood, M. G., Learish, R., Ohana, R. F., Urh, M., Simpson, D., Mendez, J., Zimmerman, K., Otto, P., Vidugiris, G., Zhu, J., Darzins, A., Klaubert, D. H., Bulleit, R. F., and Wood, K. V. (2008) HaloTag: a novel protein labeling technology for cell imaging and protein analysis, *ACS Chem Biol 3*, 373-382.
[185] Keppler, A., Gendreizig, S., Gronemeyer, T., Pick, H., Vogel, H., and Johnsson, K. (2003) A general method for the covalent labeling of fusion proteins with small molecules in vivo, *Nat. Biotechnol. 21*, 86-89.
[186] Gautier, A., Juillerat, A., Heinis, C., Correa, I. R., Jr., Kindermann, M., Beaufils, F., and Johnsson, K. (2008) An engineered protein tag for multiprotein labeling in living cells, *Chem. Biol. 15*, 128-136.
[187] Liu, J., Hanne, J., Britton, B. M., Shoffner, M., Albers, A. E., Bennett, J., Zatezalo, R., Barfield, R., Rabuka, D., Lee, J. B., and Fishel, R. (2015) An Efficient Site-Specific Method for Irreversible Covalent Labeling of Proteins with a Fluorophore, *Sci Rep 5*, 16883.

[188] Schumacher, D., Lemke, O., Helma, J., Gerszonowicz, L., Waller, V., Stoschek, T., Durkin, P. M., Budisa, N., Leonhardt, H., Keller, B. G., and Hackenberger, C. P. R. (2017) Broad substrate tolerance of tubulin tyrosine ligase enables one-step site-specific enzymatic protein labeling, *Chem Sci 8*, 3471-3478.

[189] Schumacher, D., Helma, J., Mann, F. A., Pichler, G., Natale, F., Krause, E., Cardoso, M. C., Hackenberger, C. P., and Leonhardt, H. (2015) Versatile and Efficient Site-Specific Protein Functionalization by Tubulin Tyrosine Ligase, *Angew Chem Int Ed Engl 54*, 13787-13791.

[190] Theile, C. S., Witte, M. D., Blom, A. E., Kundrat, L., Ploegh, H. L., and Guimaraes, C. P. (2013) Site-specific N-terminal labeling of proteins using sortase-mediated reactions, *Nat Protoc 8*, 1800-1807.

[191] Massa, S., Vikani, N., Betti, C., Ballet, S., Vanderhaegen, S., Steyaert, J., Descamps, B., Vanhove, C., Bunschoten, A., van Leeuwen, F. W., Hernot, S., Caveliers, V., Lahoutte, T., Muyldermans, S., Xavier, C., and Devoogdt, N. (2016) Sortase A-mediated site-specific labeling of camelid single-domain antibody-fragments: a versatile strategy for multiple molecular imaging modalities, *Contrast Media Mol Imaging 11*, 328-339.

[192] Truttmann, M. C., Wu, Q., Stiegeler, S., Duarte, J. N., Ingram, J., and Ploegh, H. L. (2015) HypE-specific nanobodies as tools to modulate HypE-mediated target AMPylation, *J Biol Chem 290*, 9087-9100.

[193] Fabricius, V., Lefebre, J., Geertsema, H., Marino, S. F., and Ewers, H. (2018) Rapid and efficient C-terminal labeling of nanobodies for DNA-PAINT, *Journal of Physics D-Applied Physics 51*, 474005.

[194] Witte, M. D., Cragnolini, J. J., Dougan, S. K., Yoder, N. C., Popp, M. W., and Ploegh, H. L. (2012) Preparation of unnatural N-to-N and C-to-C protein fusions, *Proc Natl Acad Sci U S A 109*, 11993-11998.

[195] Hudak, J. E., Barfield, R. M., de Hart, G. W., Grob, P., Nogales, E., Bertozzi, C. R., and Rabuka, D. (2012) Synthesis of heterobifunctional protein fusions using copper-free click chemistry and the aldehyde tag, *Angew. Chem. 51*, 4161-4165.

[196] Jeger, S., Zimmermann, K., Blanc, A., Grunberg, J., Honer, M., Hunziker, P., Struthers, H., and Schibli, R. (2010) Site-specific and stoichiometric modification of antibodies by bacterial transglutaminase, *Angew Chem Int Ed Engl 49*, 9995-9997.

[197] Liu, J., Hanne, J., Britton, B. M., Shoffner, M., Albers, A. E., Bennett, J., Zatezalo, R., Barfield, R., Rabuka, D., and Lee, J.-B. (2015) An efficient site-specific method for irreversible covalent labeling of proteins with a fluorophore, *Scientific reports 5*, 16883.

[198] Dennler, P., Bailey, L. K., Spycher, P. R., Schibli, R., and Fischer, E. (2015) Microbial transglutaminase and c-myc-tag: a strong couple for the functionalization of antibody-like protein scaffolds from discovery platforms, *ChemBioChem 16*, 861-867.

[199] Massa, S., Xavier, C., De Vos, J., Caveliers, V., Lahoutte, T., Muyldermans, S., and Devoogdt, N. (2014) Site-specific labeling of cysteine-tagged camelid single-domain antibody-fragments for use in molecular imaging, *Bioconjug Chem 25*, 979-988.

[200] Platonova, E., Winterflood, C. M., Junemann, A., Albrecht, D., Faix, J., and Ewers, H. (2015) Single-molecule microscopy of molecules tagged with GFP or RFP derivatives in mammalian cells using nanobody binders, *Methods 88*, 89-97.

[201] Mikhaylova, M., Cloin, B. M., Finan, K., van den Berg, R., Teeuw, J., Kijanka, M. M., Sokolowski, M., Katrukha, E. A., Maidorn, M., Opazo, F., Moutel, S., Vantard, M., Perez, F., van Bergen en Henegouwen, P. M., Hoogenraad, C. C., Ewers, H., and Kapitein, L. C. (2015) Resolving bundled microtubules using anti-tubulin nanobodies, *Nat Commun 6*, 7933.

[202] Kim, Y., Ho, S. O., Gassman, N. R., Korlann, Y., Landorf, E. V., Collart, F. R., and Weiss, S. (2008) Efficient site-specific labeling of proteins via cysteines, *Bioconjug Chem 19*, 786-791.

[203] Vugmeyster, Y., Entrican, C. A., Joyce, A. P., Lawrence-Henderson, R. F., Leary, B. A., Mahoney, C. S., Patel, H. K., Raso, S. W., Olland, S. H., Hegen, M., and Xu, X. (2012) Pharmacokinetic, biodistribution, and biophysical profiles of TNF nanobodies conjugated to linear or branched poly(ethylene glycol), *Bioconjug Chem 23*, 1452-1462.

[204] Sadeqzadeh, E., Rahbarizadeh, F., Ahmadvand, D., Rasaee, M. J., Parhamifar, L., and Moghimi, S. M. (2011) Combined MUC1-specific nanobody-tagged PEG-polyethylenimine polyplex targeting and transcriptional targeting of tBid transgene for directed killing of MUC1 over-expressing tumour cells, *J Control Release 156*, 85-91.

[205] Kijanka, M., Warnders, F. J., El Khattabi, M., Lub-de Hooge, M., van Dam, G. M., Ntziachristos, V., de Vries, L., Oliveira, S., and van Bergen En Henegouwen, P. M. (2013) Rapid optical imaging of human breast tumour xenografts using anti-HER2 VHHs site-directly conjugated to IRDye 800CW for image-guided surgery, *Eur J Nucl Med Mol Imaging 40*, 1718-1729.

[206] Pleiner, T., Bates, M., and Gorlich, D. (2018) A toolbox of anti-mouse and anti-rabbit IgG secondary nanobodies, *J Cell Biol 217*, 1143-1154.
[207] Ramos-Gomes, F., Bode, J., Sukhanova, A., Bozrova, S. V., Saccomano, M., Mitkovski, M., Krueger, J. E., Wege, A. K., Stuehmer, W., Samokhvalov, P. S., Baty, D., Chames, P., Nabiev, I., and Alves, F. (2018) Single- and two-photon imaging of human micrometastases and disseminated tumour cells with conjugates of nanobodies and quantum dots, *Sci Rep 8*, 4595.
[208] Sukhanova, A., Even-Desrumeaux, K., Kisserli, A., Tabary, T., Reveil, B., Millot, J. M., Chames, P., Baty, D., Artemyev, M., Oleinikov, V., Pluot, M., Cohen, J. H., and Nabiev, I. (2012) Oriented conjugates of single-domain antibodies and quantum dots: toward a new generation of ultrasmall diagnostic nanoprobes, *Nanomedicine 8*, 516-525.
[209] Chen, X., Li, F., and Wu, Y. W. (2015) Chemical labeling of intracellular proteins via affinity conjugation and strain-promoted cycloadditions in live cells, *Chem Commun (Camb) 51*, 16537-16540.
[210] Graulus, G. J., Ta, D. T., Tran, H., Hansen, R., Billen, B., Royackers, E., Noben, J. P., Devoogdt, N., Muyldermans, S., Guedens, W., and Adriaensens, P. (2019) Site-Selective Functionalization of Nanobodies Using Intein-Mediated Protein Ligation for Innovative Bioconjugation, *Methods Mol Biol 2033*, 117-130.
[211] Muir, T. W., Sondhi, D., and Cole, P. A. (1998) Expressed protein ligation: a general method for protein engineering, *Proc Natl Acad Sci U S A 95*, 6705-6710.
[212] Evans Jr, T. C., and Xu, M. Q. (1999) Intein-mediated protein ligation: Harnessing nature's escape artists, *Peptide Science 51*, 333-342.
[213] Sun, L., Ghosh, I., Barshevsky, T., Kochinyan, S., and Xu, M. Q. (2007) Design, preparation and use of ligated phosphoproteins: a novel approach to study protein phosphatases by dot blot array, ELISA and Western blot assays, *Methods 42*, 220-226.
[214] Evans Jr, T. C., Benner, J., and Xu, M. Q. (1998) Semisynthesis of cytotoxic proteins using a modified protein splicing element, *Protein science 7*, 2256-2264.
[215] Van Overbeke, W., Verhelle, A., Everaert, I., Zwaenepoel, O., Vandekerckhove, J., Cuvelier, C., Derave, W., and Gettemans, J. (2014) Chaperone nanobodies protect gelsolin against MT1-MMP degradation and alleviate amyloid burden in the gelsolin amyloidosis mouse model, *Mol. Ther. 22*, 1768-1778.
[216] Liu, C. C., and Schultz, P. G. (2010) Adding new chemistries to the genetic code, *Annu. Rev. Biochem. 79*, 413-444.
[217] Lee, K. J., Kang, D., and Park, H. S. (2019) Site-Specific Labeling of Proteins Using Unnatural Amino Acids, *Mol Cells 42*, 386-396.
[218] Wals, K., and Ovaa, H. (2014) Unnatural amino acid incorporation in E. coli: current and future applications in the design of therapeutic proteins, *Front Chem 2*, 15.
[219] Korkmaz, G., Holm, M., Wiens, T., and Sanyal, S. (2014) Comprehensive analysis of stop codon usage in bacteria and its correlation with release factor abundance, *J Biol Chem 289*, 30334-30342.
[220] Young, D. D., and Schultz, P. G. (2018) Playing with the Molecules of Life, *ACS Chem Biol 13*, 854-870.
[221] Chin, J. W. (2014) Expanding and reprogramming the genetic code of cells and animals, *Annu. Rev. Biochem. 83*, 379-408.
[222] Chin, J. W. (2017) Expanding and reprogramming the genetic code, *Nature 550*, 53-60.
[223] Chatterjee, A., Guo, J., Lee, H. S., and Schultz, P. G. (2013) A genetically encoded fluorescent probe in mammalian cells, *J Am Chem Soc 135*, 12540-12543.
[224] Takimoto, J. K., Dellas, N., Noel, J. P., and Wang, L. (2011) Stereochemical basis for engineered pyrrolysyl-tRNA synthetase and the efficient in vivo incorporation of structurally divergent non-native amino acids, *ACS Chem Biol 6*, 733-743.
[225] Chin, J. W., Santoro, S. W., Martin, A. B., King, D. S., Wang, L., and Schultz, P. G. (2002) Addition of p-azido-L-phenylalanine to the genetic code of Escherichia coli, *J Am Chem Soc 124*, 9026-9027.
[226] Schmidt, M. J., Weber, A., Pott, M., Welte, W., and Summerer, D. (2014) Structural basis of furan-amino acid recognition by a polyspecific aminoacyl-tRNA-synthetase and its genetic encoding in human cells, *ChemBioChem 15*, 1755-1760.
[227] Antonatou, E., Hoogewijs, K., Kalaitzakis, D., Baudot, A., Vassilikogiannakis, G., and Madder, A. (2016) Singlet Oxygen-Induced Furan Oxidation for Site-Specific and Chemoselective Peptide Ligation, *Chemistry 22*, 8457-8461.
[228] Schmidt, M. J., and Summerer, D. (2013) Red-light-controlled protein-RNA crosslinking with a genetically encoded furan, *Angew Chem Int Ed Engl 52*, 4690-4693.
[229] Furter, R. (1998) Expansion of the genetic code: site-directed p-fluoro-phenylalanine incorporation in Escherichia coli, *Protein Sci 7*, 419-426.

[230] Fleissner, M. R., Brustad, E. M., Kalai, T., Altenbach, C., Cascio, D., Peters, F. B., Hideg, K., Peuker, S., Schultz, P. G., and Hubbell, W. L. (2009) Site-directed spin labeling of a genetically encoded unnatural amino acid, *Proc Natl Acad Sci U S A 106*, 21637-21642.
[231] Axup, J. Y., Bajjuri, K. M., Ritland, M., Hutchins, B. M., Kim, C. H., Kazane, S. A., Halder, R., Forsyth, J. S., Santidrian, A. F., and Stafin, K. (2012) Synthesis of site-specific antibody-drug conjugates using unnatural amino acids, *Proceedings of the National Academy of Sciences 109*, 16101-16106.
[232] Alfonta, L., Zhang, Z., Uryu, S., Loo, J. A., and Schultz, P. G. (2003) Site-specific incorporation of a redox-active amino acid into proteins, *J Am Chem Soc 125*, 14662-14663.
[233] Schultz, K. C., Supekova, L., Ryu, Y., Xie, J., Perera, R., and Schultz, P. G. (2006) A genetically encoded infrared probe, *J Am Chem Soc 128*, 13984-13985.
[234] Cellitti, S. E., Jones, D. H., Lagpacan, L., Hao, X., Zhang, Q., Hu, H., Brittain, S. M., Brinker, A., Caldwell, J., Bursulaya, B., Spraggon, G., Brock, A., Ryu, Y., Uno, T., Schultz, P. G., and Geierstanger, B. H. (2008) In vivo incorporation of unnatural amino acids to probe structure, dynamics, and ligand binding in a large protein by nuclear magnetic resonance spectroscopy, *J Am Chem Soc 130*, 9268-9281.
[235] Xie, J., Wang, L., Wu, N., Brock, A., Spraggon, G., and Schultz, P. G. (2004) The site-specific incorporation of p-iodo-L-phenylalanine into proteins for structure determination, *Nat. Biotechnol. 22*, 1297-1301.
[236] Sakamoto, K., Murayama, K., Oki, K., Iraha, F., Kato-Murayama, M., Takahashi, M., Ohtake, K., Kobayashi, T., Kuramitsu, S., Shirouzu, M., and Yokoyama, S. (2009) Genetic encoding of 3-iodo-L-tyrosine in Escherichia coli for single-wavelength anomalous dispersion phasing in protein crystallography, *Structure 17*, 335-344.
[237] Brustad, E. M., Lemke, E. A., Schultz, P. G., and Deniz, A. A. (2008) A general and efficient method for the site-specific dual-labeling of proteins for single molecule fluorescence resonance energy transfer, *J Am Chem Soc 130*, 17664-17665.
[238] Yanagisawa, T., Ishii, R., Fukunaga, R., Kobayashi, T., Sakamoto, K., and Yokoyama, S. (2008) Multistep engineering of pyrrolysyl-tRNA synthetase to genetically encode N(epsilon)-(o-azidobenzyloxycarbonyl) lysine for site-specific protein modification, *Chem. Biol. 15*, 1187-1197.
[239] Lang, K., Davis, L., Wallace, S., Mahesh, M., Cox, D. J., Blackman, M. L., Fox, J. M., and Chin, J. W. (2012) Genetic Encoding of bicyclononynes and trans-cyclooctenes for site-specific protein labeling in vitro and in live mammalian cells via rapid fluorogenic Diels-Alder reactions, *J Am Chem Soc 134*, 10317-10320.
[240] Lee, H. S., Guo, J., Lemke, E. A., Dimla, R. D., and Schultz, P. G. (2009) Genetic incorporation of a small, environmentally sensitive, fluorescent probe into proteins in Saccharomyces cerevisiae, *J Am Chem Soc 131*, 12921-12923.
[241] Charbon, G., Brustad, E., Scott, K. A., Wang, J., Lobner-Olesen, A., Schultz, P. G., Jacobs-Wagner, C., and Chapman, E. (2011) Subcellular protein localization by using a genetically encoded fluorescent amino acid, *ChemBioChem 12*, 1818-1821.
[242] Charbon, G., Wang, J., Brustad, E., Schultz, P. G., Horwich, A. L., Jacobs-Wagner, C., and Chapman, E. (2011) Localization of GroEL determined by in vivo incorporation of a fluorescent amino acid, *Bioorg. Med. Chem. Lett. 21*, 6067-6070.
[243] Summerer, D., Chen, S., Wu, N., Deiters, A., Chin, J. W., and Schultz, P. G. (2006) A genetically encoded fluorescent amino acid, *Proc Natl Acad Sci U S A 103*, 9785-9789.
[244] Wang, J., Xie, J., and Schultz, P. G. (2006) A genetically encoded fluorescent amino acid, *J Am Chem Soc 128*, 8738-8739.
[245] Bundy, B. C., and Swartz, J. R. (2010) Site-specific incorporation of p-propargyloxyphenylalanine in a cell-free environment for direct protein-protein click conjugation, *Bioconjug Chem 21*, 255-263.
[246] Chen, X., and Wu, Y. W. (2016) Selective chemical labeling of proteins, *Org Biomol Chem 14*, 5417-5439.
[247] McKay, C. S., and Finn, M. G. (2014) Click chemistry in complex mixtures: bioorthogonal bioconjugation, *Chem. Biol. 21*, 1075-1101.
[248] Yu, Z., Pan, Y., Wang, Z., Wang, J., and Lin, Q. (2012) Genetically encoded cyclopropene directs rapid, photoclick-chemistry-mediated protein labeling in mammalian cells, *Angew Chem Int Ed Engl 51*, 10600-10604.
[249] Patterson, D. M., Nazarova, L. A., and Prescher, J. A. (2014) Finding the right (bioorthogonal) chemistry, *ACS Chem Biol 9*, 592-605.
[250] Marx, V. (2019) It's free imaging—label-free, that is, *Nature methods 16*, 1209-1212.
[251] Kumamoto, Y., Harada, Y., Takamatsu, T., and Tanaka, H. (2018) Label-free Molecular Imaging and Analysis by Raman Spectroscopy, *Acta Histochem. Cytochem. 51*, 101-110.

[252] Klein, K., Gigler, A. M., Aschenbrenner, T., Monetti, R., Bunk, W., Jamitzky, F., Morfill, G., Stark, R. W., and Schlegel, J. (2012) Label-free live-cell imaging with confocal Raman microscopy, *Biophys. J. 102*, 360-368.
[253] Kaufmann, R., Muller, P., Hausmann, M., and Cremer, C. (2011) Imaging label-free intracellular structures by localisation microscopy, *Micron 42*, 348-352.
[254] Monici, M. (2005) Cell and tissue autofluorescence research and diagnostic applications, *Biotechnol Annu Rev 11*, 227-256.
[255] Galeotti, T., van Rossum, G. D., Mayer, D. H., and Chance, B. (1970) On the fluorescence of NAD(P)H in whole-cell preparations of tumours and normal tissues, *Eur. J. Biochem. 17*, 485-496.
[256] Benson, R., Meyer, R., Zaruba, M., and McKhann, G. (1979) Cellular autofluorescence--is it due to flavins?, *Journal of Histochemistry & Cytochemistry 27*, 44-48.
[257] Dayan, D., and Wolman, M. (1993) Lipid pigments, *Prog Histochem Cytochem 25*, 1-74.
[258] Fuerst, D. E., and Jannach, J. R. (1965) Autofluorescence of Eosinophils: a Bone Marrow Study, *Nature 205*, 1333-1334.
[259] Notingher, I., and Hench, L. L. (2006) Raman microspectroscopy: a noninvasive tool for studies of individual living cells in vitro, *Expert Rev Med Devices 3*, 215-234.
[260] Raman, C. V., and Krishnan, K. S. (1928) A new type of secondary radiation, *Nature 121*, 501-502.
[261] Chernenko, T., Matthaus, C., Milane, L., Quintero, L., Amiji, M., and Diem, M. (2009) Label-free Raman spectral imaging of intracellular delivery and degradation of polymeric nanoparticle systems, *ACS Nano 3*, 3552-3559.
[262] Puppels, G. J., de Mul, F. F., Otto, C., Greve, J., Robert-Nicoud, M., Arndt-Jovin, D. J., and Jovin, T. M. (1990) Studying single living cells and chromosomes by confocal Raman microspectroscopy, *Nature 347*, 301-303.
[263] Dietzek, B., Cialla, D., Schmitt, M., and Popp, J. (2010) Introduction to the fundamentals of Raman spectroscopy, In *Confocal Raman Microscopy*, pp 21-42, Springer.
[264] Hanahan, D., and Weinberg, R. A. (2011) Hallmarks of cancer: the next generation, *Cell 144*, 646-674.
[265] Thiery, J. P. (2002) Epithelial-mesenchymal transitions in tumour progression, *Nat. Rev. Cancer 2*, 442-454.
[266] Prieto-Garcia, E., Diaz-Garcia, C. V., Garcia-Ruiz, I., and Agullo-Ortuno, M. T. (2017) Epithelial-to-mesenchymal transition in tumor progression, *Med Oncol 34*, 122.
[267] Yamaguchi, H. (2012) Pathological roles of invadopodia in cancer invasion and metastasis, *Eur. J. Cell Biol. 91*, 902-907.
[268] Donnelly, S. K., Weisswange, I., Zettl, M., and Way, M. (2013) WIP provides an essential link between Nck and N-WASP during Arp2/3-dependent actin polymerization, *Curr. Biol. 23*, 999-1006.
[269] Paterson, E. K., and Courtneidge, S. A. (2018) Invadosomes are coming: new insights into function and disease relevance, *FEBS J. 285*, 8-27.
[270] Lodish, H., Berk, A., Zipursky, S. L., Matsudaira, P., Baltimore, D., and Darnell, J. (2000) Molecular cell biology 4th edition, *National Center for Biotechnology Information, Bookshelf*.
[271] Pelaez, R., Pariente, A., Perez-Sala, A., and Larrayoz, I. M. (2019) Integrins: Moonlighting Proteins in Invadosome Formation, *Cancers (Basel) 11*, 615.
[272] Finkenstaedt-Quinn, S. A., Qiu, T. A., Shin, K., and Haynes, C. L. (2016) Super-resolution imaging for monitoring cytoskeleton dynamics, *Analyst 141*, 5674-5688.
[273] C. Wickramarachchi, D., Theofilopoulos, A. N., and Kono, D. H. (2010) Immune pathology associated with altered actin cytoskeleton regulation, *Autoimmunity 43*, 64-75.
[274] Dugina, V. B., Shagieva, G. S., and Kopnin, P. B. (2019) Biological Role of Actin Isoforms in Mammalian Cells, *Biochemistry (Mosc) 84*, 583-592.
[275] Coles, C. H., and Bradke, F. (2015) Coordinating neuronal actin-microtubule dynamics, *Curr. Biol. 25*, R677-691.
[276] Varland, S., Vandekerckhove, J., and Drazic, A. (2019) Actin Post-translational Modifications: The Cinderella of Cytoskeletal Control, *Trends Biochem. Sci. 44*, 502-516.
[277] Nurnberg, A., Kitzing, T., and Grosse, R. (2011) Nucleating actin for invasion, *Nat. Rev. Cancer 11*, 177-187.
[278] Blanchoin, L., Boujemaa-Paterski, R., Sykes, C., and Plastino, J. (2014) Actin dynamics, architecture, and mechanics in cell motility, *Physiol. Rev. 94*, 235-263.
[279] Vedula, P., and Kashina, A. (2018) The makings of the ‘actin code': regulation of actin's biological function at the amino acid and nucleotide level, *J Cell Sci 131*, jcs215509.

[280] Murakami, K., Yasunaga, T., Noguchi, T. Q., Gomibuchi, Y., Ngo, K. X., Uyeda, T. Q., and Wakabayashi, T. (2010) Structural basis for actin assembly, activation of ATP hydrolysis, and delayed phosphate release, *Cell 143*, 275-287.
[281] Carlier, M. F. (1990) Actin polymerization and ATP hydrolysis, *Adv Biophys 26*, 51-73.
[282] Bremer, A., and Aebi, U. (1992) The structure of the F-actin filament and the actin molecule, *Curr. Opin. Cell Biol. 4*, 20-26.
[283] Alblazi, K., and Siar, C. H. (2015) Cellular protrusions--lamellipodia, filopodia, invadopodia and podosomes--and their roles in progression of orofacial tumours: current understanding, *Asian Pac J Cancer Prev 16*, 2187-2191.
[284] Kudryashov, D. S., and Reisler, E. (2013) ATP and ADP actin states, *Biopolymers 99*, 245-256.
[285] Belmont, L. D., Orlova, A., Drubin, D. G., and Egelman, E. H. (1999) A change in actin conformation associated with filament instability after Pi release, *Proc Natl Acad Sci U S A 96*, 29-34.
[286] Bryce, N. S., Hardeman, E. C., Gunning, P. W., and Lock, J. G. (2019) Chemical biology approaches targeting the actin cytoskeleton through phenotypic screening, *Curr. Opin. Chem. Biol. 51*, 40-47.
[287] Bamburg, J. R., and Bernstein, B. W. (2016) Actin dynamics and cofilin-actin rods in alzheimer disease, *Cytoskeleton (Hoboken) 73*, 477-497.
[288] Kelpsch, D. J., and Tootle, T. L. (2018) Nuclear Actin: From Discovery to Function, *Anat Rec (Hoboken) 301*, 1999-2013.
[289] Murphy, D. A., and Courtneidge, S. A. (2011) The 'ins' and 'outs' of podosomes and invadopodia: characteristics, formation and function, *Nat Rev Mol Cell Biol 12*, 413-426.
[290] Tangye, S. G., Bucciol, G., Casas-Martin, J., Pillay, B., Ma, C. S., Moens, L., and Meyts, I. (2019) Human inborn errors of the actin cytoskeleton affecting immunity: way beyond WAS and WIP, *Immunol. Cell Biol. 97*, 389-402.
[291] Kalailingam, P., Tan, H. B., Jain, N., Sng, M. K., Chan, J. S. K., Tan, N. S., and Thanabalu, T. (2017) Conditional knock out of N-WASP in keratinocytes causes skin barrier defects and atopic dermatitis-like inflammation, *Sci Rep 7*, 7311.
[292] Caswell, P. T., and Zech, T. (2018) Actin-Based Cell Protrusion in a 3D Matrix, *Trends Cell Biol 28*, 823-834.
[293] Kurisu, S., and Takenawa, T. (2010) WASP and WAVE family proteins: Friends or foes in cancer invasion?, *Cancer Science 101*, 2093-2104.
[294] Frugtniet, B., Jiang, W. G., and Martin, T. A. (2015) Role of the WASP and WAVE family proteins in breast cancer invasion and metastasis, *Breast Cancer (Dove Med Press) 7*, 99-109.
[295] Schoumacher, M., Goldman, R. D., Louvard, D., and Vignjevic, D. M. (2010) Actin, microtubules, and vimentin intermediate filaments cooperate for elongation of invadopodia, *J Cell Biol 189*, 541-556.
[296] Mattila, P. K., and Lappalainen, P. (2008) Filopodia: molecular architecture and cellular functions, *Nat Rev Mol Cell Biol 9*, 446-454.
[297] Genot, E., and Gligorijevic, B. (2014) Invadosomes in their natural habitat, *Eur. J. Cell Biol. 93*, 367-379.
[298] Spuul, P., Ciufici, P., Veillat, V., Leclercq, A., Daubon, T., Kramer, I. J., and Genot, E. (2014) Importance of RhoGTPases in formation, characteristics, and functions of invadosomes, *Small GTPases 5*, e28195.
[299] Baldassarre, M., Pompeo, A., Beznoussenko, G., Castaldi, C., Cortellino, S., McNiven, M. A., Luini, A., and Buccione, R. (2003) Dynamin participates in focal extracellular matrix degradation by invasive cells, *Mol Biol Cell 14*, 1074-1084.
[300] Linder, S. (2009) Invadosomes at a glance, *J Cell Sci 122*, 3009-3013.
[301] Sibony-Benyamini, H., and Gil-Henn, H. (2012) Invadopodia: the leading force, *Eur. J. Cell Biol. 91*, 896-901.
[302] Liu, J., Yue, P., Artym, V. V., Mueller, S. C., and Guo, W. (2009) The role of the exocyst in matrix metalloproteinase secretion and actin dynamics during tumor cell invadopodia formation, *Mol Biol Cell 20*, 3763-3771.
[303] Artym, V. V., Matsumoto, K., Mueller, S. C., and Yamada, K. M. (2011) Dynamic membrane remodeling at invadopodia differentiates invadopodia from podosomes, *Eur. J. Cell Biol. 90*, 172-180.
[304] Meddens, M. B., van den Dries, K., and Cambi, A. (2014) Podosomes revealed by advanced bioimaging: what did we learn?, *Eur. J. Cell Biol. 93*, 380-387.
[305] Hoshino, D., Branch, K. M., and Weaver, A. M. (2013) Signaling inputs to invadopodia and podosomes, *J Cell Sci 126*, 2979-2989.
[306] Oikawa, T., Itoh, T., and Takenawa, T. (2008) Sequential signals toward podosome formation in NIH-src cells, *J Cell Biol 182*, 157-169.
[307] Wu, X., Suetsugu, S., Cooper, L. A., Takenawa, T., and Guan, J. L. (2004) Focal adhesion kinase regulation of N-WASP subcellular localization and function, *J Biol Chem 279*, 9565-9576.

[308] Chan, K. T., Cortesio, C. L., and Huttenlocher, A. (2009) FAK alters invadopodia and focal adhesion composition and dynamics to regulate breast cancer invasion, *J Cell Biol 185*, 357-370.
[309] Linder, S., Wiesner, C., and Himmel, M. (2011) Degrading devices: invadosomes in proteolytic cell invasion, *Annu. Rev. Cell. Dev. Biol. 27*, 185-211.
[310] Siar, C. H., Rahman, Z. A., Tsujigiwa, H., Mohamed Om Alblazi, K., Nagatsuka, H., and Ng, K. H. (2016) Invadopodia proteins, cortactin, N-WASP and WIP differentially promote local invasiveness in ameloblastoma, *J Oral Pathol Med 45*, 591-598.
[311] Ayala, I., Baldassarre, M., Giacchetti, G., Caldieri, G., Tete, S., Luini, A., and Buccione, R. (2008) Multiple regulatory inputs converge on cortactin to control invadopodia biogenesis and extracellular matrix degradation, *J Cell Sci 121*, 369-378.
[312] Buccione, R., Caldieri, G., and Ayala, I. (2009) Invadopodia: specialized tumor cell structures for the focal degradation of the extracellular matrix, *Cancer Metastasis Rev 28*, 137-149.
[313] Cmoch, A., Groves, P., and Pikuła, S. (2014) Biogenesis of invadopodia and their cellular functions, *Postepy biochemii 60*, 62.
[314] Mader, C. C., Oser, M., Magalhaes, M. A., Bravo-Cordero, J. J., Condeelis, J., Koleske, A. J., and Gil-Henn, H. (2011) An EGFR-Src-Arg-cortactin pathway mediates functional maturation of invadopodia and breast cancer cell invasion, *Cancer Res. 71*, 1730-1741.
[315] Beaty, B. T., and Condeelis, J. (2014) Digging a little deeper: the stages of invadopodium formation and maturation, *Eur. J. Cell Biol. 93*, 438-444.
[316] Castro-Castro, A., Marchesin, V., Monteiro, P., Lodillinsky, C., Rosse, C., and Chavrier, P. (2016) Cellular and Molecular Mechanisms of MT1-MMP-Dependent Cancer Cell Invasion, *Annu. Rev. Cell. Dev. Biol. 32*, 555-576.
[317] Stylli, S. S., Stacey, T. T., Verhagen, A. M., Xu, S. S., Pass, I., Courtneidge, S. A., and Lock, P. (2009) Nck adaptor proteins link Tks5 to invadopodia actin regulation and ECM degradation, *J Cell Sci 122*, 2727-2740.
[318] Busco, G., Cardone, R. A., Greco, M. R., Bellizzi, A., Colella, M., Antelmi, E., Mancini, M. T., Dell'Aquila, M. E., Casavola, V., and Paradiso, A. (2010) NHE1 promotes invadopodial ECM proteolysis through acidification of the peri-invadopodial space, *The FASEB Journal 24*, 3903-3915.
[319] Juin, A., Billottet, C., Moreau, V., Destaing, O., Albiges-Rizo, C., Rosenbaum, J., Genot, E., and Saltel, F. (2012) Physiological type I collagen organization induces the formation of a novel class of linear invadosomes, *Mol Biol Cell 23*, 297-309.
[320] Beaty, B. T., Sharma, V. P., Bravo-Cordero, J. J., Simpson, M. A., Eddy, R. J., Koleske, A. J., and Condeelis, J. (2013) beta1 integrin regulates Arg to promote invadopodial maturation and matrix degradation, *Mol Biol Cell 24*, 1661-1675, S1661-1611.
[321] Kolli-Bouhafs, K., Sick, E., Noulet, F., Gies, J. P., De Mey, J., and Ronde, P. (2014) FAK competes for Src to promote migration against invasion in melanoma cells, *Cell Death Dis 5*, e1379.
[322] Tanis, K. Q., Veach, D., Duewel, H. S., Bornmann, W. G., and Koleske, A. J. (2003) Two distinct phosphorylation pathways have additive effects on Abl family kinase activation, *Mol. Cell. Biol. 23*, 3884-3896.
[323] Takano, K., Toyooka, K., and Suetsugu, S. (2008) EFC/F-BAR proteins and the N-WASP-WIP complex induce membrane curvature-dependent actin polymerization, *EMBO J. 27*, 2817-2828.
[324] Watson, J. R., Fox, H. M., Nietlispach, D., Gallop, J. L., Owen, D., and Mott, H. R. (2016) Investigation of the Interaction between Cdc42 and Its Effector TOCA1: HANDOVER OF Cdc42 TO THE ACTIN REGULATOR N-WASP IS FACILITATED BY DIFFERENTIAL BINDING AFFINITIES, *J Biol Chem 291*, 13875-13890.
[325] Ho, H. Y., Rohatgi, R., Lebensohn, A. M., Le, M., Li, J., Gygi, S. P., and Kirschner, M. W. (2004) Toca-1 mediates Cdc42-dependent actin nucleation by activating the N-WASP-WIP complex, *Cell 118*, 203-216.
[326] Sharma, V. P., Eddy, R., Entenberg, D., Kai, M., Gertler, F. B., and Condeelis, J. (2013) Tks5 and SHIP2 regulate invadopodium maturation, but not initiation, in breast carcinoma cells, *Current Biology 23*, 2079-2089.
[327] Dominguez, R. (2016) The WH2 Domain and Actin Nucleation: Necessary but Insufficient, *Trends Biochem. Sci. 41*, 478-490.
[328] Sun, Y. D., Leong, N. T., Jiang, T., Tangara, A., Darzacq, X., and Drubin, D. G. (2017) Switch-like Arp2/3 activation upon WASP and WIP recruitment to an apparent threshold level by multivalent linker proteins in vivo, *Elife 6*.

[329] Oser, M., Yamaguchi, H., Mader, C. C., Bravo-Cordero, J. J., Arias, M., Chen, X., Desmarais, V., van Rheenen, J., Koleske, A. J., and Condeelis, J. (2009) Cortactin regulates cofilin and N-WASp activities to control the stages of invadopodium assembly and maturation, *J Cell Biol 186*, 571-587.

[330] Rohatgi, R., Nollau, P., Ho, H. Y., Kirschner, M. W., and Mayer, B. J. (2001) Nck and phosphatidylinositol 4,5-bisphosphate synergistically activate actin polymerization through the N-WASP-Arp2/3 pathway, *J Biol Chem 276*, 26448-26452.

[331] Pichot, C. S., Arvanitis, C., Hartig, S. M., Jensen, S. A., Bechill, J., Marzouk, S., Yu, J., Frost, J. A., and Corey, S. J. (2010) Cdc42-interacting protein 4 promotes breast cancer cell invasion and formation of invadopodia through activation of N-WASp, *Cancer Res. 70*, 8347-8356.

[332] Pollitt, A. Y., and Insall, R. H. (2009) WASP and SCAR/WAVE proteins: the drivers of actin assembly, *J Cell Sci 122*, 2575-2578.

[333] Eddy, R. J., Weidmann, M. D., Sharma, V. P., and Condeelis, J. S. (2017) Tumor Cell Invadopodia: Invasive Protrusions that Orchestrate Metastasis, *Trends Cell Biol 27*, 595-607.

[334] Ichetovkin, I., Grant, W., and Condeelis, J. (2002) Cofilin produces newly polymerized actin filaments that are preferred for dendritic nucleation by the Arp2/3 complex, *Current biology 12*, 79-84.

[335] Chan, A. Y., Bailly, M., Zebda, N., Segall, J. E., and Condeelis, J. S. (2000) Role of cofilin in epidermal growth factor-stimulated actin polymerization and lamellipod protrusion, *J Cell Biol 148*, 531-542.

[336] Miki, H., Sasaki, T., Takai, Y., and Takenawa, T. (1998) Induction of filopodium formation by a WASP-related actin-depolymerizing protein N-WASP, *Nature 391*, 93-96.

[337] Rohatgi, R., Ma, L., Miki, H., Lopez, M., Kirchhausen, T., Takenawa, T., and Kirschner, M. W. (1999) The Interaction between N-WASP and the Arp2/3 Complex Links Cdc42-Dependent Signals to Actin Assembly, *Cell 97*, 221-231.

[338] Lorenz, M., Yamaguchi, H., Wang, Y., Singer, R. H., and Condeelis, J. (2004) Imaging sites of N-wasp activity in lamellipodia and invadopodia of carcinoma cells, *Curr. Biol. 14*, 697-703.

[339] Hotary, K. B., Allen, E. D., Brooks, P. C., Datta, N. S., Long, M. W., and Weiss, S. J. (2003) Membrane type I matrix metalloproteinase usurps tumor growth control imposed by the three-dimensional extracellular matrix, *Cell 114*, 33-45.

[340] Nakahara, H., Howard, L., Thompson, E. W., Sato, H., Seiki, M., Yeh, Y., and Chen, W.-T. (1997) Transmembrane/cytoplasmic domain-mediated membrane type 1-matrix metalloprotease docking to invadopodia is required for cell invasion, *Proceedings of the National Academy of Sciences 94*, 7959-7964.

[341] Abram, C. L., Seals, D. F., Pass, I., Salinsky, D., Maurer, L., Roth, T. M., and Courtneidge, S. A. (2003) The adaptor protein fish associates with members of the ADAMs family and localizes to podosomes of Src-transformed cells, *J Biol Chem 278*, 16844-16851.

[342] Snoek-van Beurden, P. A. M., and Von den Hoff, J. W. (2005) Zymographic techniques for the analysis of matrix metalloproteinases and their inhibitors, *Biotechniques 38*, 73-83.

[343] Opdenakker, G., Van den Steen, P. E., and Van Damme, J. (2001) Gelatinase B: a tuner and amplifier of immune functions, *Trends in Immunology 22*, 571-579.

[344] Yu, X., Zech, T., McDonald, L., Gonzalez, E. G., Li, A., Macpherson, I., Schwarz, J. P., Spence, H., Futó, K., and Timpson, P. (2012) N-WASP coordinates the delivery and F-actin–mediated capture of MT1-MMP at invasive pseudopods, *The Journal of cell biology 199*, 527-544.

[345] Nusblat, L. M., Dovas, A., and Cox, D. (2011) The non-redundant role of N-WASP in podosome-mediated matrix degradation in macrophages, *Eur. J. Cell Biol. 90*, 205-212.

[346] Buccione, R., Orth, J. D., and McNiven, M. A. (2004) Foot and mouth: podosomes, invadopodia and circular dorsal ruffles, *Nat Rev Mol Cell Biol 5*, 647-657.

[347] Sakurai-Yageta, M., Recchi, C., Le Dez, G., Sibarita, J. B., Daviet, L., Camonis, J., D'Souza-Schorey, C., and Chavrier, P. (2008) The interaction of IQGAP1 with the exocyst complex is required for tumor cell invasion downstream of Cdc42 and RhoA, *J Cell Biol 181*, 985-998.

[348] Bravo-Cordero, J. J., Marrero-Diaz, R., Megías, D., Genís, L., García-Grande, A., García, M. A., Arroyo, A. G., and Montoya, M. C. (2007) MT1-MMP proinvasive activity is regulated by a novel Rab8-dependent exocytic pathway, *The EMBO journal 26*, 1499-1510.

[349] Ory, S., and Gasman, S. (2011) Rho GTPases and exocytosis: what are the molecular links?, In *Semin. Cell Dev. Biol.*, pp 27-32, Elsevier.

[350] Steffen, A., Le Dez, G., Poincloux, R., Recchi, C., Nassoy, P., Rottner, K., Galli, T., and Chavrier, P. (2008) MT1-MMP-dependent invasion is regulated by TI-VAMP/VAMP7, *Current Biology 18*, 926-931.

[351] Jacob, A., Jing, J., Lee, J., Schedin, P., Gilbert, S. M., Peden, A. A., Junutula, J. R., and Prekeris, R. (2013) Rab40b regulates trafficking of MMP2 and MMP9 during invadopodia formation and invasion of breast cancer cells, *J Cell Sci 126*, 4647-4658.
[352] Jacob, A., and Prekeris, R. (2015) The regulation of MMP targeting to invadopodia during cancer metastasis, *Front Cell Dev Biol 3*, 4.
[353] Yarar, D., Waterman-Storer, C. M., and Schmid, S. L. (2007) SNX9 couples actin assembly to phosphoinositide signals and is required for membrane remodeling during endocytosis, *Dev. Cell 13*, 43-56.
[354] Benesch, S., Polo, S., Lai, F. P., Anderson, K. I., Stradal, T. E., Wehland, J., and Rottner, K. (2005) N-WASP deficiency impairs EGF internalization and actin assembly at clathrin-coated pits, *J Cell Sci 118*, 3103-3115.
[355] Kessels, M. M., and Qualmann, B. (2004) The syndapin protein family: linking membrane trafficking with the cytoskeleton, *J Cell Sci 117*, 3077-3086.
[356] Li, A., Dawson, J. C., Forero-Vargas, M., Spence, H. J., Yu, X., Konig, I., Anderson, K., and Machesky, L. M. (2010) The actin-bundling protein fascin stabilizes actin in invadopodia and potentiates protrusive invasion, *Curr. Biol. 20*, 339-345.
[357] Oda, A., and Eto, K. (2013) WASPs and WAVEs: from molecular function to physiology in hematopoietic cells, *Semin. Cell Dev. Biol. 24*, 308-313.
[358] Burianek, L. E., and Soderling, S. H. (2013) Under lock and key: spatiotemporal regulation of WASP family proteins coordinates separate dynamic cellular processes, *Semin. Cell Dev. Biol. 24*, 258-266.
[359] Benesch, S., Lommel, S., Steffen, A., Stradal, T. E., Scaplehorn, N., Way, M., Wehland, J., and Rottner, K. (2002) Phosphatidylinositol 4,5-biphosphate (PIP2)-induced vesicle movement depends on N-WASP and involves Nck, WIP, and Grb2, *J Biol Chem 277*, 37771-37776.
[360] Taunton, J., Rowning, B. A., Coughlin, M. L., Wu, M., Moon, R. T., Mitchison, T. J., and Larabell, C. A. (2000) Actin-dependent propulsion of endosomes and lysosomes by recruitment of N-WASP, *J Cell Biol 148*, 519-530.
[361] Co, C., Wong, D. T., Gierke, S., Chang, V., and Taunton, J. (2007) Mechanism of actin network attachment to moving membranes: barbed end capture by N-WASP WH2 domains, *Cell 128*, 901-913.
[362] Sereni, L., Castiello, M. C., and Villa, A. (2018) Platelets in Wiskott-Aldrich syndrome: Victims or executioners?, *J Leukoc Biol 103*, 577-590.
[363] Wiskott, A. (1937) Familiarer, angeborener morbus werlhofli, *Monatsschrift Kinderheikunde 68*, 212-216.
[364] Aldrich, R. A., Steinberg, A. G., and Campbell, D. C. (1954) Pedigree demonstrating a sex-linked recessive condition characterized by draining ears, eczematoid dermatitis and bloody diarrhea, *Pediatrics 13*, 133-139.
[365] Linder, S., Nelson, D., Weiss, M., and Aepfelbacher, M. (1999) Wiskott-Aldrich syndrome protein regulates podosomes in primary human macrophages, *Proc Natl Acad Sci U S A 96*, 9648-9653.
[366] Thrasher, A. J. (2002) WASp in immune-system organization and function, *Nat. Rev. Immunol. 2*, 635-646.
[367] Alekhina, O., Burstein, E., and Billadeau, D. D. (2017) Cellular functions of WASP family proteins at a glance, *J Cell Sci 130*, 2235-2241.
[368] Miki, H., Miura, K., and Takenawa, T. (1996) N-WASP, a novel actin-depolymerizing protein, regulates the cortical cytoskeletal rearrangement in a PIP2-dependent manner downstream of tyrosine kinases, *EMBO J. 15*, 5326-5335.
[369] Kollmar, M., Lbik, D., and Enge, S. (2012) Evolution of the eukaryotic ARP2/3 activators of the WASP family: WASP, WAVE, WASH, and WHAMM, and the proposed new family members WAWH and WAML, *BMC Res Notes 5*, 88.
[370] Morris, H. T., Fort, L., Spence, H. J., Patel, R., Vincent, D. F., Park, J. H., Snapper, S. B., Carey, F. A., Sansom, O. J., and Machesky, L. M. (2018) Loss of N-WASP drives early progression in an Apc model of intestinal tumourigenesis, *J. Pathol. 245*, 337-348.
[371] Schell, C., Baumhakl, L., Salou, S., Conzelmann, A. C., Meyer, C., Helmstadter, M., Wrede, C., Grahammer, F., Eimer, S., Kerjaschki, D., Walz, G., Snapper, S., and Huber, T. B. (2013) N-wasp is required for stabilization of podocyte foot processes, *J Am Soc Nephrol 24*, 713-721.
[372] Youngstrom, M., Chattaraj, A., Michalski, P. J., Schaff, J. C., Blinov, M. L., and Loew, L. M. (2017) Multivalent Signaling Clusters have Unique Sizes Determined by Membrane Localization and Excluded Volume: the Nephrin/Nck/N-WASP System, *Biophys. J. 112*, 281a-281a.
[373] Gligorijevic, B., Wyckoff, J., Yamaguchi, H., Wang, Y., Roussos, E. T., and Condeelis, J. (2012) N-WASP-mediated invadopodium formation is involved in intravasation and lung metastasis of mammary tumors, *J Cell Sci 125*, 724-734.

[374] Yamaguchi, H., Wyckoff, J., and Condeelis, J. (2005) Cell migration in tumors, *Curr. Opin. Cell Biol. 17*, 559-564.
[375] Hou, J. X., Yang, H., Huang, X., Leng, X. H., Zhou, F. X., Xie, C. H., Zhou, Y. F., and Xu, Y. (2017) N-WASP promotes invasion and migration of cervical cancer cells through regulating p38 MAPKs signaling pathway, *American Journal of Translational Research 9*, 403-415.
[376] Isaac, B. M., Ishihara, D., Nusblat, L. M., Gevrey, J. C., Dovas, A., Condeelis, J., and Cox, D. (2010) N-WASP has the ability to compensate for the loss of WASP in macrophage podosome formation and chemotaxis, *Exp. Cell Res. 316*, 3406-3416.
[377] Volkman, B. F., Prehoda, K. E., Scott, J. A., Peterson, F. C., and Lim, W. A. (2002) Structure of the N-WASP EVH1 domain-WIP complex: insight into the molecular basis of Wiskott-Aldrich Syndrome, *Cell 111*, 565-576.
[378] Ramesh, N., Anton, I. M., Hartwig, J. H., and Geha, R. S. (1997) WIP, a protein associated with wiskott-aldrich syndrome protein, induces actin polymerization and redistribution in lymphoid cells, *Proc Natl Acad Sci U S A 94*, 14671-14676.
[379] Anton, I. M., Lu, W., Mayer, B. J., Ramesh, N., and Geha, R. S. (1998) The Wiskott-Aldrich syndrome protein-interacting protein (WIP) binds to the adaptor protein Nck, *J Biol Chem 273*, 20992-20995.
[380] Rohatgi, R., Ho, H. Y., and Kirschner, M. W. (2000) Mechanism of N-WASP activation by CDC42 and phosphatidylinositol 4, 5-bisphosphate, *J Cell Biol 150*, 1299-1310.
[381] Bieling, P., Hansen, S. D., Akin, O., Li, T. D., Hayden, C. C., Fletcher, D. A., and Mullins, R. D. (2018) WH2 and proline-rich domains of WASP-family proteins collaborate to accelerate actin filament elongation, *EMBO J. 37*, 102-121.
[382] Marchand, J.-B., Kaiser, D. A., Pollard, T. D., and Higgs, H. N. (2001) Interaction of WASP/Scar proteins with actin and vertebrate Arp2/3 complex, *Nature cell biology 3*, 76-82.
[383] Kurisu, S., and Takenawa, T. (2010) WASP and WAVE family proteins: friends or foes in cancer invasion?, *Cancer Sci. 101*, 2093-2104.
[384] Kim, A. S., Kakalis, L. T., Abdul-Manan, N., Liu, G. A., and Rosen, M. K. (2000) Autoinhibition and activation mechanisms of the Wiskott-Aldrich syndrome protein, *Nature 404*, 151-158.
[385] Mehlen, P., and Puisieux, A. (2006) Metastasis: a question of life or death, *Nat. Rev. Cancer 6*, 449-458.
[386] Liotta, L. A., and Kohn, E. C. (2003) Cancer's deadly signature, *Nat. Genet. 33*, 10-11.
[387] Leong, H. S., Robertson, A. E., Stoletov, K., Leith, S. J., Chin, C. A., Chien, A. E., Hague, M. N., Ablack, A., Carmine-Simmen, K., McPherson, V. A., Postenka, C. O., Turley, E. A., Courtneidge, S. A., Chambers, A. F., and Lewis, J. D. (2014) Invadopodia are required for cancer cell extravasation and are a therapeutic target for metastasis, *Cell Rep 8*, 1558-1570.
[388] Lennox, K. A., and Behlke, M. A. (2016) Mini-review: Current strategies to knockdown long non-coding RNAs, *J. Rare Dis. Res. Treat 1*, 66-70.
[389] Hebbrecht, T., Van Audenhove, I., Zwaenepoel, O., Verhelle, A., and Gettemans, J. (2017) VCA nanobodies target N-WASp to reduce invadopodium formation and functioning, *PLoS One 12*, e0185076.
[390] Kim, M. Y., Oskarsson, T., Acharyya, S., Nguyen, D. X., Zhang, X. H., Norton, L., and Massague, J. (2009) Tumor self-seeding by circulating cancer cells, *Cell 139*, 1315-1326.
[391] Stylli, S. S., Kaye, A. H., and Lock, P. (2008) Invadopodia: at the cutting edge of tumour invasion, *J Clin Neurosci 15*, 725-737.
[392] Leong, H. S., Robertson, A. E., Stoletov, K., Leith, S. J., Chin, C. A., Chien, A. E., Hague, M. N., Ablack, A., Carmine-Simmen, K., McPherson, V. A., Postenka, C. O., Turley, E. A., Courtneidge, S. A., Chambers, A. F., and Lewis, J. D. (2014) Invadopodia Are Required for Cancer Cell Extravasation and Are a Therapeutic Target for Metastasis, *Cell Reports 8*, 1558-1570.
[393] Desmarais, V., Yamaguchi, H., Oser, M., Soon, L., Mouneimne, G., Sarmiento, C., Eddy, R., and Condeelis, J. (2009) N-WASP and cortactin are involved in invadopodium-dependent chemotaxis to EGF in breast tumor cells, *Cell Motil. Cytoskeleton 66*, 303-316.
[394] Yamaguchi, H., Lorenz, M., Kempiak, S., Sarmiento, C., Coniglio, S., Symons, M., Segall, J., Eddy, R., Miki, H., Takenawa, T., and Condeelis, J. (2005) Molecular mechanisms of invadopodium formation: the role of the N-WASP-Arp2/3 complex pathway and cofilin, *J Cell Biol 168*, 441-452.
[395] Carlier, M.-F. (2010) *Actin-based motility*, Springer.
[396] Pichot, C. S., Arvanitis, C., Hartig, S. M., Jensen, S. A., Bechill, J., Marzouk, S., Yu, J., Frost, J. A., and Corey, S. J. (2010) Cdc42-interacting protein 4 promotes breast cancer cell invasion and formation of invadopodia through activation of N-WASp, *Cancer research 70*, 8347-8356.
[397] Miki, H., and Takenawa, T. (2003) Regulation of actin dynamics by WASP family proteins, *J Biochem 134*, 309-313.

[398] Snapper, S. B., and Rosen, F. S. (1999) The Wiskott-Aldrich syndrome protein (WASP): roles in signaling and cytoskeletal organization, *Annu. Rev. Immunol. 17*, 905-929.
[399] Yamazaki, D., Kurisu, S., and Takenawa, T. (2005) Regulation of cancer cell motility through actin reorganization, *Cancer Sci. 96*, 379-386.
[400] Bompard, G., and Caron, E. (2004) Regulation of WASP/WAVE proteins making a long story short, *The Journal of cell biology 166*, 957-962.
[401] Suetsugu, S., Miki, H., and Takenawa, T. (2002) Spatial and temporal regulation of actin polymerization for cytoskeleton formation through Arp2/3 complex and WASP/WAVE proteins, *Cell Motil. Cytoskeleton 51*, 113-122.
[402] Suetsugu, S., Miki, H., and Takenawa, T. (2001) Identification of another actin-related protein (Arp) 2/3 complex binding site in neural Wiskott-Aldrich syndrome protein (N-WASP) that complements actin polymerization induced by the Arp2/3 complex activating (VCA) domain of N-WASP, *J Biol Chem 276*, 33175-33180.
[403] McBride, H. M., Millar, D. G., Li, J. M., and Shore, G. C. (1992) A signal-anchor sequence selective for the mitochondrial outer membrane, *J Cell Biol 119*, 1451-1457.
[404] Pollitt, A. Y., and Insall, R. H. (2009) WASP and SCAR/WAVE proteins: the drivers of actin assembly, *Journal of Cell Science 122*, 2575-2578.
[405] De Clercq, S., Boucherie, C., Vandekerckhove, J., Gettemans, J., and Guillabert, A. (2013) L-plastin nanobodies perturb matrix degradation, podosome formation, stability and lifetime in THP-1 macrophages, *PLoS One 8*, e78108.
[406] Van den Abbeele, A., De Clercq, S., De Ganck, A., De Corte, V., Van Loo, B., Soror, S. H., Srinivasan, V., Steyaert, J., Vandekerckhove, J., and Gettemans, J. (2010) A llama-derived gelsolin single-domain antibody blocks gelsolin-G-actin interaction, *Cell. Mol. Life Sci. 67*, 1519-1535.
[407] Van Audenhove, I., Denert, M., Boucherie, C., Pieters, L., Cornelissen, M., and Gettemans, J. (2016) Fascin Rigidity and L-plastin Flexibility Cooperate in Cancer Cell Invadopodia and Filopodia, *J Biol Chem 291*, 9148-9160.
[408] Van Audenhove, I., and Gettemans, J. (2016) Use of Nanobodies to Localize Endogenous Cytoskeletal Proteins and to Determine Their Contribution to Cancer Cell Invasion by Using an ECM Degradation Assay, *Methods Mol Biol 1365*, 225-241.
[409] Chereau, D., Kerff, F., Graceffa, P., Grabarek, Z., Langsetmo, K., and Dominguez, R. (2005) Actin-bound structures of Wiskott-Aldrich syndrome protein (WASP)-homology domain 2 and the implications for filament assembly, *Proc Natl Acad Sci U S A 102*, 16644-16649.
[410] Chereau, D., and Dominguez, R. (2006) Understanding the role of the G-actin-binding domain of Ena/VASP in actin assembly, *J Struct Biol 155*, 195-201.
[411] Boczkowska, M., Rebowski, G., Kast, D. J., and Dominguez, R. (2014) Structural analysis of the transitional state of Arp2/3 complex activation by two actin-bound WCAs, *Nat Commun 5*, 3308.
[412] Ti, S. C., Jurgenson, C. T., Nolen, B. J., and Pollard, T. D. (2011) Structural and biochemical characterization of two binding sites for nucleation-promoting factor WASp-VCA on Arp2/3 complex, *Proc Natl Acad Sci U S A 108*, E463-471.
[413] Hetrick, B., Han, M. S., Helgeson, L. A., and Nolen, B. J. (2013) Small molecules CK-666 and CK-869 inhibit actin-related protein 2/3 complex by blocking an activating conformational change, *Chem. Biol. 20*, 701-712.
[414] Uruno, T., Liu, J., Zhang, P., Fan, Y., Egile, C., Li, R., Mueller, S. C., and Zhan, X. (2001) Activation of Arp2/3 complex-mediated actin polymerization by cortactin, *Nat. Cell Biol. 3*, 259-266.
[415] Hüfner, K., Higgs, H. N., Pollard, T. D., Jacobi, C., Aepfelbacher, M., and Linder, S. (2001) The verprolin-like central (vc) region of Wiskott-Aldrich syndrome protein induces Arp2/3 complex-dependent actin nucleation, *Journal of Biological Chemistry 276*, 35761-35767.
[416] Elbashir, S. M., Harborth, J., Lendeckel, W., Yalcin, A., Weber, K., and Tuschl, T. (2001) Duplexes of 21-nucleotide RNAs mediate RNA interference in cultured mammalian cells, *Nature 411*, 494-498.
[417] Schaefer, K. A., Wu, W. H., Colgan, D. F., Tsang, S. H., Bassuk, A. G., and Mahajan, V. B. (2017) Unexpected mutations after CRISPR-Cas9 editing in vivo, *Nat. Methods 14*, 547-548.
[418] Delanote, V., Vanloo, B., Catillon, M., Friederich, E., Vandekerckhove, J., and Gettemans, J. (2010) An alpaca single-domain antibody blocks filopodia formation by obstructing L-plastin-mediated F-actin bundling, *FASEB J. 24*, 105-118.
[419] Clark, E. S., Whigham, A. S., Yarbrough, W. G., and Weaver, A. M. (2007) Cortactin is an essential regulator of matrix metalloproteinase secretion and extracellular matrix degradation in invadopodia, *Cancer Res. 67*, 4227-4235.

[420] Clark, E. S., Brown, B., Whigham, A. S., Kochaishvili, A., Yarbrough, W. G., and Weaver, A. M. (2009) Aggressiveness of HNSCC tumors depends on expression levels of cortactin, a gene in the 11q13 amplicon, *Oncogene 28*, 431-444.
[421] Weichselbaum, R. R., Dahlberg, W., Beckett, M., Karrison, T., Miller, D., Clark, J., and Ervin, T. J. (1986) Radiation-resistant and repair-proficient human tumor cells may be associated with radiotherapy failure in head-and neck-cancer patients, *Proceedings of the National Academy of Sciences 83*, 2684-2688.
[422] Somers, K. D., Cartwright, S. L., and Schechter, G. L. (1990) Amplification of the int-2 gene in human head and neck squamous cell carcinomas, *Oncogene 5*, 915-920.
[423] Hong, V., Presolski, S. I., Ma, C., and Finn, M. G. (2009) Analysis and optimization of copper-catalyzed azide-alkyne cycloaddition for bioconjugation, *Angew Chem Int Ed Engl 48*, 9879-9883.
[424] Presolski, S. I., Hong, V. P., and Finn, M. G. (2011) Copper-Catalyzed Azide-Alkyne Click Chemistry for Bioconjugation, *Curr Protoc Chem Biol 3*, 153-162.
[425] Hong, V., Steinmetz, N. F., Manchester, M., and Finn, M. G. (2010) Labeling live cells by copper-catalyzed alkyne--azide click chemistry, *Bioconjug Chem 21*, 1912-1916.
[426] Bullions, L. C., and Levine, A. J. (1998) The role of beta-catenin in cell adhesion, signal transduction, and cancer, *Curr Opin Oncol 10*, 81-87.
[427] Zhurinsky, J., Shtutman, M., and Ben-Ze'ev, A. (2000) Plakoglobin and beta-catenin: protein interactions, regulation and biological roles, J Cell Sci 113 (Pt 18), 3127-3139.
[428] Hebbrecht, T., Liu, J., Zwaenepoel, O., Boddin, G., Van Leene, C., Decoene, K., Madder, A., Braeckmans, K., and Gettemans, J. (2020) Nanobody click chemistry for convenient site specific fluorescent labelling, single step immunocytochemistry and delivery into living cells by photoporation and live cell imaging, *New Biotechnology*
[429] Revets, H., De Baetselier, P., and Muyldermans, S. (2005) Nanobodies as novel agents for cancer therapy, *Expert Opinion on Biological Therapy 5*, 111-124.
[430] Schumacher, D., Helma, J., Schneider, A. F., Leonhardt, H., and Hackenberger, C. (2017) Chemical functionalization strategies and intracellular applications of nanobodies, *Angewandte Chemie International Edition*.
[431] Xiong, R. H., Joris, F., Liang, S. Y., De Rycke, R., Lippens, S., Demeester, J., Skirtach, A., Raemdonck, K., Himmelreich, U., De Smedt, S. C., and Braeckmans, K. (2016) Cytosolic Delivery of Nanolabels Prevents Their Asymmetric Inheritance and Enables Extended Quantitative in Vivo Cell Imaging, *Nano Letters 16*, 5975-5986.
[432] Oliveira, S., Heukers, R., Sornkom, J., Kok, R. J., and van Bergen En Henegouwen, P. M. (2013) Targeting tumors with nanobodies for cancer imaging and therapy, *J Control Release 172*, 607-617.
[433] Bertier, L., Hebbrecht, T., Mettepenningen, E., De Wit, N., Zwaenepoel, O., Verhelle, A., and Gettemans, J. (2018) Nanobodies targeting cortactin proline rich, helical and actin binding regions downregulate invadopodium formation and matrix degradation in SCC-61 cancer cells, *Biomed Pharmacother 102*, 230-241.
[434] Presolski, S. I., Hong, V. P., and Finn, M. (2011) Copper-Catalyzed Azide–Alkyne Click Chemistry for Bioconjugation, *Current protocols in chemical biology*, 153-162.
[435] Hein, J. E., and Fokin, V. V. (2010) Copper-catalyzed azide–alkyne cycloaddition (CuAAC) and beyond: new reactivity of copper (I) acetylides, *Chemical Society Reviews 39*, 1302-1315.
[436] Mann, V. R., Powers, A. S., Tilley, D. C., Sack, J. T., and Cohen, B. E. (2018) Azide–Alkyne Click Conjugation on Quantum Dots by Selective Copper Coordination, *ACS nano*.
[437] Li, S., Cai, H., He, J., Chen, H., Lam, S., Cai, T., Zhu, Z., Bark, S. J., and Cai, C. (2016) Extent of the Oxidative Side Reactions to Peptides and Proteins During the CuAAC Reaction, *Bioconjug Chem 27*, 2315-2322.
[438] Hong, V., Presolski, S. I., Ma, C., and Finn, M. (2009) Analysis and Optimization of Copper-Catalyzed Azide–Alkyne Cycloaddition for Bioconjugation, *Angewandte Chemie International Edition 48*, 9879-9883.
[439] Peyrassol, X., Laeremans, T., Gouwy, M., Lahura, V., Debulpaep, M., Van Damme, J., Steyaert, J., Parmentier, M., and Langer, I. (2016) Development by Genetic Immunization of Monovalent Antibodies (Nanobodies) Behaving as Antagonists of the Human ChemR23 Receptor, *The Journal of Immunology 196*, 2893-2901.
[440] Braun, M. B., Traenkle, B., Koch, P. A., Emele, F., Weiss, F., Poetz, O., Stehle, T., and Rothbauer, U. (2016) Peptides in headlock--a novel high-affinity and versatile peptide-binding nanobody for proteomics and microscopy, *Sci Rep 6*, 19211.

[441] Maier, J., Traenkle, B., and Rothbauer, U. (2015) Real-time analysis of epithelial-mesenchymal transition using fluorescent single-domain antibodies, *Scientific reports 5*, 13402.
[442] Truttmann, M. C., Wu, Q., Stiegeler, S., Duarte, J. N., Ingram, J., and Ploegh, H. L. (2015) HypE-specific nanobodies as tools to modulate HypE-mediated target AMPylation, *Journal of Biological Chemistry 290*, 9087-9100.
[443] Wang, Q., Chan, T. R., Hilgraf, R., Fokin, V. V., Sharpless, K. B., and Finn, M. G. (2003) Bioconjugation by copper(I)-catalyzed azide-alkyne [3 + 2] cycloaddition, *J Am Chem Soc 125*, 3192-3193.
[444] Graulus, G.-J., Ta, D. T., Tran, H., Hansen, R., Billen, B., Royackers, E., Noben, J.-P., Devoogdt, N., Muyldermans, S., and Guedens, W. (2019) Site-selective functionalization of nanobodies using intein-mediated protein ligation for innovative bioconjugation.
[445] Oliveira, S., Schiffelers, R. M., van der Veeken, J., van der Meel, R., Vongpromek, R., van Bergen En Henegouwen, P. M., Storm, G., and Roovers, R. C. (2010) Downregulation of EGFR by a novel multivalent nanobody-liposome platform, *J Control Release 145*, 165-175.
[446] van der Meel, R., Oliveira, S., Altintas, I., Haselberg, R., van der Veeken, J., Roovers, R. C., van Bergen en Henegouwen, P. M., Storm, G., Hennink, W. E., Schiffelers, R. M., and Kok, R. J. (2012) Tumor-targeted Nanobullets: Anti-EGFR nanobody-liposomes loaded with anti-IGF-1R kinase inhibitor for cancer treatment, *J Control Release 159*, 281-289.
[447] Gray, M. A., Tao, R. N., DePorter, S. M., Spiegel, D. A., and McNaughton, B. R. (2016) A Nanobody Activation Immunotherapeutic that Selectively Destroys HER2-Positive Breast Cancer Cells, *Chembiochem 17*, 155-158.
[448] Harmand, T. J., Bousbaine, D., Chan, A., Zhang, X. H., Liu, D. R., Tam, J. P., and Ploegh, H. L. (2018) One-Pot Dual Labeling of IgG 1 and Preparation of C-to-C Fusion Proteins Through a Combination of Sortase A and Butelase 1, *Bioconjugate Chemistry 29*, 3245-3249.
[449] Nguyen, G. K., Kam, A., Loo, S., Jansson, A. E., Pan, L. X., and Tam, J. P. (2015) Butelase 1: A Versatile Ligase for Peptide and Protein Macrocyclization, *J Am Chem Soc 137*, 15398-15401.
[450] Fabricius, V., Lefèbre, J., Geertsema, H., Marino, S. F., and Ewers, H. (2018) Rapid and efficient C-terminal labeling of nanobodies for DNA-PAINT, *Journal of Physics D: Applied Physics 51*, 474005.
[451] Thueng-in, K., Thanongsaksrikul, J., Srimanote, P., Bangphoomi, K., Poungpair, O., Maneewatch, S., Choowongkomon, K., and Chaicumpa, W. (2012) Cell Penetrable Humanized-VH/VHH That Inhibit RNA Dependent RNA Polymerase (NS5B) of HCV, *Plos One 7*, e49254.
[452] Chen, I., Dorr, B. M., and Liu, D. R. (2011) A general strategy for the evolution of bond-forming enzymes using yeast display, *Proc Natl Acad Sci U S A 108*, 11399-11404.
[453] Wang, L., and Schultz, P. G. (2001) A general approach for the generation of orthogonal tRNAs, *Chem. Biol. 8*, 883-890.
[454] Adli, M. (2018) The CRISPR tool kit for genome editing and beyond, *Nat Commun 9*, 1911.
[455] Omodamilola, O., and Ibrahim, A. (2018) CRISPR Technology; Advantages, Limitations and Future Direction, *J Biomed Pharm Sci 1*, 2.
[456] Cho, S., Park, S. G., Lee, D. H., and Park, B. C. (2004) Protein-protein interaction networks: from interactions to networks, *J Biochem Mol Biol 37*, 45-52.
[457] Parsons, M., Monypenny, J., Ameer-Beg, S. M., Millard, T. H., Machesky, L. M., Peter, M., Keppler, M. D., Schiavo, G., Watson, R., Chernoff, J., Zicha, D., Vojnovic, B., and Ng, T. (2005) Spatially distinct binding of Cdc42 to PAK1 and N-WASP in breast carcinoma cells, *Mol. Cell. Biol. 25*, 1680-1695.
[458] Harlander, R. S., Way, M., Ren, Q., Howe, D., Grieshaber, S. S., and Heinzen, R. A. (2003) Effects of ectopically expressed neuronal Wiskott-Aldrich syndrome protein domains on Rickettsia rickettsii actin-based motility, *Infect. Immun. 71*, 1551-1556.
[459] Banzai, Y., Miki, H., Yamaguchi, H., and Takenawa, T. (2000) Essential role of neural Wiskott-Aldrich syndrome protein in neurite extension in PC12 cells and rat hippocampal primary culture cells, *J Biol Chem 275*, 11987-11992.
[460] Gomez, T. S., Gorman, J. A., de Narvajas, A. A., Koenig, A. O., and Billadeau, D. D. (2012) Trafficking defects in WASH-knockout fibroblasts originate from collapsed endosomal and lysosomal networks, *Mol Biol Cell 23*, 3215-3228.
[461] Cramer, K., Bolender, A. L., Stockmar, I., Jungmann, R., Kasper, R., and Shin, J. Y. (2019) Visualization of Bacterial Protein Complexes Labeled with Fluorescent Proteins and Nanobody Binders for STED Microscopy, *Int J Mol Sci 20*, 3376.
[462] Seitz, K. J., and Rizzoli, S. O. (2019) GFP nanobodies reveal recently-exocytosed pHluorin molecules, *Sci Rep 9*, 7773.

[463] Sograte-Idrissi, S., Oleksiievets, N., Isbaner, S., Eggert-Martinez, M., Enderlein, J., Tsukanov, R., and Opazo, F. (2019) Nanobody Detection of Standard Fluorescent Proteins Enables Multi-Target DNA-PAINT with High Resolution and Minimal Displacement Errors, *Cells 8*, 48.

[464] Guimaraes, C. P., Witte, M. D., Theile, C. S., Bozkurt, G., Kundrat, L., Blom, A. E., and Ploegh, H. L. (2013) Site-specific C-terminal and internal loop labeling of proteins using sortase-mediated reactions, *Nat Protoc 8*, 1787-1799.

[465] Celikkan, F. T., Mungan, C., Sucu, M., Uysal, F., Kahveci, S., Hayme, S., Kuscu, N., Ozkavukcu, S., Celik-Ozenci, C., and Can, A. (2019) Glyoxal Does Not Preserve Cellular Proteins as Accurately as PFA: A Microscopical Survey of Epitopes, *bioRxiv*, 625863.

[466] Singh, H., Bishen, K. A., Garg, D., Sukhija, H., Sharma, D., and Tomar, U. (2019) Fixation and Fixatives: Roles and Functions—A Short Review, *Dental Journal of Advance Studies*.

[467] Richter, K. N., Revelo, N. H., Seitz, K. J., Helm, M. S., Sarkar, D., Saleeb, R. S., D'Este, E., Eberle, J., Wagner, E., and Vogl, C. (2018) Glyoxal as an alternative fixative to formaldehyde in immunostaining and super-resolution microscopy, *The EMBO journal 37*, 139-159.

[468] Sabatini, D. D., Bensch, K., and Barrnett, R. J. (1963) Cytochemistry and electron microscopy. The preservation of cellular ultrastructure and enzymatic activity by aldehyde fixation, *J Cell Biol 17*, 19-58.

[469] Melan, M. A. (1994) Overview of cell fixation and permeabilization, In *Immunocytochemical Methods and Protocols*, pp 55-66, Springer.

[470] Schnell, U., Dijk, F., Sjollema, K. A., and Giepmans, B. N. (2012) Immunolabeling artifacts and the need for live-cell imaging, *Nat. Methods 9*, 152-158.

Acknowledgments - Dankwoord

Acknowledgments - Dankwoord

Als laatste onderdeel van mijn doctoraat is het uiteraard belangrijk om een aantal mensen op te sommen die mij geholpen hebben om de eindmeet te halen, zowel direct als indirect, fysiek als mentaal. Ik ben dan misschien niet degene die altijd het meest te vertellen had of heeft, toch ben ik zeer blij dat ik jullie allemaal heb mogen ontmoeten.

Allereerst wil ik **Jan**, mijn promotor, bedanken om mij de kans te geven mijn master thesis en doctoraat te mogen uitvoeren onder zijn supervisie. Zonder u had ik niet gestaan waar ik nu sta met mijn bagage over de nanobody technologie en fundamenteel kankeronderzoek. Hoewel het verkrijgen van financiering niet altijd van een leien dakje liep, ben ik zeer blij dat ik een kleine vier jaar als doctoraatstudent bij labo Gettemans heb mogen doorbrengen. Ook **Isabel** wil ik hiervoor bedanken om mij tijdens mijn thesisjaar de tips tricks aan te leren die ik nog veelvuldig gebruikt heb doorheen de daaropvolgende jaren. Je was een topbegeleider en een behulpzame, toffe collega! Zelfs nadat je al lang nieuw werk had, vond je het niet erg dat ik je met wetenschappelijke problemen lastig viel. Naast het wetenschappelijke, kon ik steeds ook terecht voor van alles en nog wat. Ook **Leen** bedankt voor de hulp bij mijn lastige vragen rond microscopie en voor het fijne gezelschap samen met Laura in Praag. Gesprekken met jou werkten steeds inspirerend. Daarnaast wil ik ook de personen bedanken waarmee er tijdens de afgelopen jaren we samenwerkingen werden opgezet. Hierbij bedank ik **prof. Annemieke Madder** en **Klaas Decoene**, die ons steeds hielpen bij de zoektocht naar een ideaal onnatuurlijk aminozuur en de chemische achtergrond hierbij. Hoewel het kort was maar toch zeer leerrijk, wil ik onze collega's in Nijmegen, **prof. Alessandra Cambi** en **Ben Joosten**, bedanken om mij daar een aantal dagen te ontvangen en mij wegwijs te maken in de wereld van super resolutie microscopie. Last, but not least, I will thank prof. Kevin Braekmans and Jing Liu for their great support and help in the photoporation experiments. You really helped in the improvements and progression of research in combination with fluorescent nanobodies. We could not achieve the same results without you.

Toen ik op Rommelaere kwam thesissen, werd ik opgenomen in het fijne gezelschap 'labo Gettemans'. In die tijd raakten we bij het middageten niet eens allemaal rond onze tafel. Den bureau boven bestond uit Isabel, Laurence, Ciska en de pas gestarte Anneleen en den bureau beneden met Adriaan, Wouter, Jonas, Els en niet te vergeten den Olivier. Door de goede

groepssfeer tijdens mijn thesisjaar, kon ik nog geen afscheid nemen van de groep en ben ik gegaan voor een PhD. Waar ik tot op heden nog steeds geen spijt van heb. **Laurence**, met jouw heb ik wel het grootste paniekmomentje tijdens mijn doctoraat beleefd, toen we op de terugweg van Helsinki het vliegtuig moesten nemen. Ik heb nog nooit zo snel als dan van de incheckbalie naar de gate gegaan als toen. Uiteindelijk was er geen probleem en hadden we onze beweging voor de dag ook weer gehad. Naast dat momentje heb ik genoten van u gezelschap en de vele verhalen je telkens te vertellen had. **Adriaan**, jij kon ook vertellen als de beste en je was net de wandelende encyclopedie van labo Gettemans. Jammer dat je je schilpadden hebt moeten achterlaten, maar ik vermoed dat het je wel bevalt in het verre Amerika. **Els**, onze sympathieke ambtenaar en laatste West-Vlaming van de groep. Hoewel je al even weg bent, bleef je steeds vertegenwoordigd. Je zelf gevouwen bootje plakt nog steeds aan mijn PC-scherm en de "West-Vlamingen zijn ook maar mensen" hangt nog steeds op. Jij was er altijd om uitjes van 'Labo Gettemans' uitgevoerd te krijgen waarvoor ik blij ben, zoals de escape room, de sportdag (waar Anneleen ook steeds overtuigend voor was), het kerstfeestje (waarvoor je de doorslag gaf in 2019), … Maar ondertussen is er een klein LB'tje geboren :) die nu je volle aandacht zal opeisen. Dikke proficiat, Els en Joren! Samen met **Anneleen,** is er regelmatig een bureaustoelendans gedaan. Er werd telkens doorgeschoven van bureau om uiteindelijk rechtover elkaar te komen zitten zodat we telkens van achter de PC schermen moesten piepen om ons beklag te doen ;). En als laatste vrouw, heb je 'Labo Gettemans' moeten achterlaten waardoor groep Gettemans duidelijk een mannenbastion werd. De laatste vrouwelijke touch wordt gemist, alsook je rechttoe rechtaan opmerkingen, maar ik merkte wel dat 'den bureau beneden' samen met Chloé daarmee ook op goede weg was :p. Hoewel er enkel mannen overbleven, heb ik de veelbesproken poster nog niet zien verschijnen. Als er een model gevonden is, wil ik altijd helpen de foto te maken en/of hem dan in het groot te helpen ophangen ;) . **Tijs** en **Olivier**, jullie vormen een ideaal duo om 'den bureau beneden' in eer te houden en jullie doen dat uitstekend. Hou den bureau boven maar in de gaten, voor zolang we er nog een hebben. Veel succes trouwens met de verhuis. Dat worden leuke tijden om zo alles te versleuren met jullie 'drietjes', maar wie weet doen jullie nog 'de ontdekking van de eeuw' in de gebouwen, kasten, … van het Rommelaere complex ;). En **Tijs**, hoewel het drukke verhuisperiode wordt, zal het voor u nog drukker worden met het schrijven van je artikels, revisie en doctoraat. Niettemin, ben ik ervan overtuigd dat je de kwaliteiten voor een doctoraatstitel meer dan verdiend hebt en hoop ik van harte dat je hem ook krijgt. Ik duim alvast voor een eenvoudige revisie. Als jij nog geen doctoraatstitel zou verdienen, weet ik het ook niet meer. **Olivier**, onze vaste rots in de branding en pro in alles wat nanobodies aanbelangt. Bedankt om mij tijdens mijn doctoraat te helpen met raad en daad als ik op problemen stootte. Als we een overvloed aan confituur aardbeien hebben, weet ik u te vinden :p . En tot slot, **Brian**, de laatste aanwinst van de groep. Hoewel het zeer rustig al worden, zou ik aanraden om er toch je hoofd goed bij te houden en geen verstrooide professor te worden, waar ik misschien niet altijd een goed voorbeeld van was tijdens je thesisjaar, maar we zullen er het UV verhaal niet bijhalen deze keer :p. Probeer er ook zelf wat druk achter te zetten, want vier jaar vliegen snel voorbij. **@Olivier, Tijs & Brian**, ik ben trouwens blij dat ik nog steeds welkom was om te crashen net voor de avondlessen. Zo kon ik trouwens de

veranderingen en roddels in Rommelaere op de voet blijven opvolgen, alsook de frustraties over de thesisstudenten.

Ook **Emily** wil ik eens in de kijker zetten. Hoewel jij het de laatste jaren ook niet altijd even gemakkelijk hebt gehad en kanker van dichtbij hebt moeten ervaren, ben je steeds je aangename zelf gebleven. Ik heb u dan wel regelmatig opgezadeld met veel werk door al mijn producties, maar je bleef altijd vriendelijk de stapels isomo dozen verzamelen die nog steeds goed van pas komen. Ook **Patrick** wil ik hiervoor bedanken.

Vervolgens gaat een doctoraat ook gepaard met het begeleiden van thesisstudenten. Ook jullie wil ik bedanken. Hoewel jullie er zowel op goede als op de kwade dagen waren, we hebben het altijd zo leuk mogelijk proberen maken en meet succes. Uiteraard kan **Brian** het meest over negatieve resultaten meespreken, maar deze zijn daarom niet minder belangrijk dan de positieve resultaten. Hoewel dat laatste uiteraard aangenamer is, maar ondertussen weet je ook wat onderzoek inhoudt. *Witte geit* nog, **Emma**, alle onze plezante momenten? Er zijn er te veel om op te noemen, een jaar om niet te vergeten. Samen met Anne-Sophie brachten jullie ongetwijfeld leven in de brouwerij. En nogmaals bedankt om mij te helpen met de gelabelde nanobodies in dat weekend om rond te geraken voor Nijmegen! Uiteraard is er nog 'mijn' (of bij wie is het nu precies) laatste thesisstudente, **Chloé**. Hoewel het voor u ook niet gemakkelijk is om in verschillende groepen en zonder vaste begeleider uw experimenten uit te voeren, doe je dat uitstekend. Je zou nochtans een aanwinst zijn voor labo Gettemans. Zeker nu ik al getuige ben van het vrolijke trio dat je vormt met Tijs en Olivier :D . Ondanks onze vooroordelen die we hebben over de VIVES studenten, wil ik **Gaëlle** toch nog eens extra bedanken voor alles wat ze gedaan heeft. Zonder jouw ging het zo snel niet vooruit gegaan zijn en ik denk wel dat je het al weet, maar jij bent echt wel de uitzondering op de regel. Zo'n top studente!

Uiteraard de ***freaky five*** (en aanhangsels ;)), jullie hebben ook bijgedragen aan mijn doctoraat door de ontstress sessies, de gezellige babbels met hapje en drankje, … kortom het gezelschap die we ondertussen al sinds het derde middelbaar vormen. Ik kijk telkens uit naar de volgende gelegenheid. Ik wil Nele nog eens extra bedanken, aangezien zij nog niet iets meer rechtstreeks bijgedragen door het zware werk van het nalezen van dit naslagwerk op fouten, het opvangen van gestrande pendelaars tijdens sneeuwdagen en het verplicht Chinees moeten eten telkens ik daar was :p .

Natuurlijk niet alleen oude vrienden hebben voor het plezier gezorgd in mijn vrije tijd, ook de **fotografievriendjes** uiteraard (Nele, Ruth, Els en Sin). Ik ben blij dat ik zo snel bij het groepje ben kunnen migreren en vind het altijd aangenaam om met jullie te vertoeven al dan niet met camera in de hand. Eenmaal ik verder in de kooklessen reeks zit, zal ik jullie uiteraard eens uitnodigen om mijn kookkunsten uit te testen, maar ik kan geen beloften doen op het eindresultaat ;) . Ook jij, **Jules**, bedankt voor de etentjes die we afgelopen jaren te weinig doen, hoewel de kookles er nu verandering in brengt. Ik ben blij dat we op die manier terug regelmatiger samenkomen.

Uiteraard ook een bedanking voor het thuisfront. Bedankt **mama en papa** voor de nog steeds warme ontvangst na de werkdag en om mij mee te nemen op de mooie onvergetelijke reizen die we ondertussen gedaan hebben. Daarnaast, waren jullie eveneens vertegenwoordigd op Rommelaere. Ik denk dat ze er ondertussen onze aardbeien ook wel al herkennen. Die verdienste is uiteraard ook van **Stijn**. Jammer genoeg moeten we het nu zonder jou verder doen, maar ook **Annelies** bedankt voor alles. Jij bent een top vrouw, hoe je er steeds in slaagt om alles te regelen met je twee kleine sloebers, **Warre en Lander**. Echt chapeau! Het is ook mooi te zien dat je Stijn extra in eer houdt door je rond 19 augustus telkens weer in te zetten voor het eetfeSTIJN. Ook mede daardoor kan 'Kom op tegen kanker' onderzoek steunen, waardoor ik ook een jaar onderzoek kon doen. Als laatste nog een bedanking aan **Ineke en haar kroost**, want ook jullie werden vertegenwoordigd op Rommelaere met jouw ambachtelijke ijscrème die telkens terug in de smaak viel!

Nu we toch bezig zijn, ik ben dan misschien geen man van veel woorden, maar dat wil niet zeggen dat ik daarvoor jullie niet in mijn hart gesloten heb. Nog eens bedankt aan iedereen die ik reeds vermelde, maar ook alle andere mensen die de afgelopen jaren mijn pad kruisten en rechtstreeks of onrechtstreeks invloed hebben gehad. Dus dikke merci aan iedereen, ookal kan ik door Covid-19 dit niet in persoon zeggen!!!